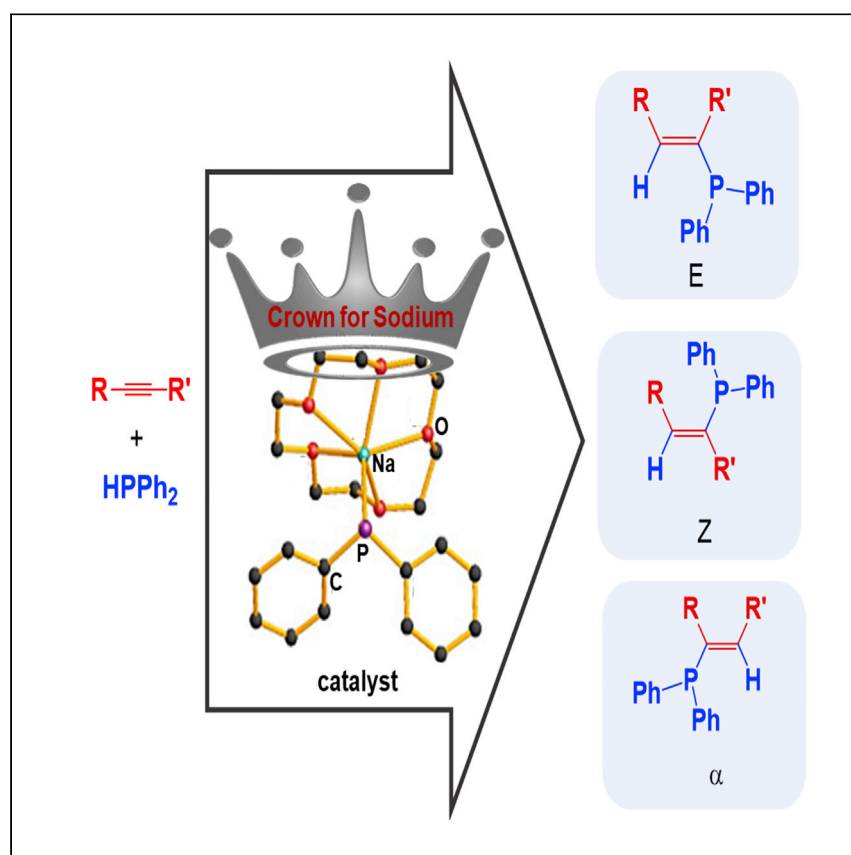


Article

Catalytic hydrophosphination of alkynes using structurally diverse sodium diphenylphosphide donor complexes



Michael T. Whitelaw, Sumanta Banerjee, Alan R. Kennedy, Alexander van Teijlingen, Tell Tuttle, Robert E. Mulvey

r.e.mulvey@strath.ac.uk

Highlights

Four crystallographically characterized sodium diphenylphosphide donor complexes

Screening of complexes as catalysts in hydrophosphination applications of alkynes

Detailed DFT analysis probing different catalytic mechanisms

Homogeneous catalysis relies heavily on the use of precious transition metal catalysts. Here, Whitelaw et al. describe the use of a series of alternative, structurally well-defined compounds based on the earth-abundant metal sodium, which can catalyze hydrophosphination reactions of alkynes leading to alkenes.

Article

Catalytic hydrophosphination of alkynes using structurally diverse sodium diphenylphosphide donor complexes

Michael T. Whitelaw,¹ Sumanta Banerjee,¹ Alan R. Kennedy,¹ Alexander van Teijlingen,¹ Tell Tuttle,¹ and Robert E. Mulvey^{1,2,*}

SUMMARY

Currently, there is a drive to develop the organoelement chemistry of sodium, the most abundant alkali metal on earth, as an alternative to that of rarer lithium, with the prime focus on sustainability. Organolithium compounds have been essential to the success of synthetic chemistry for more than a century, although their implementation has been essentially confined to stoichiometric synthesis. Here, we report on synthetic, structural, catalytic, mechanistic, and theoretical studies of a series of sodium diphenylphosphides, having unique structures defined by the Lewis base donor *D* solvating the Lewis acidic sodium cation. These donor complexes are explored as hydrophosphination catalysts on reacting $\text{Ph}_2\text{P-H}$ with a range of alkynes and prove to be generally effective under ambient conditions, especially when $n = 1$ in $[(\text{Ph}_2\text{PNa}(\text{D})_n)_x]$. Density functional theory (DFT) studies have shed light on the possible mechanisms of these catalytic cycles and how they relate to the *E*, *Z*, or α isomer formed.

INTRODUCTION

Phosphorus-containing compounds are invaluable due to their extensive applications in areas such as agriculture, pharmaceuticals, and organometallic catalysis.⁵ Fertilizers,⁶ antibiotics,⁶ and flame retardants⁷ are just three examples of the diverse roles that phosphorus compounds have that benefit the everyday lives of humankind. It follows, then, that hydrophosphination, the process of inserting a phosphorus-hydrogen bond into an unsaturated carbon-carbon or carbon-heteroatom bond, is of significant interest in modern research. Much current focus is on catalytic hydrophosphination as it provides a pathway to higher product yields with lower reaction times and less-demanding conditions. The first metal-catalyzed hydrophosphination was reported over 30 years ago in a seminal communication by Pringle and Smith,⁸ who used a Pt(0) complex to catalyze phosphine addition to acrylonitrile. In the intervening years, significant advances have been made using a plethora of catalyst types.^{9–18} Reports of “catalyst-free” systems have also emerged.^{19,20} With scientists shifting more of their research toward sustainability issues and the development of green chemistry, it would be desirable if the less-abundant and generally more toxic precious transition metal catalysts could be replaced with more-abundant and less-toxic main-group alternatives. Toward that goal, progress has been made, with, for example, reports of Ca, Sr, Ba, Al, and Ge-based catalysts,^{21–24} while our own group has contributed the heterobimetallic lithium aluminate catalyst $^i\text{Bu}_3\text{AlPPh}_2\text{Li}(\text{THF})_3$.²⁵

Organoalkali-metal compounds have long been one of the most widely used classes of reagents in the history of synthetic chemistry, with organosodium and

¹WestCHEM, Department of Pure and Applied Chemistry, University of Strathclyde, Glasgow G1 1XL, UK

²Lead contact

*Correspondence: r.e.mulvey@strath.ac.uk
<https://doi.org/10.1016/j.xcrp.2022.100942>

organopotassium compounds first reported in 1858 by Wanklyn,²⁶ while organolithium compounds, by far the most utilized organoalkali-metal reagents, were introduced by Schlenk and Holtz in 1917.²⁷ The numerous applications of s-block complexes have been the subject of many review articles, highlighting the importance of these compounds.^{28–34} Nearly all of these applications have been within the confines of stoichiometric chemistry. On the other hand, d-block metals have dominated the catalysis world for decades. With advantages of high earth abundance (especially sodium and potassium), low cost, environmental friendliness, and relatively low toxicity compared with their d-block counterparts, alkali-metal-based compounds could become prize assets within the catalytic world moving forward, which is why the “ignition” has now been pressed and the development of alkali-metal homogeneous catalysis is starting to accelerate. Here, our interests lie in developing organosodium-based catalysts for hydrophosphination. The use of alkali metals in hydrophosphination chemistry was achieved as early as 1966 by Aguiar and Archibald³⁵ when they studied the addition of lithium diphenylphosphide to phenylacetylene in stoichiometric reactions. Related work was reported in 1970 by Issleib, Boehme, and Rockstroh when they reacted lithium and potassium diphenylphosphides stoichiometrically with acetylenes.³⁶ Since then, hydrophosphination has been advanced to the catalytic regime with other alkali-metal catalysts, such as KO^tBu^{37–40} and KHMDS (HMDS = 1, 1, 1, 3, 3, 3-hexamethyldisilazide).⁴¹

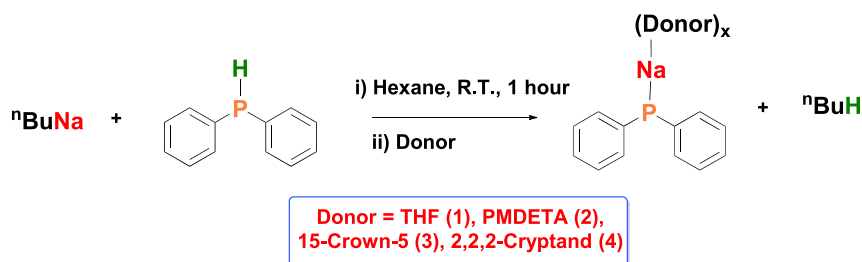
The study of sodium compounds for carrying out various chemical transformations is an area currently undergoing a resurgence.^{30,42–47} In our aforementioned research on employing a heterobimetallic lithium aluminate compound for catalytic hydrophosphination of various alkynes, alkenes, and carbodiimides,²⁵ monometallic lithium diphenylphosphide was also screened for comparison and, although it gave slightly lower yields than the aluminate ⁱBu₃AlPPh₂Li(THF)₃, it was still catalytically competent. Given that sodium is both more abundant than lithium and its compounds are generally more reactive than lithium compounds, it left us pondering whether sodium could be a more effective and more sustainable replacement for its lighter congener in catalytic hydrophosphination processes. To address this question, we have therefore synthesized and structurally characterized four monometallic sodium diphenylphosphide complexes and tested their catalytic competence in the hydrophosphination of benchmark alkenes and alkynes.

RESULTS AND DISCUSSION

Synthesis and characterization

Although sodium diphenylphosphide has been synthesized previously via metalation of the parent secondary phosphine Ph₂PH by benzyl sodium,⁴⁸ transmetalation of LiPPh₂ with NaO^tBu,⁴⁹ or by direct metalation using sodium dispersion,^{50,51} we found it convenient to make it by a simple deprotonative metalation reaction between *n*-butylsodium⁵² and Ph₂PH in a 1:1 stoichiometric ratio in hexane solution. This produced a bright yellow suspension, to which a stoichiometric quantity of a polydentate Lewis base donor ligand was added, either PMDETA (*N,N,N',N'',N''*-pentamethyldiethylenetriamine), 15-crown-5, or 2,2,2-cryptand, while monodentate tetrahydrofuran (THF) was added in excess. Each of these solutions deposited crystals of a suitable quality for X-ray crystallographic determination, which established them to be [(Ph₂PNa.(THF)₂)_∞] (1), [(Ph₂PNa.PMDETA)₂] (2), [Ph₂PNa.15-crown-5] (3), and [(Ph₂P)[−](Na.2,2,2-cryptand)⁺] (4) (Scheme 1).

These crystalline products were isolated in yields of 57%, 79%, 55%, and 21% respectively. As would be expected, the set of compounds displayed a trend of



Scheme 1. Procedure for the synthesis of the Lewis base-supported sodium diphenylphosphide complexes 1–4

lowering aggregation state with increasing denticity of the Lewis base donor ligand, with the THF-solvate a polymer, the PMDETA-solvate a dimer, the 15-crown-5-solvate a monomer, and the highest dentate 2,2,2-cryptand sequestering the sodium cation to generate a charge-separated ion pair. Figure 1 shows the asymmetric units of 1–4; while Figure 2 gives more extended views of the aggregated structures of 1 and 2.

As can be seen from Tables S1 and S2 in the supplemental information, there are significant differences in the metrics between the different complexes 1–3. Structural data for compound 4 can also be found in the supplemental information (Tables S3 and S4) and has been omitted from the above tables due to the complexity of the compound and the lack of any Na–P contact. The sodium cations in each compound have different coordination numbers and adopt different geometries; it is 4-coordinate in 1, adopting a tetrahedral geometry (mean bond angle of 109.5°), 5-coordinate in 2, adopting a distorted trigonal bipyramidal geometry where P2 and N2 occupy the axial positions (bond angle of 170.12° [6]) and P1, N1, and N3 lie equatorially (bond angles ranging from 110.05° [14] to 125.47° [11]), and is 6-coordinate in 3 with a distorted trigonal prismatic geometry having a mean bond angle of 89.16° around the edges of the coordination sphere and 127.3° diagonally across it. The geometry of the phosphorus atoms change across the set of compounds also, from 4-coordinate distorted tetrahedral in 1 and 2 (mean bond angles of 116.8° and 106.2° respectively) to 3-coordinate distorted trigonal pyramidal in 3 with a mean bond angle of 102.3°. As of 18 November 2021, searching for [Ph₂PNa.THF] in the Cambridge Structural Database⁵³ reveals a single hit in the dimeric

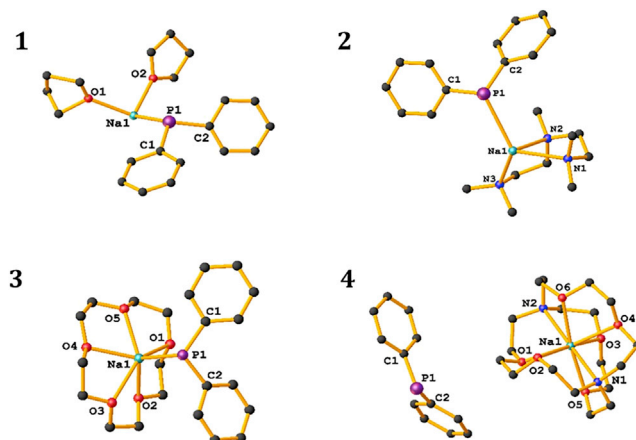


Figure 1. Mononuclear structural units of 1–4 with key atom labeling
H atoms have been removed for clarity.

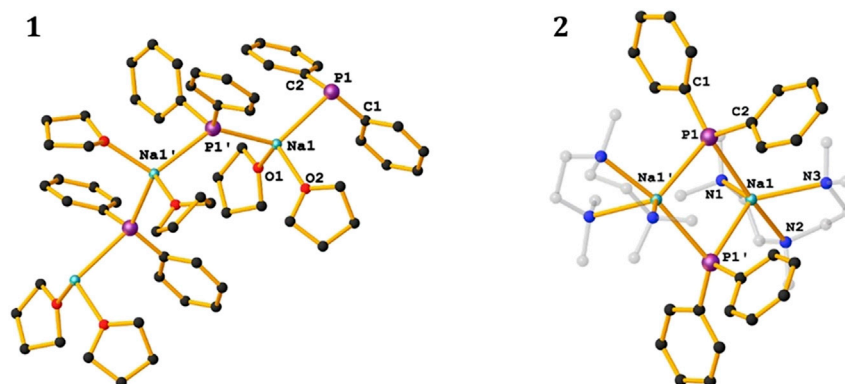


Figure 2. Part of the polymeric structure of 1 and dimeric structure of 2 with key atom labeling
H atoms have been removed for clarity. PMDETA ligands in 2 have been set to 60% transparency for clarity. Here and elsewhere, for compound 1, the prime symbol “'” indicates the symmetry operation $x + 1/2, 1 - y, z$; and for compound 2, it indicates $1 - x, y, 3/2 - z$.

sodium bis(2,6-diisopropylphenyl)phosphide,⁴⁸ with each sodium atom being solvated by two THF units, and two Na–P bonds (lengths of 2.9246(8) Å and 3.0178(8) Å), both considerably longer than the 2.825(2) Å observed in 1. When [Ph₂PNa.PMDETA] is searched, two hits show,^{48,54} one monomeric compound with the previously mentioned bis(2,6-diisopropylphenyl)phosphide anion, and another involving a monomeric phosphinimide complex. These have Na–P bond lengths of 2.8745(12) Å and 2.9619(11) Å respectively, this time notably shorter than the 2.9499(17) Å and 3.036(2) Å in 2. Finally, searching for [Ph₂PNa.O₅] brings up one hit,⁵⁵ namely a sodium bis(2-oxy-3,5-di-*tert*-butyl)tert-butylphosphide polymer with one glyme molecule solvating each sodium cation, and an extra glyme molecule bridging between sodium cations. This gives a Na–P bond length of 2.8757(14) Å, which is in good agreement with the 2.8742(8) Å found in 3. This paucity of structural hits also underlines the novelty of the new compounds 1–4.

Catalytic hydrophosphination studies

Next, we moved on to quantifying the comparative effectiveness of the solvated sodium phosphides for catalytic hydrophosphination of the model alkyne, phenylacetylene PhC≡CH (Table 1). Since our previous hydrophosphination work using the heterobimetallic catalyst ^tBu₃AlPPh₂Li(THF)₃ required a 10 mol % catalyst loading at 110°C,²⁵ we viewed this as a logical starting point for our new aluminum-free phosphides. However, simple visual inspections suggested that compounds 3 and 4 were reacting significantly faster than the 30-min measurement mark, so we therefore lowered the temperature for these reactions to room temperature. Pleasingly, both compounds still produced quantitative conversion to the hydrophosphinated alkene products in 30 min. The conversions in Table 1 were calculated by ¹H NMR spectroscopy using adamantane as the internal standard and are based on the consumption of diphenylphosphine starting material.

Entries 1, 2, 5, and 6 were therefore taken as the optimized conditions for each catalyst. The catalysts were each tested on 11 different substrates and the full set of results are collated in Figure 3. The stereoselectivities obtained in each case are also noted. Phosphide 1 was shown to be the least efficient catalyst as it required the most demanding conditions and produced the lowest conversions. Notably, however, it was still able to convert 4-cyanophenylacetylene, 3-phenyl-1-propyne, and methyl acrylate in just 30 min at room temperature in good to excellent conversions (entries e, f, and k). Understandably, the more challenging aliphatic substrates

Table 1. Optimization of hydrophosphination conditions using phenylacetylene as model substrate

Entry	Catalyst	Temperature (°C)	Time (h)	Conversion (%) ^a
1	1	110	1	72
2	2	110	1	99
3	3	110	<0.5	99
4	4	110	<0.5	99
5	3	RT	0.5	99
6	4	RT	0.5	99

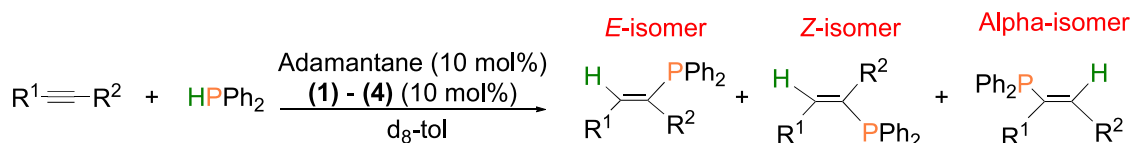
RT, room temperature.

^aConversions are based on the consumption of HPPH₂ within the reaction and were calculated from the ¹H NMR spectra using adamantane as the internal standard.

4-phenyl-1-butyne and 1-octyne required 3 h at 110°C in order to obtain moderate to good conversions (entries g and h), whereas the most difficult 3-hexyne produced only a 10% conversion after a full 24 h at 110°C (entry i).

Phosphide 2 performed marginally better than 1 and notably was more efficient when electron-withdrawing substituents were present, quantitatively converting 4-trifluoromethyl phenylacetylene and 4-cyanophenylacetylene in 30 min at room temperature (entries d and e); it also only required these conditions for the more activated methyl acrylate (entry k). Longer times were necessary to successfully convert 3-phenyl-1-propyne, 4-phenyl-1-butyne and 1-octyne, producing good to moderate conversions in each case (entries f, g, and h). Interestingly, 3 h were also required to convert styrene using 2 (entry j). Finally, phosphide 2 secured a slightly better result with 3-hexyne than 1, but the conversion was still poor (entry i). Moving to monomeric 3, this proved significantly more reactive than the previous two phosphides and quantitatively converted all but three of the substrates under the standard conditions, with 4-phenyl-1-butyne producing a low conversion, and 1-octyne requiring 3 h at 110°C (entries g and h). A good result was obtained with the obstinate 3-hexyne, albeit still requiring harsh conditions (24 h at 110°C, entry i). Compound 4 proved to be the most efficient catalyst of the set with the non-activated aliphatic alkynes the only substrates that required deviation from standard mild conditions. Notwithstanding, 1-octyne required 3 h to secure a good conversion, and 4 was the only compound to successfully hydrophosphinate 1-octyne at room temperature (entry h), demonstrating its heightened reactivity, and while 3-hexyne did still require 24 h at 110°C, 4 was the only catalyst to obtain quantitative conversion of this substrate (entry i). In order to examine whether or not the alkali metal is necessary, we attempted the hydrophosphination of phenylacetylene, catalyzed by the ammonium analogue [Bu₄N]⁺[Ph₂P]⁻. After 3 h at 110°C there was only a 13% conversion observed, and this did not change when left for a further 72 h at room temperature. This result demonstrates the necessity of the alkali metal in our work. Significant work by Wipff and co-workers⁵⁶ on the molecular dynamic simulations of 2,2,2-cryptand encapsulating a series of alkali-metal cations suggest that some of the sodium surface is available for reactivity, which may explain in part the high reactivity of compound 4.

In order to obtain selected yields of products as well as conversions, we repeated four of the above catalytic reactions and each reaction was quenched with an



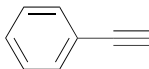
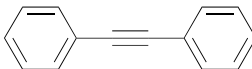
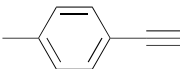

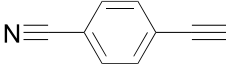
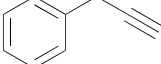
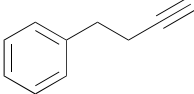
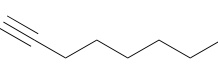
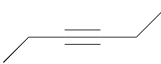
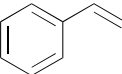
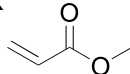
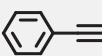
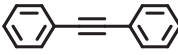
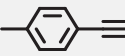
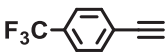
<p>A</p>  <p>(1) 72% (49:51) (2) 99% (83:17) (3) 99% (45:55) (4) 99% (28:72)</p>	<p>B</p>  <p>(1) 99% (96:4) (2) 99% (94:6) (3) 99% (35:65) (4) 99% (100:0)</p>	<p>C</p>  <p>(1) 92% (19:81) (2) 99% (31:69) (3) 99% (17:83) (4) 99% (13:87)</p>
<p>D</p>  <p>(1) 99% (64:36) (2) 99%^c (81:19) (3) 99% (68:32) (4) 99% (48:52)</p>	<p>E</p>  <p>(1) 82%^c (70:0:30)* (2) 99%^c (85:11:4)* (3) 99% (50:0:50)* (4) 99% (84:16)</p>	<p>F</p>  <p>(1) 96%^c (79:21) (2) 88%^a (82:18) (3) 99% (85:15) (4) 99% (95:5)</p>
<p>G</p>  <p>(1) 77%^a (47:53) (2) 99%^a (52:28:20)* (3) 23% (43:57) (4) 83% (51:49)</p>	<p>H</p>  <p>(1) 53%^a (4:55:41)* (2) 63%^a (25:38:37)* (3) 99%^a (41:14:45)* (4) 79%^d (2:55:43)*</p>	<p>I</p>  <p>(1) 10%^b (100:0) (2) 20%^b (100:0) (3) 80%^b (100:0) (4) 99%^b (100:0)</p>
<p>J</p>  <p>(1) 99% (2) 99%^a (3) 99% (4) 99%</p>	<p>K</p>  <p>(1) 71%^c (2) 86%^c (3) 99% (4) 99%</p>	

Figure 3. Hydrophosphination of unsaturated substrates A–K using (1)–(4) as catalyst

Conversions based on consumption of HPPH₂ calculated from ¹H NMR spectra using adamantane as an internal standard. E:Z ratios in parentheses and determined from ³¹P NMR. General conditions: (1) 1 h, 110°C; (2) 1 h, 110°C; (3) 30 min, room temperature; (4) 30 min, room temperature. ^a3 h at 110°C; ^b24 h at 110°C; ^c30 min, room temperature; ^d3 h, room temperature; *E:Z:α.

Table 2. Yields obtained from hydrophosphination of selected substrates, using 3 as a catalyst, after chromatographic separation using a silica-packed column

$\text{R}^1\text{C}\equiv\text{R}^2 + \text{HPPH}_2 \xrightarrow[\text{d}_8\text{-tol, R.T., 30 mins}]{\text{Ph}_2\text{PNa.15C5 (10 mol\%)}} \text{H}-\text{C}(\text{R}^1)=\text{C}(\text{R}^2)-\text{PPh}_2 + \text{H}-\text{C}(\text{R}^1)=\text{C}(\text{R}^2)-\text{PPh}_2$						
Entry	Substrate	Time (h)	Temperature (°C)	Conversion (%)	Yield (%)	E:Z
1		0.5	RT	99	86	42:58
2		0.5	RT	99	73	91:9
3		0.5	RT	99	86	65:35
4		0.5	RT	99	76	23:77

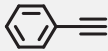
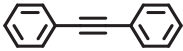
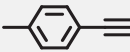
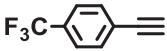
EtOAc/water mixture before being run through a column packed with silica and using a 1:19 EtOAc/hexane eluant mixture. This allowed us to obtain yield by mass for four of our substrates, with compound 3 being employed as the catalyst in each case. It should be noted that although compound 4 produced better catalytic results, 3 was employed as the model catalyst throughout these further studies due to its higher stability, making it easier to isolate, store, and use from a consistent batch. Displayed in Table 2, the results show a general decrease from the conversions but the isolated yields are still good with the lowest one at 73%. The corresponding turnover numbers (TONs) and turnover frequencies (TOFs) have been determined using NMR spectroscopy and the results are presented in the [supplemental information](#) (Table S5). In 2019, Schmidt et al.⁵⁷ reported the use of the *N,N*-dimethylbenzylamine-derived lanthanum catalyst, La(Dmba)₃ for the hydrophosphination of various alkynes. Applying a 5 mol % catalyst loading, they required 12 h at room temperature to obtain an 87% yield of hydrophosphinated phenylacetylene and 48 h for a 65% yield of hydrophosphinated diphenylacetylene, whereas our compounds 3 and 4 required 30 min at room temperature for 99% conversions of each, and 3 obtained 86% and 73% yields of phenylacetylene and diphenylacetylene respectively. Another example is that of Westerhausen¹ in 2008, where he hydrophosphinated diphenylacetylene using a calcium catalyst, and although this did achieve quantitative conversion, it required a 20 mol % catalyst loading and 12 h at 75°C.

While our new methodology is not stereoselective, it is interesting to note the ratio of isomers obtained in each case. With some exceptions, the stereoselectivity appeared to be more dependent on the substrate rather than the catalyst, with each substrate producing similar stereoselectivities irrespective of the catalyst involved, suggesting similar mechanistic pathways. For example, the presence of an electron-donating group favored production of the Z isomer, whereas electron-withdrawing groups favored production of the E isomer. There were also a few cases where significant quantities of the α isomer were observed, where the two non-hydrogen substituents are attached to the same carbon atom.

We first wanted to investigate the effect of changing temperature on the stereoselectivity of the reaction. Using 3 as an example, E:Z ratios of 45:55 and 35:65 were found for phenylacetylene and diphenylacetylene, respectively. When these

Table 3. Comparative stereoselectivity study with changing temperature using 3 as the catalyst

$$R^1 \equiv R^2 + H-PPh_2 \xrightarrow[\text{d}_8\text{-tol, R.T., 30 mins}]{\text{Adamantane (10 mol\%), Ph}_2\text{PNa}\cdot 15C_5\text{ (10 mol\%)}} \begin{matrix} H & R^2 \\ | & | \\ R^1 & -C=C- \\ | & | \\ H & PPh_2 \end{matrix} + \begin{matrix} H & PPh_2 \\ | & | \\ R^1 & -C=C- \\ | & | \\ H & PPh_2 \end{matrix} \xrightarrow{110^\circ C, 1 \text{ hour}} \begin{matrix} H & PPh_2 \\ | & | \\ R^1 & -C=C- \\ | & | \\ H & PPh_2 \end{matrix}$$

Entry	Substrate	Time (h)	Temperature (°C)	E:Z	Time (h)	Temperature (°C)	E:Z
1		0.5	RT	45:55	1	110	96:4
2		0.5	RT	35:65	1	110	97:3
3		0.5	RT	17:83	1	110	17:83
4		0.5	RT	68:32	1	110	68:32

reaction solutions are either left at room temperature for significantly longer (approximately 17 h) or heated to 110°C for 1 h, the ratios change to 96:4 and 97:3 respectively. Furthermore, when the reaction was carried out with phenylacetylene at the lower temperature of –20°C, a 20:80 E:Z ratio was observed (see [supplemental information](#)). These findings are consistent with the Z isomer being the kinetically favored product and the E isomer the thermodynamically favored product.

Next, we sought to shed light on the mechanism behind this isomerization process, as it could potentially lead us to achieve better stereoselectivity in the future. We first investigated the effect of temperature on the stereoselectivity ([Table 3](#)) and used four of the previously investigated substrates, encapsulating terminal and internal alkynes, as well as alkynes containing both electron-donating and electron-withdrawing groups. The crown ether monomer 3 was utilized as the catalyst throughout this part of the study. While the first two substrates produced promising results with nearly quantitative stereoselectivity to E upon heating, entries 3 and 4 demonstrate the inherent complexity of this process, as the electronics of the substituent groups on these alkyne substrates appear to have a clear and notable impact on the isomerization, showing no change upon heating.

Schmidt et al.⁵⁷ also discussed a potential isomerization mechanism with their aforementioned La(Dmba)₃ catalyst and proposed that the substrates were temporarily undergoing double hydrophosphination. This would produce an alkane intermediate, allowing free rotation of the carbon-carbon bond, before β-phosphide elimination re-formed the alkene product in the more favorable E conformation ([Figure 4](#)). To add merit to this hypothesis, they demonstrated that reducing the quantity of phosphine in the reaction selectively produced the Z isomer, whereas alternatively increasing the quantity of phosphine selectively produced the E isomer. To investigate whether or not our system could be undergoing a similar process, we attempted the same reaction. However, no difference was observed in our system when the phosphine concentration was increased or reduced, implying that our system proceeds by a different mechanism.

In 1966, Aguiar and Archibald³⁵ published work showing the stoichiometric and stereoselective addition of phosphines to alkynes via lithium diphenylphosphide. They showed that, by carrying out their reactions in THF and adding a primary amine to the mixture (e.g., *n*-butylamine), they witnessed E selectivity. In contrast, when

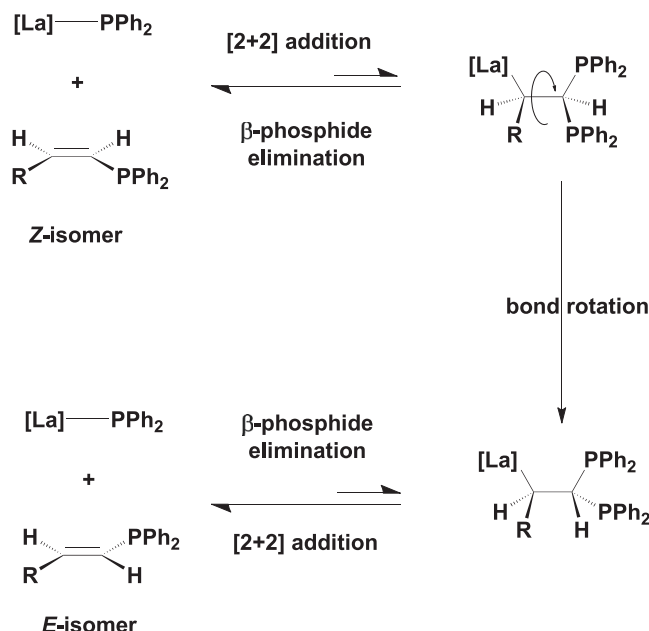


Figure 4. Potential isomerization mechanism proposed by Schmidt et al. for their lanthanum-catalyzed hydrophosphination

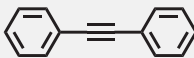
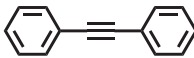
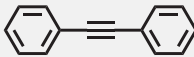
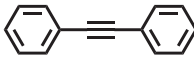
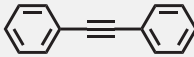
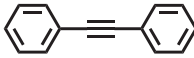
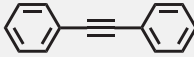
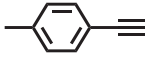
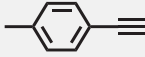
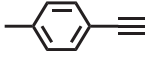
Reproduced with permission from Basiouny et al.⁵⁷ Copyright 2019, American Chemical Society.

they added a secondary amine (e.g., *N*-methylaniline), there was a stereoselective switch to the Z isomer. Interestingly, they also noted that this was not the case on changing their polar metal phosphide source to sodium from lithium. Regardless, we decided to attempt this method with our sodium system, and the results are displayed in Table 4.

While Aguiar and Archibald carried out their process stoichiometrically, we opted to attempt this catalytically and began by using $[\text{NaPPh}_2]_\infty$ in d_8 -THF to replicate the conditions used by Aguiar and Archibald (entries 1–3) and found that the stereoselectivity does change when a sodium catalyst is used in the presence of either a primary or secondary amine. We then moved to using one of our own catalysts for this purpose (entries 4–7) and found that the choice of solvent was significant, observing no change in the stereoselectivity of hydrophosphination of diphenylacetylene when the reaction was run in d_8 -toluene. That notwithstanding, we were able to partially control the stereoselectivity of diphenylacetylene using 3 in d_8 -THF, obtaining an E:Z ratio of 97:3 when a primary amine was added, and reversing this to 30:70 on changing to a secondary amine additive. When we attempted this method on 4'-methylphenylacetylene, a substrate that has been shown to be Z selective previously, there was unfortunately no notable difference when a primary or secondary amine was added to the reaction (entries 8–10).

There have been other reports of main-group metal-catalyzed hydrophosphination over the past few years; for example, Webster et al. reported their use of $[\text{GeCl}\{\text{N}(\text{SiMe}_3)_2\}_3]$ as a pre-catalyst for hydrophosphination in 2020 and showcased the good performance of this catalyst as it only required a 5 mol % catalyst loading and had a wide-ranging substrate scope.²⁴ However, one of the main limitations of their system was the longer reaction time with internal alkynes, with durations as long as 96 h in one case. This was shown not to be a problem in our sodium work. Our catalysts, for example, were all able to quantitatively convert

Table 4. Stereoselectivity study by adding primary or secondary amines to the reaction mixture

Entry	Substrate	Catalyst	Solvent	Amine	Conversion (%)	E:Z
1		[NaPPh ₂] _∞	d ₈ -THF	no amine	99	41:59
2		[NaPPh ₂] _∞	d ₈ -THF	n-butylamine	99	91:9
3		[NaPPh ₂] _∞	d ₈ -THF	N-methylaniline	99	23:77
4		3	d ₈ -toluene	n-butylamine	99	30:70
5		3	d ₈ -THF	no amine	99	67:73
6		3	d ₈ -THF	n-butylamine	99	97:3
7		3	d ₈ -THF	N-methylaniline	99	30:70
8		3	d ₈ -THF	no amine	99	10:90
9		3	d ₈ -THF	n-butylamine	99	9:91
10		3	d ₈ -THF	N-methylaniline	99	7:93

All reactions were complete in 30 min at room temperature.

diphenylacetylene to the respective hydrophosphinated product either in 1 h at 110°C (1 and 2) or in 30 min at room temperature (3 and 4), whereas the germanium catalyst reported by Webster et al. required 48 h at room temperature to obtain an 81% conversion. The reported germanium catalyst also struggled with stereoselectivity, something we were also familiar with. Two years prior to this, the Webster group also demonstrated the ability of KHMDS to carry out catalytic double hydrophosphination.⁴¹ A 10 mol % catalyst loading was required, along with longer reaction times than were required for our system (6 h). It is worth noting that we have not observed double hydrophosphination in any of our work.

In an early seminal piece of work, Knochel and Bunlaksanansorn introduced the use of KO^tBu for hydrophosphination in 2002³⁹ and disclosed the ability of this easy-to-obtain and cheap starting material as a catalyst. Their work required a 20 mol % loading of the catalyst though, and the product yields spanned the range 63%–88%, notably lower than what was generally observed with our catalysts. There were also no alkynes tested in Knochel's study, only activated alkene substrates. Manners et al. also carried out work with KO^tBu, albeit for the purpose of homo- and heterodehydrocoupling of phosphines,⁴⁰ but it is worth noting that reported intermediates in their work are hydrophosphination products. While they do carry out these reactions with only a 10 mol % loading of their potassium catalyst, the process requires harsh conditions (e.g., 130°C in THF for 16 h). Intrigued by these publications, we attempted the hydrophosphination of phenylacetylene and 3-hexyne using

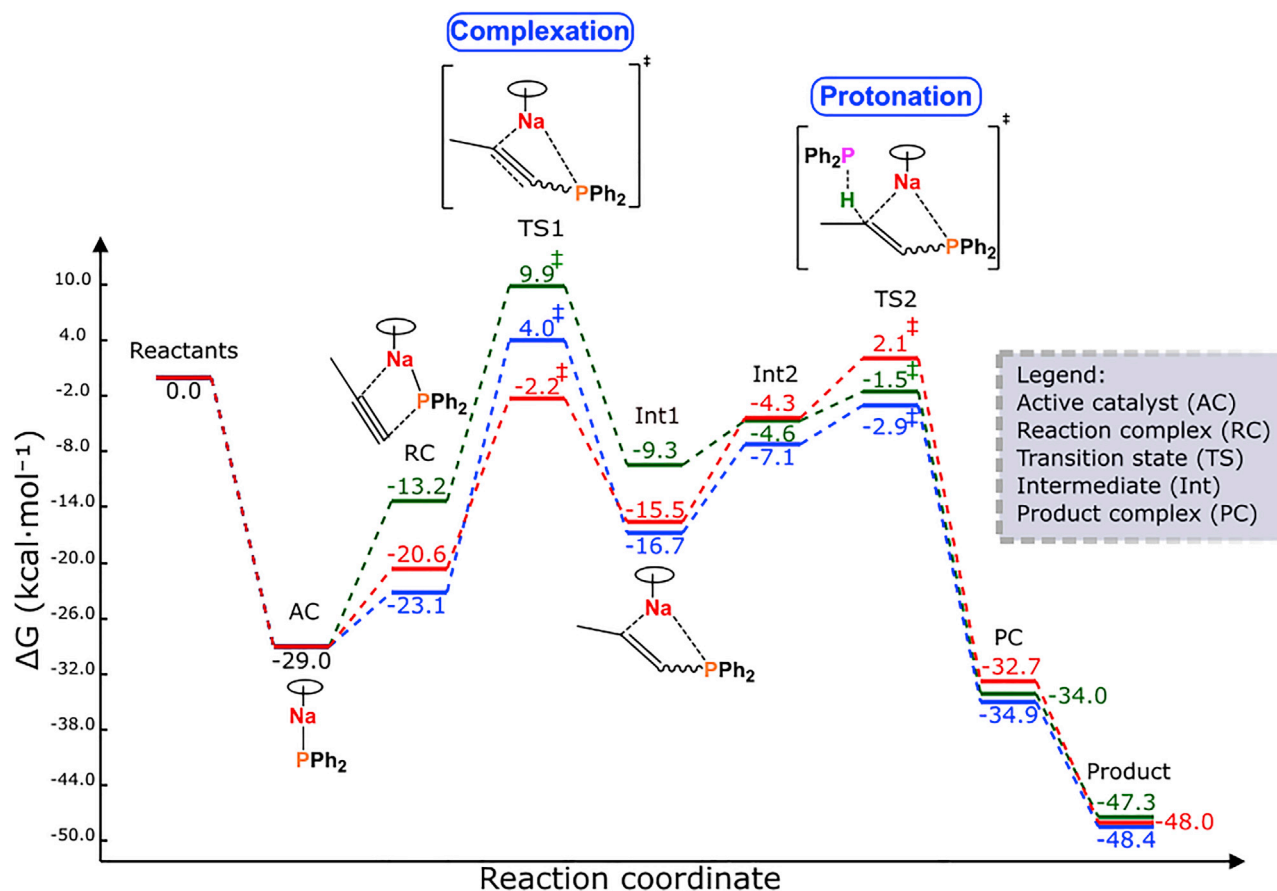


Figure 5. Competitive energy profiles for the formation of the α isomer, E isomer, and Z isomer
 α isomer (green), E isomer (blue), and Z isomer (red).

KO^tBu as the pre-catalyst; this resulted in quantitative conversion of phenylacetylene in 2 h at 110°C (E:Z 35:65) and an 8% conversion of 3-hexyne after 29 h at 110°C . When a catalytic quantity of 18-crown-6 was added to this reaction, a 78% conversion of 3-hexyne was obtained after 47 h at 110°C . While these results do reinforce the conclusion that KO^tBu can be successfully used as a pre-catalyst for the hydrophosphination of alkynes, these preliminary results show that it is not as efficient as compounds 3 and 4 described in this work.

DFT studies

In an attempt to gain insight into the mechanism behind our sodium-catalyzed hydrophosphinations, and the formation of each isomer, we turned our attention to density functional theory (DFT) studies. For calculational simplicity, we employed the diphenylphosphine-analogue of compound 3 as the catalyst in these studies, diphenylphosphine as the phosphorus reagent, and 1-propyne as the benchmark substrate, to investigate the catalytic process, carried out in toluene solvent. All calculations were performed using the Gaussian 16³ program with the M06-L⁴ function and def2tzvp² basis set using an ultrafine integral with the toluene solvent modeled via the CPCM (conductor-like polarizable continuum model) method.⁵⁸ Reaction pathways were confirmed by following the intrinsic reaction coordinates (IRC)^{2,59} in both directions from the optimized transition states; followed by optimization and frequency calculations of the resulting minima to yield reaction complexes and intermediates. Figure 5 shows competitive energy profiles for the α , E, and Z

isomers, from which it can be seen that the Z isomer has a lower initial energy barrier ($\Delta G^* \text{ AC} \rightarrow \text{TS1} = 26.8 \text{ kcal/mol}$) from the active sodium phosphide catalyst (AC), therefore showing it to be the kinetic product consistent with our reasoning from the experimental observations with the E isomer ($\Delta G^* \text{ AC} \rightarrow \text{TS1} = 33.0 \text{ kcal/mol}$) and α -isomer ($\Delta G^* \text{ AC} \rightarrow \text{TS1} = 38.8 \text{ kcal/mol}$) tending toward inaccessible, and indeed the α -isomer is not observed experimentally for this reaction. However, when the first intermediate of the Z isomer is formed (Int1), the relative barrier height for the forward ($\Delta G^* \text{ Int1} \rightarrow \text{TS2} = 17.6 \text{ kcal/mol}$) is higher than the backward reaction ($\Delta G^* \text{ Int1} \rightarrow \text{TS1} = 13.3 \text{ kcal/mol}$) and as such the reverse reaction to form the reaction complex (RC) can provide new starting material for the E isomer, as the energies and molecular orientations of the E/Z RC are similar. This isomerization pathway is also feasible for the E-isomer intermediate; however, it is much less accessible than the Z isomer due to the forward reaction ($\Delta G^* \text{ Int1} \rightarrow \text{TS2} = 13.7 \text{ kcal/mol}$) being favorable for the E isomer over the backward reaction ($\Delta G^* \text{ Int1} \rightarrow \text{TS1} = 20.7 \text{ kcal/mol}$), suggesting that, once the E isomer intermediate is formed via the higher-energy transition state, the reaction continues to form the thermodynamic product. This does not provide an easy route to the α isomer as the energy of that RC is significantly higher and the reactant is orientated differently with respect to the catalyst (visualizations of the 3 RCs are shown in the [supplemental information, Figure S150](#)). The intermediate structure is the only structure that can be isomerized in these systems, as following the second transition state (TS2) the exergonic nature of the reaction shows the protonation step to be irreversible. The E/Z relative energy barriers are achievable at the experimental conditions. Moreover, the subtle variations in the barrier height of the forward and backward barriers for the Z isomer is suggestive of the role that the substituents of the alkyne substrate can play in determining the stereoselectivity. That is, small changes in the substrate can result in significant relative ordering of the forward and backward barrier heights and consequently the ratio of isomers generated. From these computational data, we were able to propose a plausible general mechanism by which this catalytic hydrophosphination proceeds, for the formation of the α , E, and Z isomers. This mechanism of formation of the E and Z isomers is displayed in [Figure 6](#) and the mechanism for the α isomer can be found in [Figure S149](#) of the [supplemental information](#).

The cycle begins with an initial deprotonation step in order to form the AC, followed by coordination of the catalyst to the alkyne substrate, forming the RC. The test reaction with the NBu_4^+ salt as stated above bears testimony to the nature of the RC, where the roles of both the Na^+ and the phosphide anion are important. There is then a complexation step, the rate-determining step, which leads to transition state 1 (TS1). This then undergoes formal insertion, producing an alkene intermediate (Int1) before a second equivalent of phosphine approaches and coordinates to the alkene, resulting in intermediate 2 (Int2). A second complexation step is observed to generate transition state 2 (TS2), which is followed by a formal protonation step to replace the sodium atom with a proton and form the product complex (PC) where the newly regenerated sodium phosphide catalyst is still coordinated to the phosphorus atom of the alkene. Finally, this undergoes a dissociation step to release the product and fully regenerate the catalyst.

To summarize, in this work we have reported the synthesis and structural characterization of four new sodium diphenylphosphide compounds, each existing in a different aggregation state owing to the specific Lewis base donor ligand employed. We then compared and contrasted their ability to act as catalysts for the $\text{Ph}_2\text{P-H}$ hydrophosphination of a range of alkenes and alkynes. It was observed that lowering the aggregation

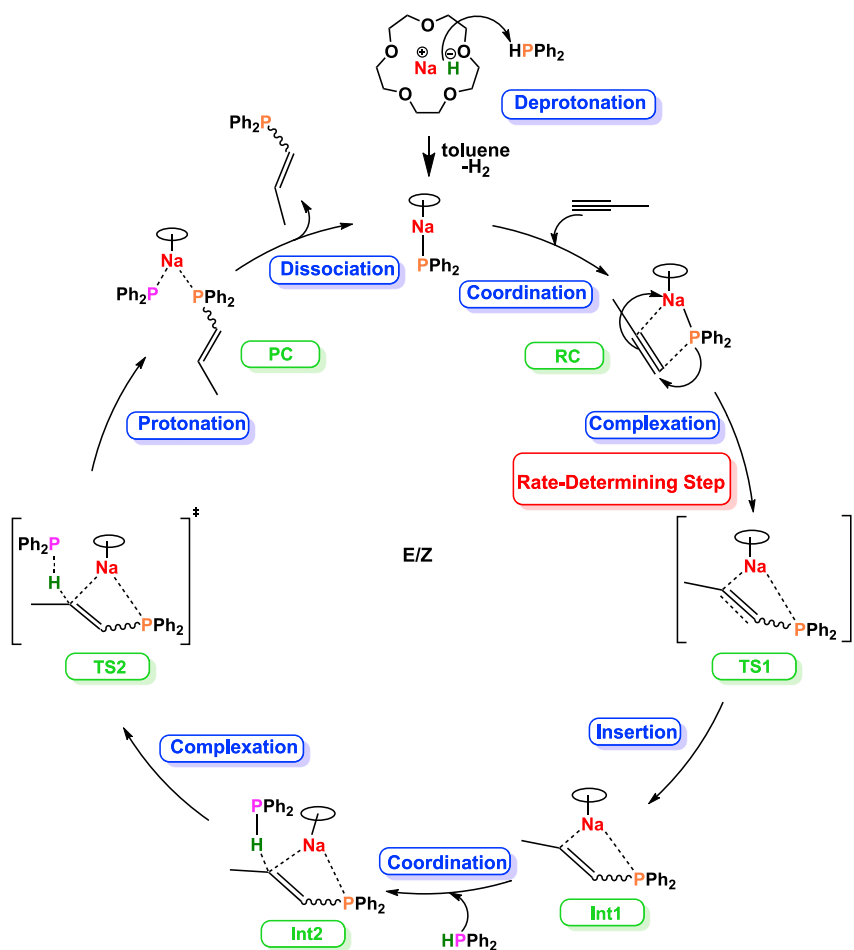


Figure 6. Proposed catalytic cycle for the hydrophosphination of 1-propyne with diphenylphosphine, catalyzed by $\text{Ph}_2\text{PNa} \cdot 15\text{-crown-5}$, in toluene

Note that the mechanisms for formation of both the E and Z isomers differ only in the direction by which the catalyst approaches; therefore, they have been combined into one cycle with a wavy bond to denote the differing stereochemistry.

state of the compounds increases catalytic performance, with the monomeric 15-crown-5 solvate (3) and the charge-separated ion pair, where 2,2,2-cryptand is the donor ligand (4) performing exceptionally well under ambient conditions. We also noted the stereoselectivity for each substrate and attempts thus far to obtain a completely stereoselective process have been unsuccessful. DFT studies have been used to propose possible mechanisms for the hydrophosphination of alkynes that provide insight into the complicated pattern of the E/Z isomer ratios obtained in these catalytic reactions that suggests a high dependency on the particular substrate studied. Collectively, this work advances the development of earth-abundant homogeneous catalysts for fundamentally important chemical transformations, and further work on improving the design of alkali-metal catalysts is ongoing.

EXPERIMENTAL PROCEDURES

Resource availability

Lead contact

Further information and requests for resources should be directed to and will be fulfilled by the lead contact, Robert Mulvey (r.e.mulvey@strath.ac.uk).

Materials availability

Hexane, THF, and toluene were dried by heating to reflux over sodium benzophenone ketyl and then distilled under nitrogen prior to use. D₈-toluene and d₈-THF were degassed by freeze-pump-thaw methods and stored over activated 4 Å molecular sieves prior to use. All reagents were purchased from commercial sources and used as received, unless stated otherwise. PMDETA was distilled and stored over activated 4 Å molecular sieves prior to use. ⁿBuNa was synthesized according to literature procedures and stored as a white powder in the glovebox freezer.⁵²

Data and code availability

Data used within this publication can be accessed at <https://doi.org/10.15129/0498dbe7-f5cc-414b-9a30-cc5208f3527f>. Click or tap if you trust this link: <https://doi.org/10.15129/0498dbe7-f5cc-414b-9a30-cc5208f3527f>.

NMR spectra were recorded on a Bruker AV3 or AV 400 MHz spectrometer operating at 400.03 MHz for ¹H, 100.59 MHz for ¹³C, 376.40 MHz for ¹⁹F, and 161.93 MHz for ³¹P. All ¹³C and ¹⁹F spectra were proton decoupled. ¹H, ¹³C{¹H}, ¹⁹F{¹H}, and ³¹P chemical shifts are expressed in parts per million (δ, ppm) and referenced to residual solvent peaks. HSQC (heteronuclear single quantum coherence) measurements were recorded on an AV 400 MHz spectrometer operating at 400.13 MHz, using the pulse program hsqcedetgp. X-ray data for compound 1 were measured with a Rigaku Synergy-i instrument and for compounds 2–4 were measured with an Oxford Diffraction Gemini S instrument. Data collection and processing used CrysAlisPro software.¹ All structures were solved and then refined to convergence against *F*² using all independent reflections by the full-matrix least-squares method using SHELXL-2018 implemented within WINGX or Olex2.^{2,3,4} Crystals of 1 were cut from fragile thin sheets of material. These were found to shatter at low temperature and so a collection temperature of 230 K was used. Even at this higher temperature, the samples were observed to bend upon mounting. These material properties resulted in non-ideal diffraction behavior and a relatively low-quality final model. This model does, however, confirm the atomic connectivity of this compound. In all structures, non-hydrogen atoms were refined using anisotropic thermal parameters. Two THF ligands of 1 and a C₂H₄ section of the crown ether in 3 were treated as disordered. All of these groups were modeled with atoms split over two sites and with appropriate restraints and constraints applied to ensure normal geometries and displacement behaviors. Selected geometric parameters for 1–4 are given in Tables S1–S4. Selected crystallographic data for all structures are shown in Tables S6 and S7. The TON and TOF values have been determined for selected substrates and have been included in Table S5. Crystallographic data have been deposited in the Cambridge Crystallographic Data Centre (CCDC) under accession numbers: 2124351–2124354. These data can be obtained free of charge from the CCDC at http://www.ccdc.cam.ac.uk/data_request/cif.

Experimental procedures and product characterization

All reactions and manipulations were performed under a protective argon atmosphere using standard glovebox techniques, or under a protective nitrogen atmosphere using standard Schlenk techniques.

Synthesis of [(Ph₂PNa.(THF)₂)]_∞ (1)

To a suspension of ⁿBuNa (0.24 g; 3 mmol) in hexane (10 mL) was added HPPh₂ (0.51 mL; 3 mmol) and this was stirred at room temperature for 1 h. To the resulting bright yellow suspension was added THF (3 mL) while heating the suspension with a heat gun; this resulted in formation of a clear, yellow solution. Once allowed to cool

to room temperature, the solution was stored at -30°C and a crop of yellow needle-like crystals were obtained overnight. These were isolated by filtration (0.602 g; 1.71 mmol; 57% yield). ^1H NMR (400.03 MHz, d_8 -toluene, 300K): δ 1.374 (m, J = 3.20 Hz, 8H, CH_2 of THF); 3.416 (m, J = 6.40 Hz, 8H, CH_2 of THF); 6.786 (t, J = 7.16 Hz, 4H, CH of phenyl groups); 6.956 (m, J = 7.44, 4H, CH of phenyl groups); 7.603 (t, J = 7.13 Hz, 2H, p -CH of phenyl groups) ppm. ^{31}P NMR (161.93 MHz, d_8 -toluene, 300K): δ -36.09 (s) ppm. $^{13}\text{C}\{^1\text{H}\}$ NMR (100.59 MHz, d_8 -toluene, 300K): δ 25.73 (s, CH_2 of THF); 67.83 (s, CH_2 of THF); 122.20 (s, CH of phenyl groups); 128.45 (s, CH of phenyl groups); 131.36 (s, CH of phenyl groups); 131.52 (s, C of phenyl groups) ppm. Elemental analysis (CHN): expected value C = 68.18, H = 7.39, N = 0.00; found C = 66.10, H = 6.77, N = 0.00.

Synthesis of $[(\text{Ph}_2\text{PNa.PMDETA})_2]$ (2)

To a suspension of NaO^tBu (0.48 g; 5 mmol) in hexane (20 mL) was added 3.125 mL of $^n\text{BuLi}$ solution (1.6 M solution in hexane; 5 mmol) and this was stirred at room temperature for 2 h. To the resulting white suspension was added HPPH_2 (0.85 mL; 5 mmol), which immediately formed a yellow suspension and was stirred at room temperature for a further hour before PMDETA (1.05 mL; 5 mmol) was added and the yellow solution stored at -30°C overnight. The yellow amorphous solid, which was found to be impure by NMR, was filtered and resuspended in toluene (30 mL). To this yellow suspension was added a further 1.05 mL of PMDETA (5 mmol) and the suspension was heated to reflux temperature for 3 h, resulting in the formation of an orange solution. The solution was allowed to slowly cool to room temperature and a crop of yellow block crystals were obtained. These were isolated by filtration (1.5004 g; 3.94 mmol; 79% yield). ^1H NMR (400.03 MHz, d_8 -toluene, 300K): δ 2.043 (s, 23H, all proton resonances for PMDETA); 6.833 (t, J = 7.23 Hz, 2H, p -CH of phenyl groups); 7.124 (t, J = 7.61 Hz, 4H, CH of phenyl groups); 7.898 (t, J = 6.42 Hz, 4H, CH of phenyl groups) ppm. ^{31}P NMR (161.93 MHz, d_8 -toluene, 300K): δ -21.11 (s) ppm. $^{13}\text{C}\{^1\text{H}\}$ NMR (100.59 MHz, d_8 -toluene, 300K): δ 43.28 (s, CH_3 of PMDETA); 45.67 (s, CH_3 of PMDETA); 57.95 (s, CH_2 of PMDETA); 58.02 (s, CH_2 of PMDETA); 120.52 (s, CH of phenyl groups); 128.26 (s, CH of phenyl groups); 130.47 (s, CH of phenyl groups); 130.63 (s, C of phenyl groups) ppm. Elemental analysis (CHN): expected value C = 66.14, H = 8.66, N = 11.02; found C = 64.48, H = 8.79, N = 10.77.

Synthesis of $[(\text{Ph}_2\text{PNa.15-crown-5})]$ (3)

To a suspension of $^n\text{BuNa}$ (0.4 g; 5 mmol) in hexane (10 mL) was added HPPH_2 (0.85 mL; 5 mmol) and this was stirred at room temperature for 1 h. To the yellow suspension was added 15-crown-5 (0.98 mL; 5 mmol) resulting in a red/orange suspension, which was allowed to stir at room temperature for a further hour before THF (2–3 mL) was added along with heating with a heat gun to form a clear red solution. This was stored at -30°C and a crop of red block crystals were obtained overnight; these were isolated by filtration (0.8254 g; 1.93 mmol; 39% yield). ^1H NMR (400.03 MHz, d_8 -toluene, 300K): δ 3.355 (s, 20H, CH_2 of 15-crown-5); 6.995 (m, 4H, CH of phenyl groups); 7.276 (m, 4H, CH of phenyl groups); 8.010 (m, 2H, p -CH of phenyl groups) ppm. ^{31}P NMR (161.93 MHz, d_8 -toluene, 300K): δ -17.62 (s) ppm. $^{13}\text{C}\{^1\text{H}\}$ NMR (100.59 MHz, d_8 -toluene, 300K): δ 70.61 (s, CH_2 of 15-crown-5); 127.46 (s, CH of phenyl groups); 128.49 (s, CH of phenyl groups); 134.35 (s, CH of phenyl groups); 137.20 (s, C of phenyl groups) ppm. Elemental analysis (CHN): expected value C = 61.68, H = 7.01, N = 0.00; found C = 59.58, H = 7.16, N = 0.00.

Synthesis of $[(\text{PPh}_2)^-(\text{Na.2,2,2-cryptand})^+]$ (4)

To a suspension of $^n\text{BuNa}$ (0.16 g; 2 mmol) in hexane (10 mL) was added HPPH_2 (0.34 mL; 2 mmol) and this was stirred at room temperature for 1 h. To the yellow

suspension was added 2,2,2-cryptand (0.752 g; 2 mmol) and this formed a red suspension, which was allowed to stir for a further hour at room temperature before THF (5 mL) was added with heating from a heat gun, resulting in formation of a red solution. This was allowed to cool to room temperature and, once cool, a crop of red needle-like crystals were obtained. These were isolated by filtration (0.2519 g; 0.43 mmol; 21.5% yield). ^1H NMR (400.03 MHz, d_8 -toluene, 300K): δ 2.468 (t, J = 4.48 Hz, 12H, CH_2 of cryptand); 3.442 (t, J = 5.11 Hz, 12H, CH_2 of cryptand); 3.606 (s, 12H, CH_2 of cryptand); 6.715 (t, J = 6.97 Hz, 2H, CH of phenyl groups); 6.967 (m, 4H, CH of phenyl groups); 7.905 (t, J = 5.84 Hz, 4H, CH of phenyl groups) ppm. ^{31}P NMR (161.93 MHz, d_8 -toluene, 300K): δ 2.25 (s) ppm. $^{13}\text{C}\{^1\text{H}\}$ NMR (100.59 MHz, d_8 -toluene, 300K): δ 57.14 (s, CH_2 of cryptand); 70.39 (s, CH_2 of cryptand); 71.40 (s, CH_2 of cryptand); 116.75 (s, CH of phenyl groups); 127.24 (s, CH of phenyl groups); 128.49 (s, CH of phenyl groups); 137.73 (s, C of phenyl groups) ppm. Elemental analysis (CHN) was not possible due to the instability of this compound.

General catalytic procedure

A 10 mol % loading of the desired catalyst (1–4) was added to 0.5 mL of d_8 -toluene solution containing adamantane as an internal standard (0.05 mmol; 0.007 g), the substrate precursor (0.6 mmol), and HPPH_2 (0.5 mmol; 0.085 mL). This reaction mixture was contained in a sealed J. Young's tap NMR tube and the reaction was regularly monitored by ^1H and ^{31}P NMR until complete consumption of the HPPH_2 had occurred, determined by integration against the adamantane standard. Using catalysts 1 and 2, the reactions were all carried out at 110°C unless otherwise specified. Reactions using catalysts 3 and 4 were carried out at room temperature unless otherwise specified. For isomerization studies by temperature, the reaction mixture was monitored by ^1H and ^{31}P NMR at room temperature for 30 min before being heated to 110°C for 1 h and measured again. For the low-temperature study, the catalyst was added to the NMR tube at -20°C and monitored by ^1H and ^{31}P NMR at this temperature before being allowed to warm up to room temperature. For isomerization studies by amine additive, a stoichiometric quantity of either *N*-methylaniline (0.055 mL; 0.5 mmol) or *n*-butylamine (0.05 mL; 0.5 mmol) was added to the mixture before addition of the catalyst. These reactions were all carried out in d_8 -THF, unless otherwise specified, and at room temperature.

SUPPLEMENTAL INFORMATION

Supplemental information can be found online at <https://doi.org/10.1016/j.xcrp.2022.100942>.

ACKNOWLEDGMENTS

We wish to express our gratitude to the Leverhulme Trust for generous funding (grant award RPG-2019-264) and the University of Strathclyde for an REA (research excellence award) studentship to M.T.W. Computational results were obtained using the Engineering and Physical Sciences Research Council (EPSRC)-funded ARCHIE-WeSt High Performance Computer (www.archie-west.ac.uk; EPSRC grant no. EP/K000586/1). Professor Eva Hevia (University of Bern) is thanked for her insightful comments at the manuscript preparation stage. We also wish to thank London Metropolitan University for carrying out the elemental analyses.

AUTHOR CONTRIBUTIONS

M.T.W. conducted the bulk of experimental work, formal analysis, validation, and writing. A.R.K. conducted formal analysis. S.B. conducted experimental work and formal analysis. A.v.T. conducted computational analysis and DFT studies. T.T.

conducted writing, review and editing, supervision, and computational analysis. R.E.M. conducted writing, review and editing, supervision, project conception, and administration.

DECLARATION OF INTERESTS

The authors declare no competing interests.

Received: December 9, 2021

Revised: May 6, 2022

Accepted: May 25, 2022

Published: June 21, 2022

REFERENCES

- Al-Shboul, T.M.A., Görls, H., Görls, H., and Westerhausen, M. (2008). Calcium-mediated hydrophosphination of diphenylethyne and diphenylbutadiene as well as crystal structure of 1, 4-diphenyl-1, 4-bis(diphenylphosphanyl) buta-1, 3-diene. *Inorg. Chem. Commun.* 11, 1419–1421. <https://doi.org/10.1016/j.inoche.2008.09.019>.
- Weigend, F., and Ahlrichs, R. (2005). Balanced basis sets of split valence, triple zeta valence and quadruple zeta valence quality for H to Rn: design and assessment of accuracy. *Phys. Chem. Chem. Phys.* 7, 3297. <https://doi.org/10.1039/b508541a>.
- Frisch, M.J., Trucks, G.W., Schlegel, H.B., Scuseria, G.E., Robb, M.A., Cheeseman, J.R., Scalmani, G., Barone, V., Petersson, G.A., Nakatsuji, H., et al. (2016). *Gaussian 16* (Wallingford, CT: Gaussian, Inc).
- Zhao, Y., and Truhlar, D.G. (2006). A new local density functional for main-group thermochemistry, transition metal bonding, thermochemical kinetics, and noncovalent interactions. *J. Chem. Phys.* 125, 194101. <https://doi.org/10.1063/1.2370993>.
- Dillon, K.B., Mathey, F., and Nixon, J.F. (1998). *Phosphorus: The Carbon Copy* (John Wiley and Sons).
- Nazarov, A.A., and Dyson, P.J. (2011). Metal phosphorus complexes as antitumor agents. In *Phosphorus Compounds: Advanced Tools in Catalysis and Material Sciences*, L.G.M. Peruzzini, ed. (Springer), pp. 445–462.
- Wendels, S., Chavez, T., Bonnet, M., Salmeia, K.A., and Gaan, S. (2017). Recent developments in organophosphorus flame retardants containing P-C bond and their applications. *Materials* 10, 784. <https://doi.org/10.3390/ma10070784>.
- Pringle, P.G., and Smith, M.B. (1990). Platinum(0)-Catalysed hydrophosphination of acrylonitrile. *J. Chem. Soc.* 23, 1701. <https://doi.org/10.1039/c39900001701>.
- Takaki, K., Komeyama, K., Kobayashi, D., Kawabata, T., and Takehira, K. (2006). Hydrophosphination of alkynes and related reactions catalyzed by rare-earth amides. *J. Alloys Compd.* 408–412, 432–436. <https://doi.org/10.1016/j.jallcom.2004.11.088>.
- Kamitani, M., Itazaki, M., Tamiya, C., and Nakazawa, H. (2012). Regioselective double hydrophosphination of terminal arylacetylenes catalyzed by an iron complex. *J. Am. Chem. Soc.* 134, 11932–11935. <https://doi.org/10.1021/ja304818c>.
- Rosenberg, L. (2013). Mechanisms of metal-catalyzed hydrophosphination of alkenes and alkynes. *ACS Catal.* 3, 2845–2855. <https://doi.org/10.1021/cs400685c>.
- Ghebreab, M.B., Bange, C.A., and Waterman, R. (2014). Intermolecular zirconium-catalyzed hydrophosphination of alkenes and dienes with primary phosphines. *J. Am. Chem. Soc.* 136, 9240–9243. <https://doi.org/10.1021/ja503036z>.
- Bange, C.A., and Waterman, R. (2016). Challenges in catalytic hydrophosphination. *Chem. Eur J.* 22, 12598–12605. <https://doi.org/10.1002/chem.201602749>.
- Pullarkat, S.A. (2015). Recent progress in palladium-catalyzed asymmetric hydrophosphination. *Synthesis* 48, 493–503. <https://doi.org/10.1055/s-0035-1560556>.
- Cristina Silva Costa, D. (2020). Additions to non-activated alkenes: recent advances. *Arab. J. Chem.* 13, 799–834. <https://doi.org/10.1016/j.arabjc.2017.07.017>.
- Glueck, D.S. (2020). Metal-catalyzed P-C bond formation via P-H oxidative addition: fundamentals and recent advances. *J. Org. Chem.* 85, 14276–14285. <https://doi.org/10.1021/acs.joc.0c00667>.
- Hirano, K., and Miura, M. (2017). Recent advances in diphosphination of alkynes and alkenes. *Tetrahedron. Lett.* 58, 4317–4322. <https://doi.org/10.1016/j.tetlet.2017.10.018>.
- Zang, B., Ma, X., Yan, B., Ni, C., Yu, H., Yang, Z., and Roesky, H.W. (2021). An efficient catalytic method for the hydrophosphination of heterocumulenes with diethylzinc as precatalyst without a solvent. *Dalton Trans.* 50, 15488–15492.
- Bissessar, D., Egly, J., Achard, T., Steffanut, P., and Bellemin-Lapponnaz, S. (2019). Catalyst-free hydrophosphination of alkenes in presence of 2-methyltetrahydrofuran: a green and easy access to a wide range of tertiary phosphines. *RSC Adv.* 9, 27250–27256. <https://doi.org/10.1039/c9ra04896k>.
- Moglie, Y., González-Soria, M.J., Martín-García, I., Radivoy, G., and Alonso, F. (2016). Catalyst- and solvent-free hydrophosphination and multicomponent hydrothiophosphination of alkenes and alkynes. *Green Chem.* 18, 4896–4907. <https://doi.org/10.1039/c6gc00903d>.
- Crimmin, M.R., Barrett, A.G.M., Hill, M.S., Hitchcock, P.B., and Procopiou, P.A. (2007). Calcium-catalyzed intermolecular hydrophosphination. *Organometallics* 26, 2953–2956. <https://doi.org/10.1021/om070200k>.
- Sarazin, Y., and Carpentier, J.F. (2020). Molecular s-block catalysts for alkene hydrophosphination and related reactions. In *Early Main Group Metal Catalysis: Concepts and Reactions*, S. Harder, ed. (Wiley-VCH), pp. 93–121.
- Kriek, S., and Westerhausen, M. (2020). H-N and H-P bond addition to alkynes and heterocumulenes. In *Early Main Group Metal Catalysis: Concepts and Reactions*, S. Harder, ed. (Wiley-VCH), pp. 123–149.
- Barrett, A.N., Sanderson, H.J., Mahon, M.F., and Webster, R.L. (2020). Hydrophosphination using [GeCl{N(SiMe₃)₂}₃] as a pre-catalyst. *Chem. Commun.* 56, 13623–13626. <https://doi.org/10.1039/d0cc05792d>.
- Pollard, V.A., Young, A., McLellan, R., Kennedy, A.R., Tuttle, T., and Mulvey, R.E. (2019). Lithium aluminate-catalyzed hydrophosphination applications. *Angew. Chem. Int. Ed.* 131, 12419–12424. <https://doi.org/10.1002/ange.201906807>.
- Wanklyn, J.A. (1858). On some new Ethyl-compounds containing the Alkali-metals. *Proc. R. Soc.* 9, 341–345.
- Schlenk, W., and Holtz, J. (1917). Über die einfachsten metallorganischen Alkaliverbindungen. *Ber. Dtsch. Chem. Ges.* 50, 262–274. <https://doi.org/10.1002/cber.19170500142>.
- Robertson, S.D., Uzelac, M., and Mulvey, R.E. (2019). Alkali-metal-mediated synergistic effects in polar main group organometallic chemistry. *Chem. Rev.* 119, 8332–8405. <https://doi.org/10.1021/acs.chemrev.9b00047>.
- Gentner, T.X., and Mulvey, R.E. (2020). Alkali-metal mediation: diversity of applications in main-group organometallic chemistry. *Angew. Chem. Int. Ed.* 60, 9247–9262. <https://doi.org/10.1002/anie.202010963>.

30. Asako, S., Nakajima, H., and Takai, K. (2019). Organosodium compounds for catalytic cross-coupling. *Nature Catalysis* 2, 297–303. <https://doi.org/10.1038/s41929-019-0250-6>.
31. Weiss, E. (1993). Structures of organo alkali metal complexes and related compounds. *Angew. Chem.* 32, 1501–1523. <https://doi.org/10.1002/anie.199315013>.
32. Ruhlandt-Senge, K., Henderson, K.W., and Andrews, P.C. (2007). Alkali metal organometallics - structure and bonding. In *Comprehensive Organometallic Chemistry III*, R.H.C.D.M.P. Mingos, ed. (Elsevier), pp. 1–65.
33. Harvey, M.J. (2014). Alkali-metals: organometallic chemistry. In *Encyclopedia of Inorganic and Bioinorganic Chemistry*, R.A. Scott, ed. (John Wiley & Sons Ltd.), pp. 1–13.
34. Smith, J.D. (1999). Organometallic compounds of the heavier alkali metals. *Adv. Organomet. Chem.* 43, 267–343.
35. Aguiar, A.M., and Archibald, T.G. (1966). The stereospecific addition of organophosphides to terminal alkynes. *Tetrahedron Lett.* 7, 5471–5475. [https://doi.org/10.1016/s0040-4039\(00\)70125-0](https://doi.org/10.1016/s0040-4039(00)70125-0).
36. Issleib, K., Böhme, H., and Rockstroh, C. (1970). Alkali-Phosphorverbindungen und ihr reaktives Verhalten. LXIV [1]. Zur Umsetzung von Alkali-phenylphosphid mit Phenylacetylen. *J. Prakt. Chem.* 312, 571–577. <https://doi.org/10.1002/prac.19703120405>.
37. Bookham, J.L., McFarlane, W., Thornton-Pett, M., and Jones, S. (1990). Stereoselective addition reactions of diphenylphosphine: meso- and rac-1, 2-diphenyl-1, 2-bis(diphenylphosphino)ethane and their group 6 metal tetracarbonyl complexes. Crystal structures of the molybdenum derivatives. *J. Chem. Soc. Dalton Trans.* 3621. <https://doi.org/10.1039/dt9900003621>.
38. Bookham, J.L., Smithies, D.M., Wright, A., Thornton-Pett, M., and McFarlane, W. (1998). Stereoselective addition of diphenylphosphine to substituted diphenylethyne: synthetic, NMR and X-ray crystallographic studies. *J. Chem. Soc. Dalton Trans.* 811–818. <https://doi.org/10.1039/a707210d>.
39. Bunlaksananusorn, T., and Knochel, P. (2002). t-BuOK-Catalyzed addition phosphines to functionalized alkenes: a convenient synthesis of polyfunctional phosphine derivatives. *Tetrahedron Lett.* 43, 5817–5819. [https://doi.org/10.1016/s0040-4039\(02\)01177-2](https://doi.org/10.1016/s0040-4039(02)01177-2).
40. Wu, L., Annibale, V.T., Jiao, H., Brookfield, A., Collison, D., and Manners, I. (2019). Homo- and heterodehydrocoupling of phosphines mediated by alkali-metal catalysts. *Nat. Commun.* 10, 2786. <https://doi.org/10.1038/s41467-019-09832-4>.
41. Coles, N.T., Mahon, M.F., and Webster, R.L. (2018). 1, 1-diphosphines and divinylphosphines via base-catalyzed hydrophosphination. *Chem. Commun.* 54, 10443–10446. <https://doi.org/10.1039/c8cc05890c>.
42. Gissot, A., Becht, J.-M., Desmurs, J.R., Pévère, V., Wagner, A., and Mioskowski, C. (2002). Directed ortho-metalation, a new insight into organosodium chemistry. *Angew. Chem.* 41, 340–343. [https://doi.org/10.1002/1521-3773\(2002118\)41:2<340::aid-anie340>3.0.co;2-d](https://doi.org/10.1002/1521-3773(2002118)41:2<340::aid-anie340>3.0.co;2-d).
43. Ma, Y., Algera, R.F., and Collum, D.B. (2016). Sodium diisopropylamide in N, N-dimethylethylamine: reactivity, selectivity and synthetic utility. *J. Org. Chem.* 81, 11312–11315. <https://doi.org/10.1021/acs.joc.6b02287>.
44. Huang, Y., Chan, G.H., and Chiba, S. (2017). Amide-directed C-H sodiation by a sodium hydride/iodide composite. *Angew. Chem. Int. Ed.* 129, 6644–6647. <https://doi.org/10.1002/ange.201702512>.
45. Weidmann, N., Ketels, M., and Knochel, P. (2018). Sodiation of arenes and heteroarenes in continuous flow. *Angew. Chem. Int. Ed.* 57, 10748–10751. <https://doi.org/10.1002/anie.201803961>.
46. Nozawa-Kumada, K., Iwakawa, Y., Onuma, S., Shigeno, M., and Kondo, Y. (2020). NaH-mediated direct C-H arylation in the presence of 1, 10-phenanthroline. *Chem. Commun.* 56, 7773–7776. <https://doi.org/10.1039/d0cc00730g>.
47. Kim, H., Lee, J.H., Hwang, H., and An, D.K. (2020). Quantitative NaH catalytic hydroboration of aldimines. *New J. Chem.* 44, 11330–11335. <https://doi.org/10.1039/d0nj01423k>.
48. Izod, K., Evans, P., and Waddell, P.G. (2017). Desolvation and aggregation of sterically demanding alkali metal diarylphosphides. *Dalton Trans.* 46, 13824–13834. <https://doi.org/10.1039/c7dt02238g>.
49. Izod, K., Liddle, S.T., Clegg, W., and Harrington, R.W. (2006). Amino-functionalised diarylphosphide complexes of the alkali metals and lanthanum. *Dalton Trans.* 3431–3437. <https://doi.org/10.1039/b601938b>.
50. Ye, J., Zhang, J.Q., Saga, Y., Onozawa, S.Y., Kobayashi, S., Sato, K., Fukaya, N., and Han, L.B. (2020). Ready approach to organophosphines from ArCl via selective cleavage of C–P bonds by sodium. *Organometallics* 39, 2682–2694. <https://doi.org/10.1021/acs.organomet.0c00295>.
51. Asako, S., Takahashi, I., Nakajima, H., Ilies, L., and Takai, K. (2021). Halogen–sodium exchange enables efficient access to organosodium compounds. *Commun. Chem.* 4, 76. <https://doi.org/10.1038/s42004-021-00513-2>.
52. Schade, C., Bauer, W., and Von Ragué Schleyer, P. (1985). n-Butylsodium: the preparation, properties and NMR spectra of a hydrocarbon- and tetrahydrofuran-soluble reagent. *J. Org. Chem.* 295, c25–c28. [https://doi.org/10.1016/0022-328x\(85\)80326-0](https://doi.org/10.1016/0022-328x(85)80326-0).
53. Allen, F.H. (2002). The Cambridge Structural Database: a quarter of a million crystal structures and rising. *Acta Crystallogr.* 58, 380–388. <https://doi.org/10.1107/s0108768102003890>.
54. Ellermann, J., Schütz, M., Heinemann, F.W., and Moll, M. (1998). Synthesis and Crystal Structure of N, N, N', N', N"-pentamethyl-diethylene-triamine-cocordinated Sodium bis(diphenylphosphanyl) amide and a 12-crown-4 derivative. *Z. Anorg. Allg. Chem.* 624, 257–262. [https://doi.org/10.1002/\(sici\)1521-3749\(199802\)624:2<257::aid-zaac257>3.0.co;2-0](https://doi.org/10.1002/(sici)1521-3749(199802)624:2<257::aid-zaac257>3.0.co;2-0).
55. Hsu, Y.-L., and Liang, L.-C. (2010). Alkali metal complexes of a tert-butylphosphine-bridged biphenolate ligand. *Organ* 29, 6201–6208. <https://doi.org/10.1021/om100495e>.
56. Troxler, L., and Wipff, G. (1994). Conformation and dynamics of 18-crown-6, cryptand 222, and their cation complexes in acetonitrile studied by molecular dynamics simulations. *J. Am. Chem. Soc.* 116, 1468–1480. <https://doi.org/10.1021/ja00083a036>.
57. Basiouny, M.M.I., Dollard, D.A., and Schmidt, J.A.R. (2019). Regioselective single and double hydrophosphination and hydrophosphinylation of unactivated alkynes. *ACS Catal.* 9, 7143–7153. <https://doi.org/10.1021/acscatal.9b01538>.
58. Barone, V., and Cossi, M. (1998). Quantum calculation of molecular energies and energy gradients in solution by a conductor solvent model. *J. Phys. Chem.* 102, 1995–2001. <https://doi.org/10.1021/jp9716997>.
59. Fukui, K. (1981). The path of chemical reactions - the IRC approach. *Acc. Chem. Res.* 14, 363–368. <https://doi.org/10.1021/ar00072a001>.

Cell Reports Physical Science, Volume 3

Supplemental information

**Catalytic hydrophosphination of alkynes using
structurally diverse sodium diphenylphosphide
donor complexes**

Michael T. Whitelaw, Sumanta Banerjee, Alan R. Kennedy, Alexander van Teijlingen, Tell Tuttle, and Robert E. Mulvey

Contents

Characterisation of Compounds

NMR of $[(\text{Ph}_2\text{PNa} \cdot (\text{THF})_2)_\infty]$, **1**

NMR of $[(\text{Ph}_2\text{PNa} \cdot \text{PMDETA})_2]$, **2**

NMR of $[\text{Ph}_2\text{PNa} \cdot 15\text{-crown-5}]$, **3**

NMR of $[(\text{Ph}_2\text{P})^- (\text{Na} \cdot 2,2,2\text{-cryptand})^+]$, **4**

Hydrophosphination Using **1** as a Catalyst

Hydrophosphination Using **2** as a Catalyst

Hydrophosphination Using **3** as a Catalyst

Hydrophosphination Using **4** as a Catalyst

Stereoselectivity Study with Temperature

Stereoselectivity Study with Amine Additives

Isolation of Hydrophosphination Products

Computational Data

X-Ray Crystallographic Parameters for **1-4**

Table S1. Selected bond lengths (Å) of compounds **1 – 3**

Table S2. Selected bond angles (°) of compounds **1 – 3**

Table S3. Key bond lengths (Å) for compound **4**

Table S4. Key bond angles (°) for compound **4**

Table S5. Turnover number (TON) and Turnover frequency (TOF) of selected substrates using **3** as catalyst

Table S6: Selected Crystal Structure Data and Refinement Details for Compounds **1** and **2**

Table S7: Selected Crystal Structure Data and Refinement Details for Compounds **3** and **4**

Characterisation of Compounds
NMR of $[(\text{Ph}_2\text{PNa} \cdot (\text{THF})_2)_\infty]$, **1**

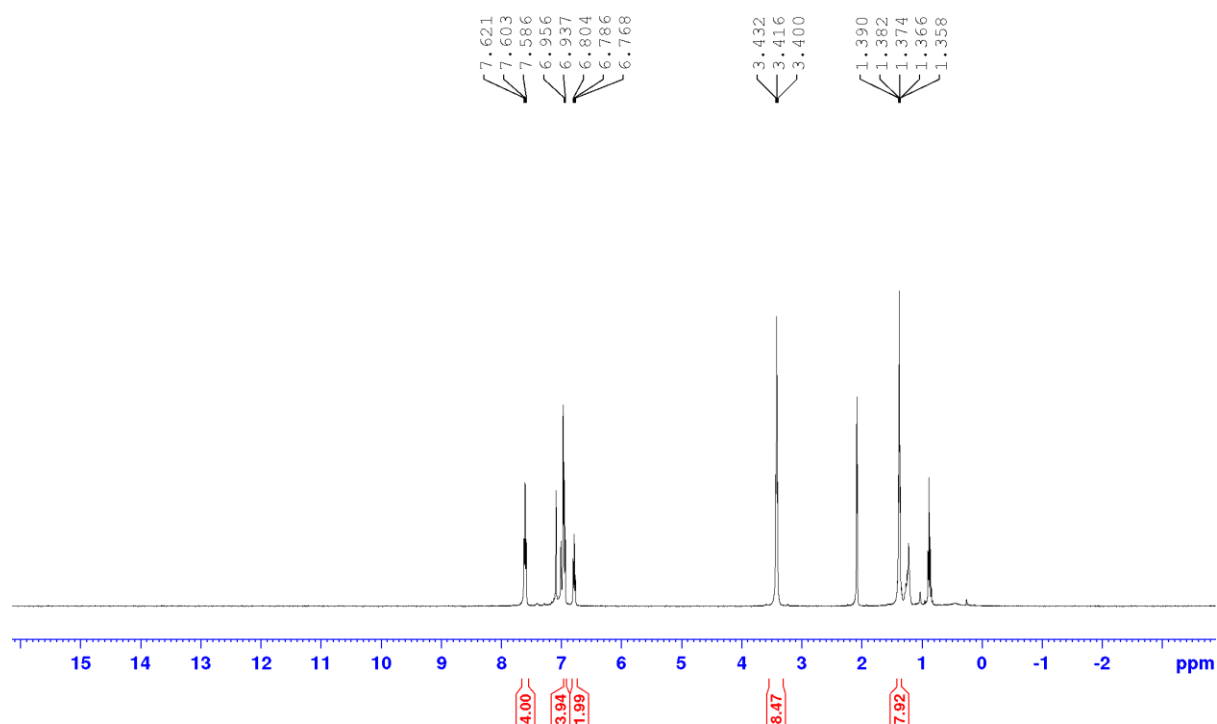


Figure S1: ^1H NMR spectrum of $[(\text{Ph}_2\text{PNa} \cdot (\text{THF})_2)_\infty]$, **1**, in d_8 -toluene.

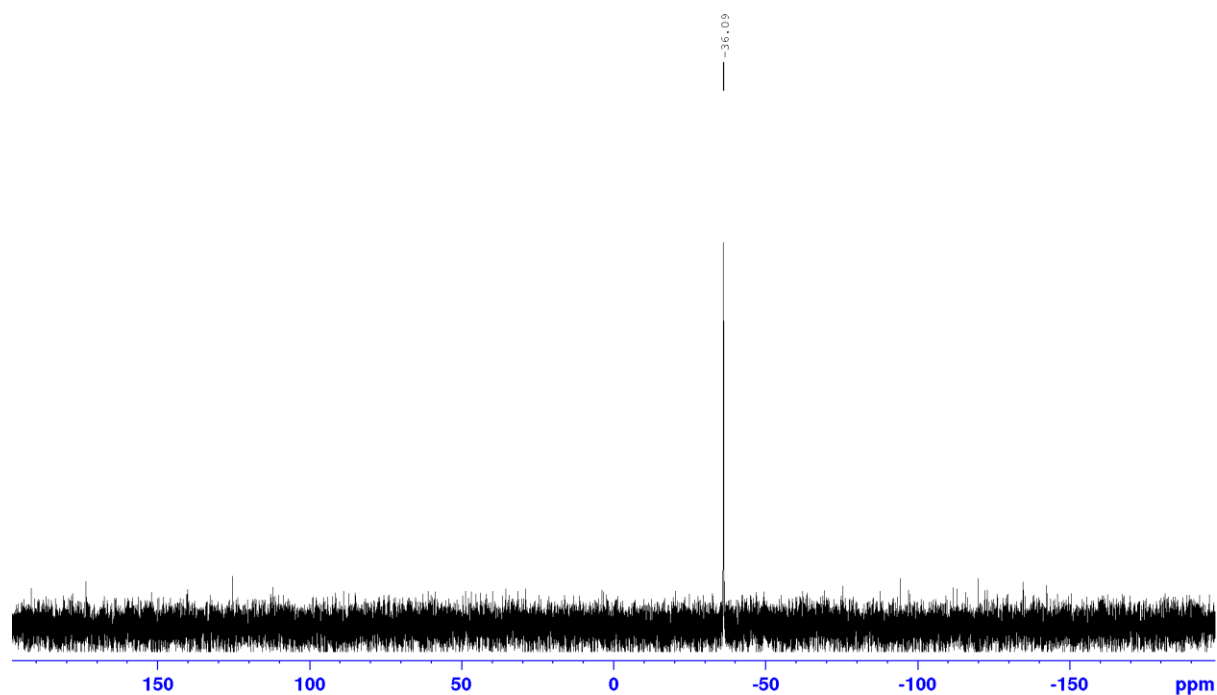


Figure S2: ^{31}P NMR spectrum of $[(\text{Ph}_2\text{PNa} \cdot (\text{THF})_2)_\infty]$, **1**, in d_8 -toluene.

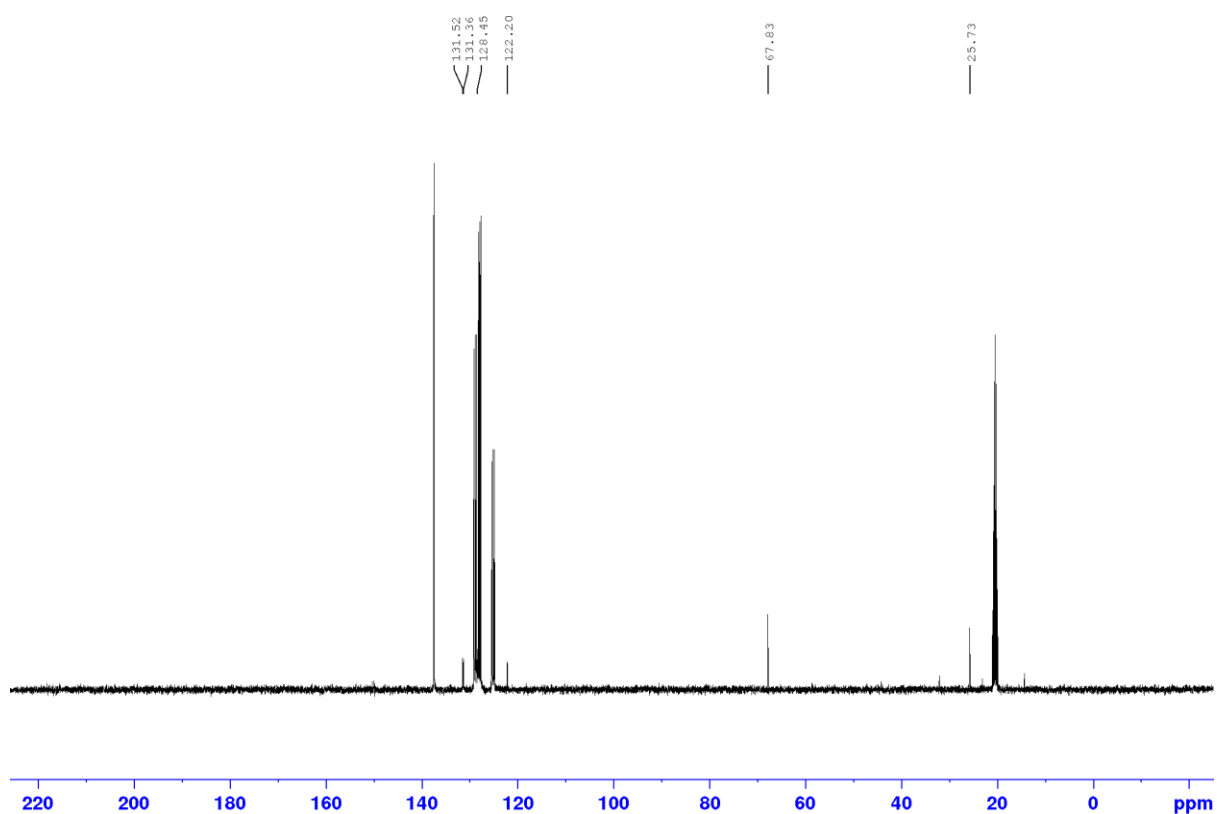


Figure S3: $^{13}\text{C}\{^1\text{H}\}$ NMR spectrum of $[(\text{Ph}_2\text{PNa} \cdot (\text{THF})_2)_\infty]$, **1**, in d_8 -toluene.

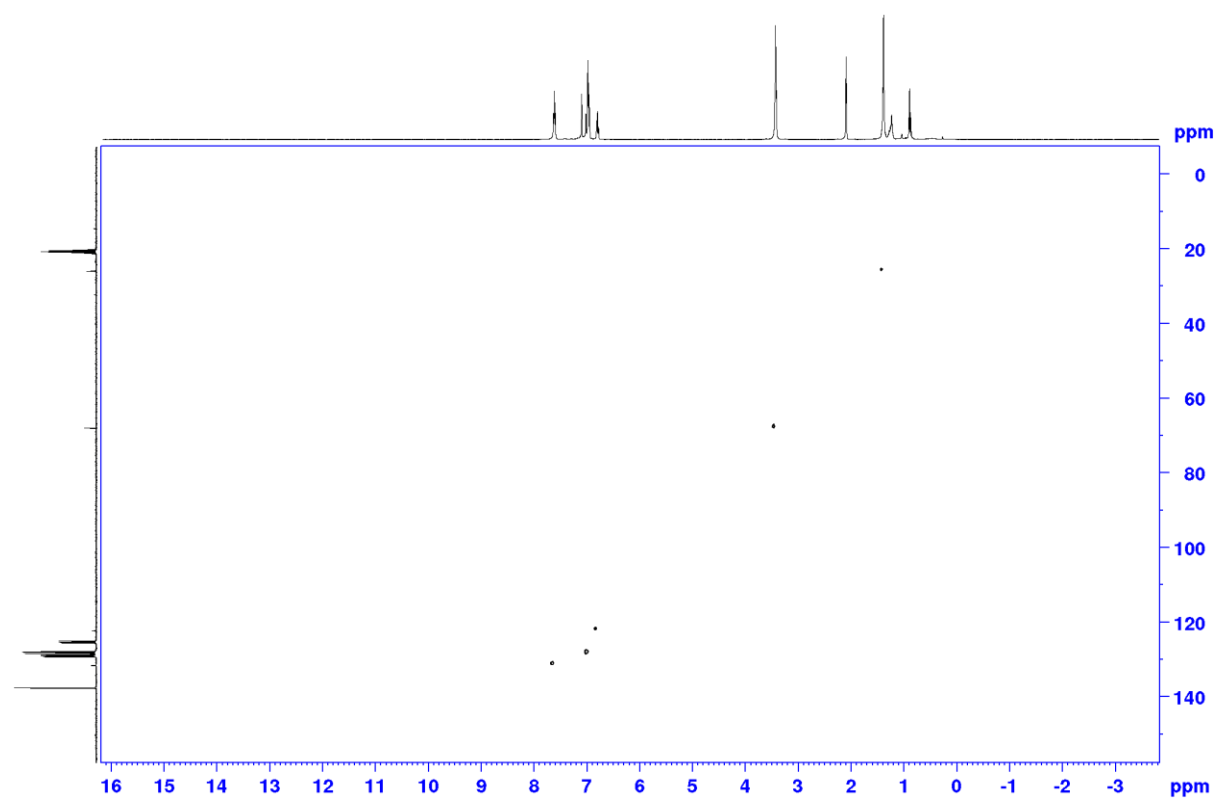


Figure S4: HSQC NMR spectrum of $[(\text{Ph}_2\text{PNa} \cdot (\text{THF})_2)_\infty]$, **1**, in d_8 -toluene.

NMR of $[(\text{Ph}_2\text{PNa.PMDETA})_2]$, **2**

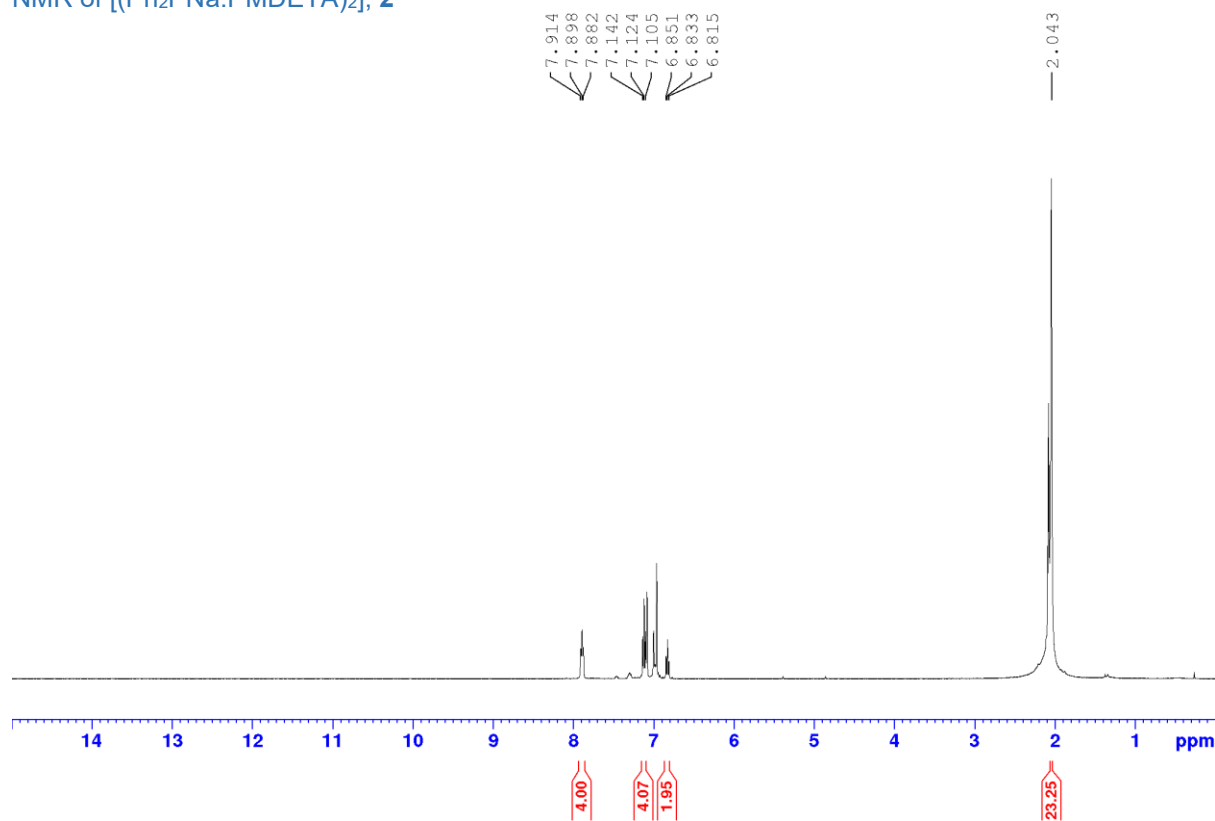


Figure S5: ^1H NMR spectrum of $[(\text{Ph}_2\text{PNa.PMDETA})_2]$, **2**, in d_8 -toluene.

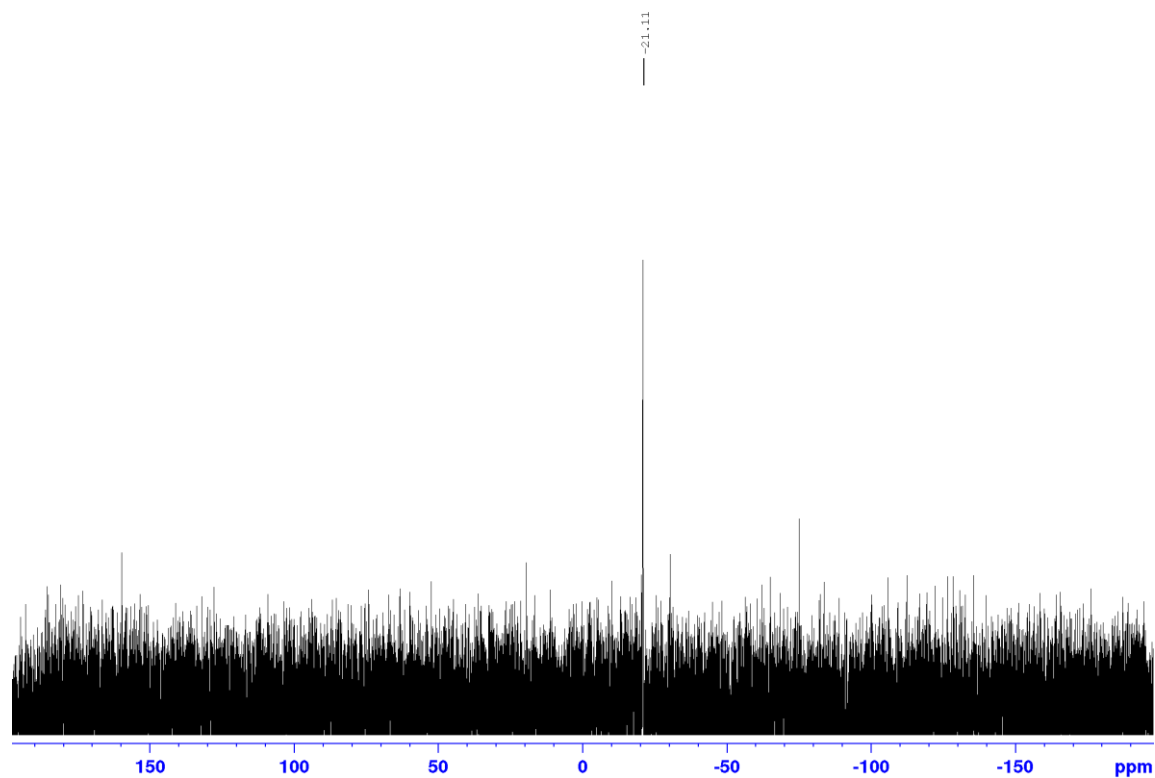


Figure S6: ^{31}P NMR spectrum of $[(\text{Ph}_2\text{PNa.PMDETA})_2]$, **2**, in d_8 -toluene.

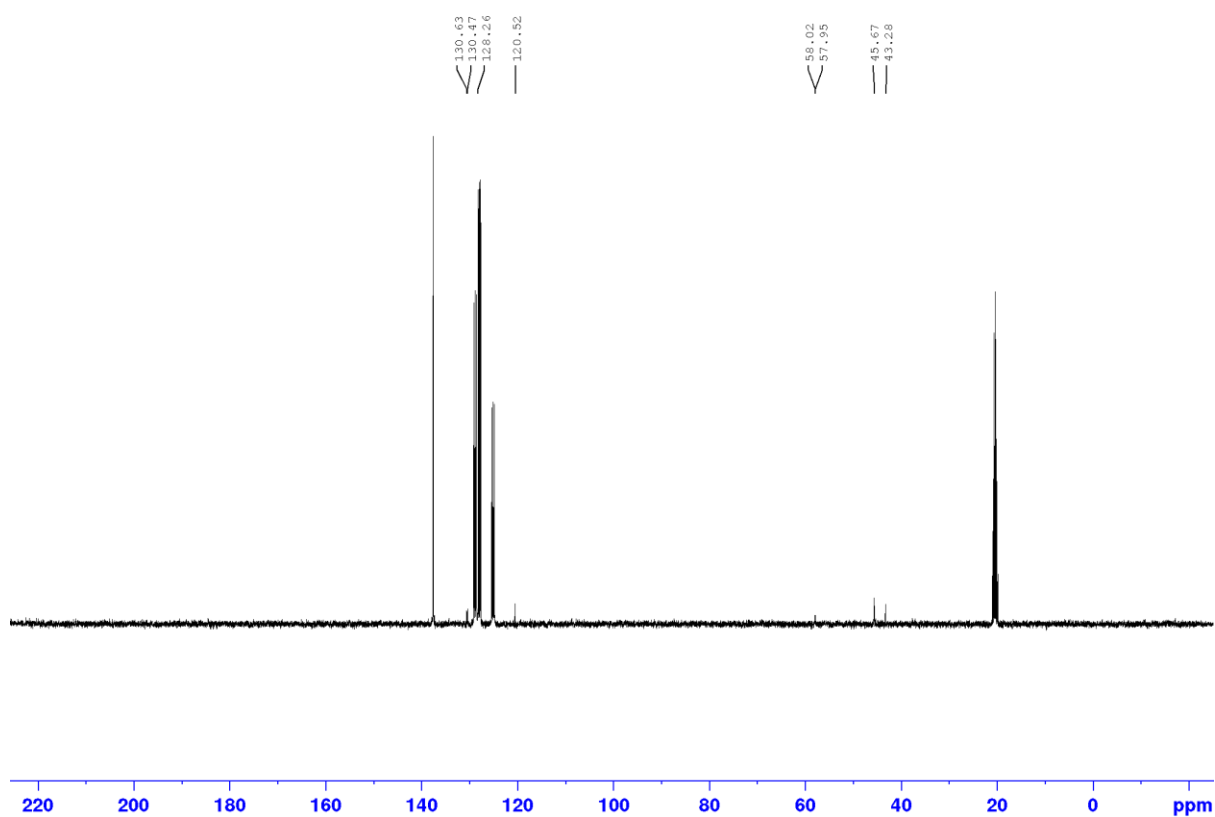


Figure S7: $^{13}\text{C}\{^1\text{H}\}$ NMR spectrum of $[(\text{Ph}_2\text{PNa.PMDETA})_2]$, **2**, in d_8 -toluene.

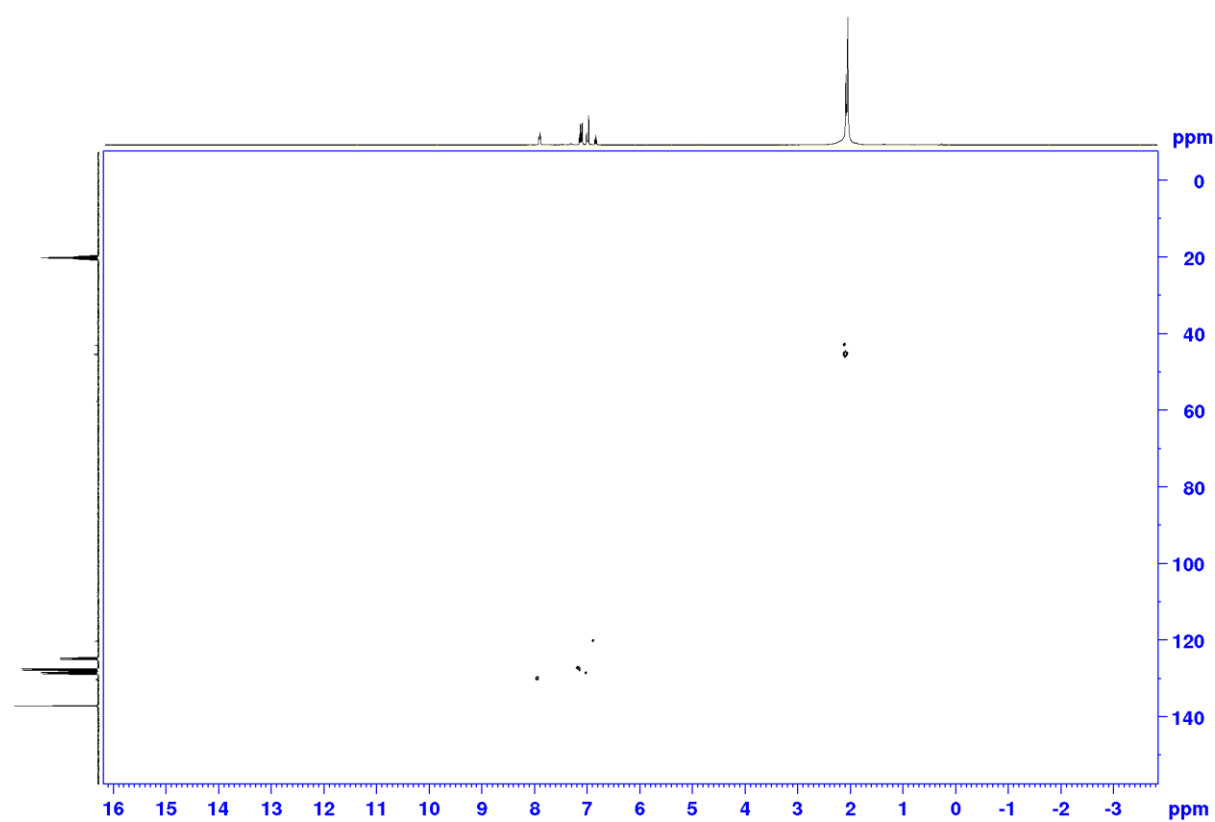


Figure S8: HSQC NMR spectrum of $[(\text{Ph}_2\text{PNa.PMDETA})_2]$, **2**, in d_8 -toluene.

NMR of [Ph₂PNa.15-crown-5], **3**

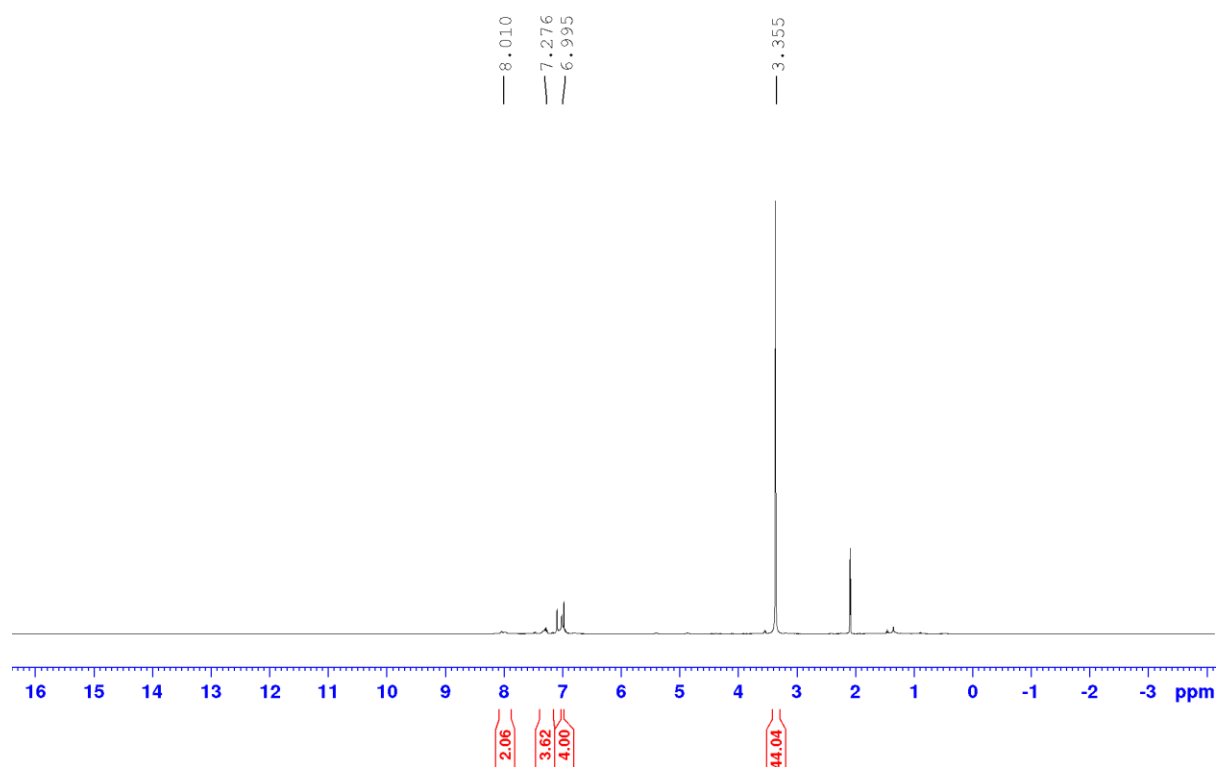


Figure S9: ¹H NMR spectrum of [Ph₂PNa.15-crown-5], **3**, in d₈-toluene.

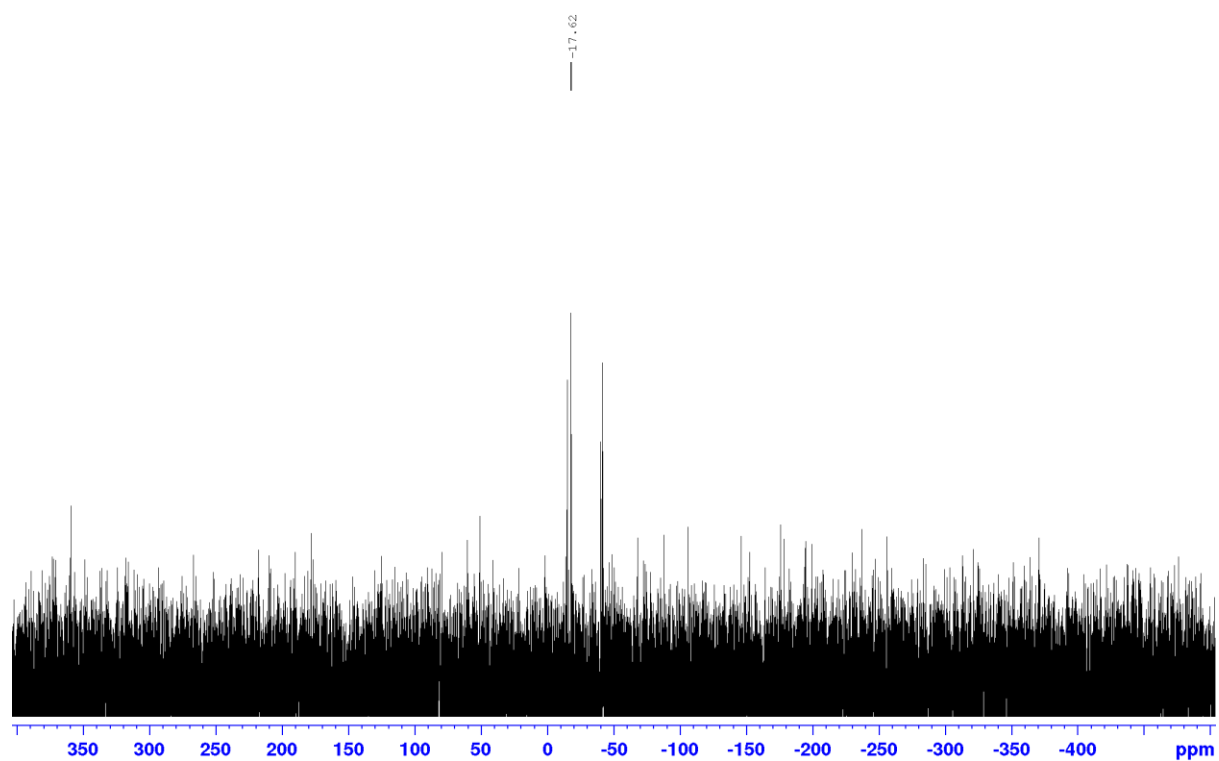


Figure S10: ³¹P NMR spectrum of [Ph₂PNa.15-crown-5], **3**, in d₈-toluene.

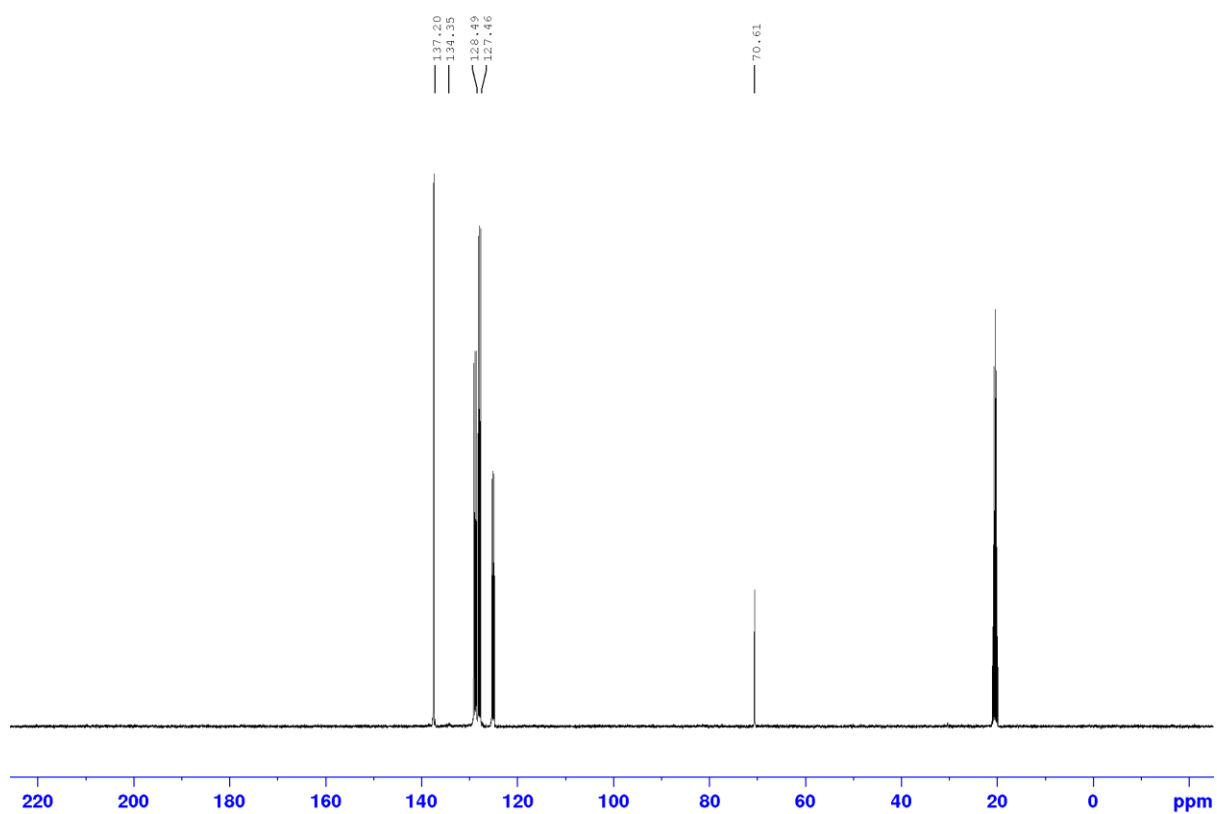


Figure S11: $^{13}\text{C}\{^1\text{H}\}$ NMR spectrum of $[\text{Ph}_2\text{PNa.15-crown-5}]$, **3**, in d_8 -toluene.

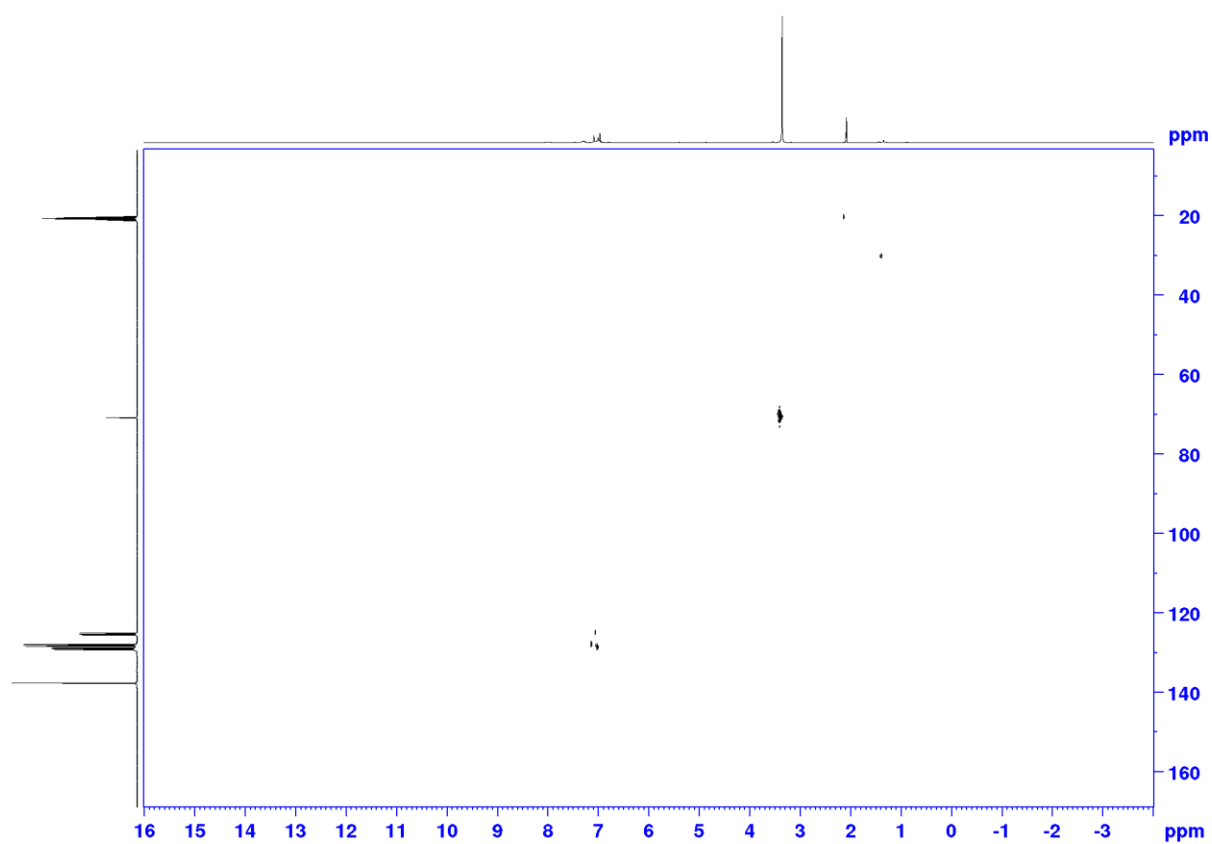


Figure S12: HSQC NMR spectrum of $[\text{Ph}_2\text{PNa.15-crown-5}]$, **3**, in d_8 -toluene.

NMR of $[(\text{Ph}_2\text{P})^- (\text{Na} \cdot 2,2,2\text{-cryptand})^+]$, **4**

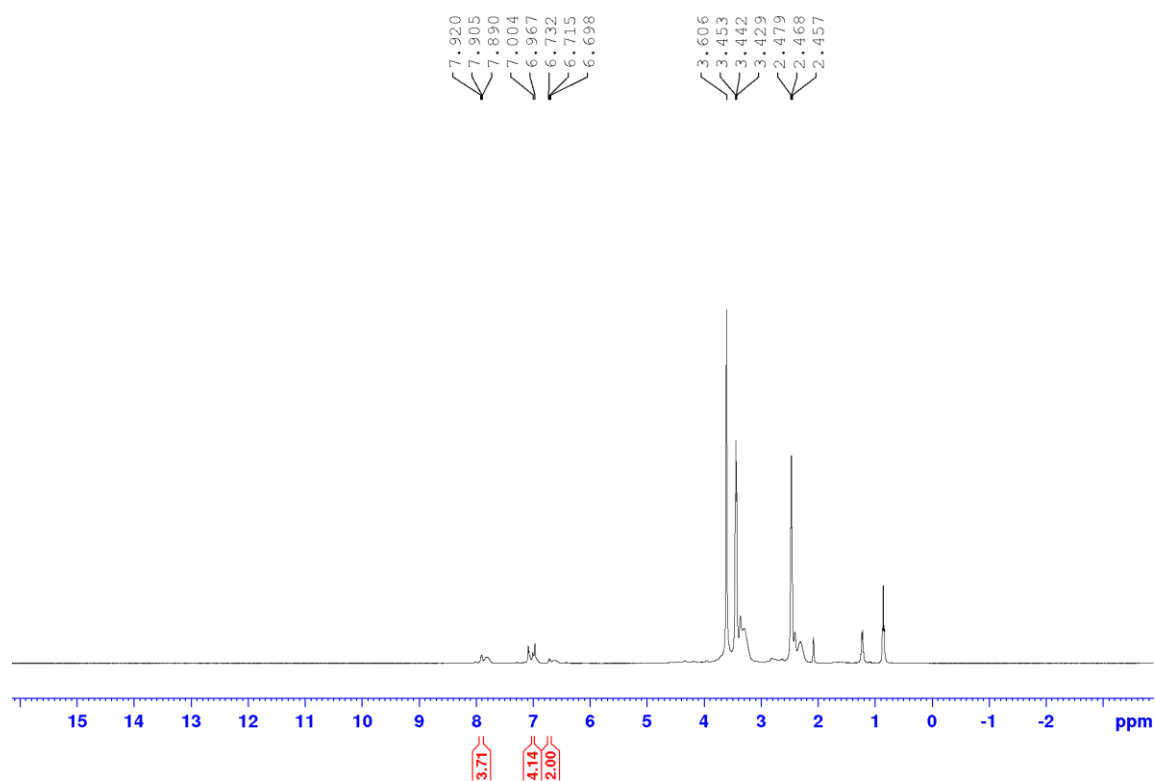


Figure S13: ^1H NMR spectrum of $[(\text{PPh}_2)^- (\text{Na} \cdot 2,2,2\text{-cryptand})^+]$, **4**, in d_8 -toluene.

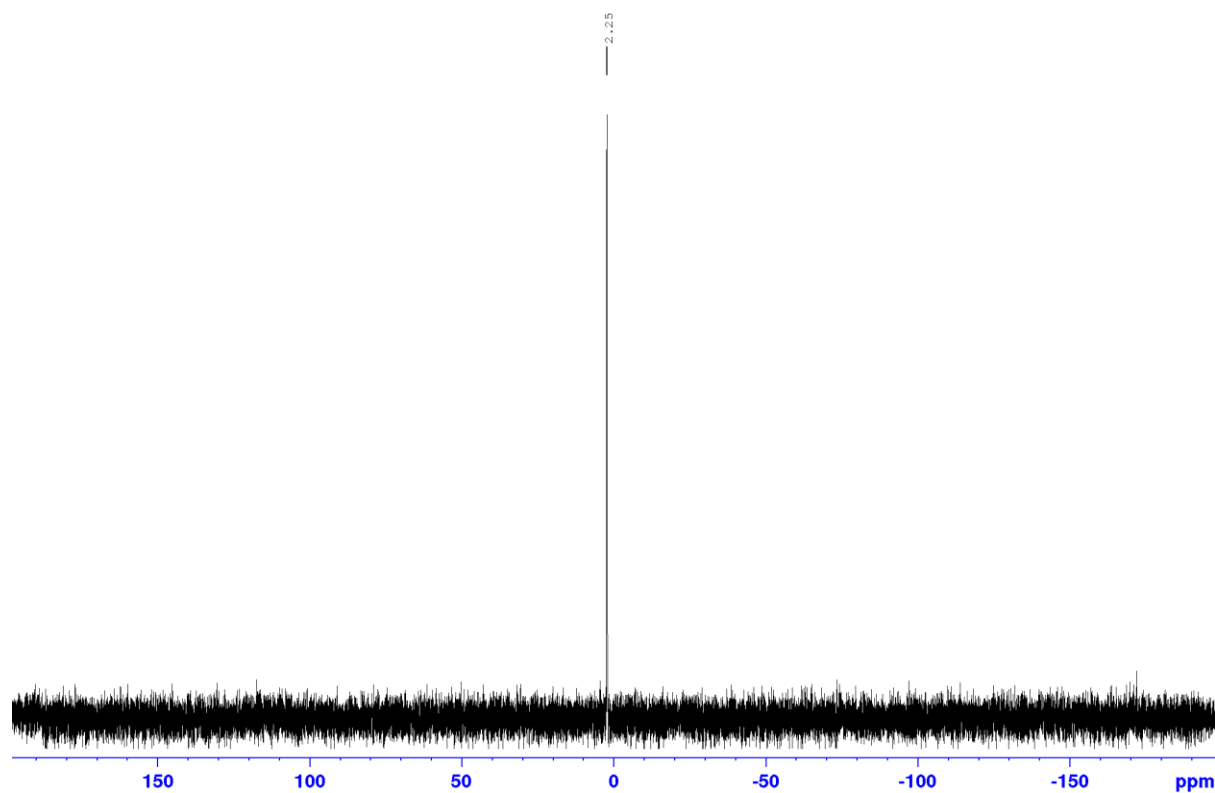


Figure S14: ^{31}P NMR spectrum of $[(\text{PPh}_2)^- (\text{Na} \cdot 2,2,2\text{-cryptand})^+]$, **4**, in d_8 -toluene.

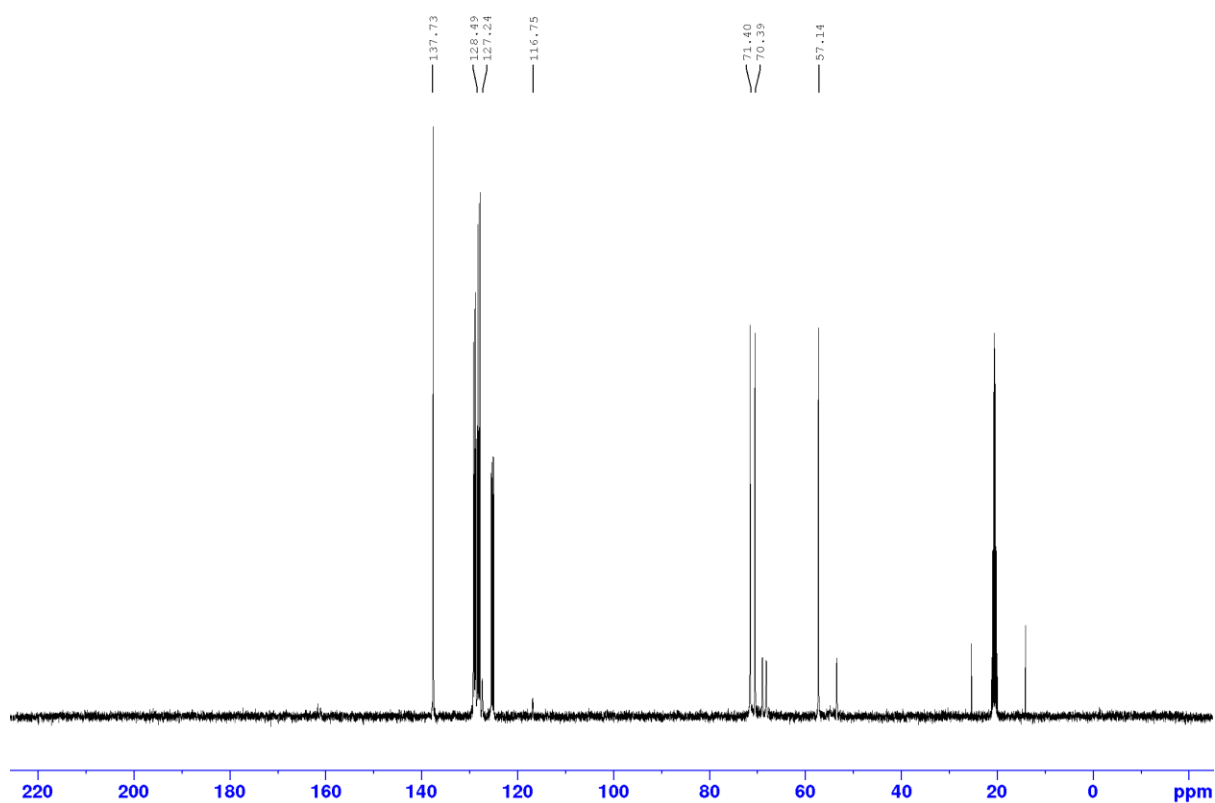


Figure S15: $^{13}\text{C}\{^1\text{H}\}$ NMR spectrum of $[(\text{PPh}_2)^- (\text{Na} \cdot 2,2,2\text{-cryptand})^+]$, **4**, in d_8 -toluene.

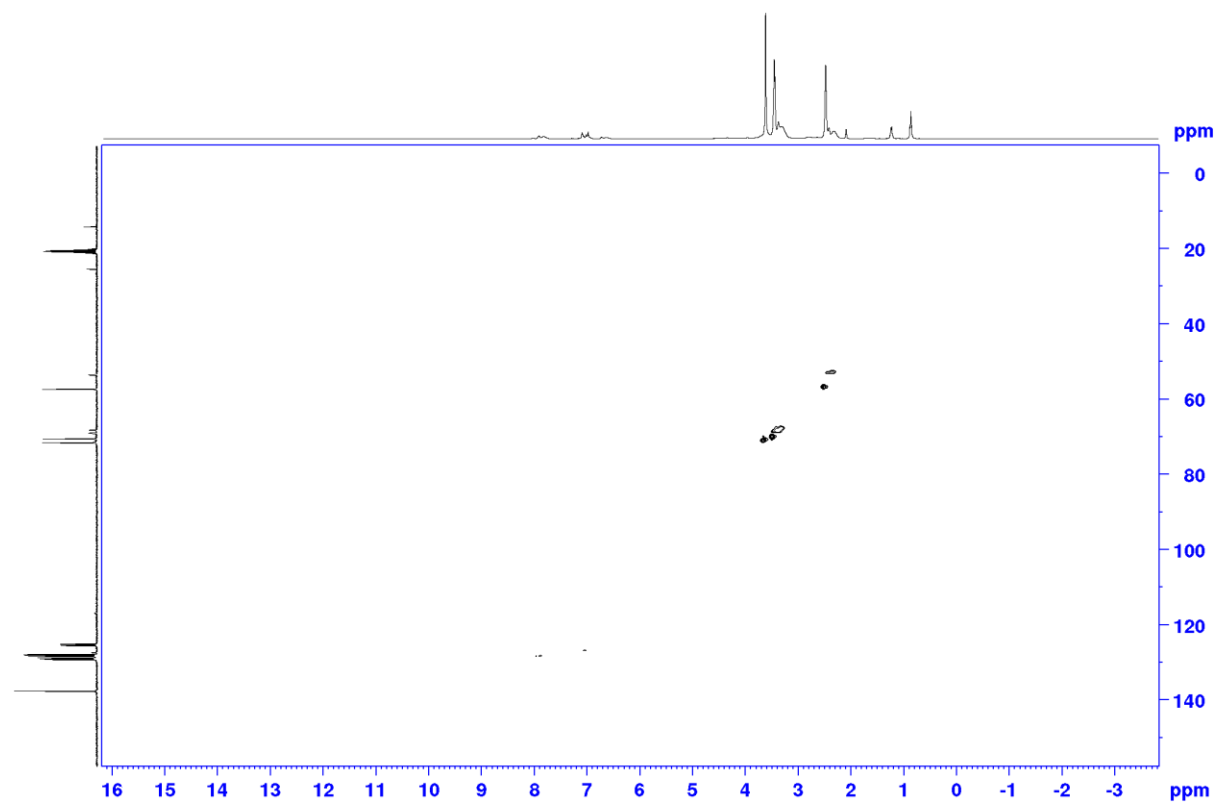


Figure S16: HSQC NMR spectrum of $[(\text{PPh}_2)^- (\text{Na} \cdot 2,2,2\text{-cryptand})^+]$, **4**, in d_8 -toluene.

Hydrophosphination Using **1** as a Catalyst

Phenylacetylene catalysed by **1**

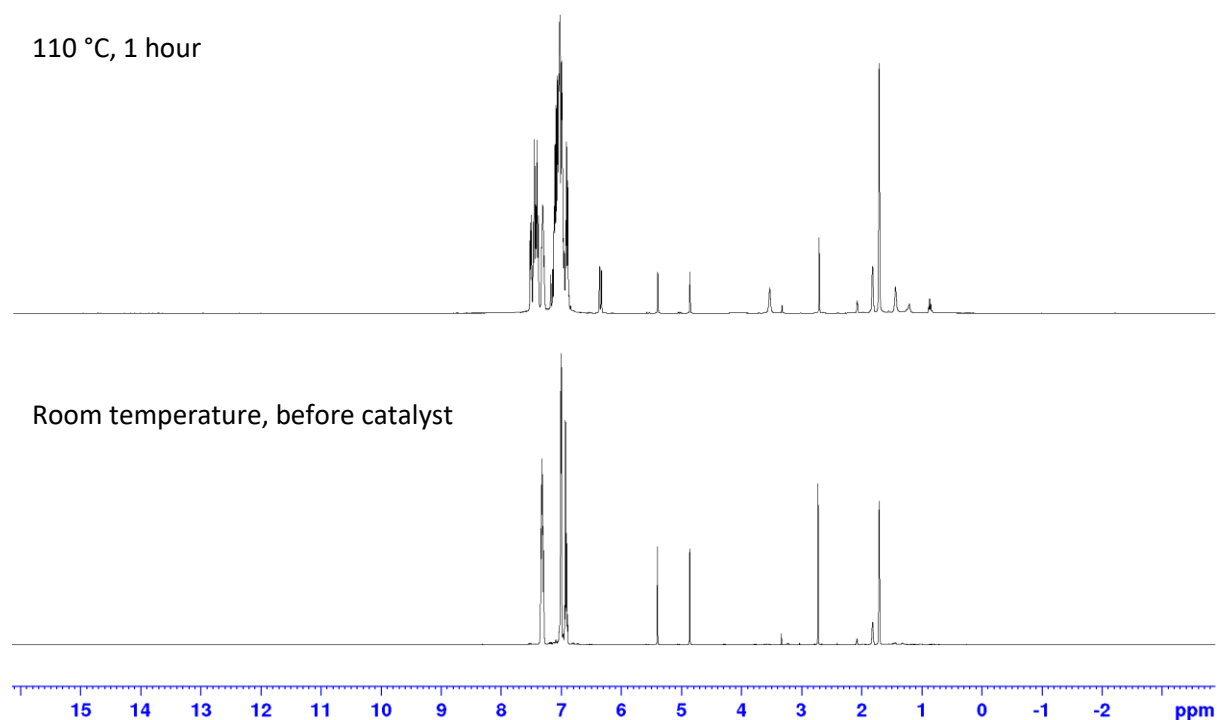


Figure S17: ¹H NMR spectrum for the hydrophosphination of phenylacetylene catalysed by **1** (10 mol%) in d₈-toluene.

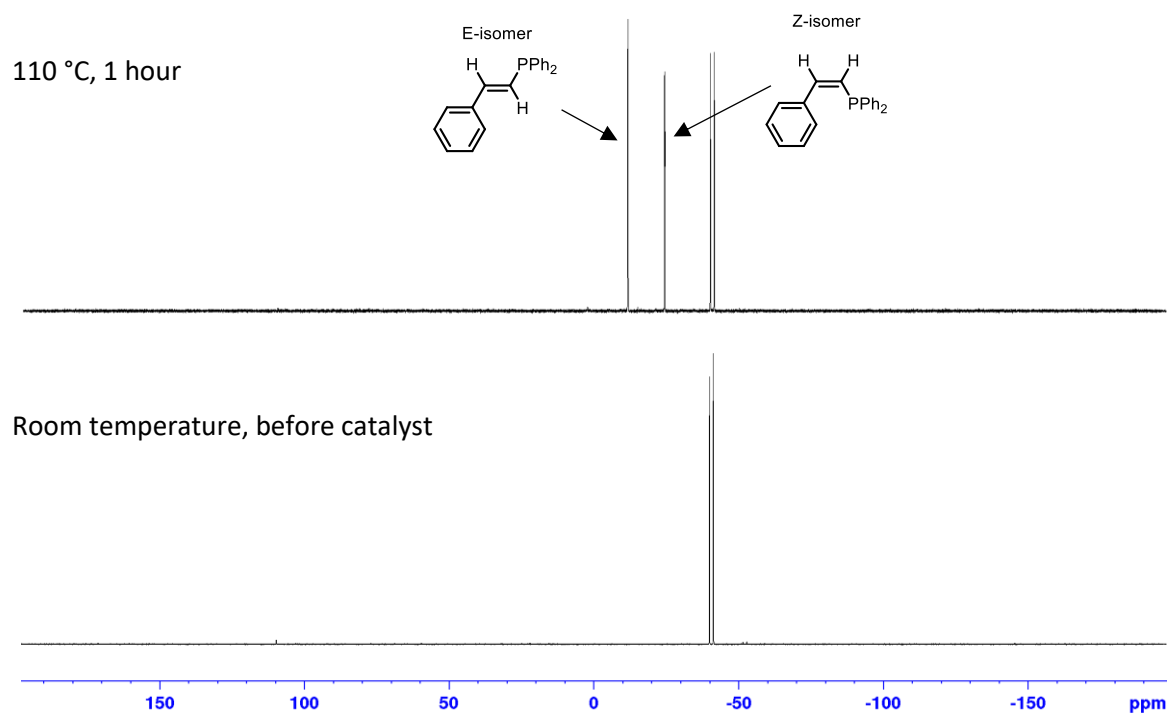


Figure S18: ³¹P NMR spectrum for the hydrophosphination of phenylacetylene catalysed by **1** (10 mol%) in d₈-toluene.

Diphenylacetylene catalysed by **1**

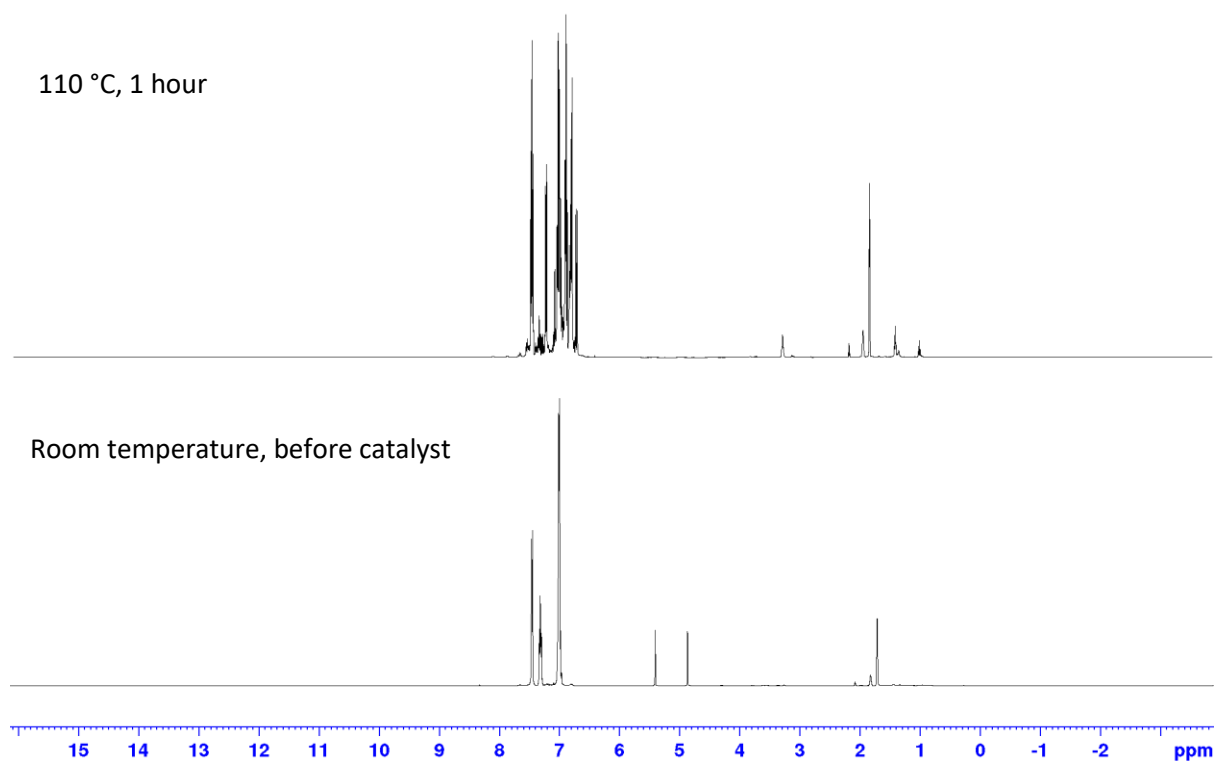


Figure S19: ¹H NMR spectrum for the hydrophosphination of diphenylacetylene catalysed by **1** (10 mol%) in d₈-toluene.

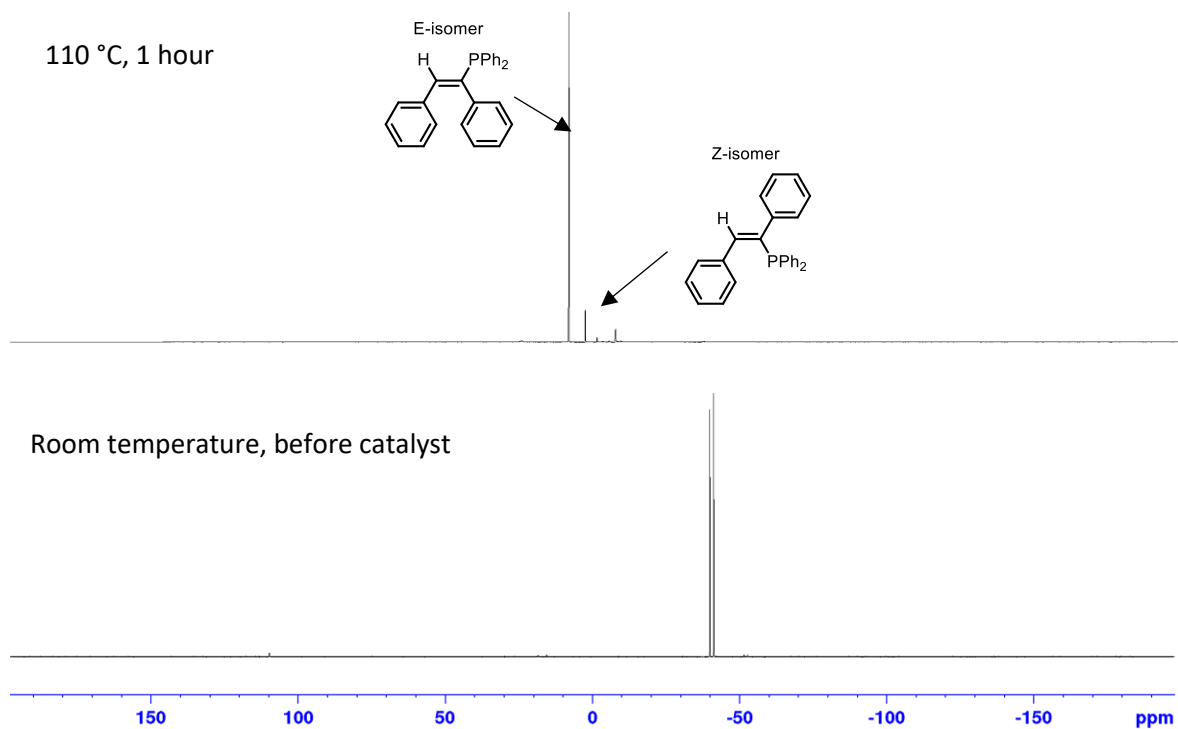
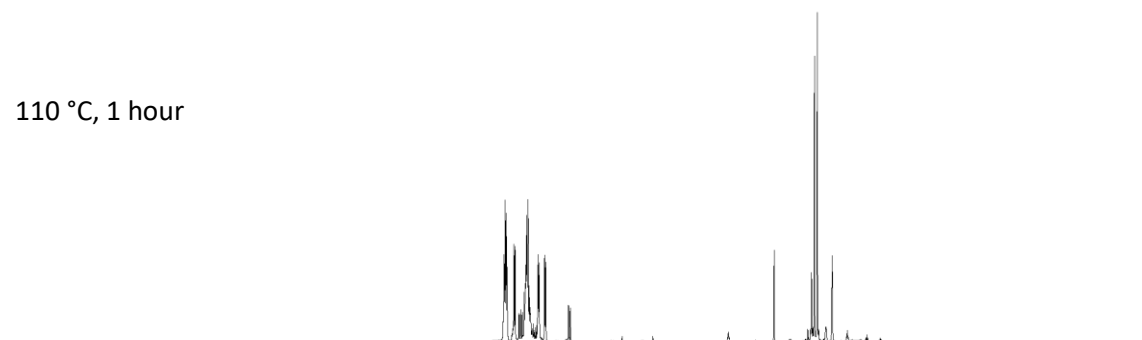


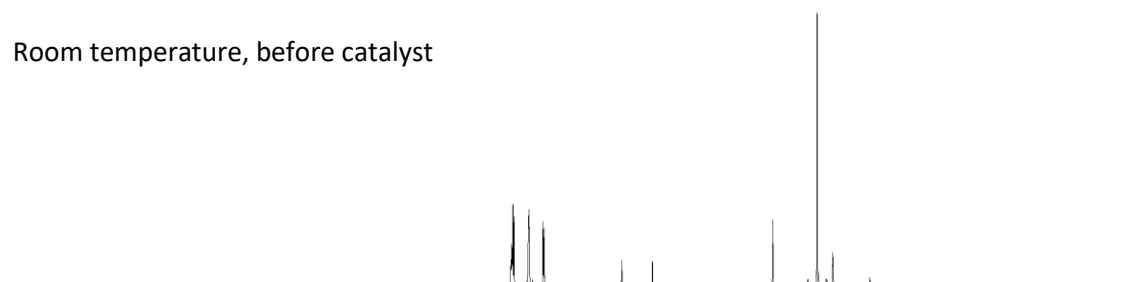
Figure S20: ³¹P NMR spectrum for the hydrophosphination of diphenylacetylene catalysed by **1** (10 mol%) in d₈-toluene.

4'-Methylphenylacetylene catalysed by **1**

110 °C, 1 hour



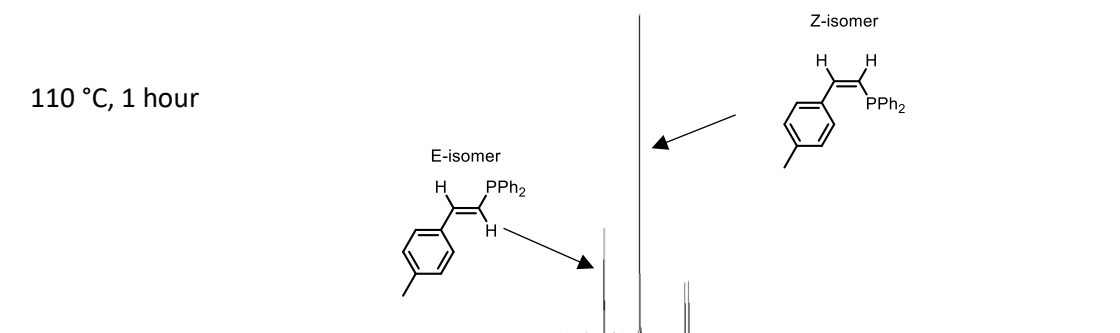
Room temperature, before catalyst



15 14 13 12 11 10 9 8 7 6 5 4 3 2 1 0 -1 -2 ppm

Figure S21: ¹H NMR spectrum for the hydrophosphination of 4'-methylphenylacetylene catalysed by **1** (10 mol%) in d₈-toluene.

110 °C, 1 hour



Room temperature, before catalyst



150 100 50 0 -50 -100 -150 ppm

Figure S22: ³¹P NMR spectrum for the hydrophosphination of 4'-methylphenylacetylene catalysed by **1** (10 mol%) in d₈-toluene.

4'-Trifluoromethylphenylacetylene catalysed by **1**

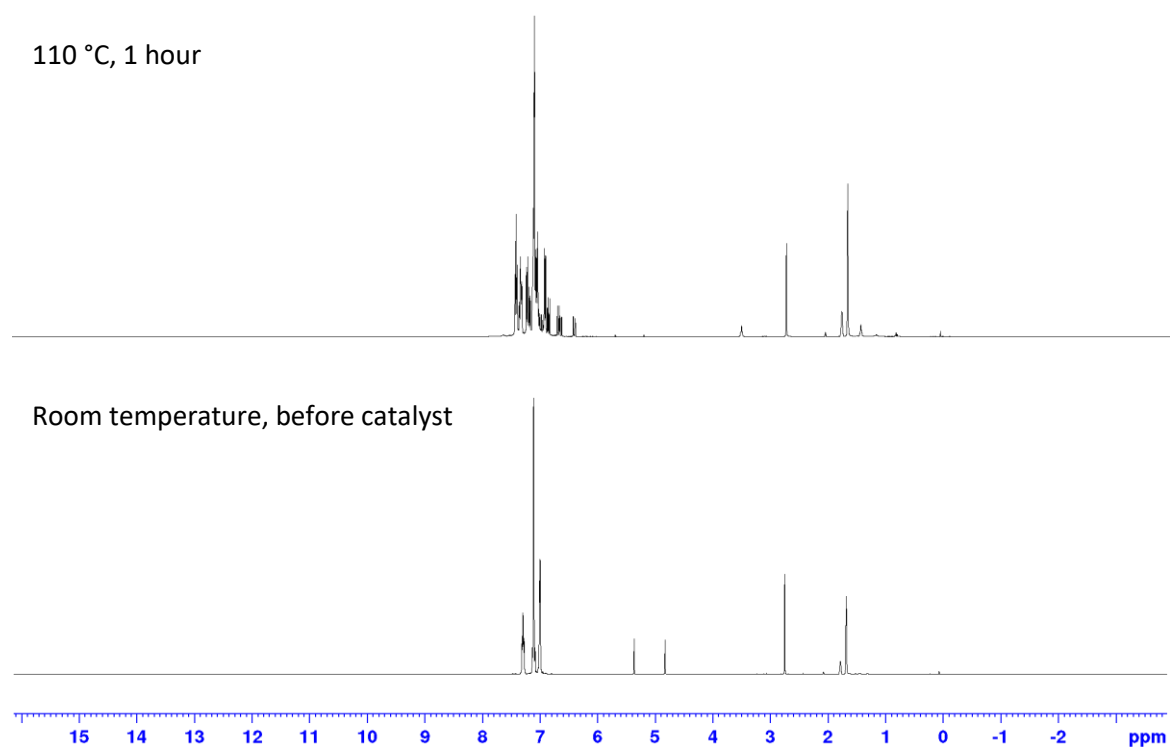


Figure S23: ¹H NMR spectrum for the hydrophosphination of 4'-trifluoromethylphenylacetylene catalysed by **1** (10 mol%) in d₈-toluene.

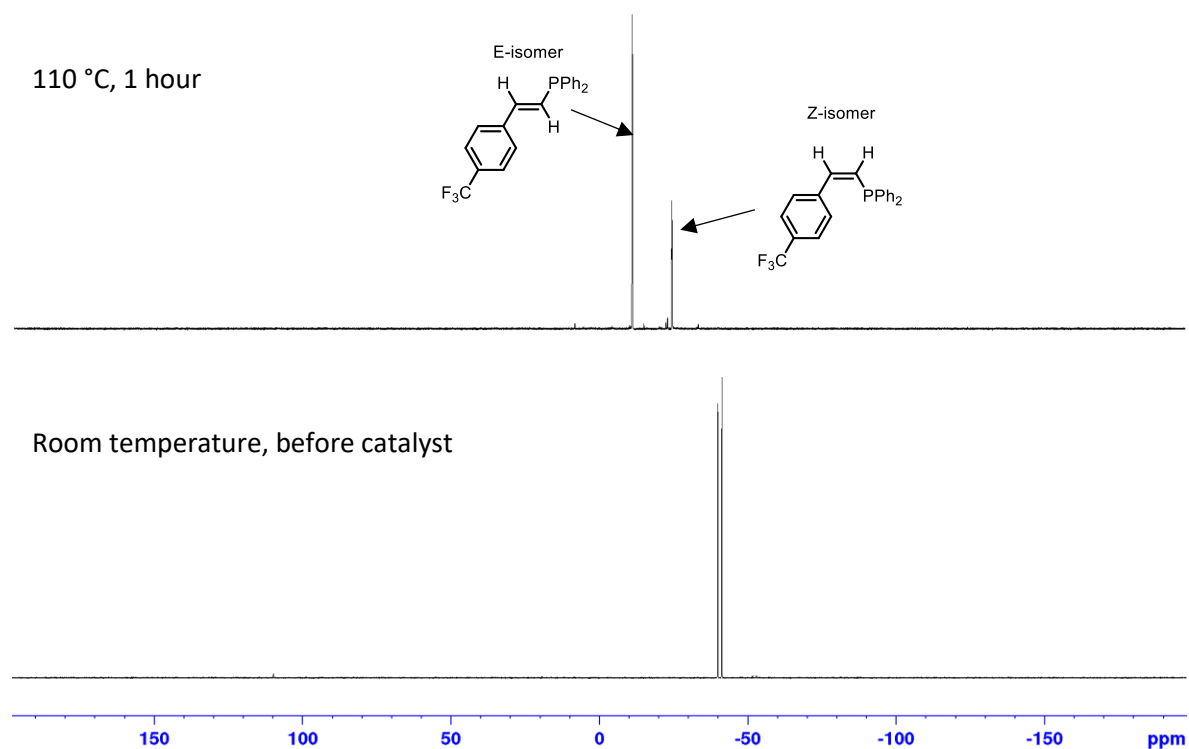


Figure S24: ³¹P NMR spectrum for the hydrophosphination of 4'-trifluoromethylphenylacetylene catalysed by **1** (10 mol%) in d₈-toluene.

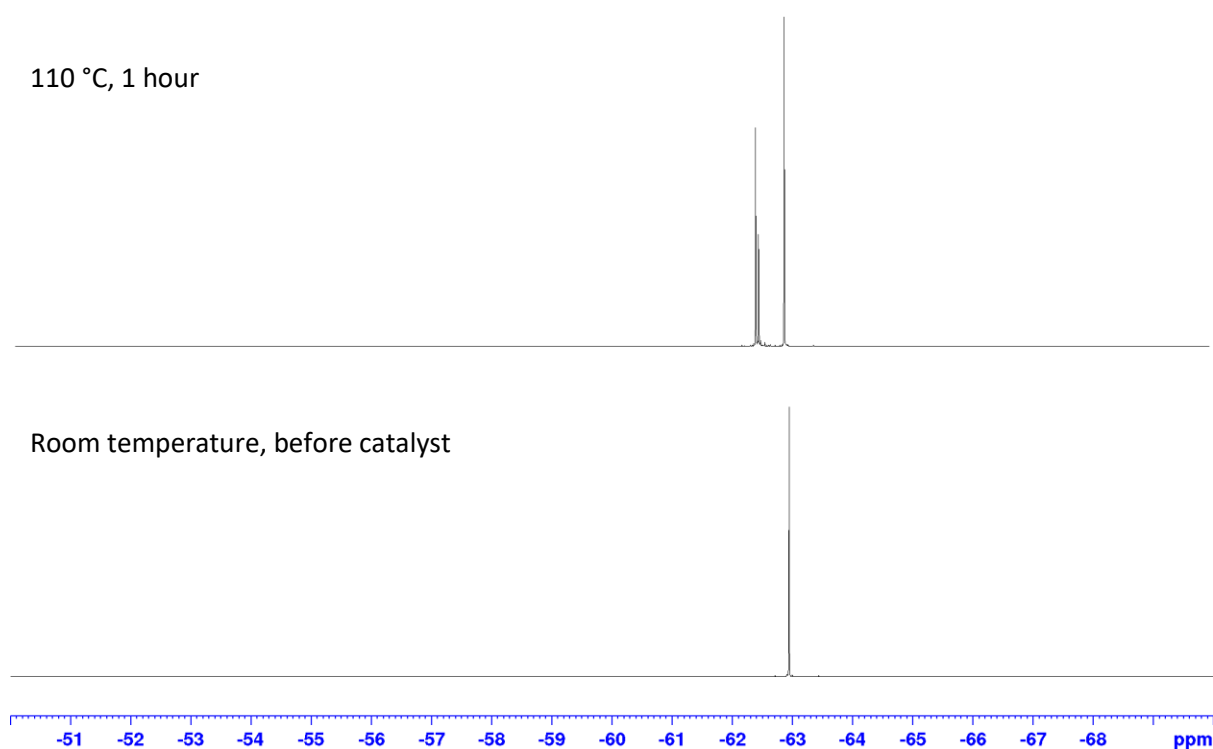


Figure S25: $^{19}\text{F}\{^1\text{H}\}$ NMR spectrum for the hydrophosphination of 4'-trifluoromethylphenylacetylene catalysed by **1** (10 mol%) in d_8 -toluene.

4-Cyanophenylacetylene catalysed by **1**

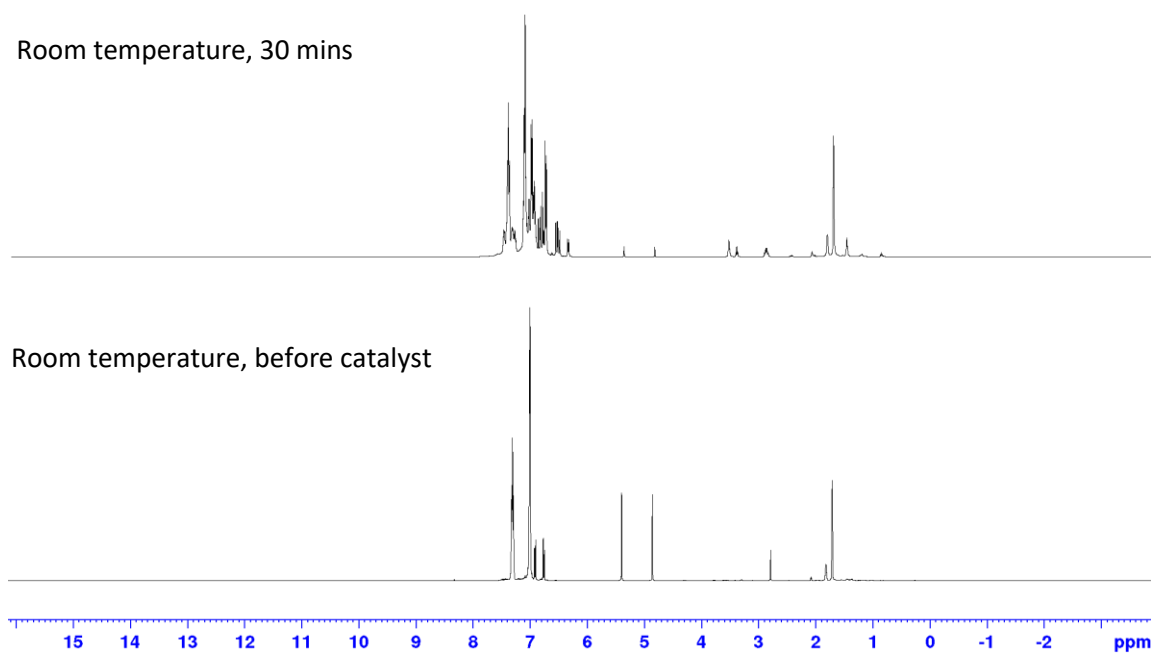


Figure S26: ^1H NMR spectrum for the hydrophosphination of 4-cyanophenylacetylene catalysed by **1** (10 mol%) in d_8 -toluene.

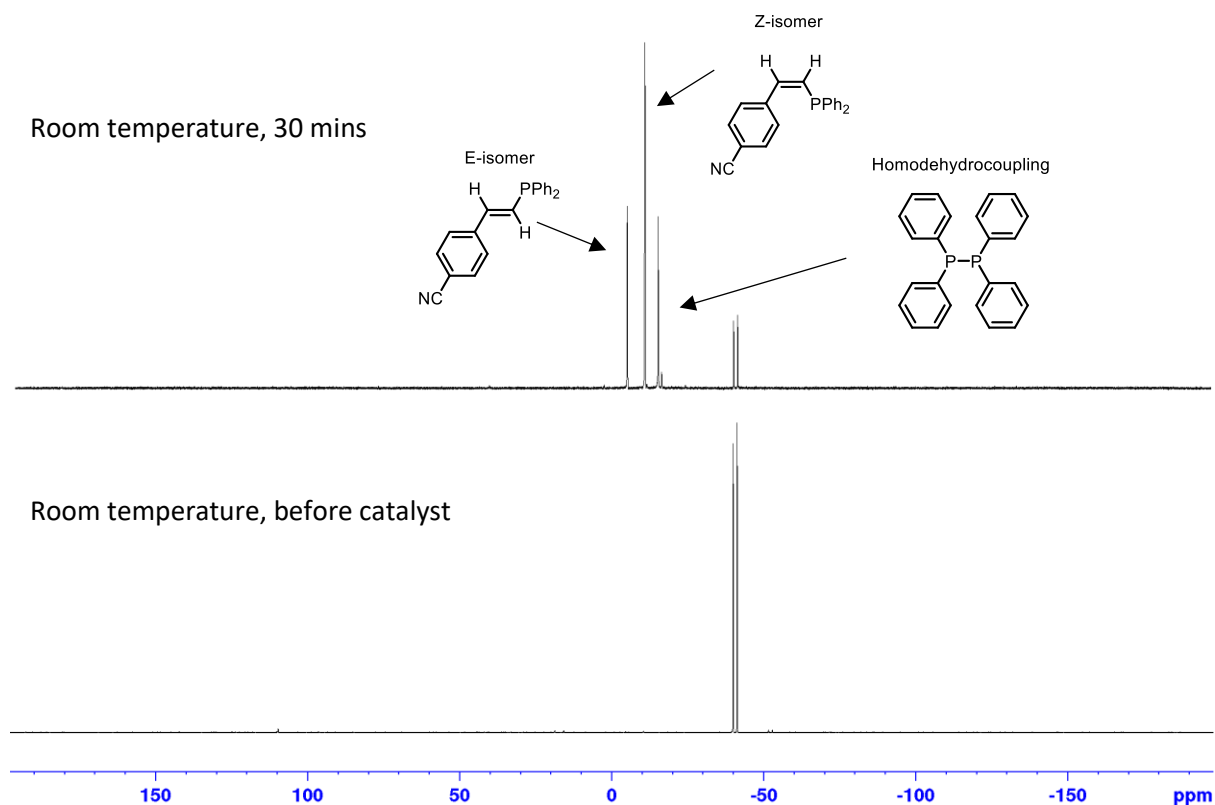


Figure S27: ^{31}P NMR spectrum for the hydrophosphination of 4-cyanophenylacetylene catalysed by **1** (10 mol%) in d_8 -toluene.

3-Phenyl-1-propyne catalysed by **1**

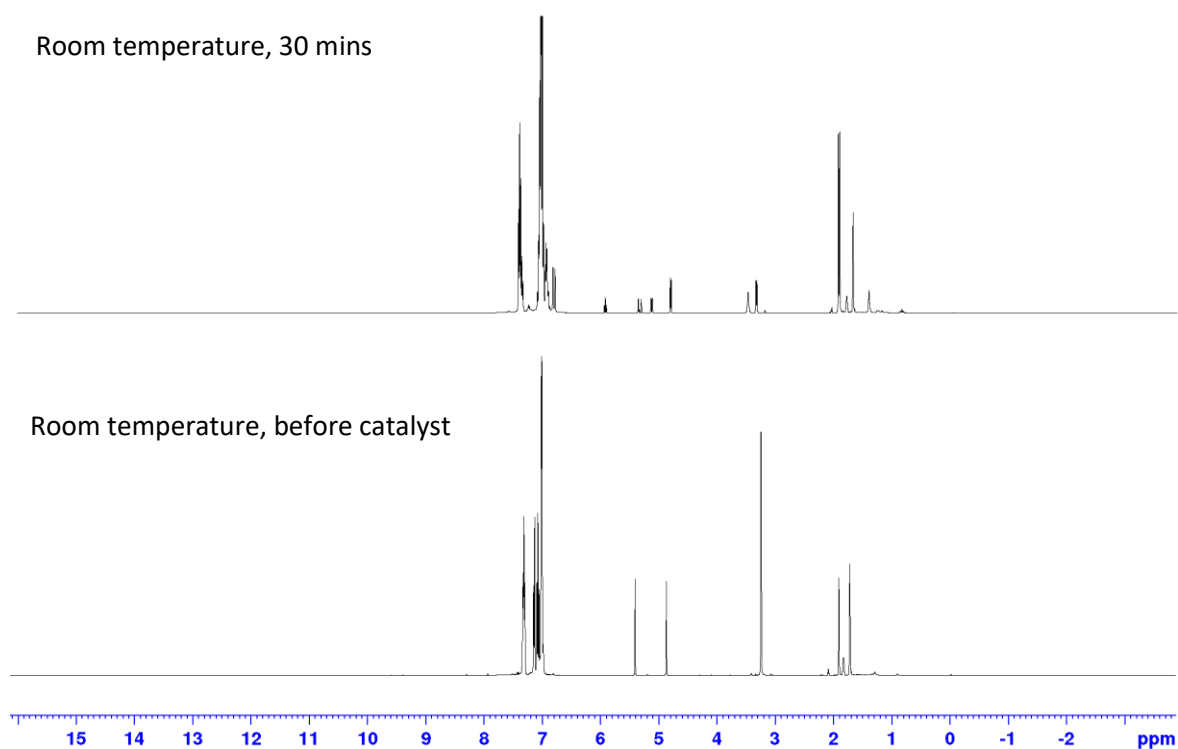


Figure S28: ^1H NMR spectrum for the hydrophosphination of 3-phenyl-1-propyne catalysed by **1** (10 mol%) in d_8 -toluene.

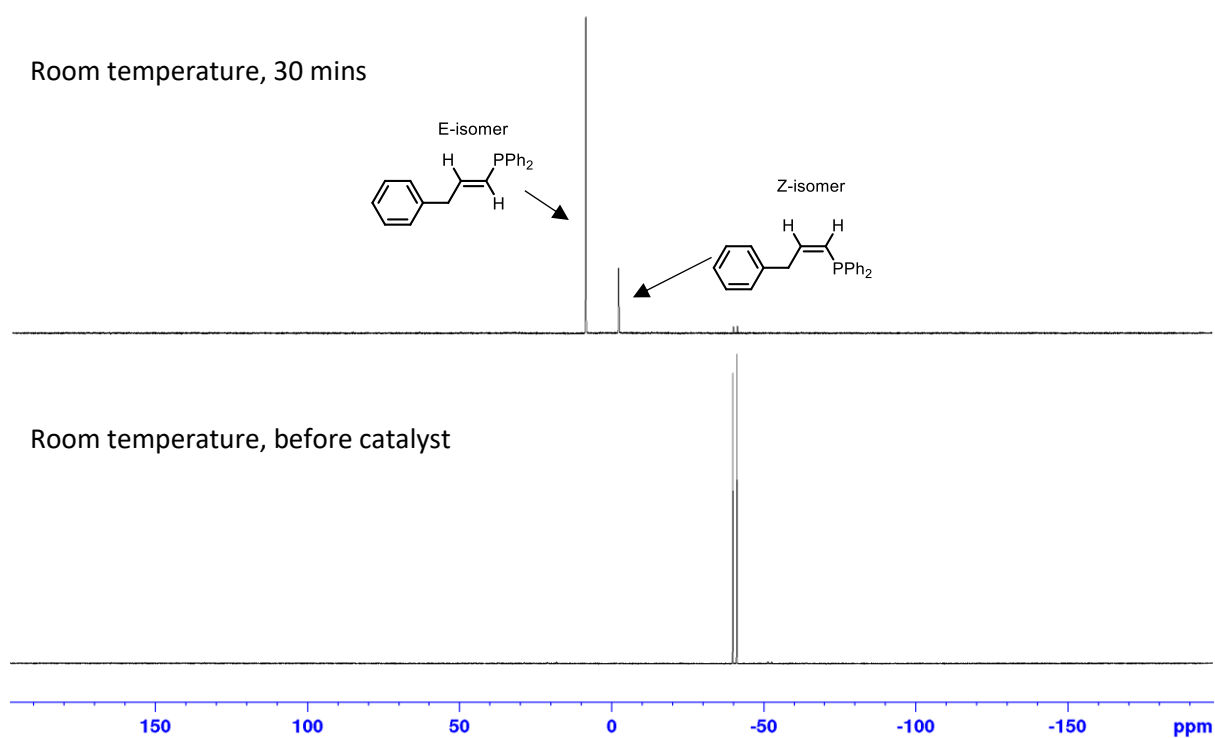


Figure S29: ^{31}P NMR spectrum for the hydrophosphination of 3-phenyl-1-propyne catalysed by **1** (10 mol%) in d_8 -toluene.

4-Phenyl-1-butyne catalysed by **1**

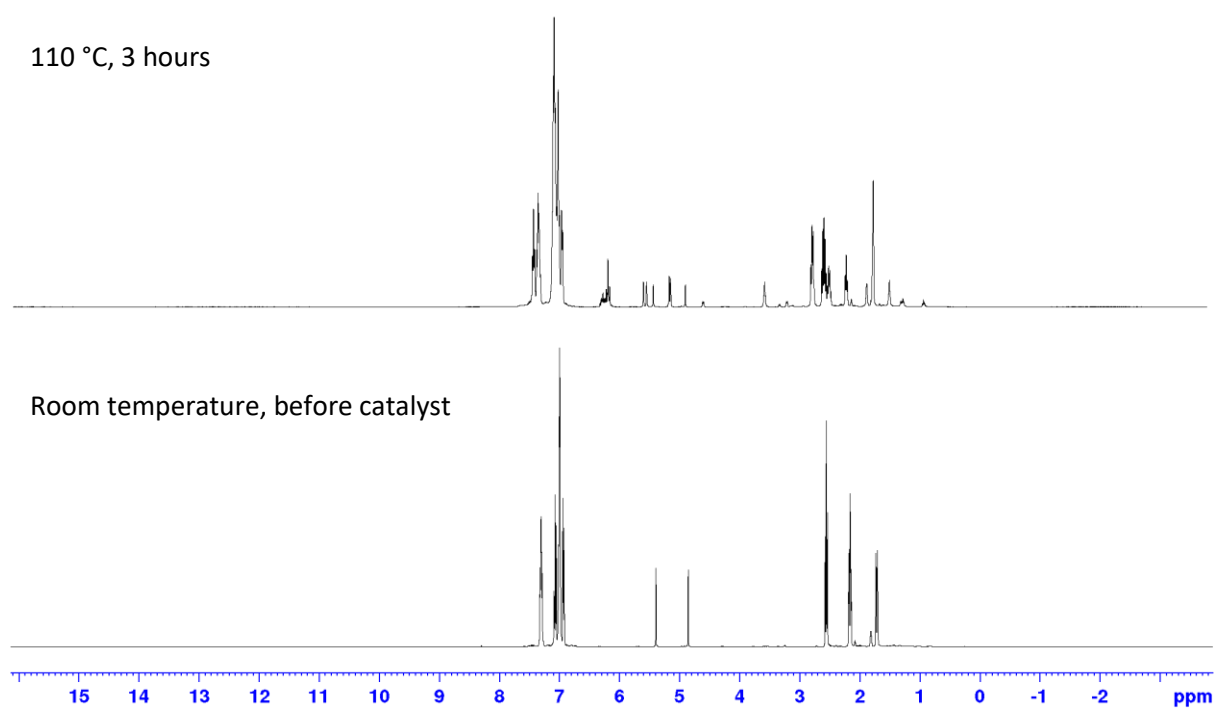


Figure S30: ^1H NMR spectrum for the hydrophosphination of 4-phenyl-1-butyne catalysed by **1** (10 mol%) in d_8 -toluene.

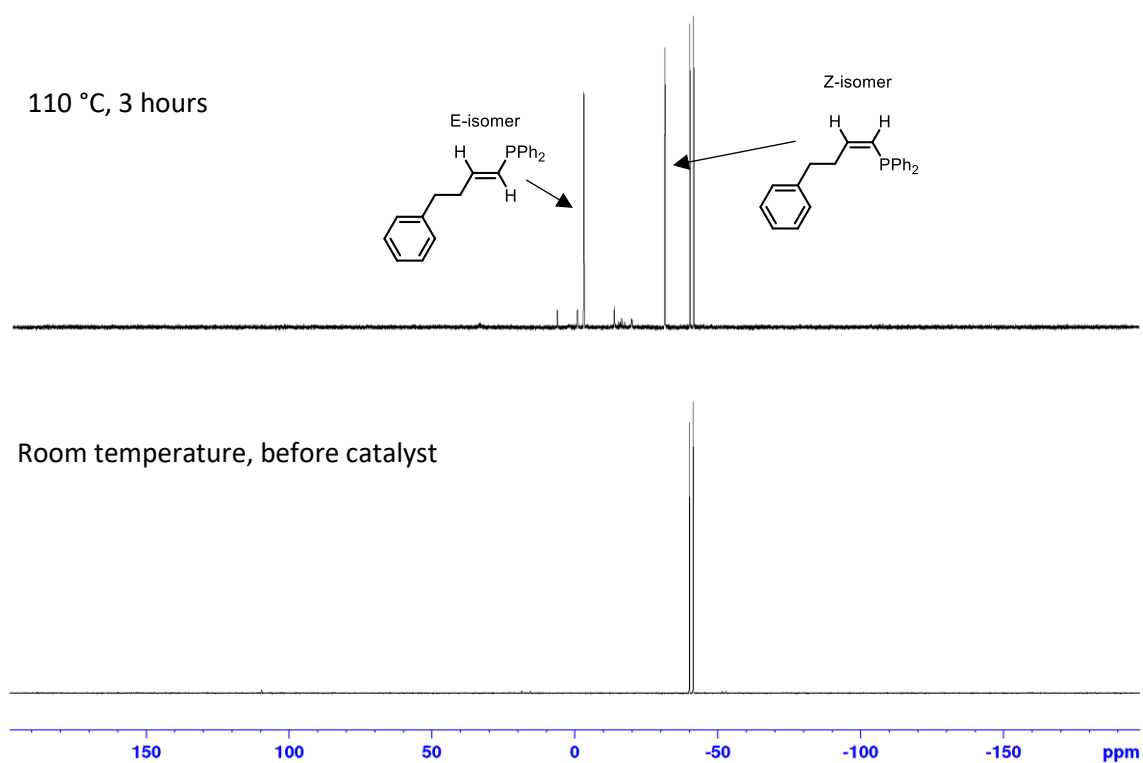


Figure S31: ^{31}P NMR spectrum for the hydrophosphination of 4-phenyl-1-butyne catalysed by **1** (10 mol%) in d_8 -toluene.

1-Octyne catalysed by **1**

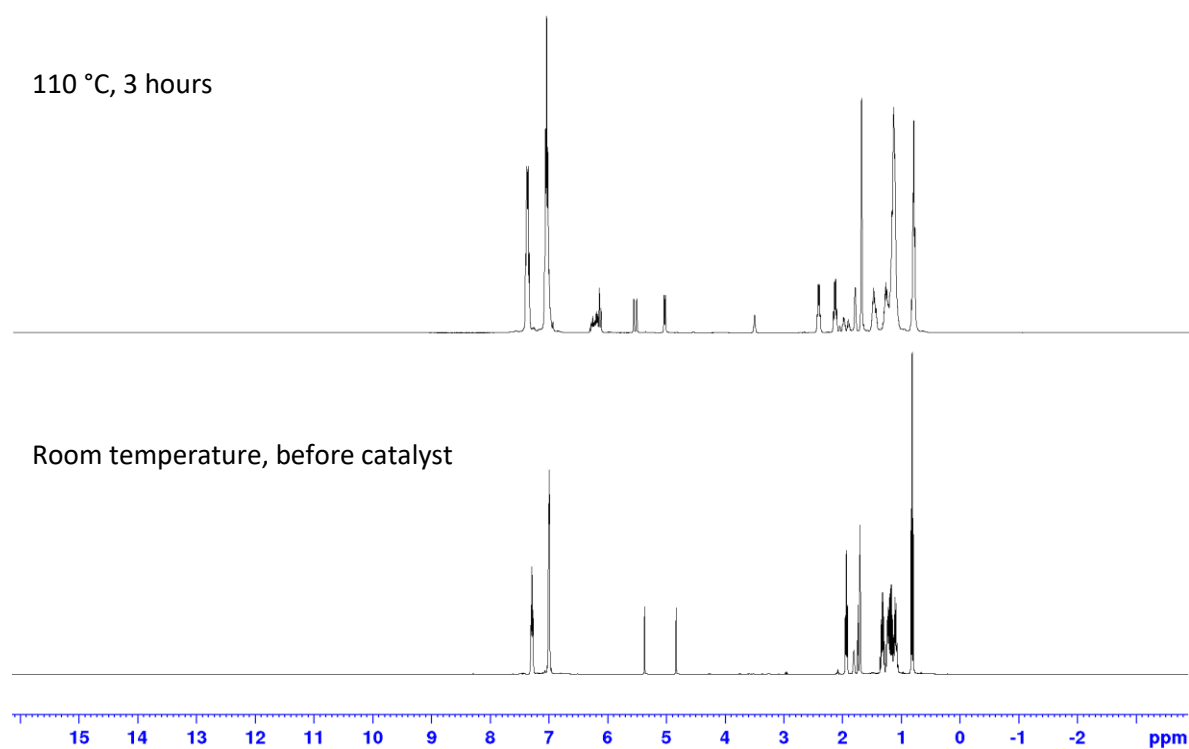


Figure S32: ^1H NMR spectrum for the hydrophosphination of 1-octyne catalysed by **1** (10 mol%) in d_8 -toluene.

110 °C, 3 hours

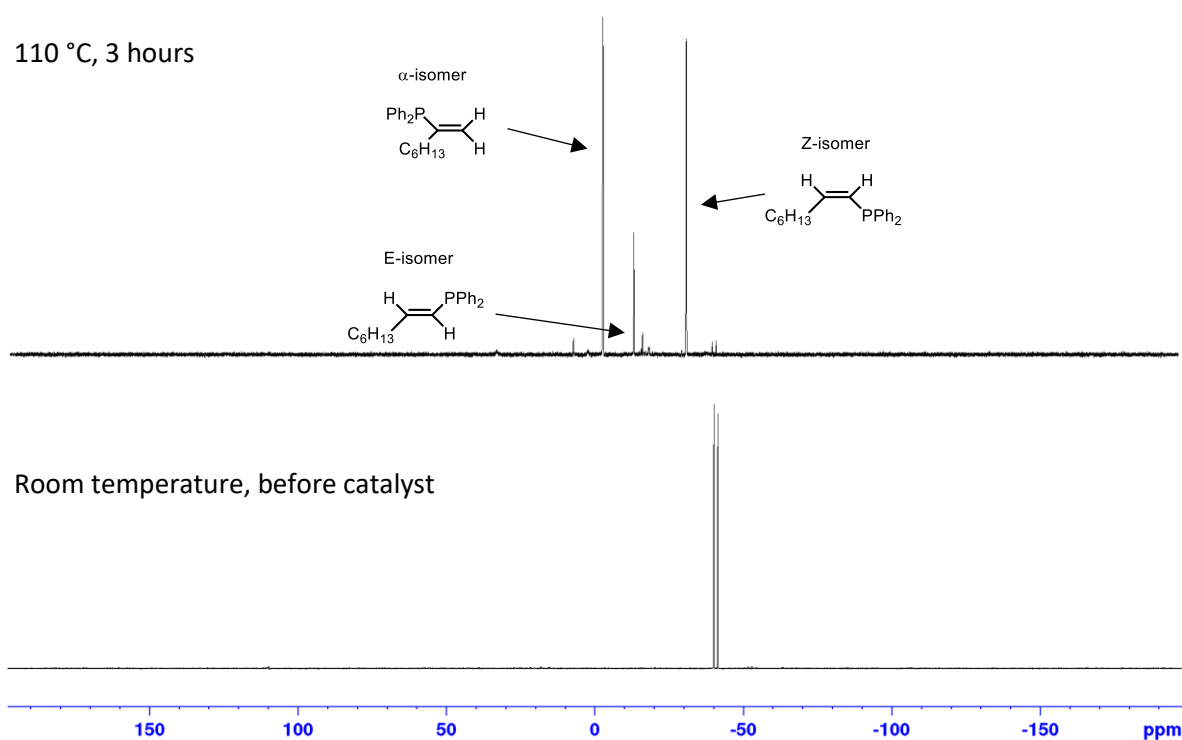


Figure S33: ^{31}P NMR spectrum for the hydrophosphination of 1-octyne catalysed by **1** (10 mol%) in d_8 -toluene.

3-Hexyne catalysed by **1**

110 °C, 24 hours

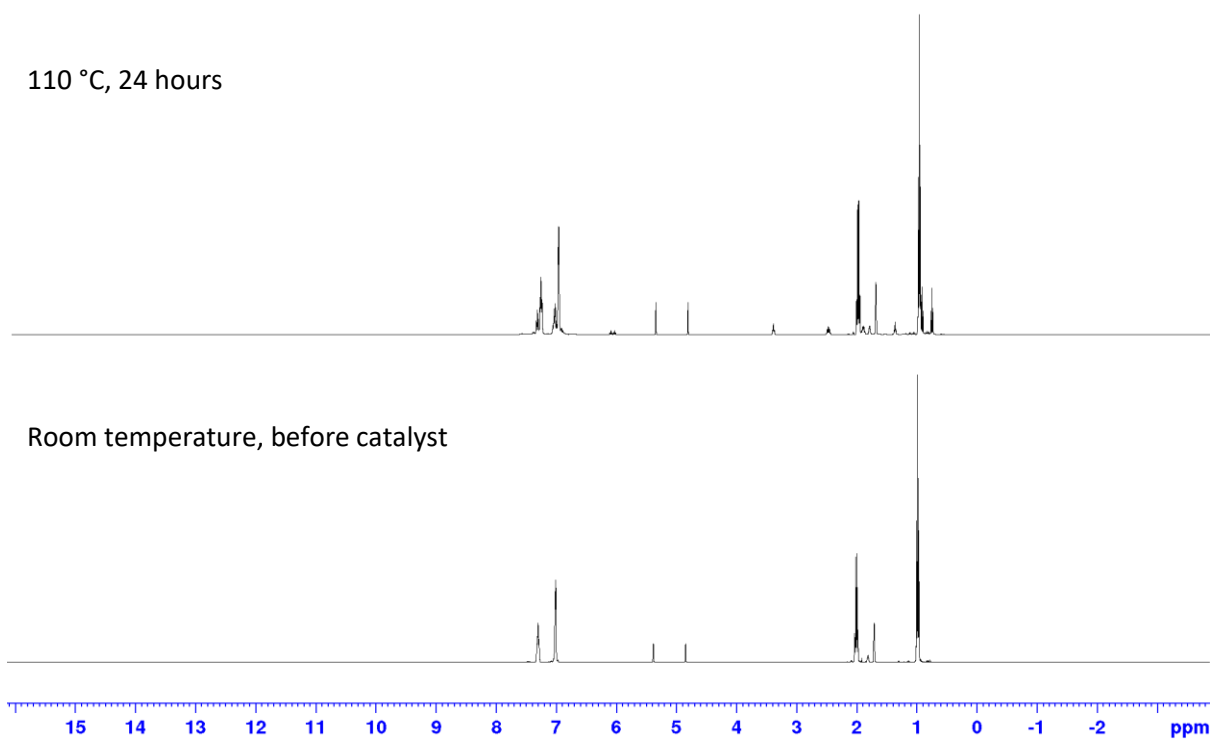


Figure S34: ^1H NMR spectrum for the hydrophosphination of 3-hexyne catalysed by **1** (10 mol%) in d_8 -toluene.

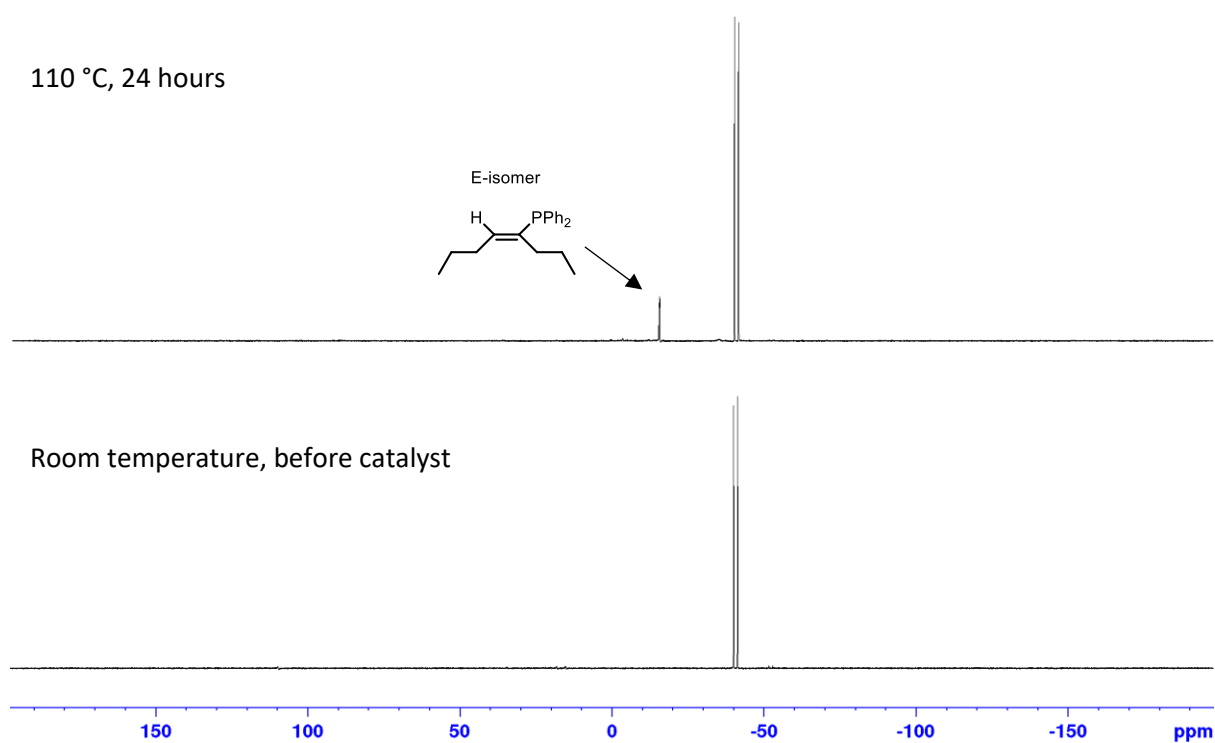


Figure S35: ^{31}P NMR spectrum for the hydrophosphination of 3-hexyne catalysed by **1** (10 mol%) in d_8 -toluene.

Styrene catalysed by **1**

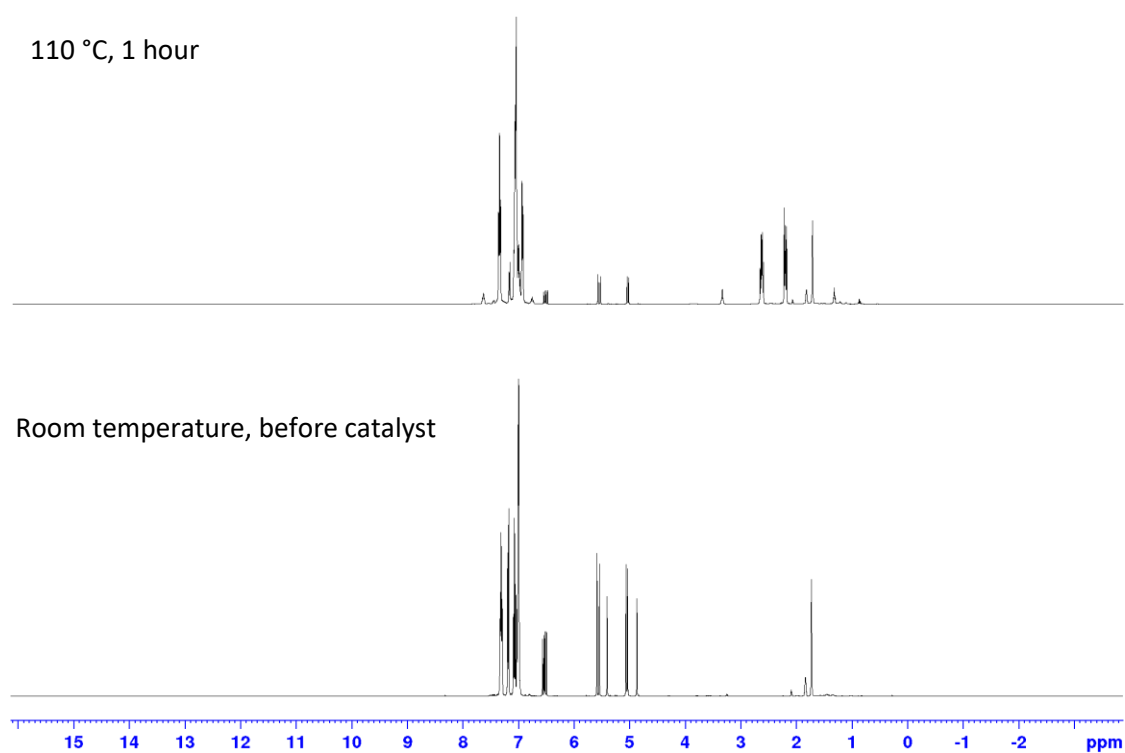


Figure S36: ^1H NMR spectrum for the hydrophosphination of styrene catalysed by **1** (10 mol%) in d_8 -toluene.

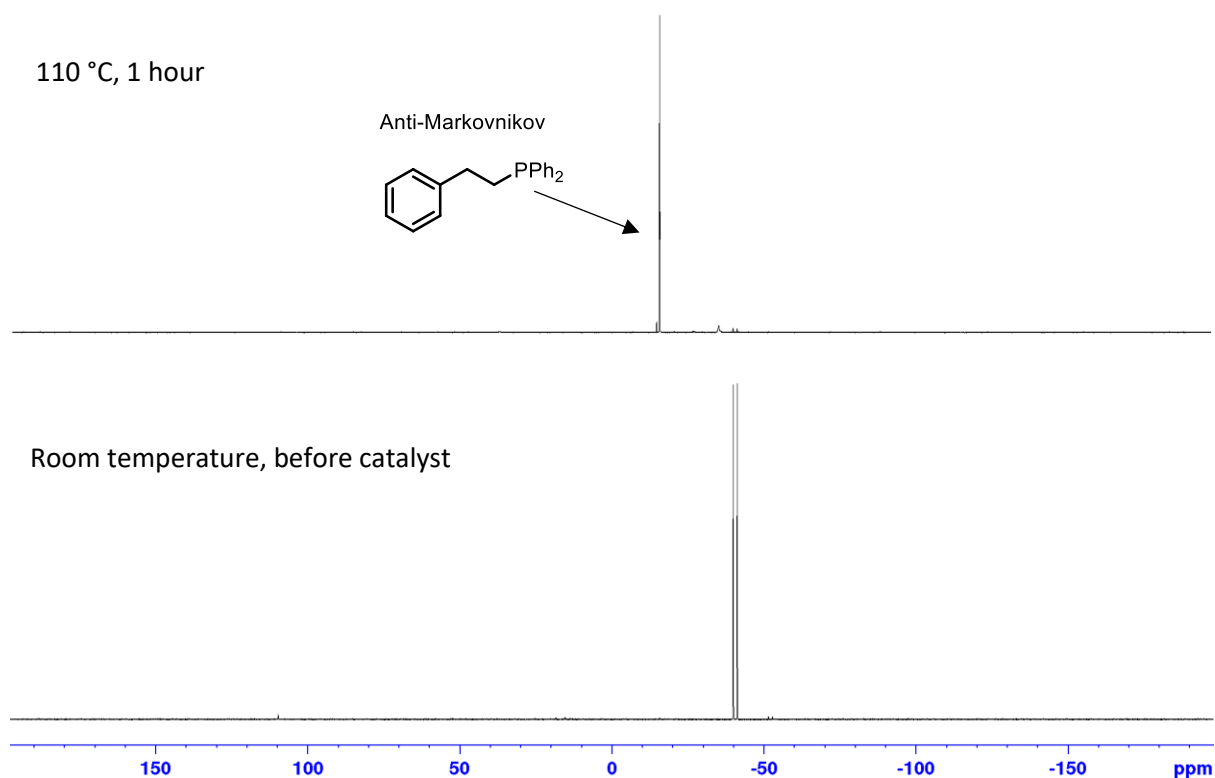


Figure S37: ^{31}P NMR spectrum for the hydrophosphination of styrene catalysed by **1** (10 mol%) in d_8 -toluene.

Methyl acrylate catalysed by **1**

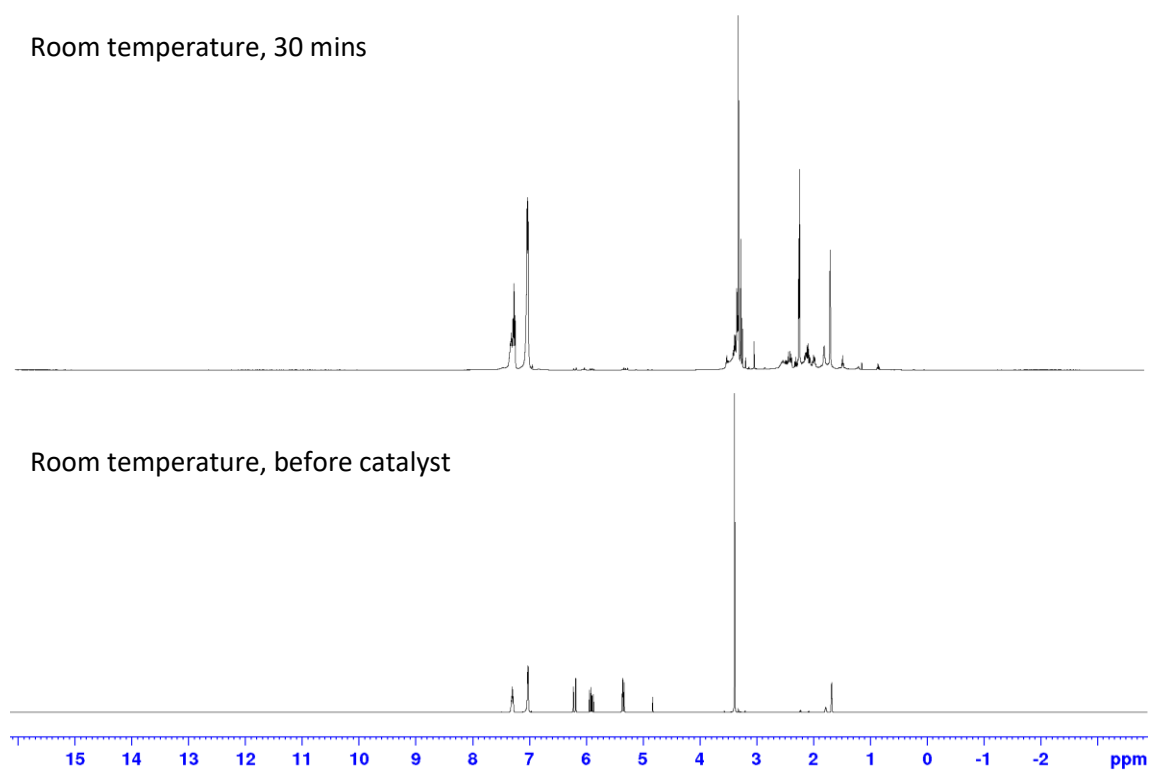


Figure S38: ^1H NMR spectrum for the hydrophosphination of methyl acrylate catalysed by **1** (10 mol%) in d_8 -toluene.

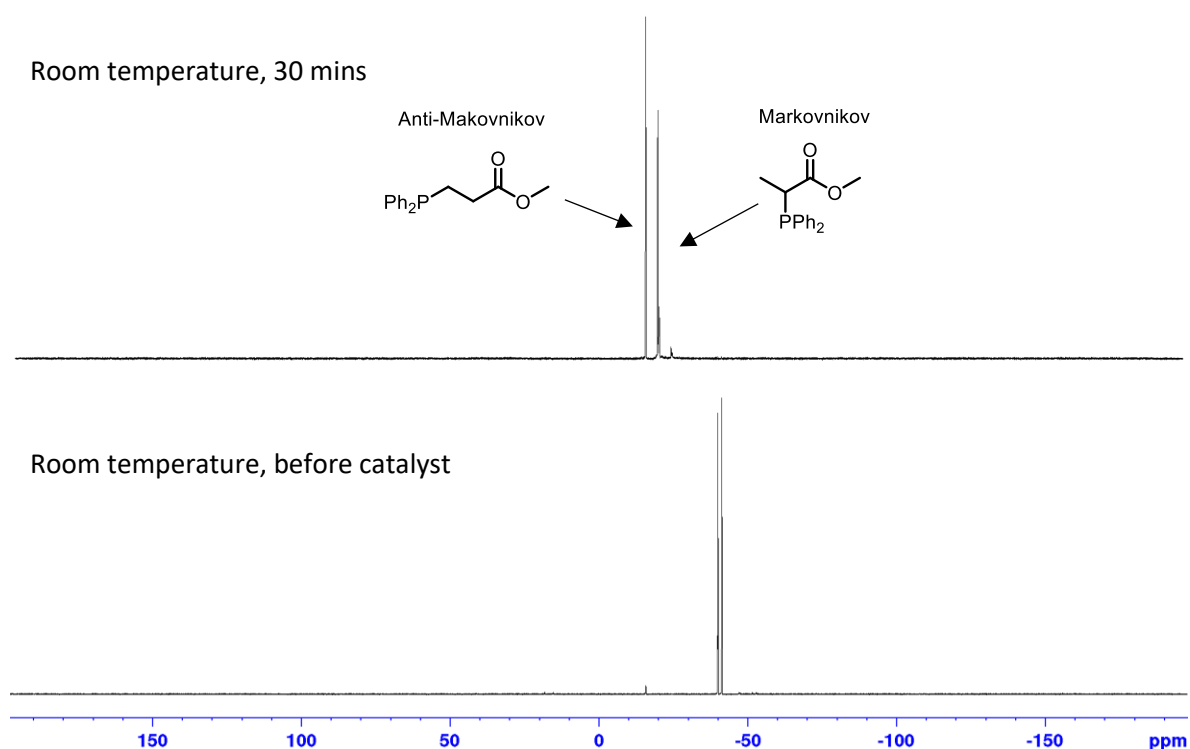


Figure S39: ^{31}P NMR spectrum for the hydrophosphination of methyl acrylate catalysed by **1** (10 mol%) in d_8 -toluene.

Hydrophosphination Using **2** as a Catalyst

Phenylacetylene catalysed by **2**

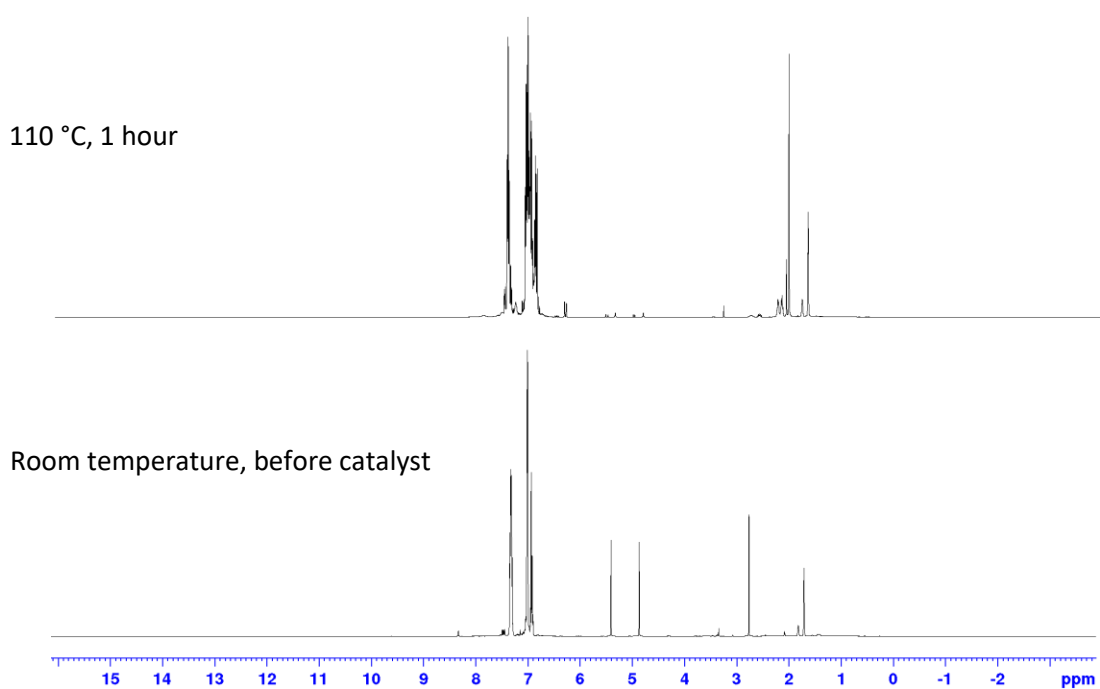


Figure S40: ^1H NMR for the hydrophosphination of phenylacetylene catalysed by **2** (10 mol%) in d_8 -toluene.

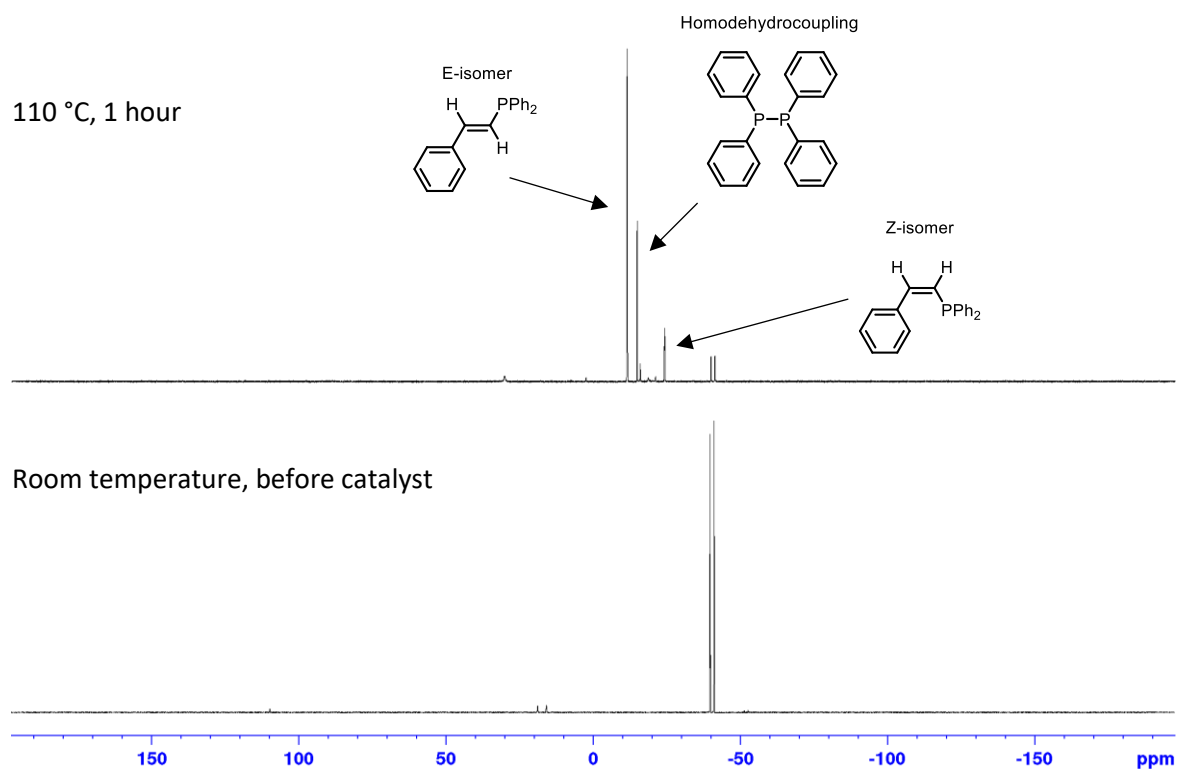


Figure S41: ^{31}P NMR for the hydrophosphination of phenylacetylene catalysed by **2** (10 mol%) in d_8 -toluene.

Diphenylacetylene catalysed by **2**

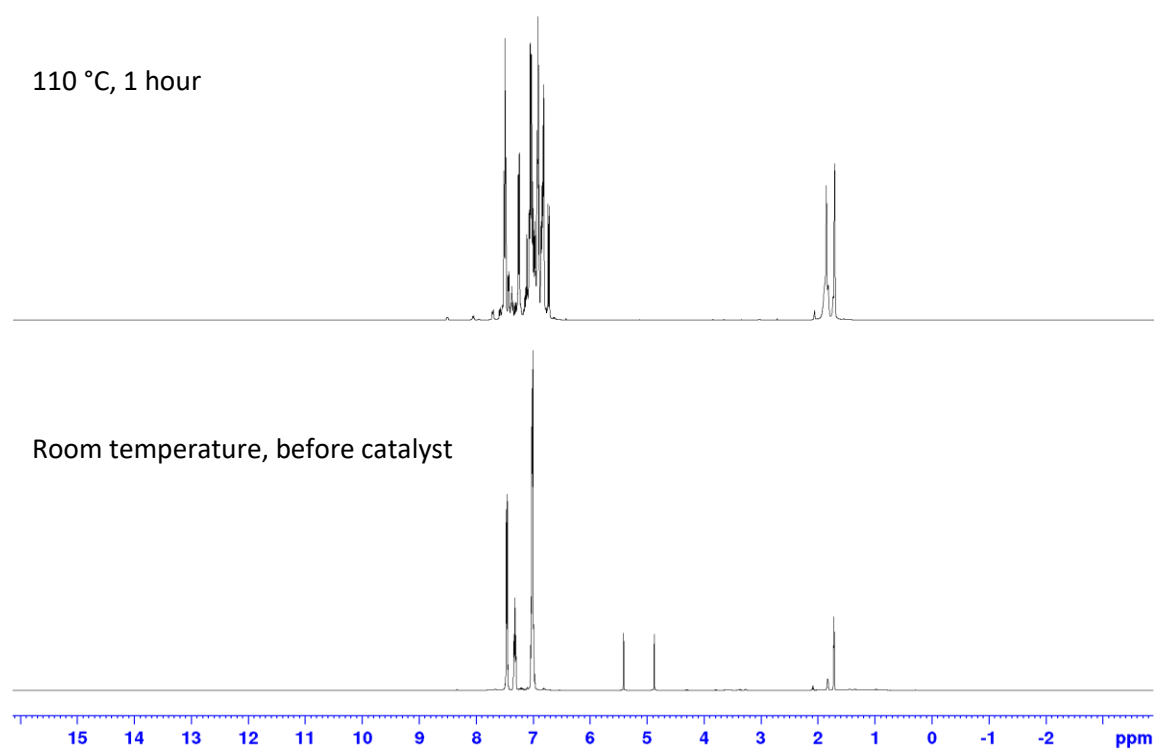


Figure S42: ^1H NMR spectrum for the hydrophosphination of diphenylacetylene catalysed by **2** (10 mol%) in d_8 -toluene.

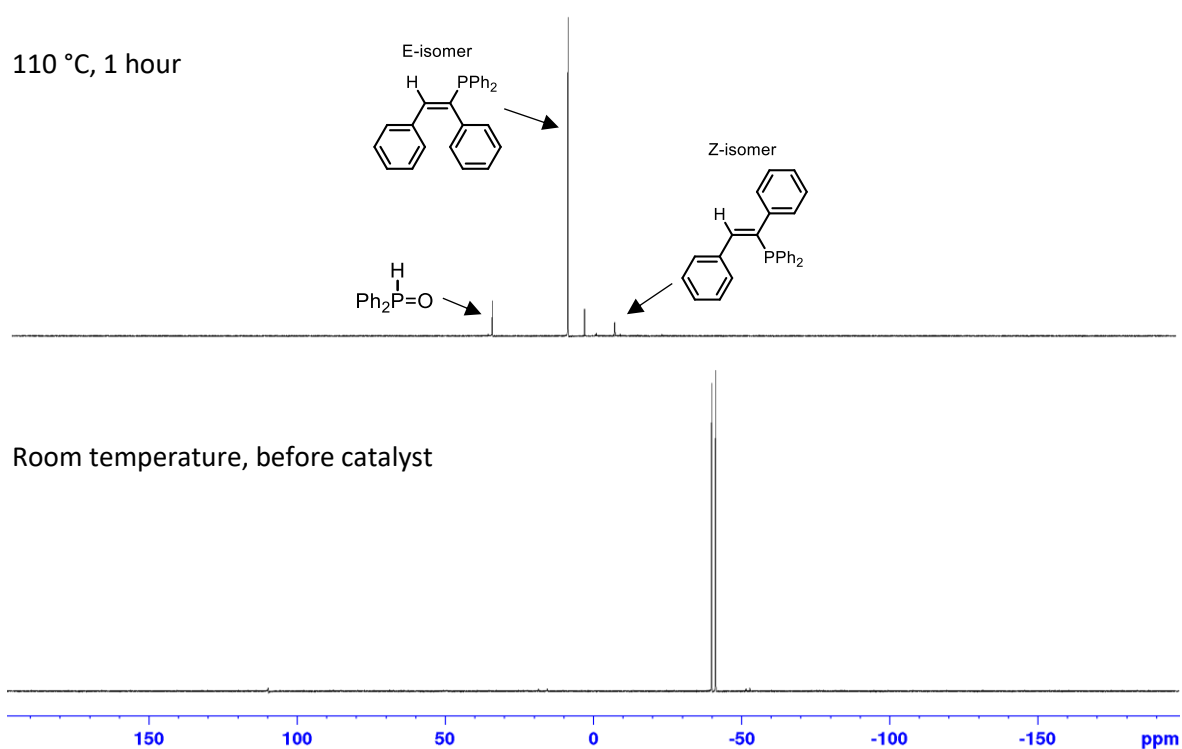


Figure S43: ^{31}P NMR spectrum for the hydrophosphination of diphenylacetylene catalysed by **2** (10 mol%) in d_8 -toluene.

4'-Methylphenylacetylene catalysed by **2**

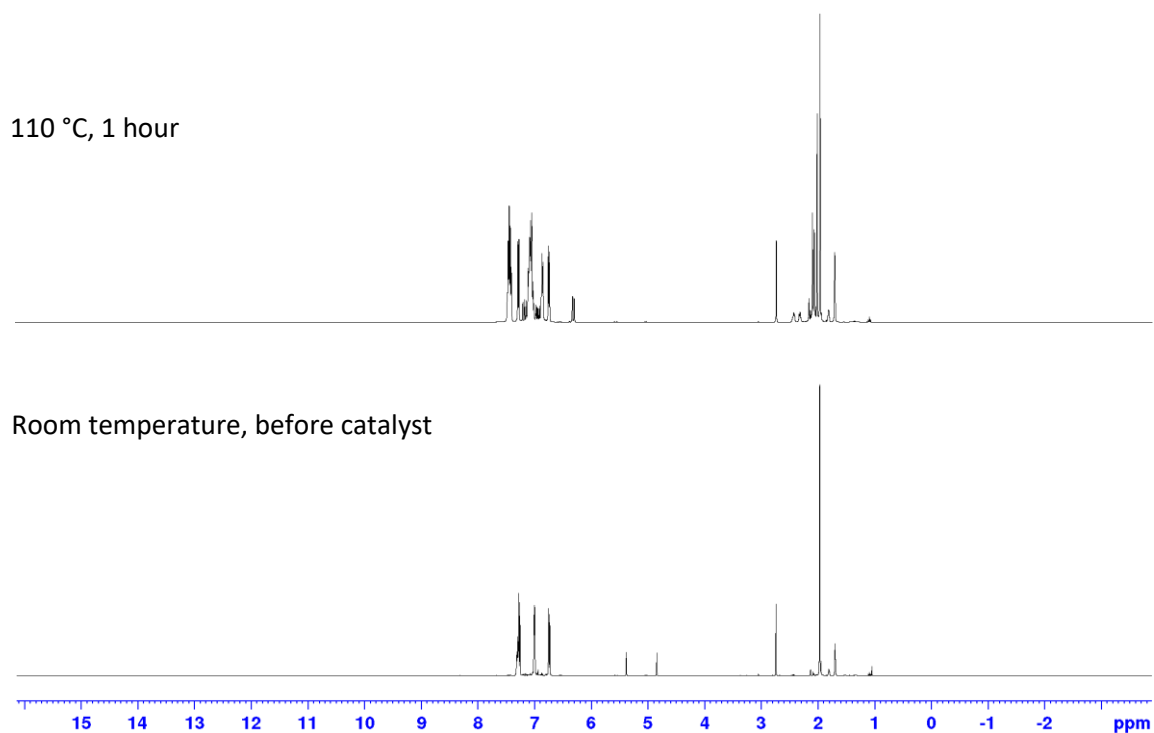


Figure S44: ^1H NMR spectrum for the hydrophosphination of 4'-methylphenylacetylene catalysed by **2** (10 mol%) in d_8 -toluene.

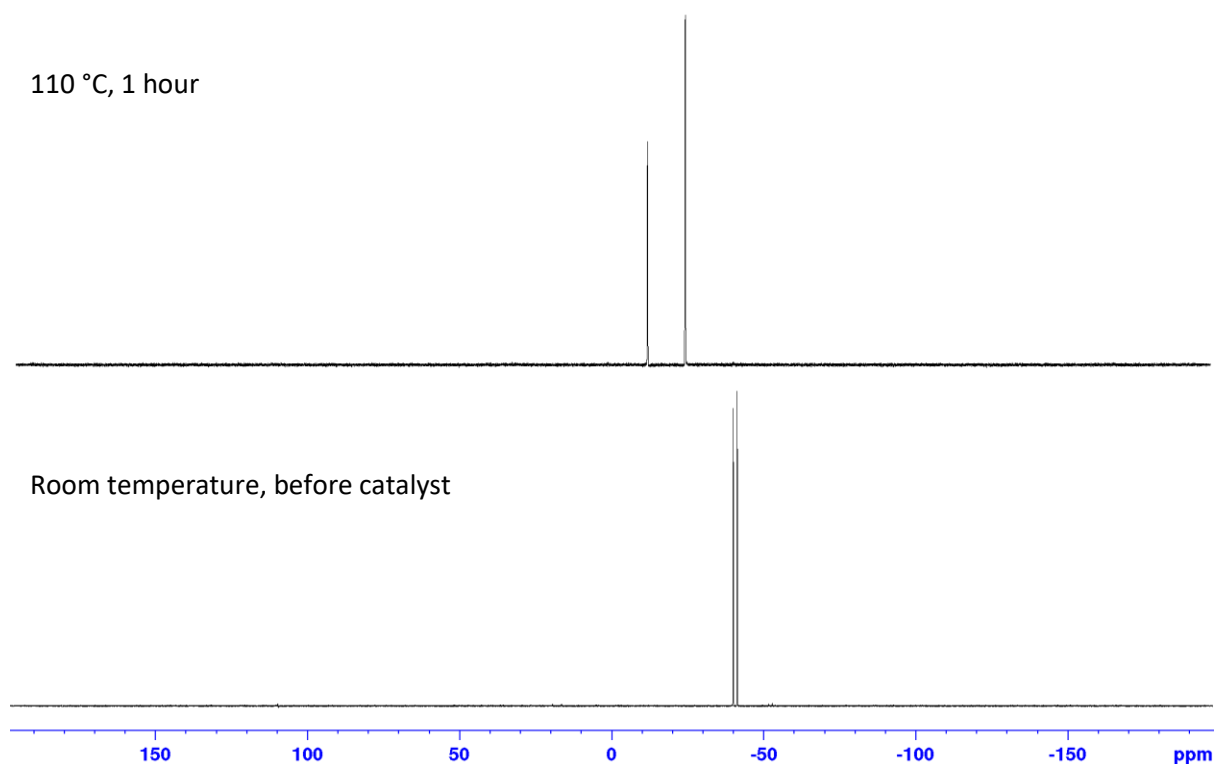


Figure S45: ^{31}P NMR spectrum for the hydrophosphination of 4'-methylphenylacetylene catalysed by **2** (10 mol%) in d_8 -toluene.

4'-Trifluoromethylphenylacetylene catalysed by **2**

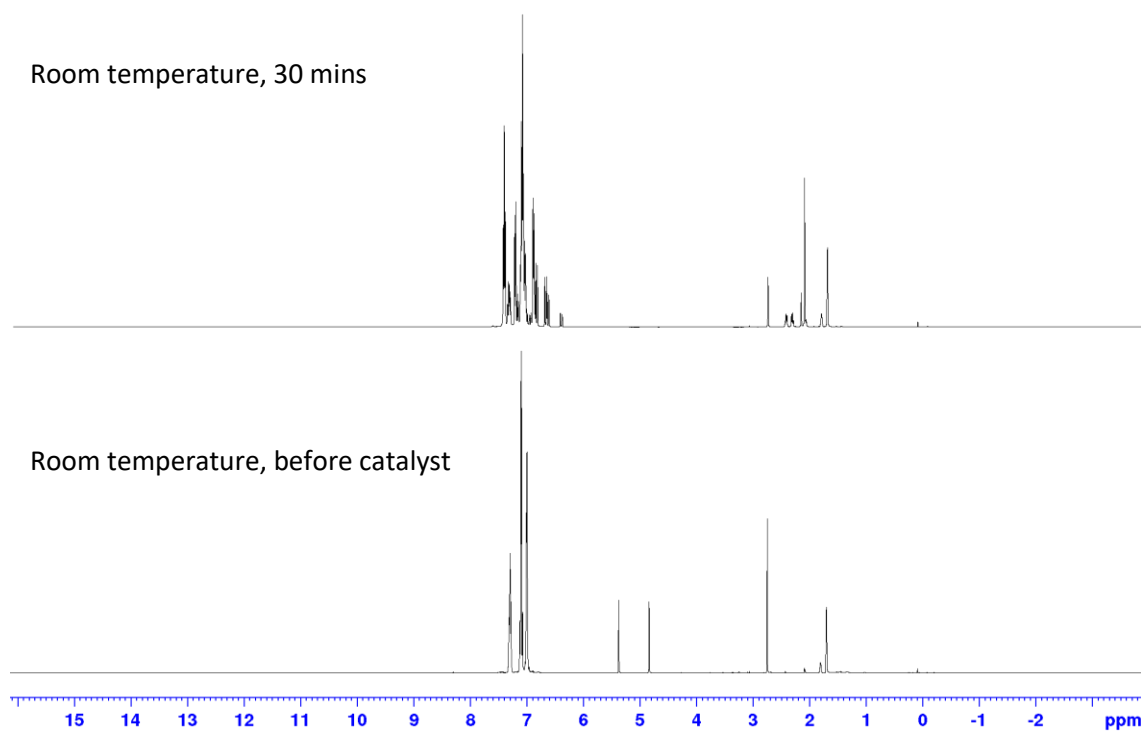


Figure S46: ^1H NMR spectrum for the hydrophosphination of 4'-trifluoromethylphenylacetylene catalysed by **2** (10 mol%) in d_8 -toluene.

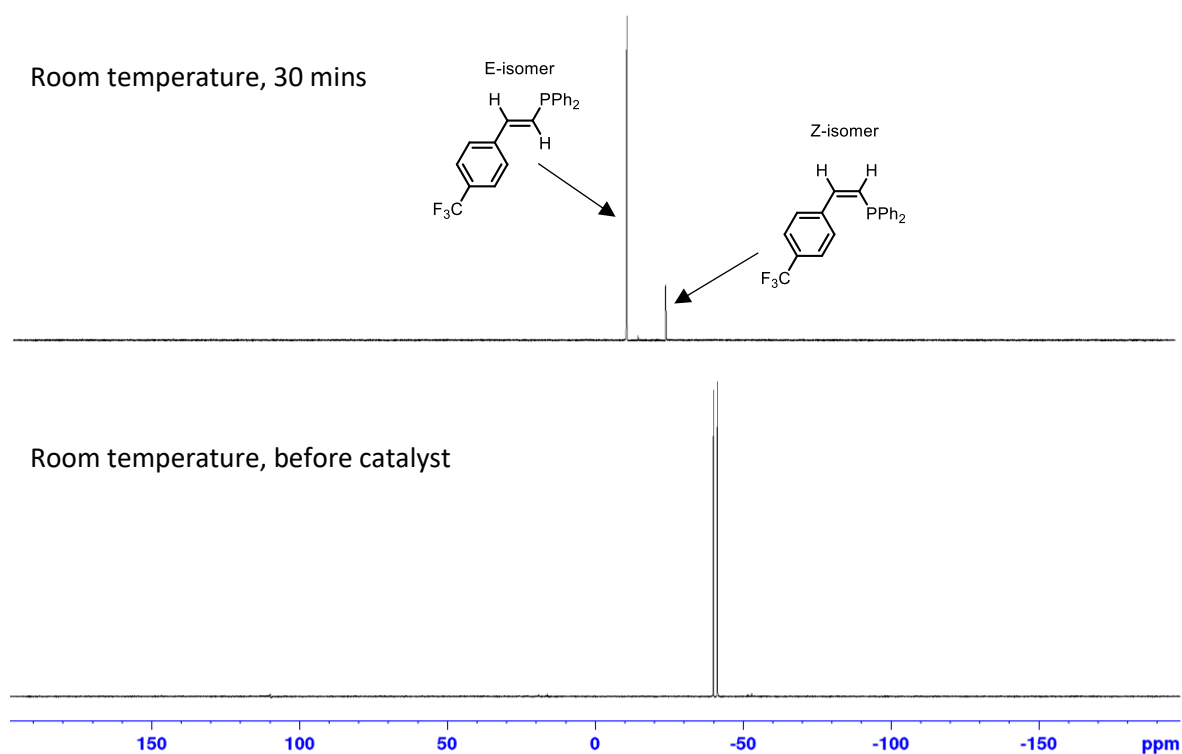


Figure S47: ^{31}P NMR spectrum for the hydrophosphination of 4'-trifluoromethylphenylacetylene catalysed by **2** (10 mol%) in d_8 -toluene.

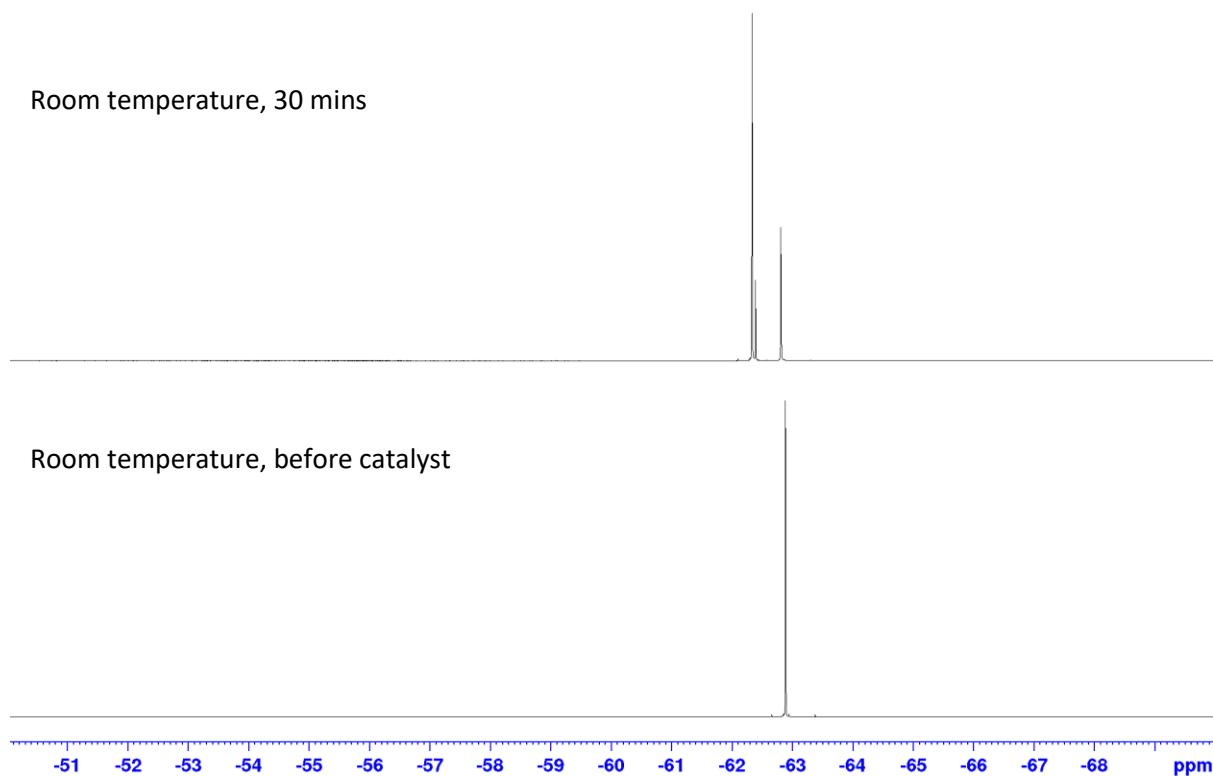


Figure S48: $^{19}\text{F}\{^1\text{H}\}$ NMR spectrum for the hydrophosphination of 4'-trifluoromethylphenylacetylene catalysed by **2** (10 mol%) in d_8 -toluene.

4-Cyanophenylacetylene catalysed by **2**

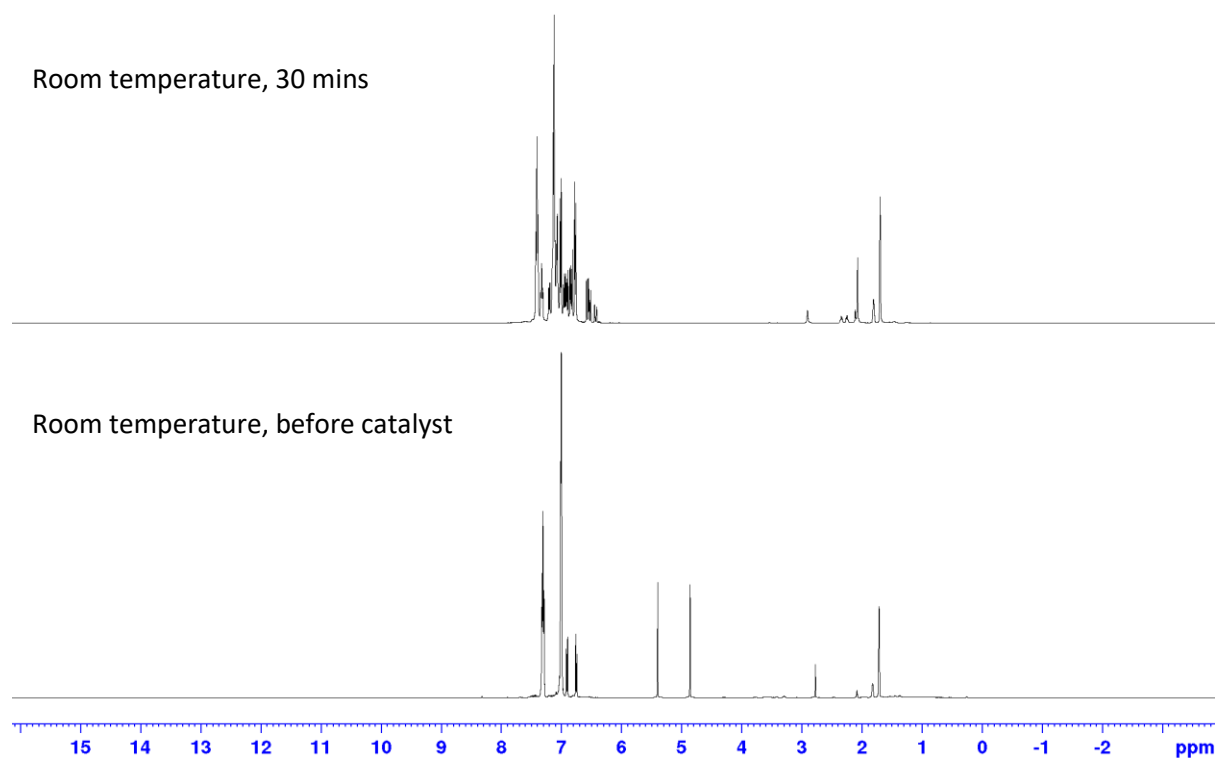


Figure S49: ^1H NMR spectrum for the hydrophosphination of 4-cyanophenylacetylene catalysed by **2** (10 mol%) in d_8 -toluene.

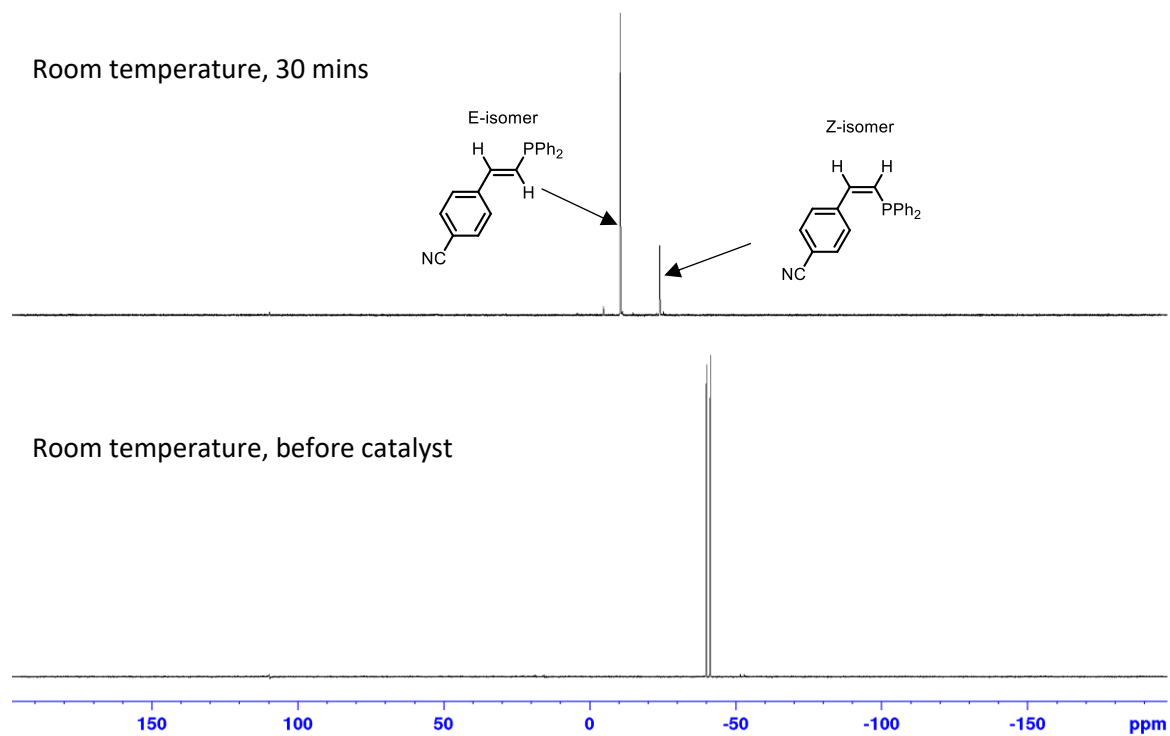


Figure S50: ^{31}P NMR spectrum for the hydrophosphination of 4-cyanophenylacetylene catalysed by **2** (10 mol%) in d_8 -toluene.

3-Phenyl-1-propyne catalysed by **2**

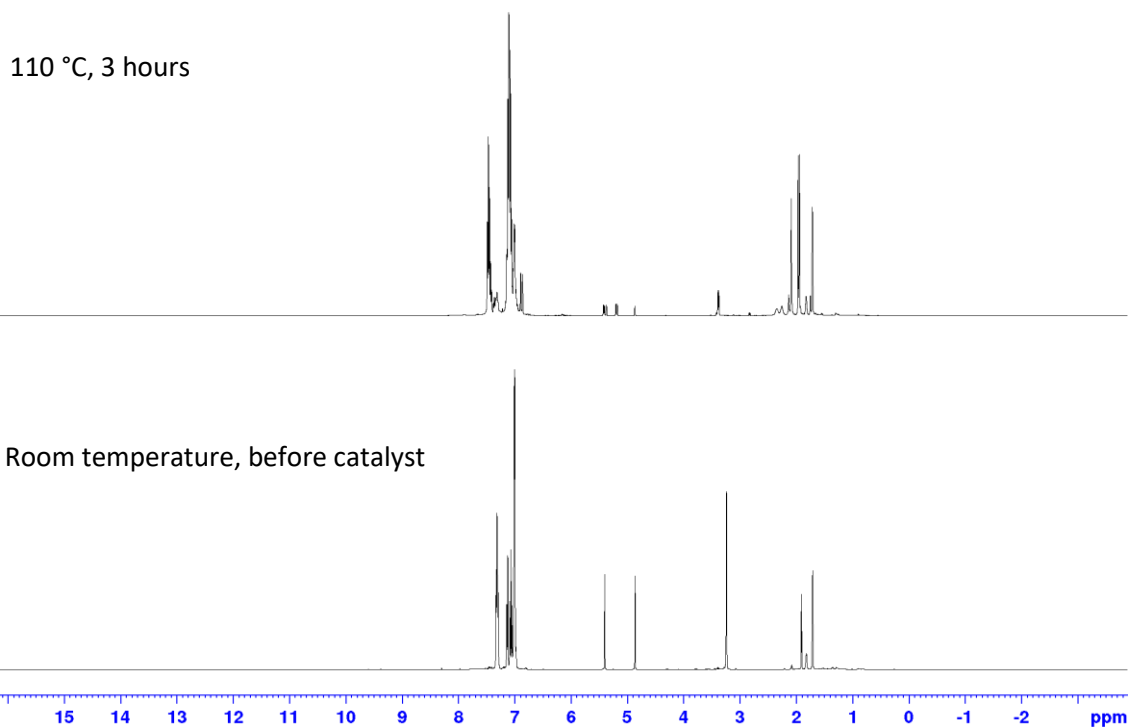


Figure S51: ^1H NMR spectrum for the hydrophosphination of 3-phenyl-1-propyne catalysed by **2** (10 mol%) in d_8 -toluene.

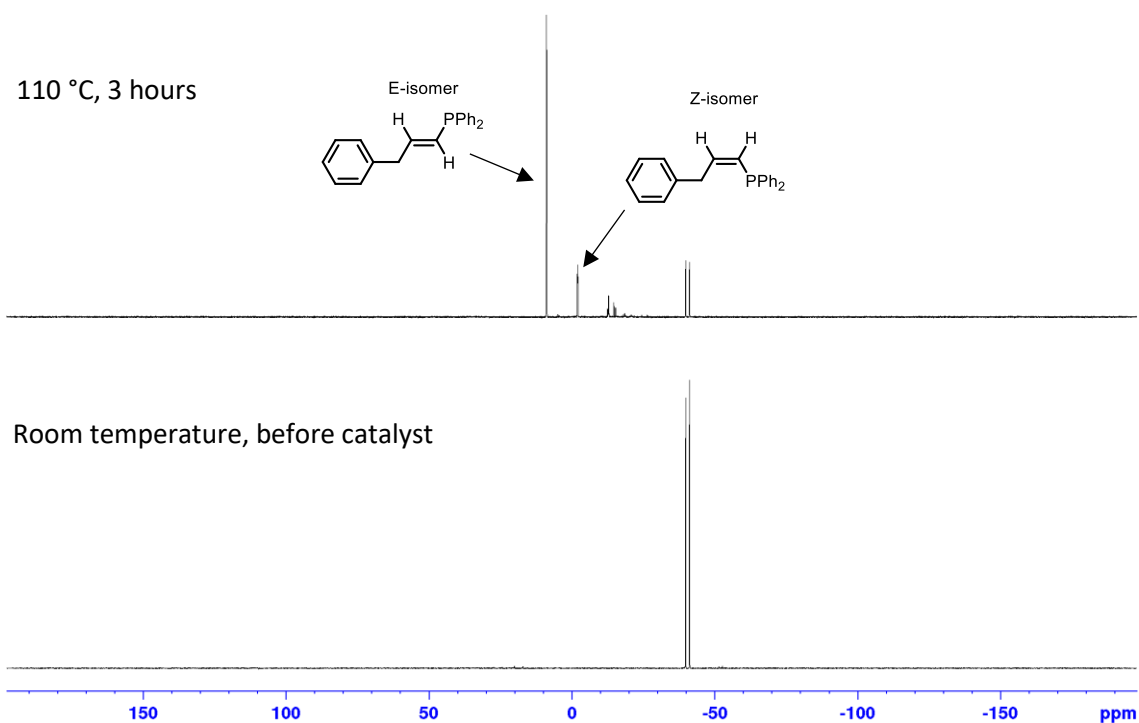


Figure S52: ^{31}P NMR spectrum for the hydrophosphination of 3-phenyl-1-propyne catalysed by **2** (10 mol%) in d_8 -toluene.

4-Phenyl-1-butyne catalysed by **2**

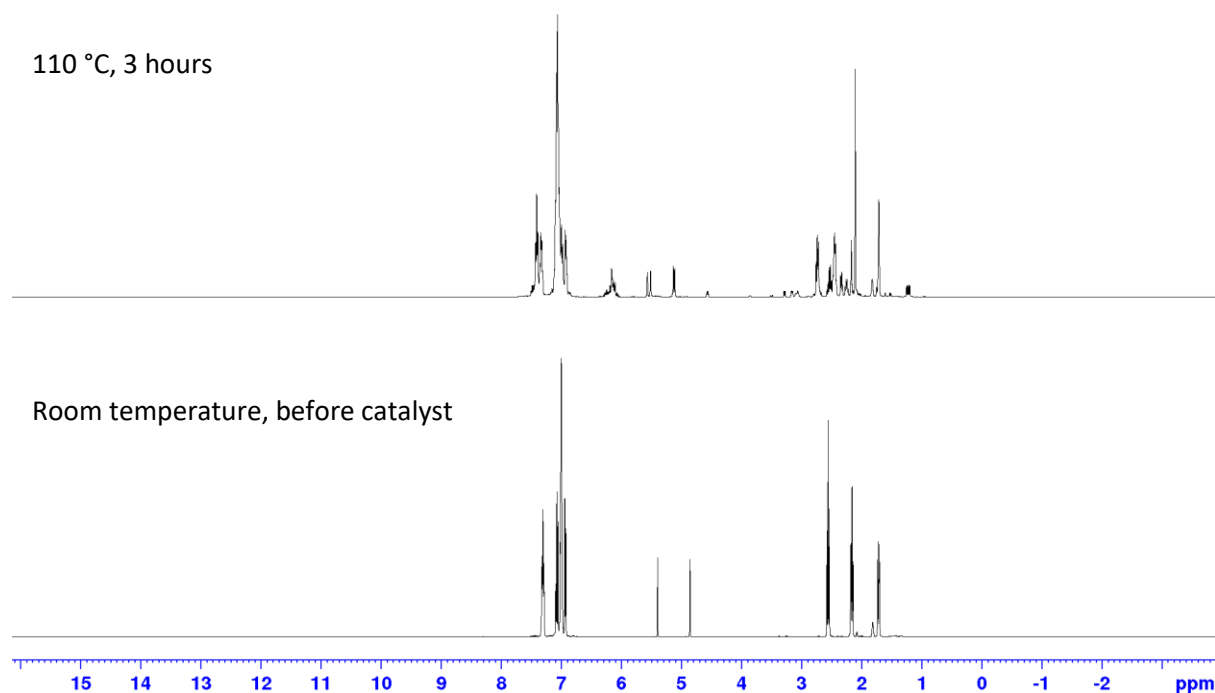


Figure S53: ^1H NMR spectrum for the hydrophosphination of 4-phenyl-1-butyne catalysed by **2** (10 mol%) in d_8 -toluene.

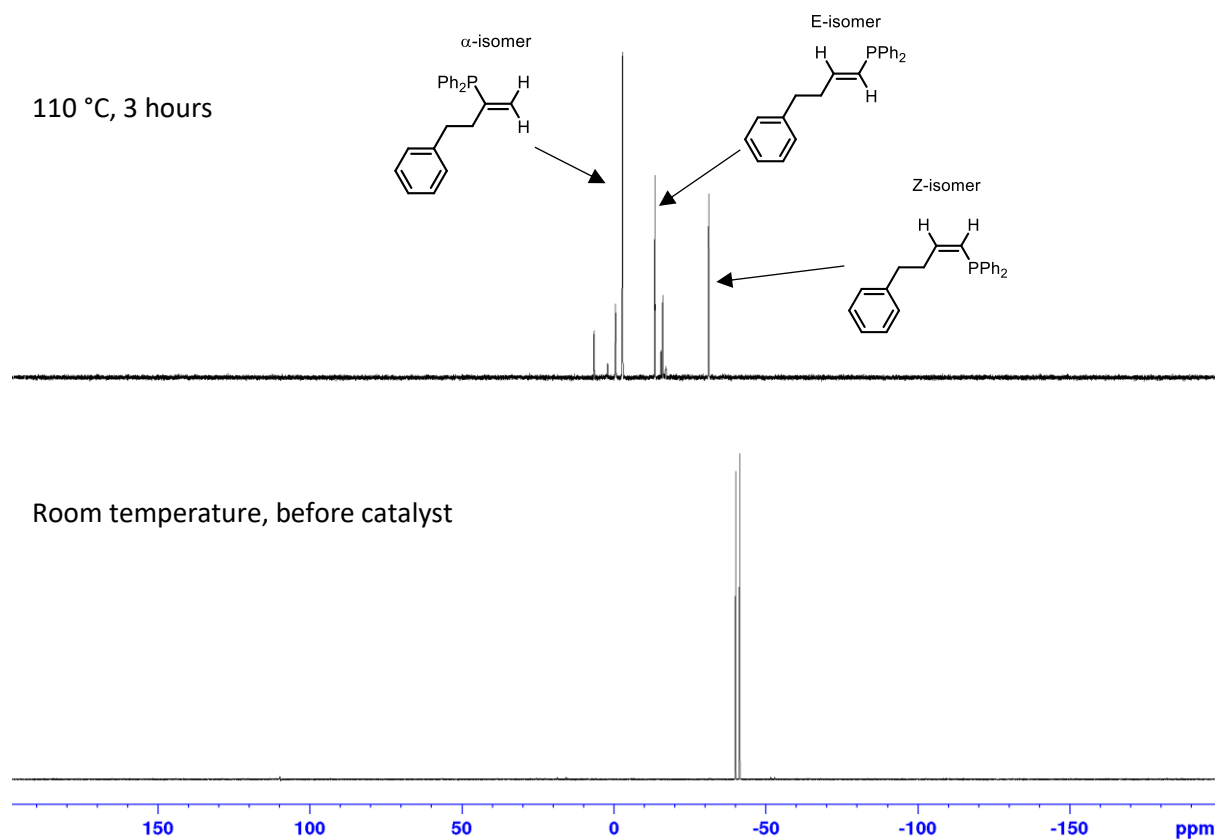


Figure S54: ^{31}P NMR spectrum for the hydrophosphination of 4-phenyl-1-butyne catalysed by **2** (10 mol%) in d_8 -toluene.

1-Octyne catalysed by **2**

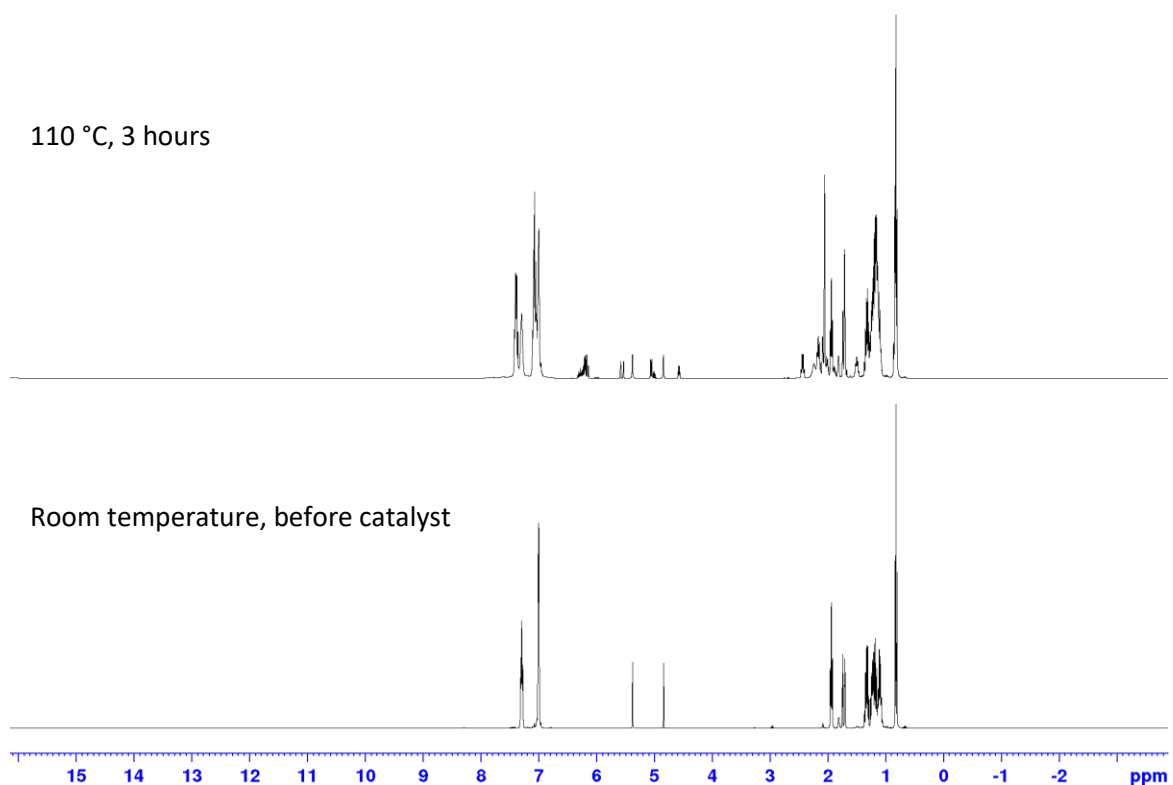


Figure S55: ^1H NMR spectrum for the hydrophosphination of 1-octyne catalysed by **2** (10 mol%) in d_8 -toluene.

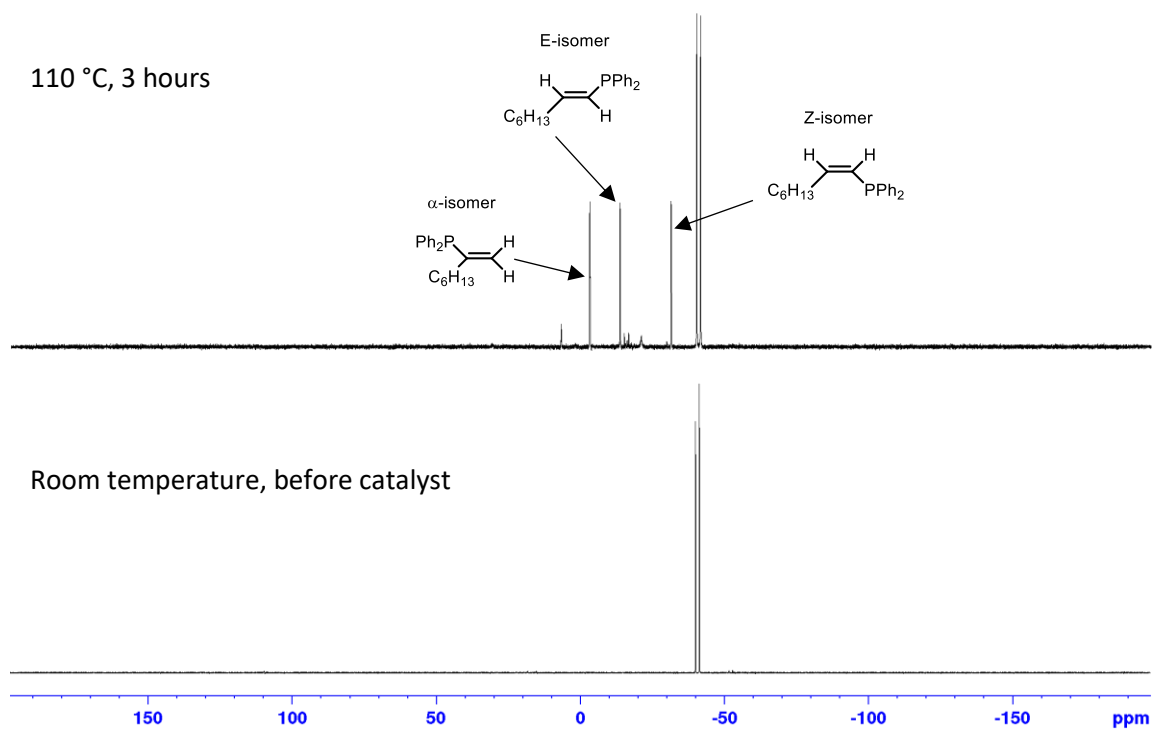
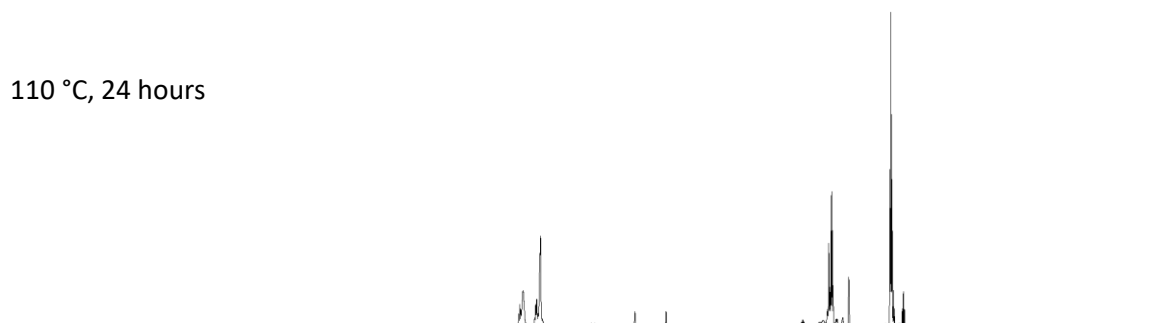


Figure S56: ^{31}P NMR spectrum for the hydrophosphination of 1-octyne catalysed by **2** (10 mol%) in d_8 -toluene.

3-Hexyne catalysed by **2**

110 °C, 24 hours



Room temperature, before catalyst

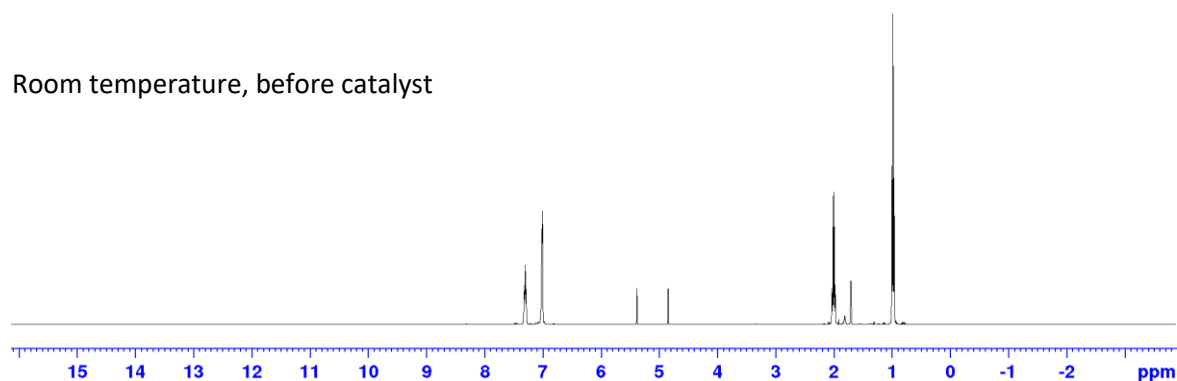
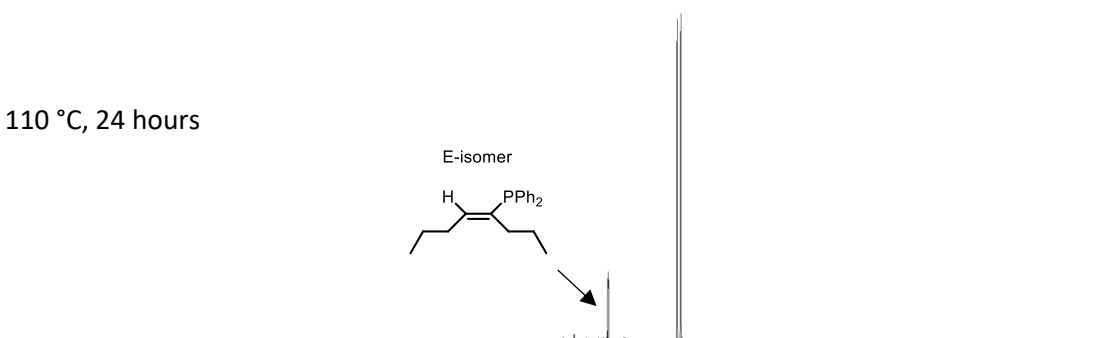


Figure S57: ¹H NMR spectrum for the hydrophosphination of 3-hexyne catalysed by **2** (10 mol%) in d₈-toluene.

110 °C, 24 hours



Room temperature, before catalyst

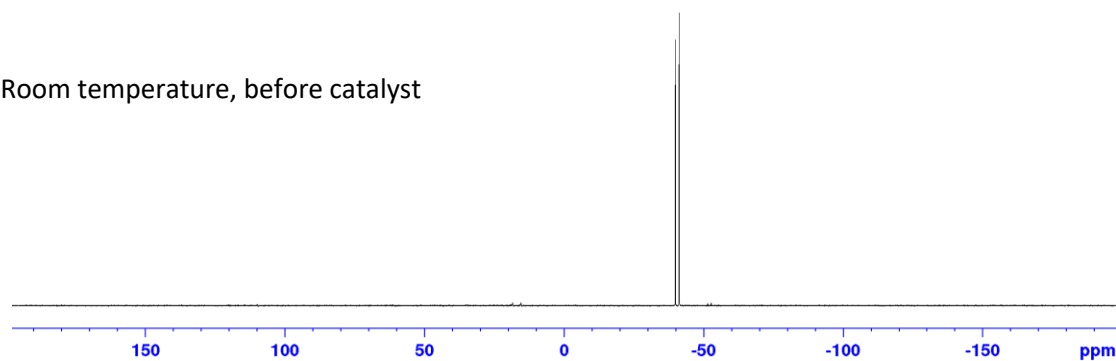


Figure S58: ³¹P NMR spectrum for the hydrophosphination of 3-hexyne catalysed by **2** (10 mol%) in d₈-toluene.

Styrene catalysed by **2**

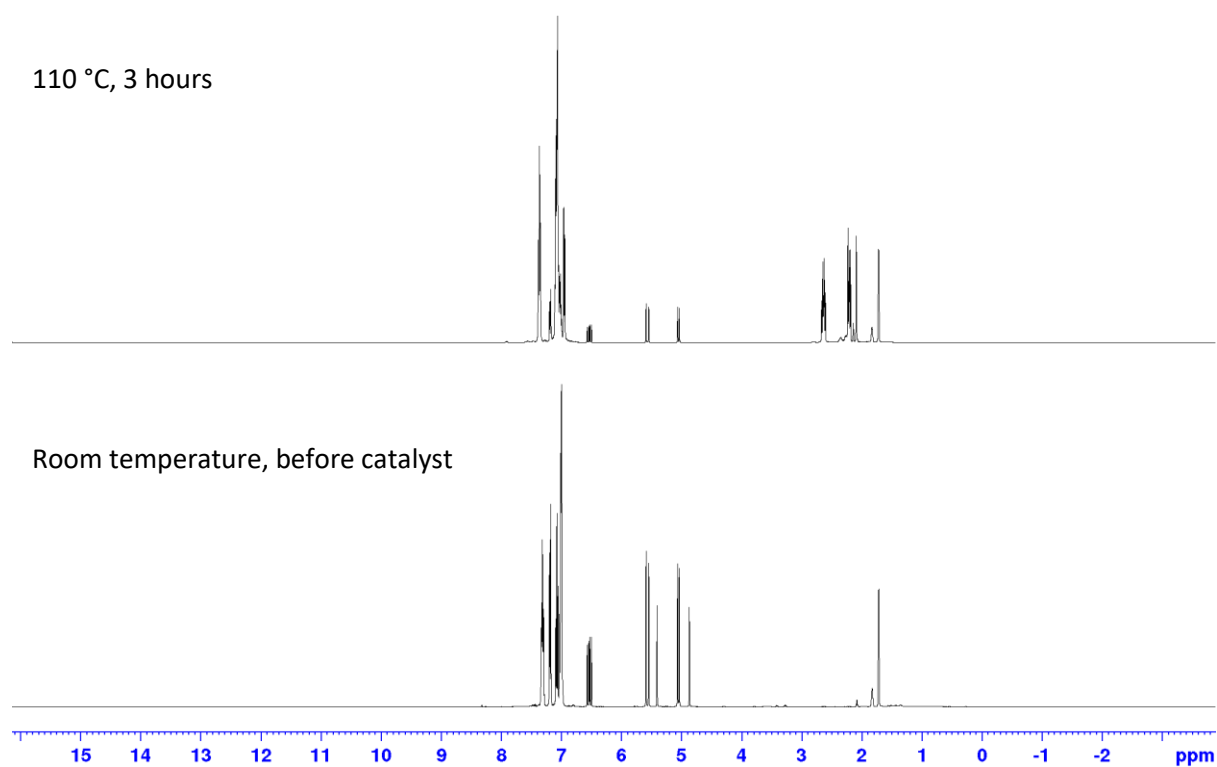


Figure S59: ¹H NMR spectrum for the hydrophosphination of styrene catalysed by **2** (10 mol%) in d₈-toluene.

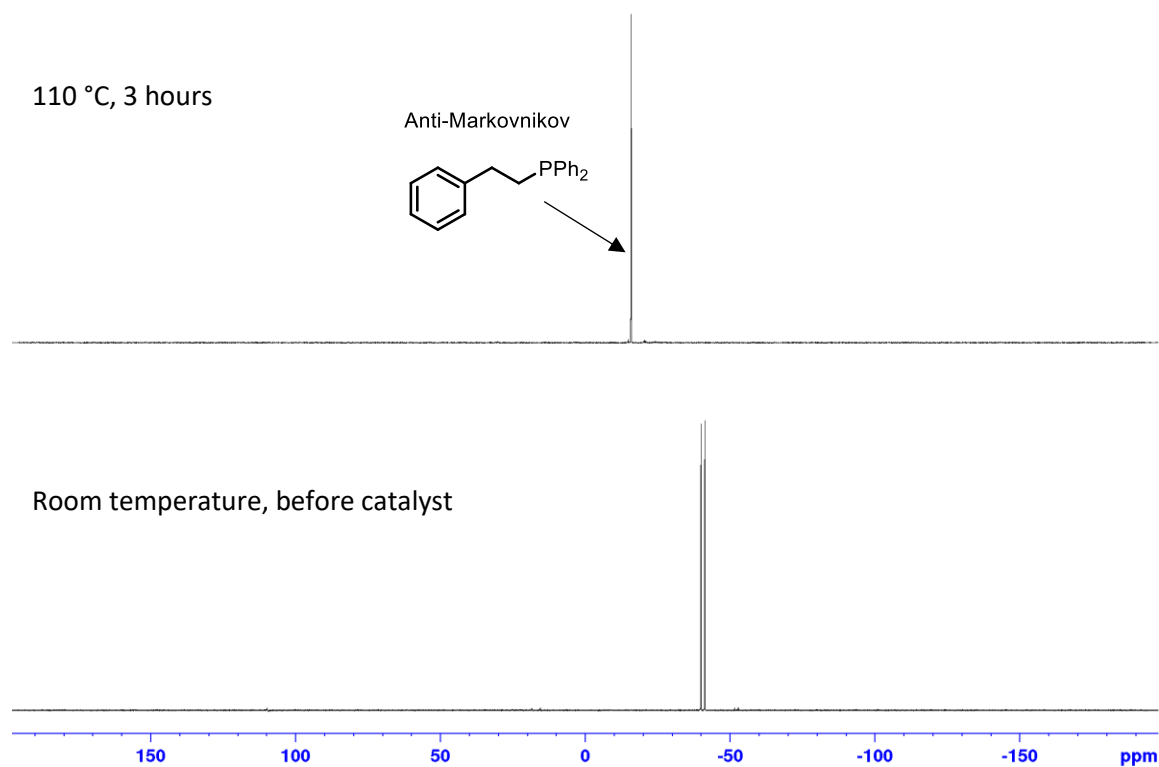


Figure S60: ³¹P NMR spectrum for the hydrophosphination of styrene catalysed by **2** (10 mol%) in d₈-toluene.

Methyl acrylate catalysed by **2**

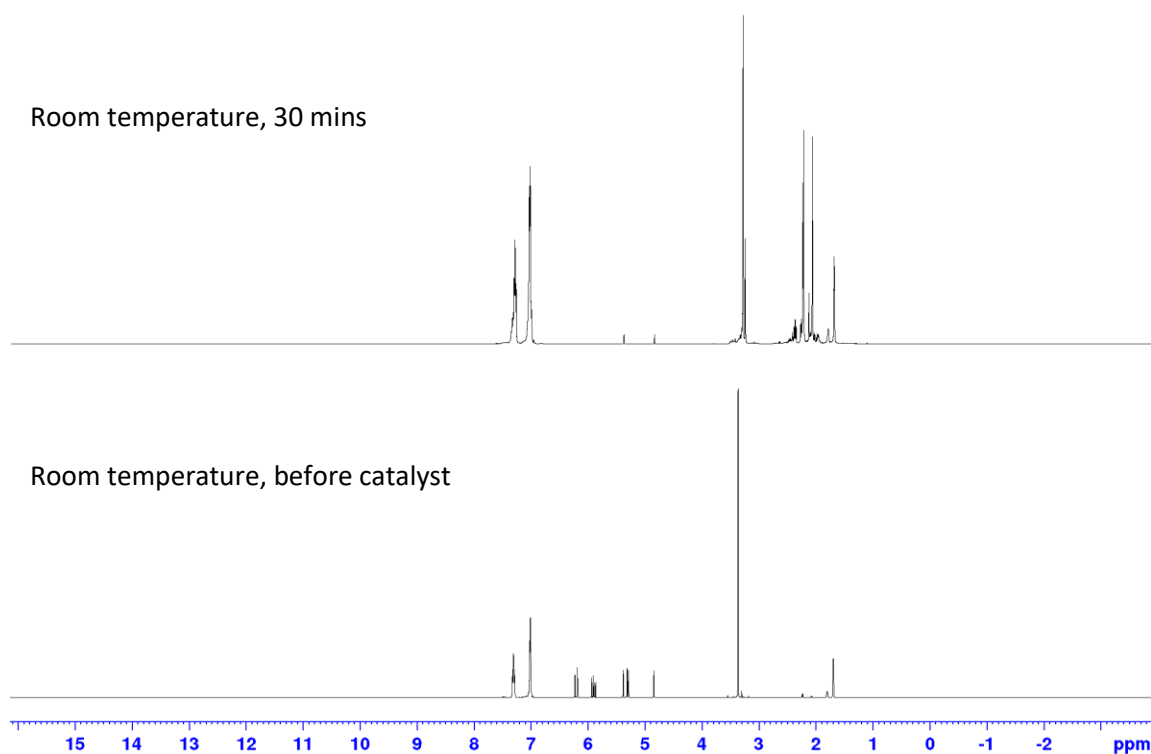


Figure S61: ^1H NMR spectrum for the hydrophosphination of methyl acrylate catalysed by **2** (10 mol%) in d_8 -toluene.

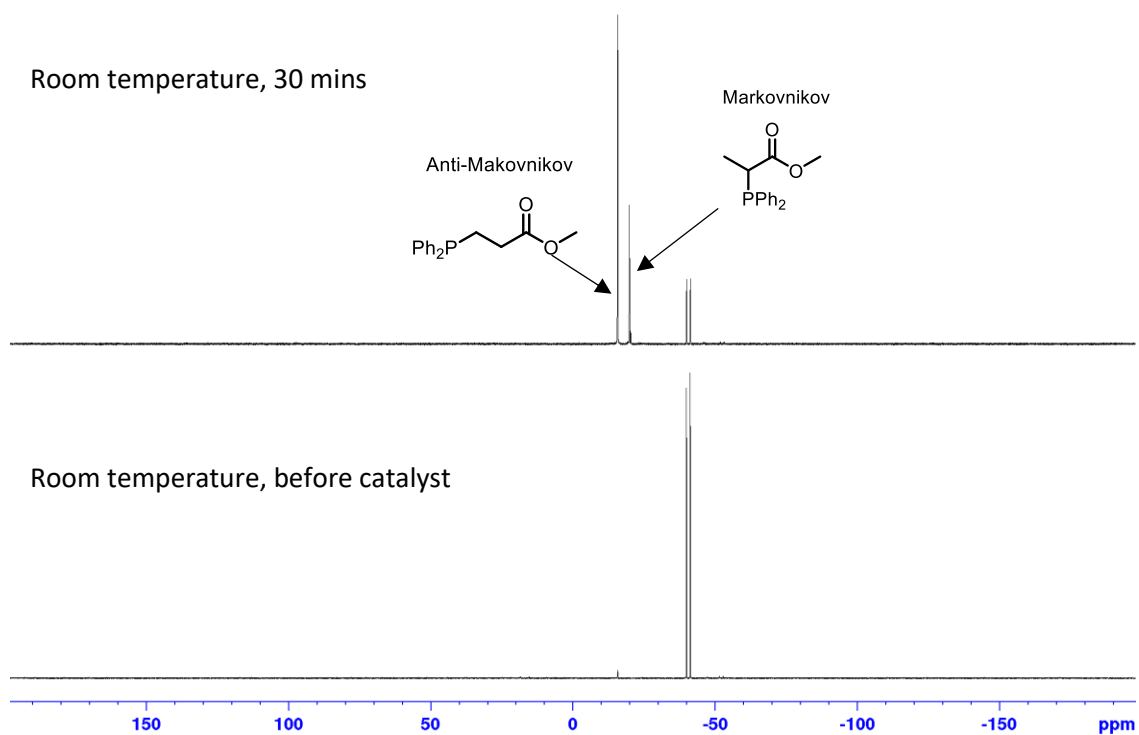


Figure S62: ^{31}P NMR spectrum for the hydrophosphination of methyl acrylate catalysed by **2** (10 mol%) in d_8 -toluene.

Hydrophosphination Using **3** as a Catalyst

Phenylacetylene catalysed by **3**

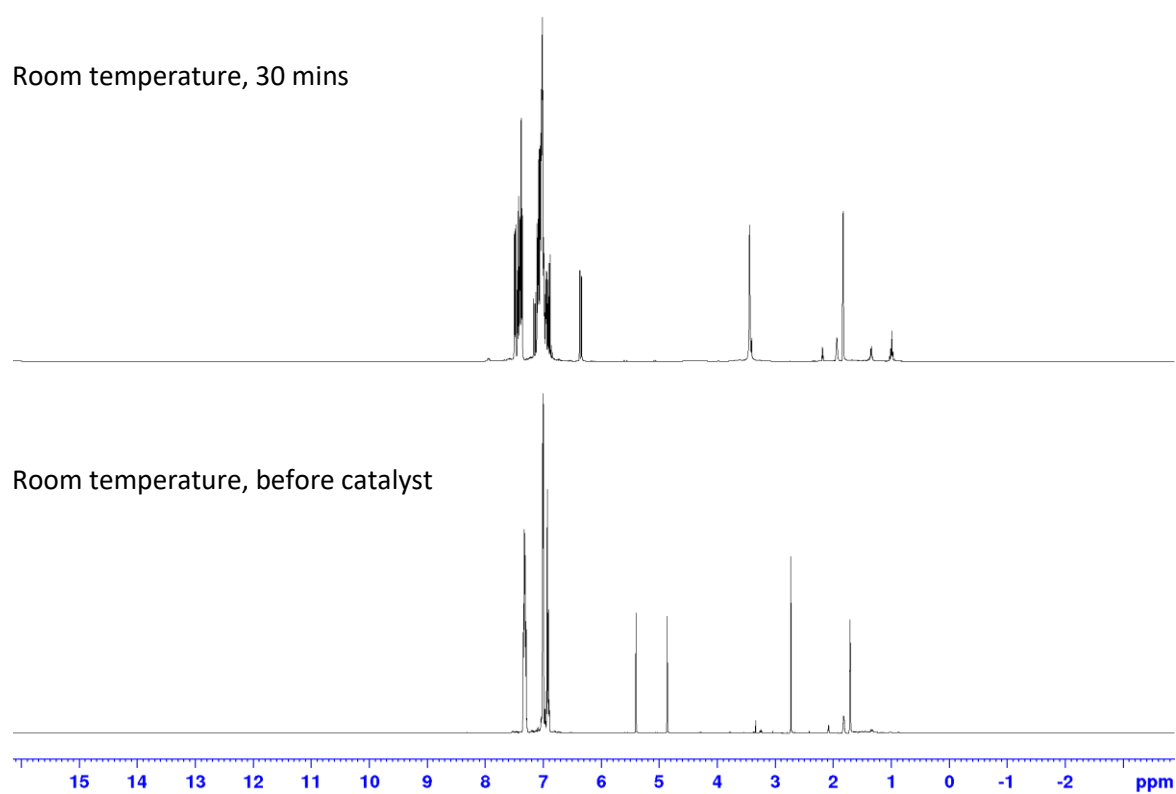


Figure S63: ^1H NMR spectrum for the hydrophosphination of phenylacetylene catalysed by **3** (10 mol%) in d_8 -toluene.

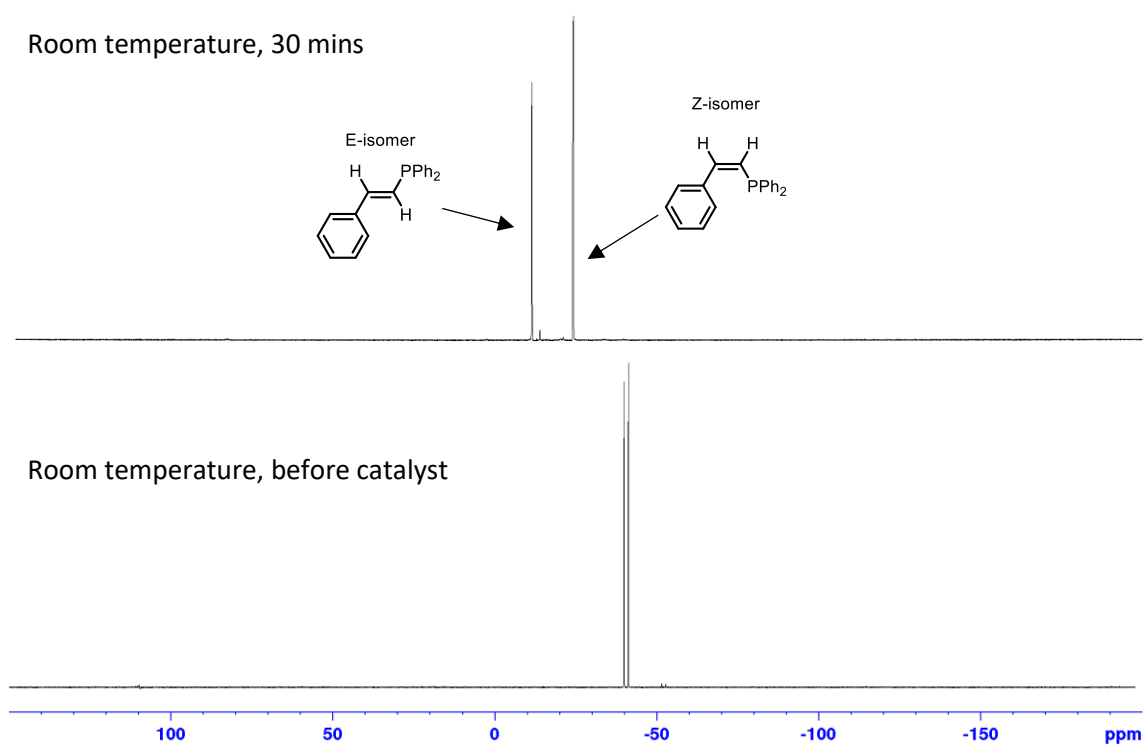


Figure S64: ^{31}P NMR spectrum for the hydrophosphination of phenylacetylene catalysed by **3** (10 mol%) in d_8 -toluene.

Diphenylacetylene catalysed by **3**

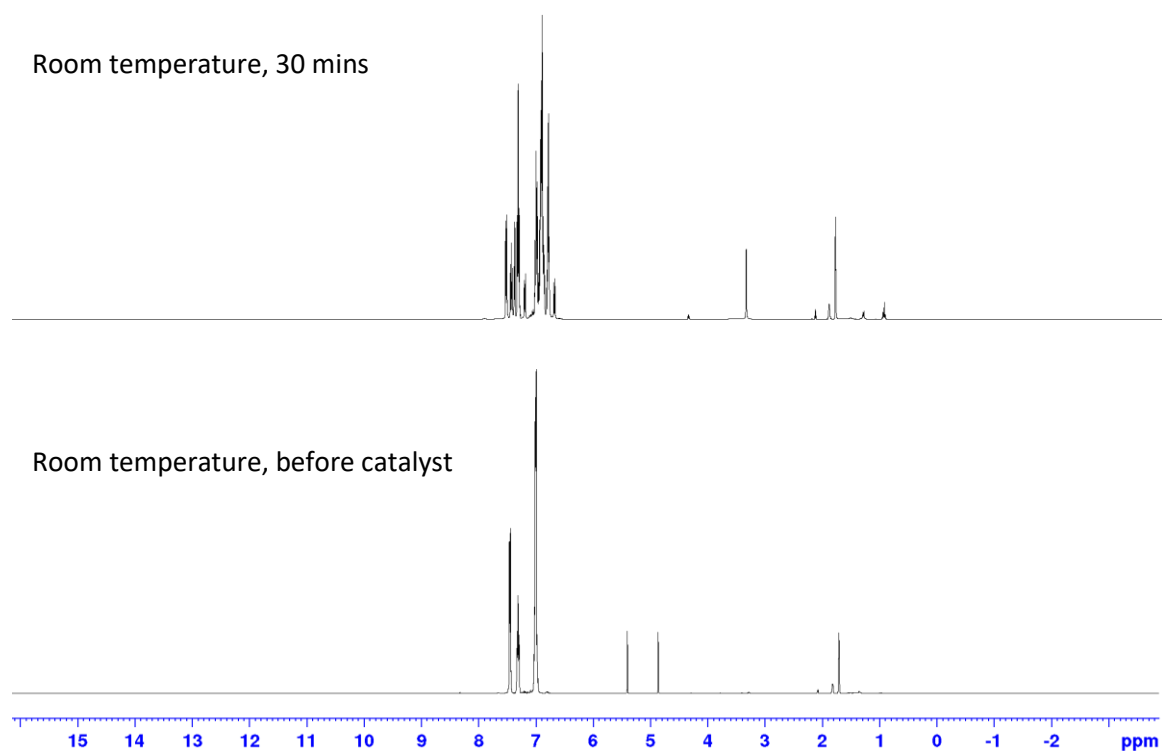


Figure S65: ^1H NMR spectrum for the hydrophosphination of diphenylacetylene catalysed by **3** (10 mol%) in d_8 -toluene.

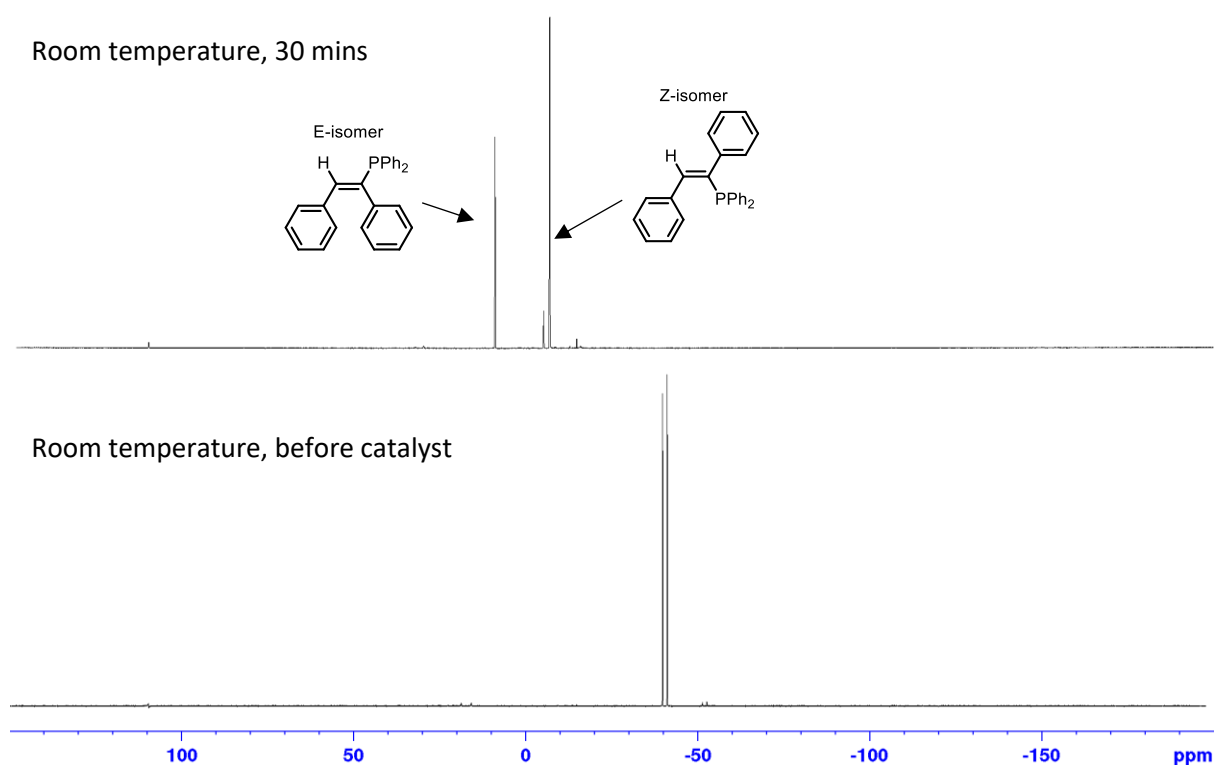


Figure S66: ^{31}P NMR spectrum for the hydrophosphination of diphenylacetylene catalysed by **3** (10 mol%) in d_8 -toluene.

4'-Methylphenylacetylene catalysed by **3**

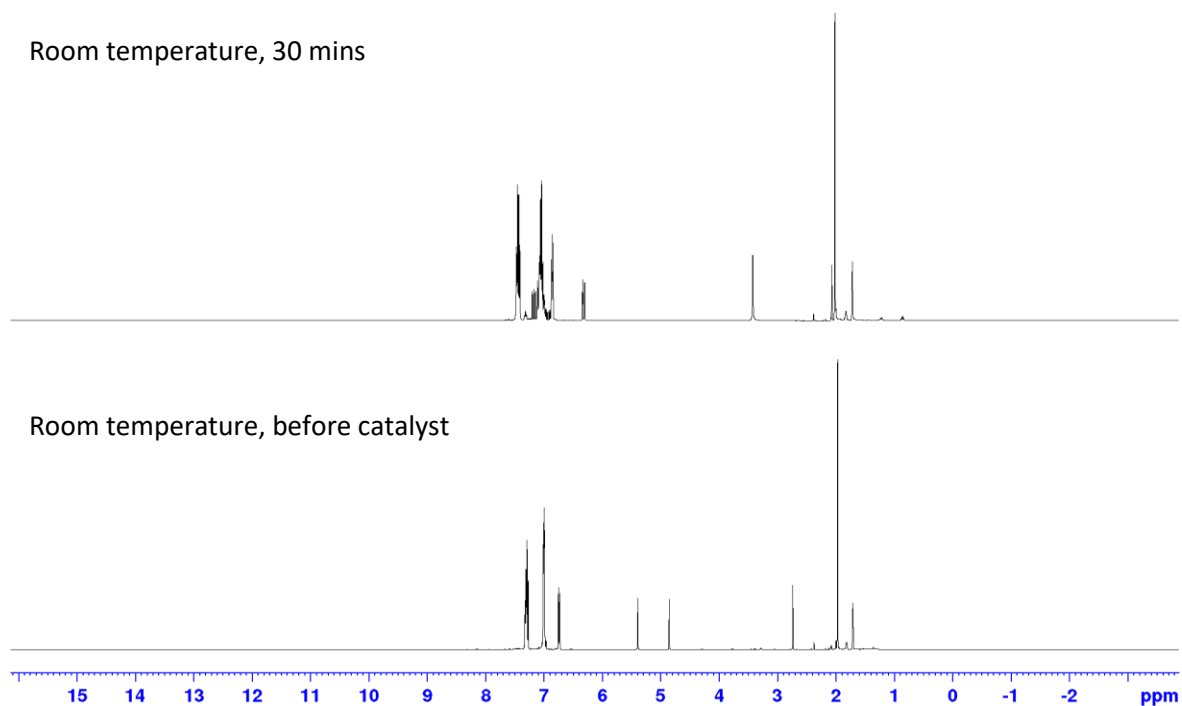


Figure S67: ^1H NMR spectrum for the hydrophosphination of 4'-methylphenylacetylene catalysed by **3** (10 mol%) in d_8 -toluene.

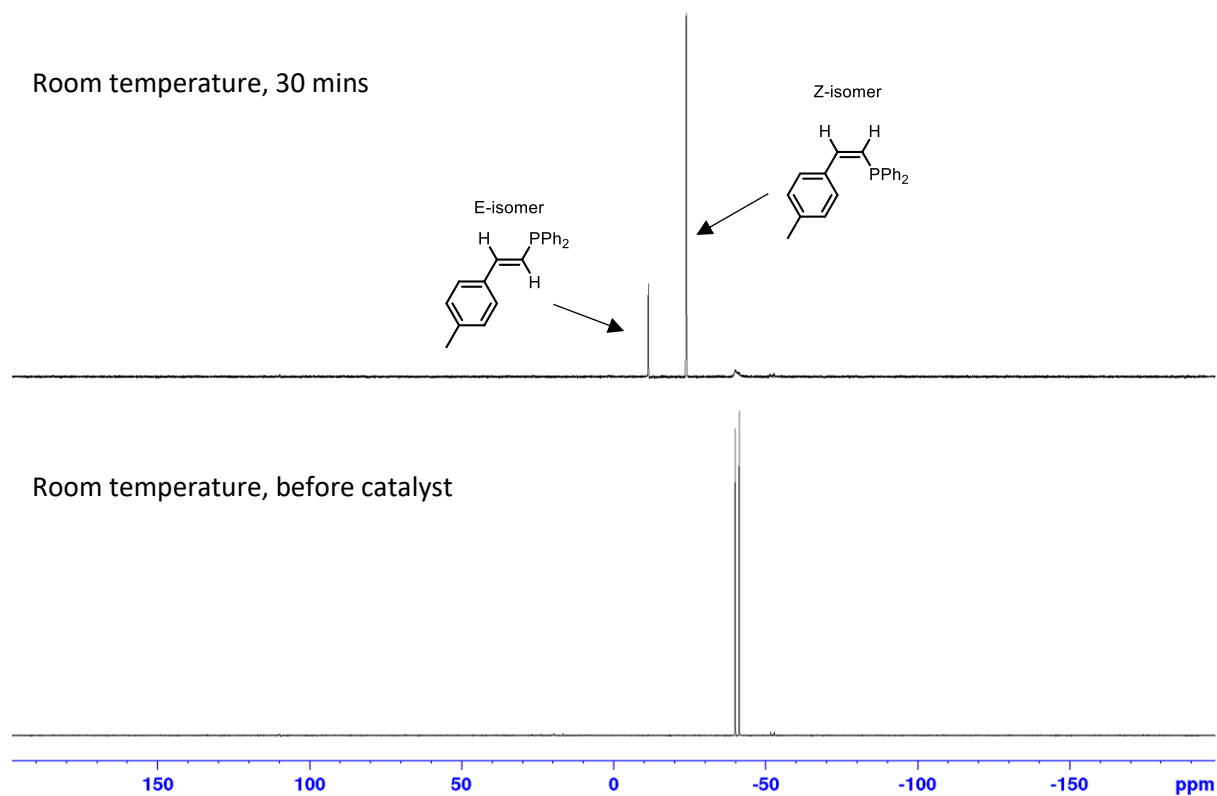


Figure S68: ^{31}P NMR spectrum for the hydrophosphination of 4'-methylphenylacetylene catalysed by **3** (10 mol%) in d_8 -toluene.

4'-Trifluoromethylphenylacetylene catalysed by **3**

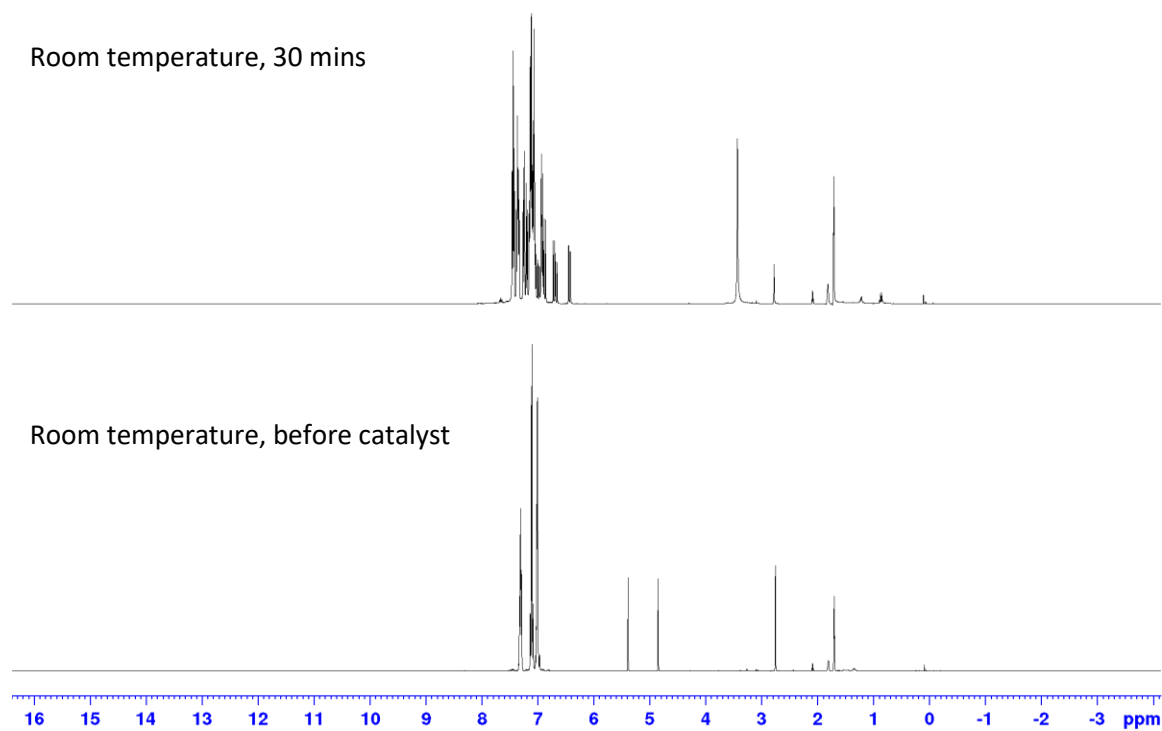


Figure S69: ^1H NMR spectrum for the hydrophosphination of 4'-trifluoromethylphenylacetylene catalysed by **3** (10 mol%) in d_8 -toluene.

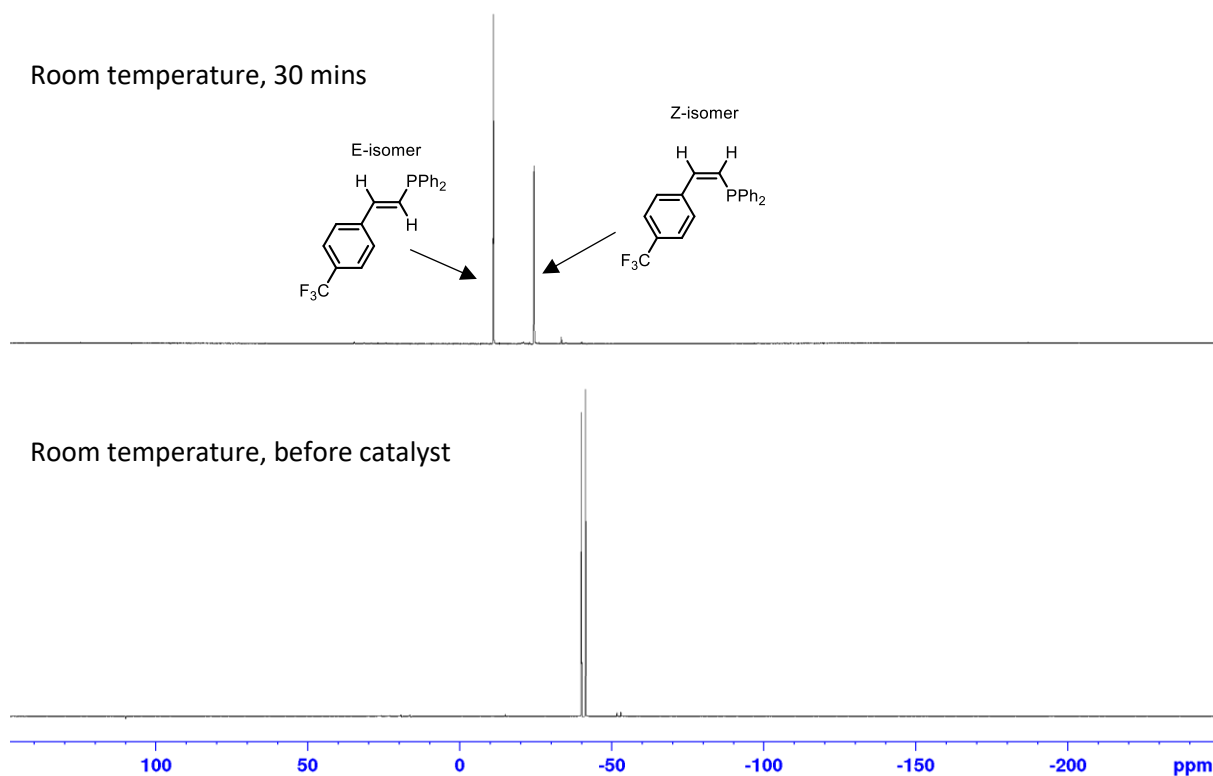


Figure S70: ³¹P NMR spectrum for the hydrophosphination of 4'-trifluoromethylphenylacetylene catalysed by **3** (10 mol%) in d₈-toluene.

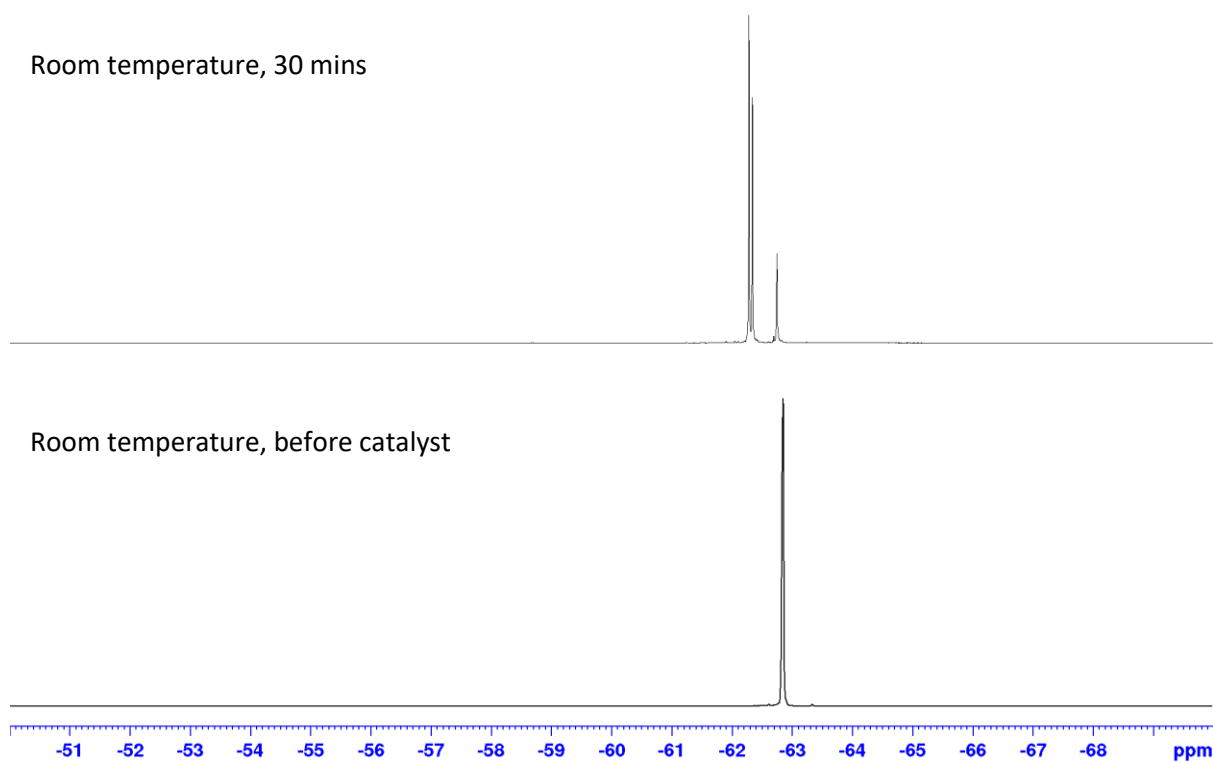


Figure S71: ¹⁹F{¹H} NMR spectrum for the hydrophosphination of 4'-trifluoromethylphenylacetylene catalysed by **3** (10 mol%) in d₈-toluene.

4-Cyanophenylacetylene catalysed by **3**

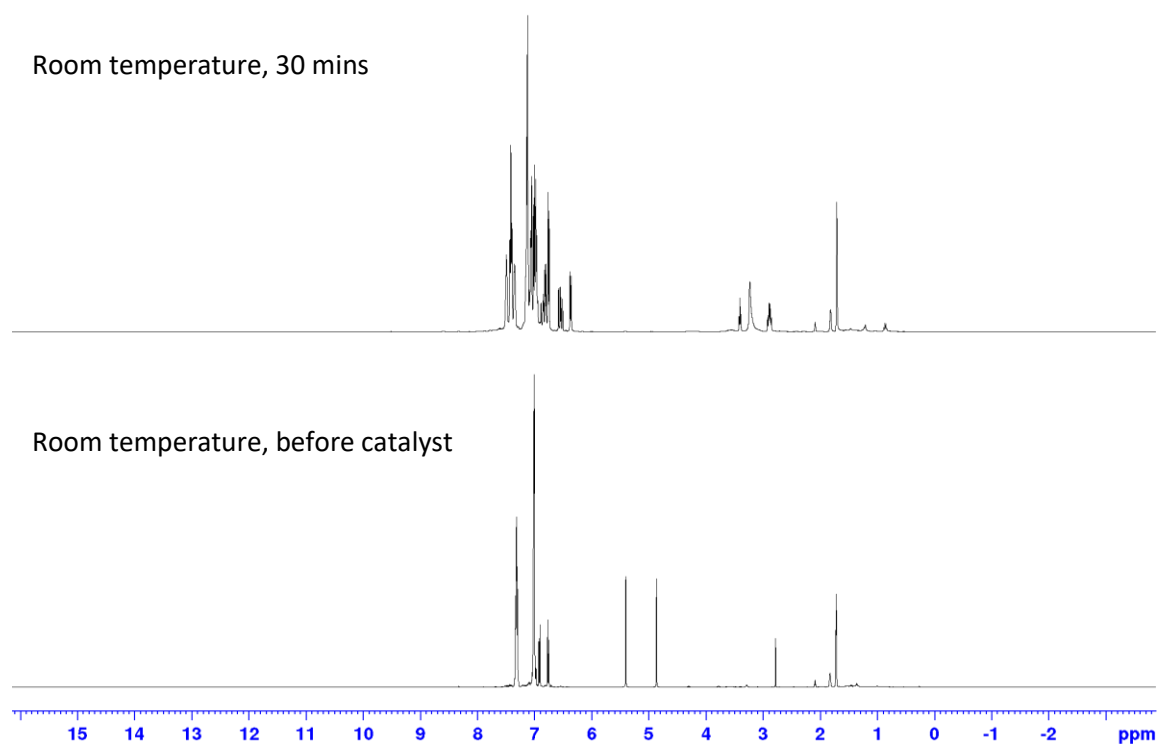


Figure S72: ¹H NMR spectrum for the hydrophosphination of 4-cyanophenylacetylene catalysed by **3** (10 mol%) in d₈-toluene.

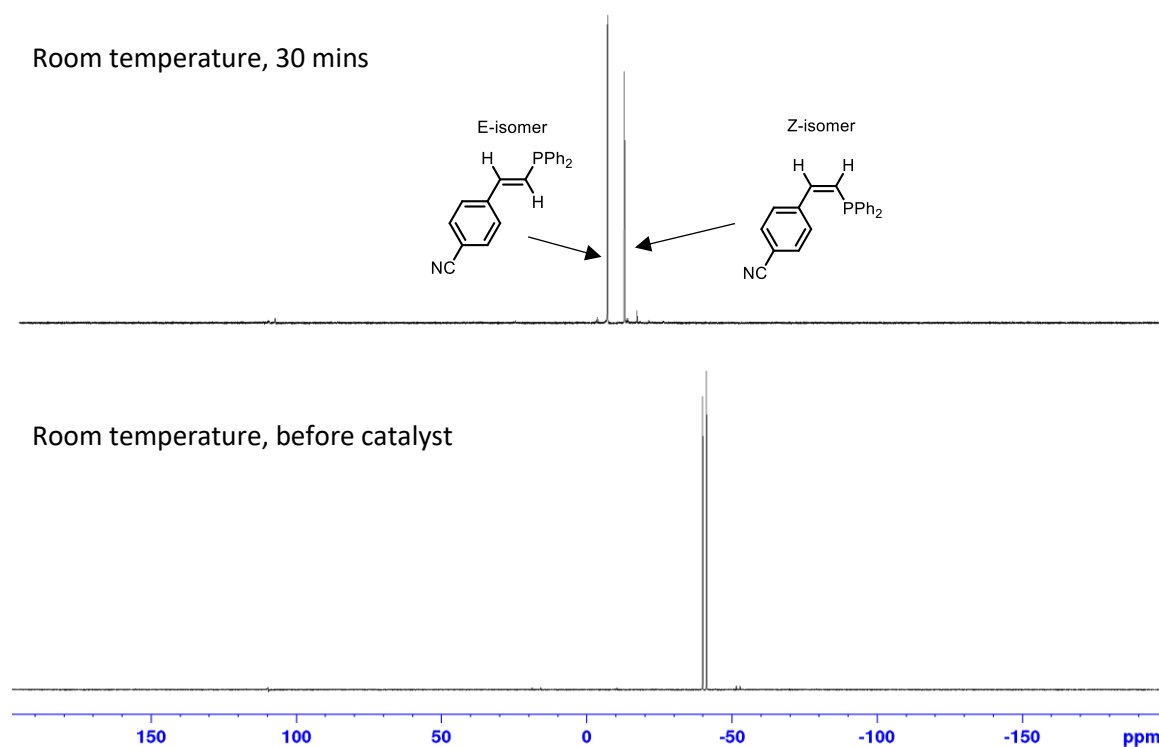


Figure S73: ³¹P NMR spectrum for the hydrophosphination of 4-cyanophenylacetylene catalysed by **3** (10 mol%) in d₈-toluene.

3-Phenyl-1-propyne catalysed by **3**

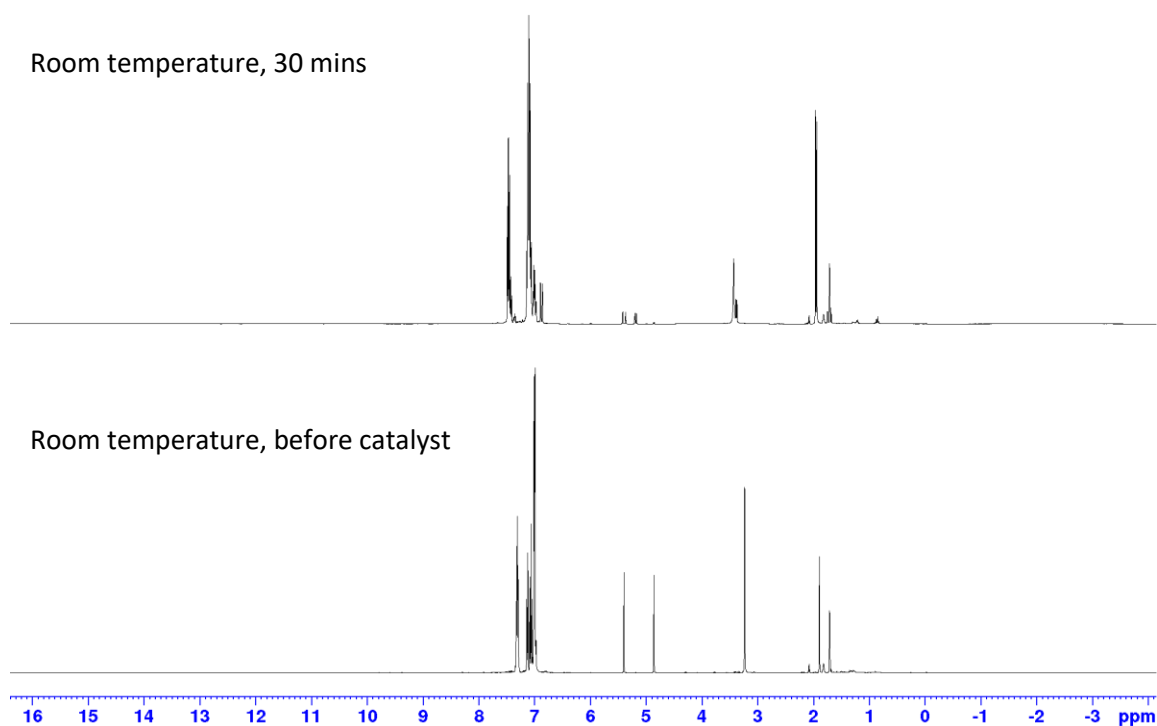


Figure S74: ¹H NMR spectrum for the hydrophosphination of 3-phenyl-1-propyne catalysed by **3** (10 mol%) in d₈-toluene.

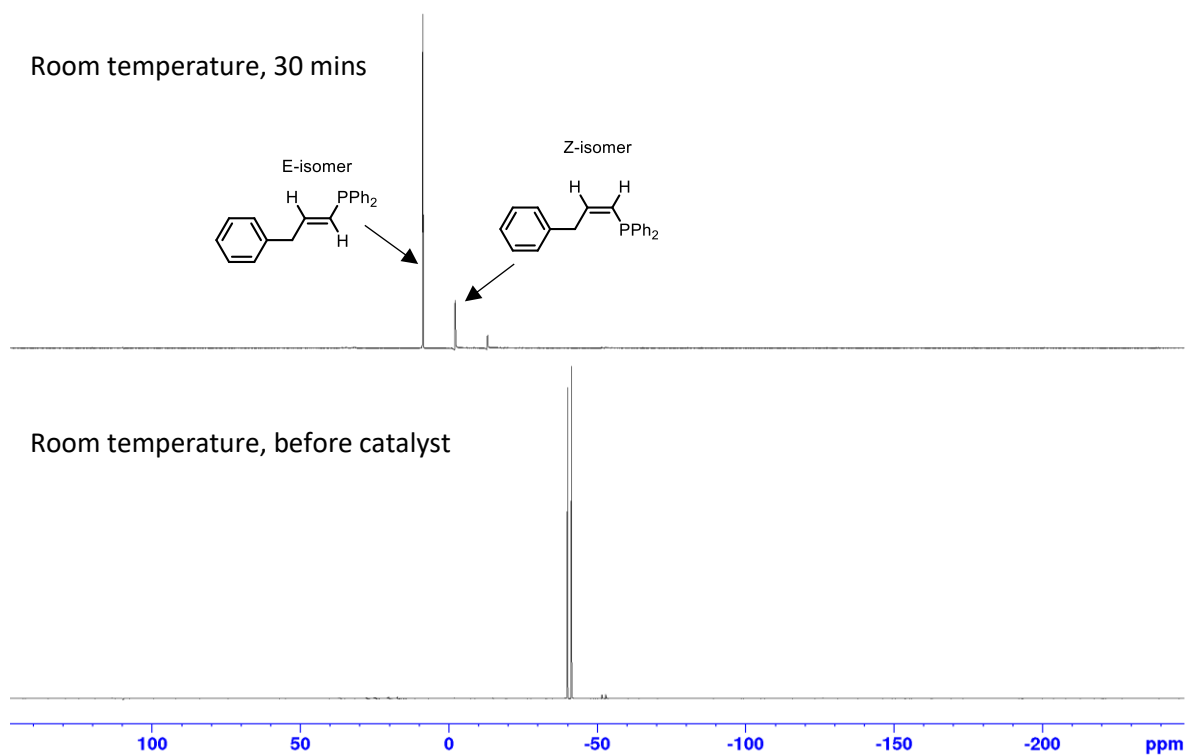


Figure S75: ³¹P NMR spectrum for the hydrophosphination of 3-phenyl-1-propyne catalysed by **3** (10 mol%) in d₈-toluene.

4-Phenyl-1-butyne catalysed by **3**

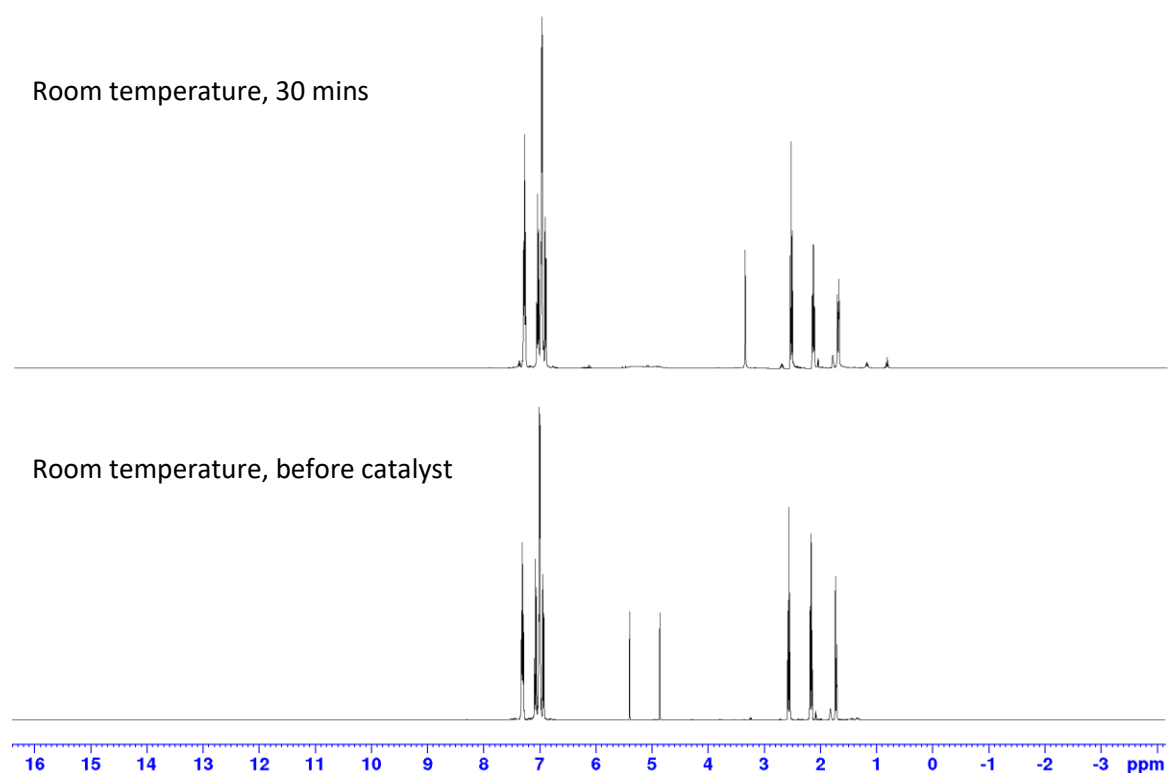


Figure S76: ^1H NMR spectrum for the hydrophosphination of 4-phenyl-1-butyne catalysed by **3** (10 mol%) in d_8 -toluene.

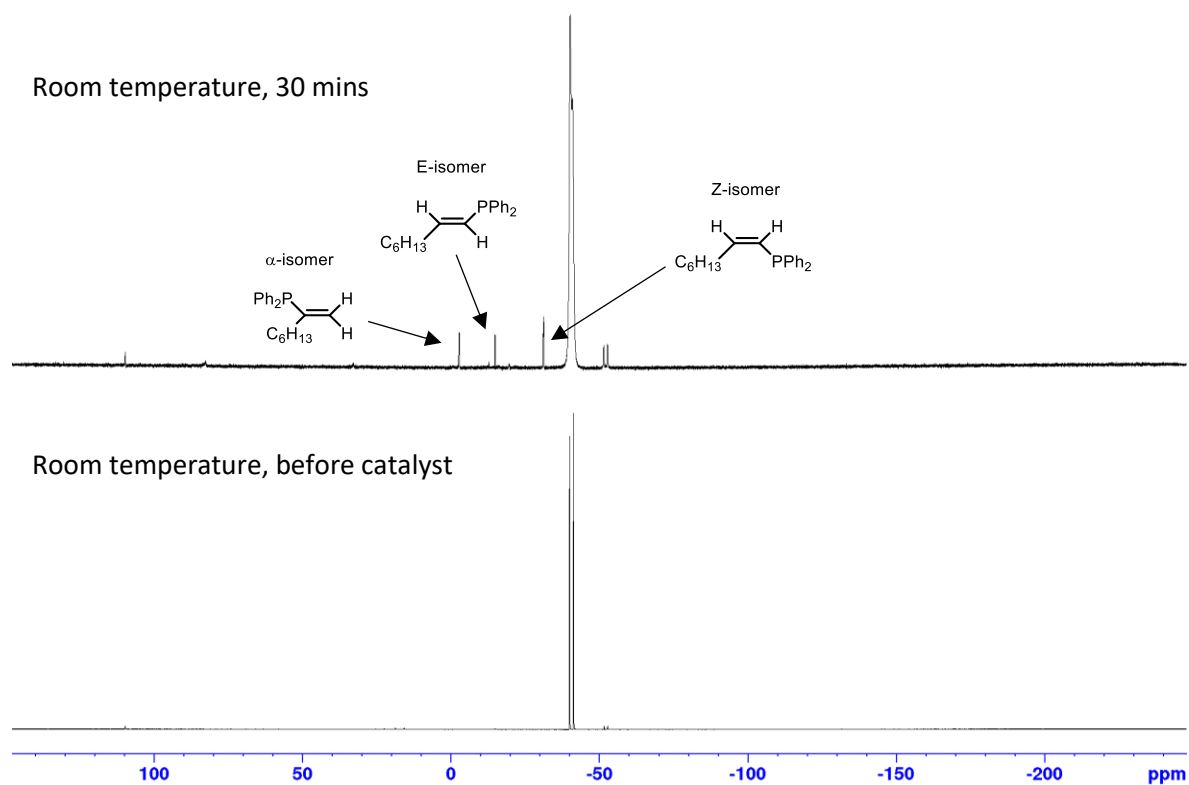


Figure S77: ^{31}P NMR spectrum for the hydrophosphination of 4-phenyl-1-butyne catalysed by **3** (10 mol%) in d_8 -toluene.

1-Octyne catalysed by **3**

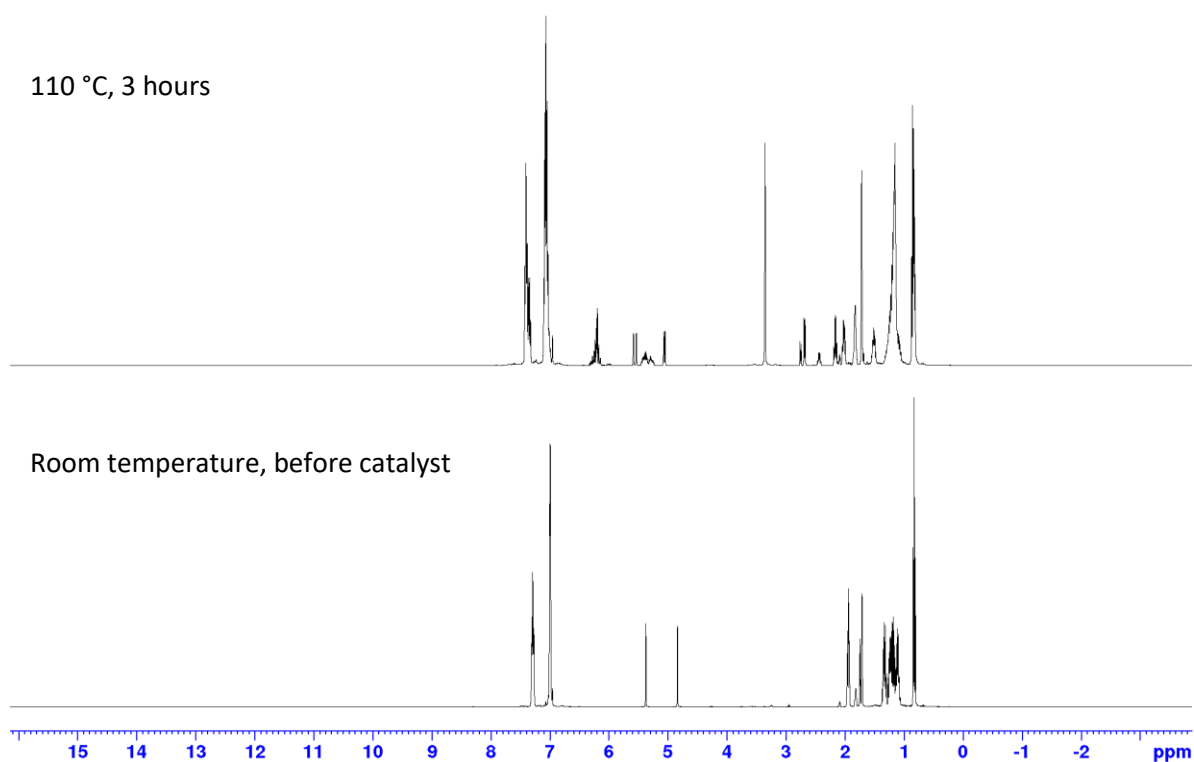


Figure S78: ^1H NMR spectrum for the hydrophosphination of 1-octyne catalysed by **3** (10 mol%) in d_8 -toluene.

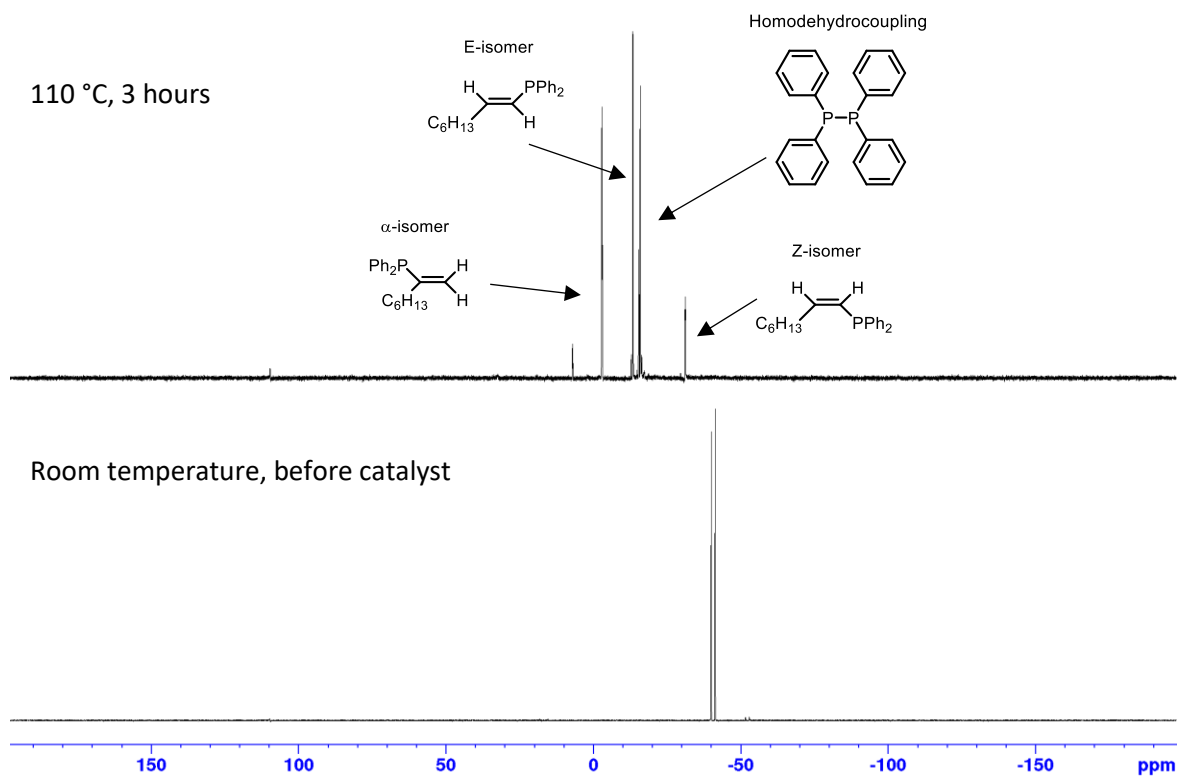


Figure S79: ^{31}P NMR spectrum for the hydrophosphination of 1-octyne catalysed by **3** (10 mol%) in d_8 -toluene.

3-Hexyne catalysed by **3**

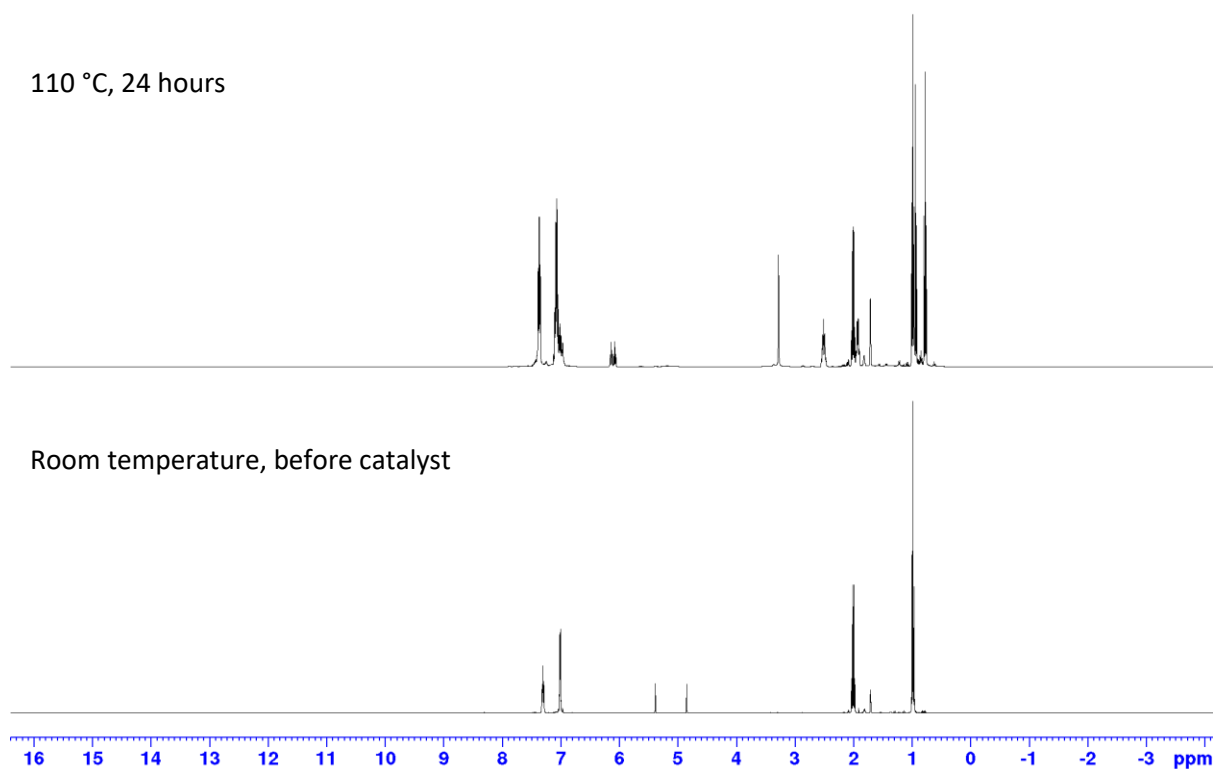


Figure S80: ^1H NMR spectrum for the hydrophosphination of 3-hexyne catalysed by **3** (10 mol%) in d_8 -toluene.

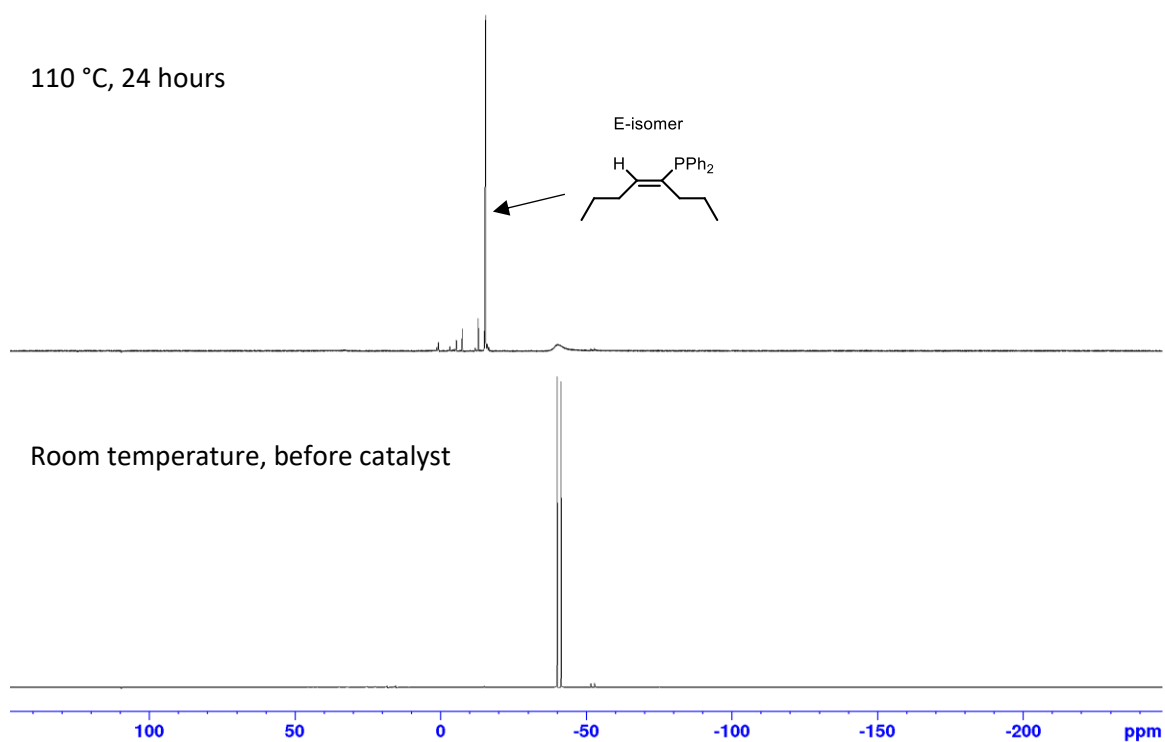


Figure S81: ^{31}P NMR spectrum for the hydrophosphination of 3-hexyne catalysed by **3** (10 mol%) in d_8 -toluene.

Styrene catalysed by **3**

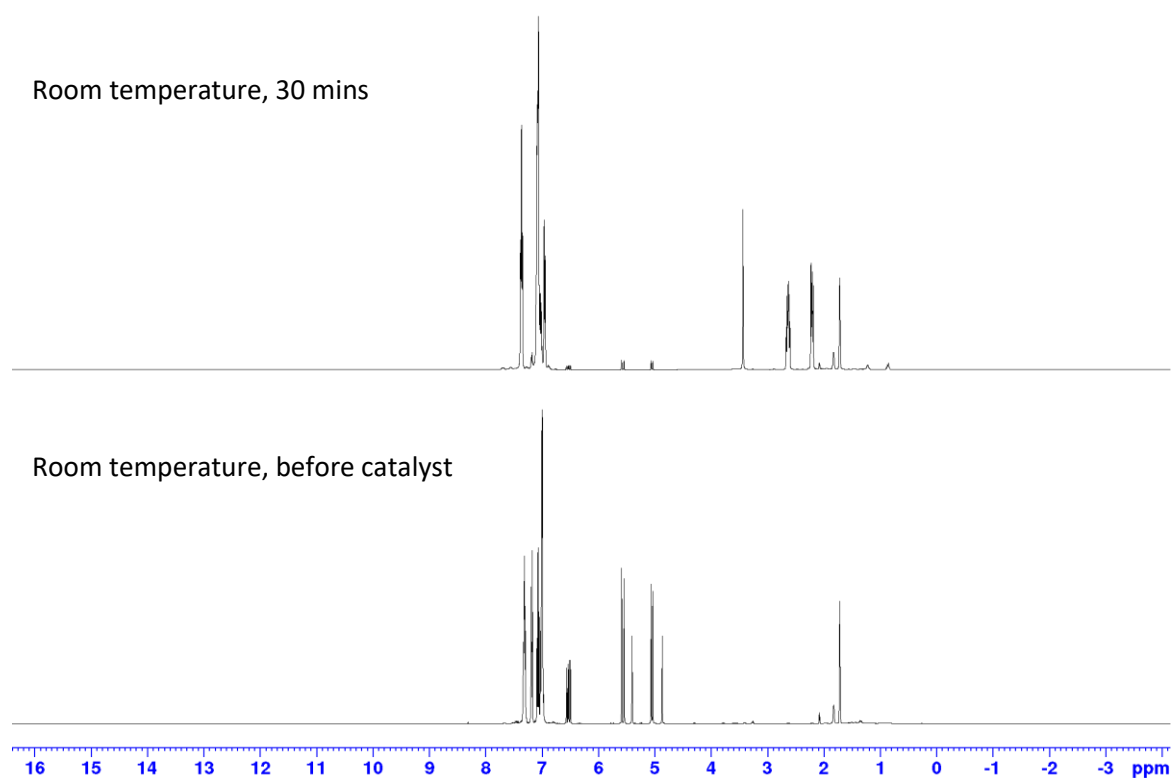


Figure S82: ¹H NMR spectrum for the hydrophosphination of styrene catalysed by **3** (10 mol%) in d₈-toluene.

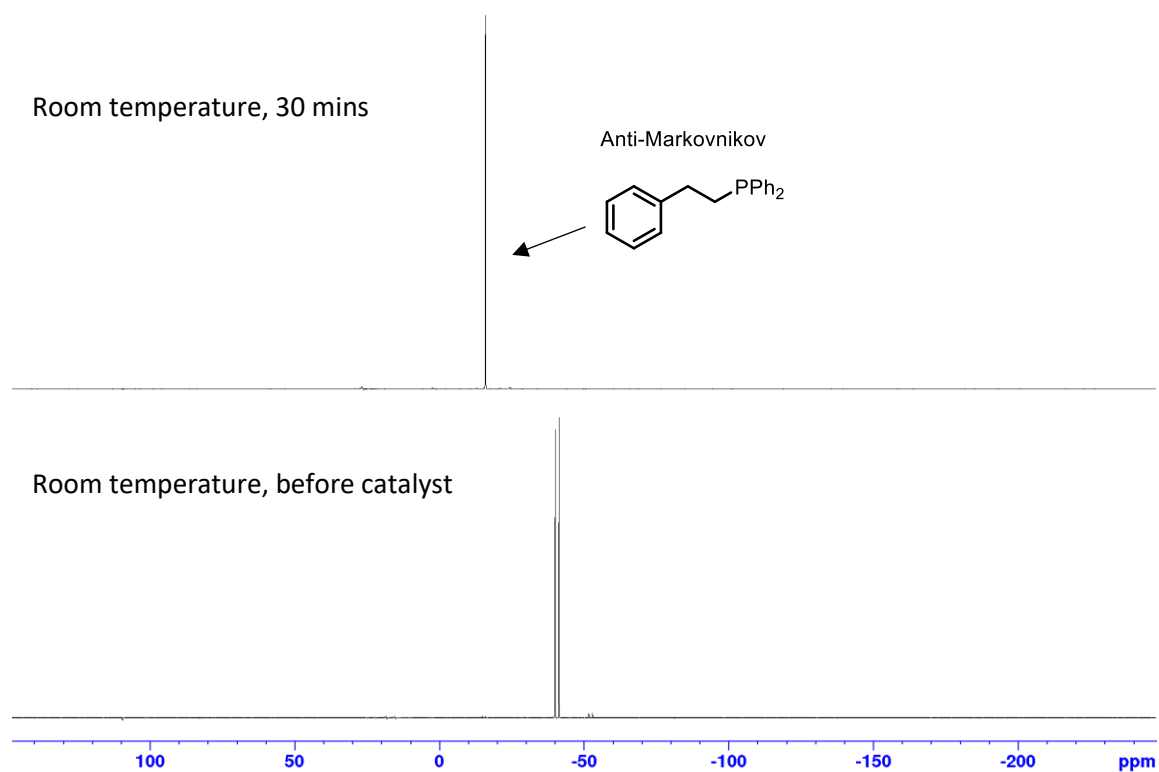


Figure S83: ³¹P NMR spectrum for the hydrophosphination of styrene catalysed by **3** (10 mol%) in d₈-toluene.

Methyl acrylate catalysed by **3**

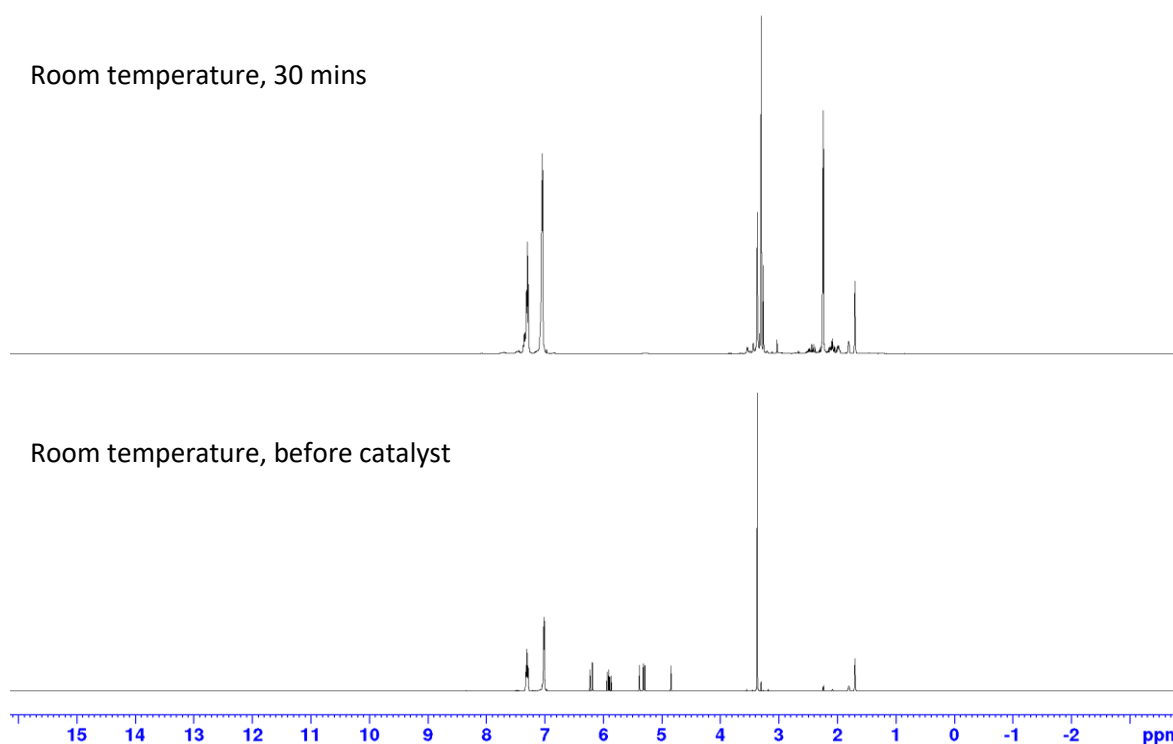


Figure S84: ^1H NMR spectrum for the hydrophosphination of methyl acrylate catalysed by **3** (10 mol%) in d_8 -toluene.

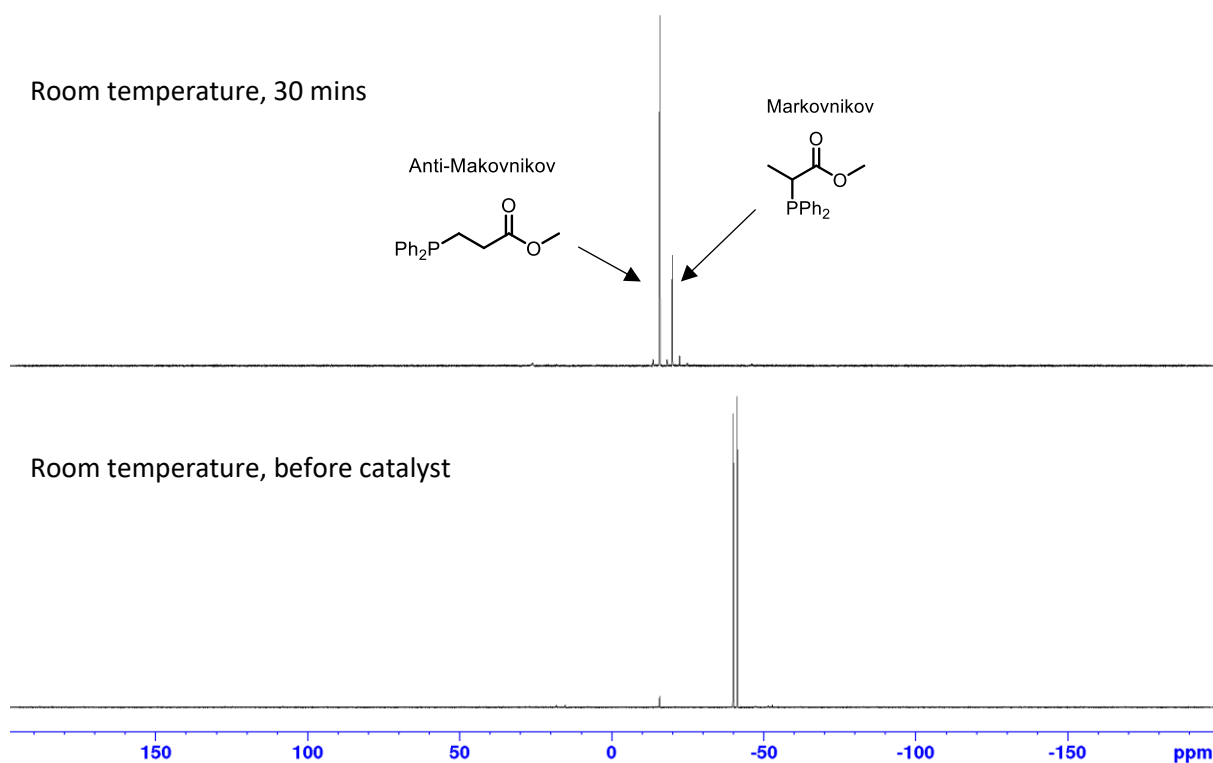


Figure S85: ^{31}P NMR spectrum for the hydrophosphination of methyl acrylate catalysed by **3** (10 mol%) in d_8 -toluene.

Hydrophosphination Using **4** as a Catalyst

Phenylacetylene catalysed by **4**

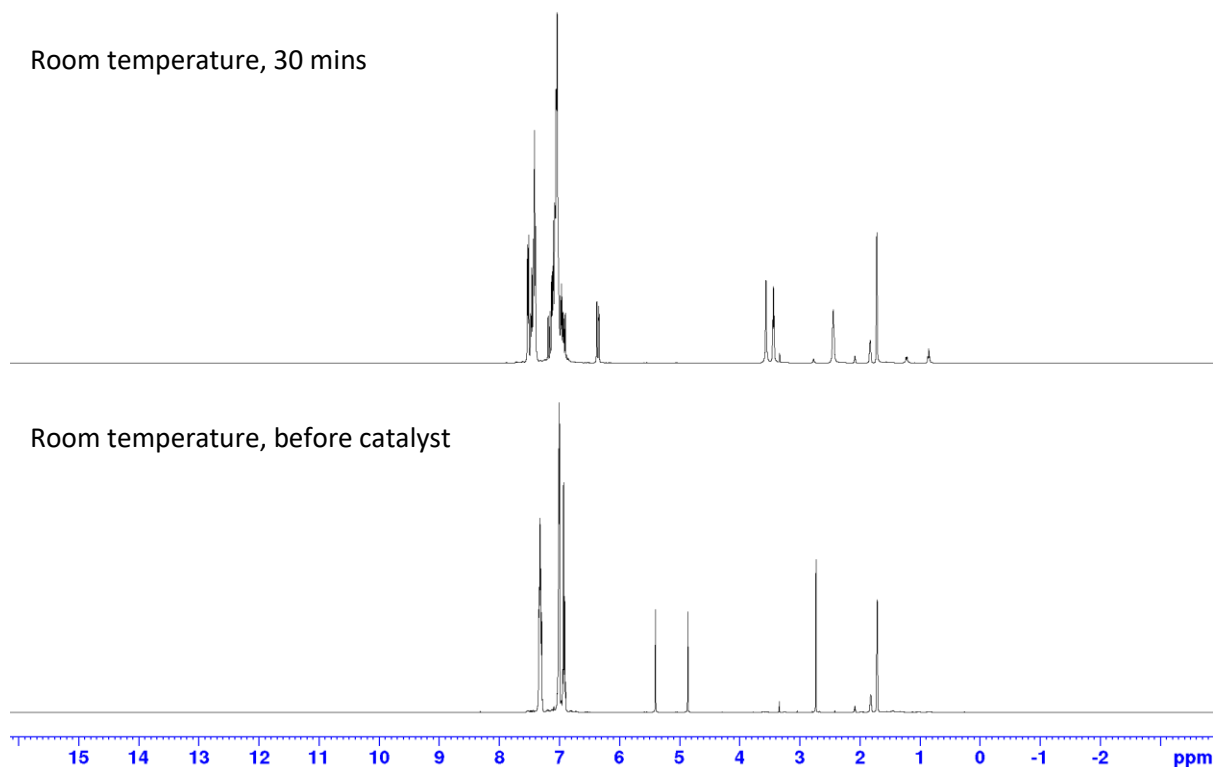


Figure S86: ¹H NMR spectrum for the hydrophosphination of phenylacetylene catalysed by **4** (10 mol%) in d₈-toluene.

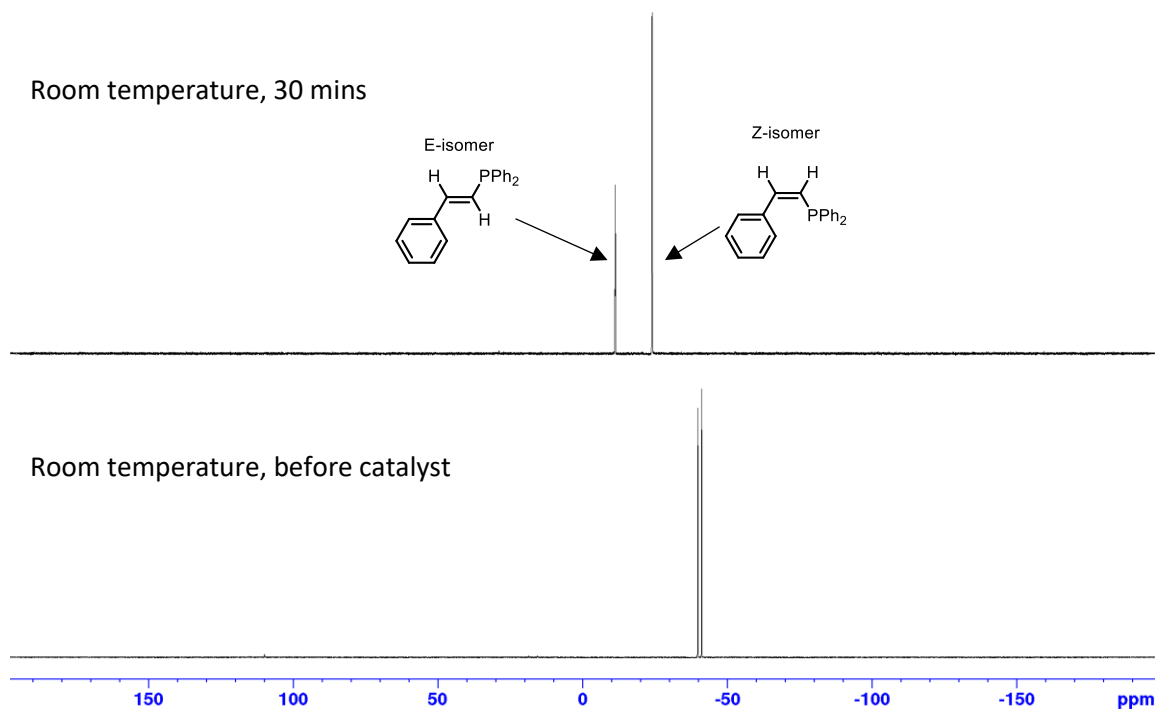


Figure S87: ³¹P NMR spectrum for the hydrophosphination of phenylacetylene catalysed by **4** (10 mol%) in d₈-toluene.

Diphenylacetylene catalysed by **4**

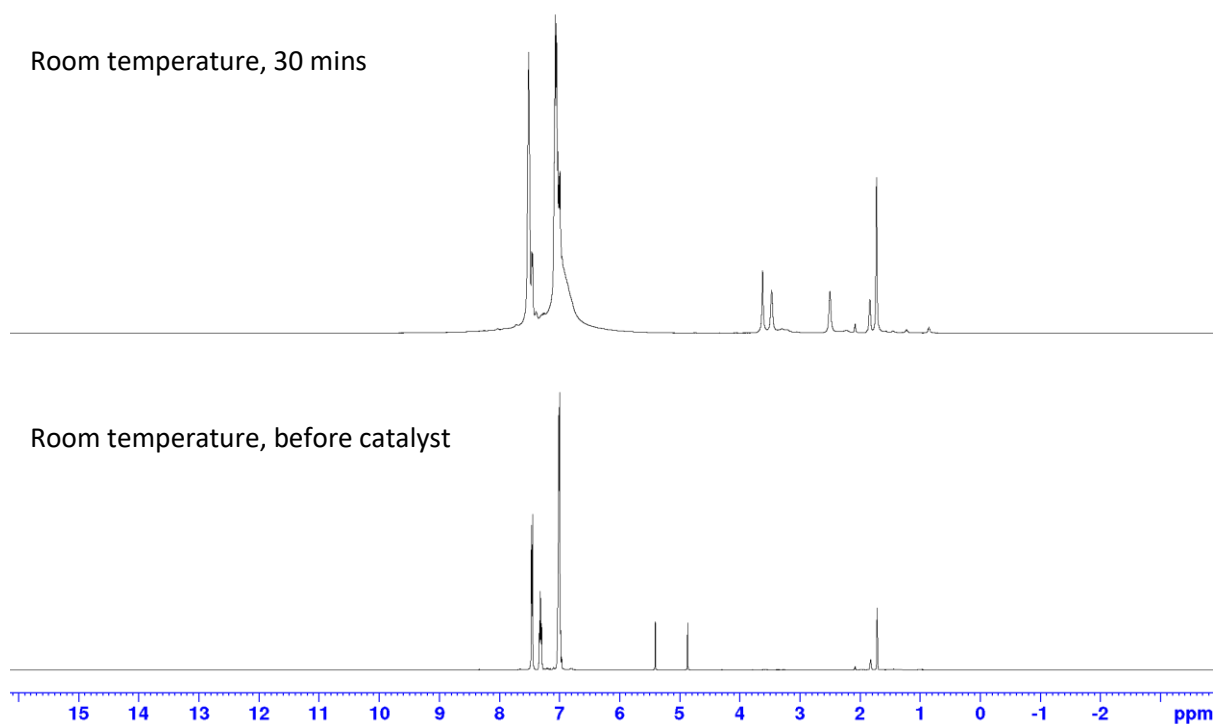


Figure S88: ¹H NMR spectrum for the hydrophosphination of diphenylacetylene catalysed by **4** (10 mol%) in d₈-toluene.

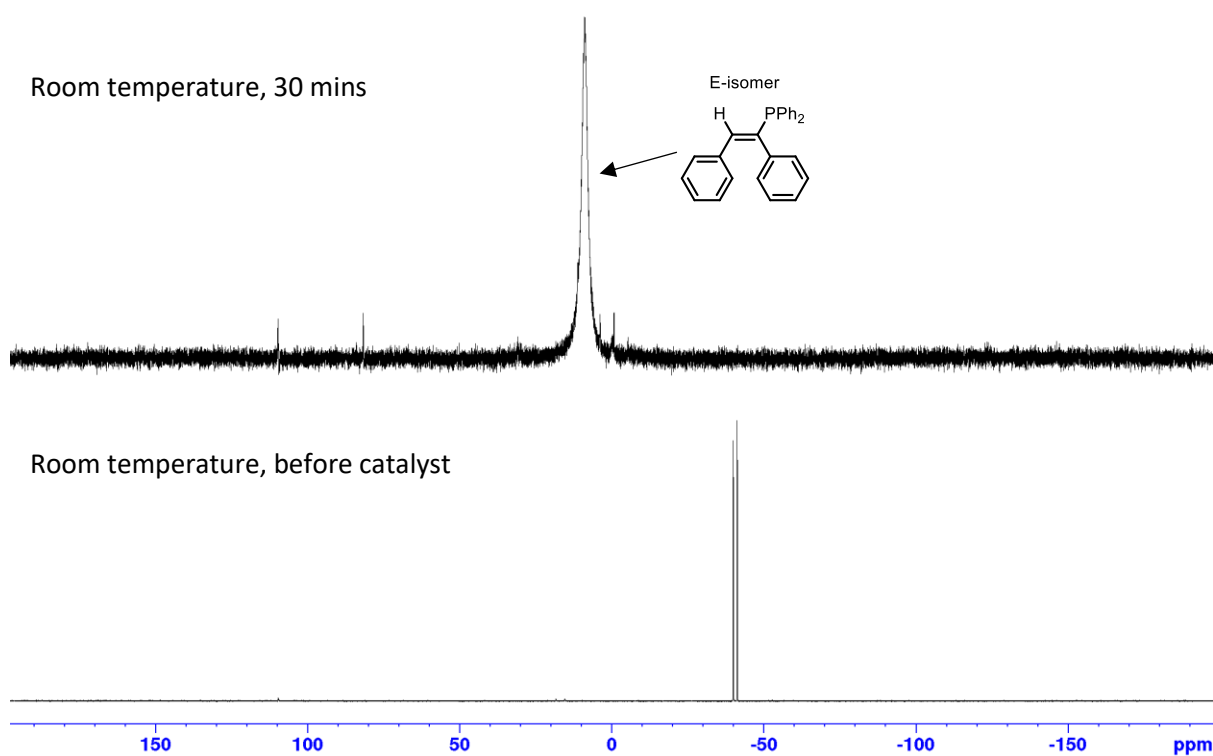


Figure S89: ³¹P NMR spectrum for the hydrophosphination of diphenylacetylene catalysed by **4** (10 mol%) in d₈-toluene.

4'-Methylphenylacetylene catalysed by **4**

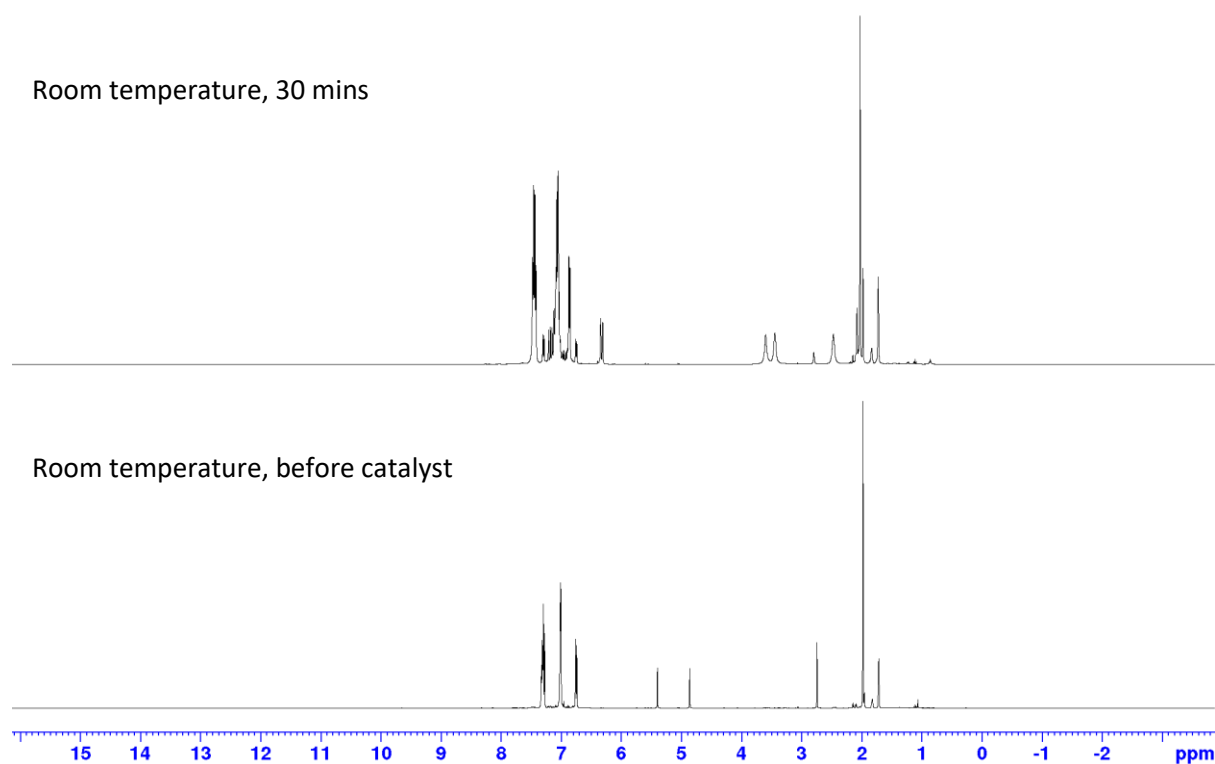


Figure S90: ¹H NMR spectrum for the hydrophosphination of 4'-methylphenylacetylene catalysed by **4** (10 mol%) in d₈-toluene.

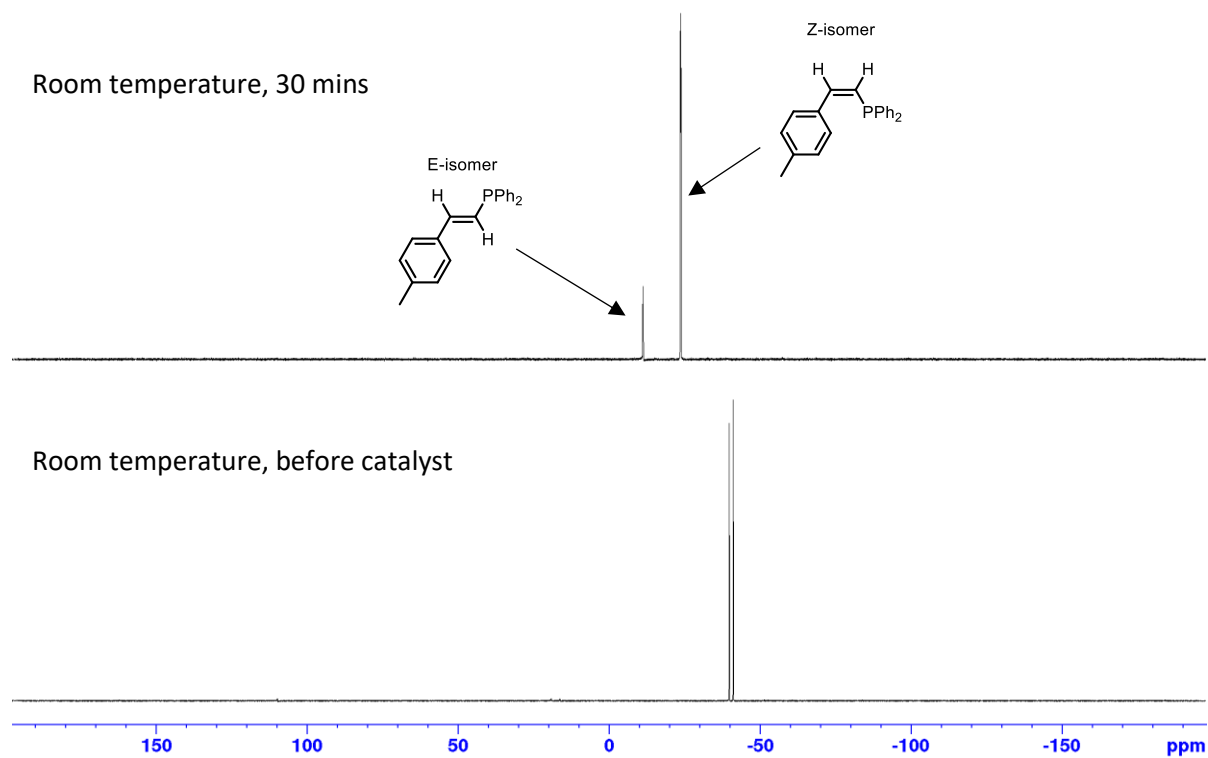


Figure S91: ³¹P NMR spectrum for the hydrophosphination of 4'-methylphenylacetylene catalysed by **4** (10 mol%) in d₈-toluene.

4'-Trifluoromethylphenylacetylene catalysed by **4**

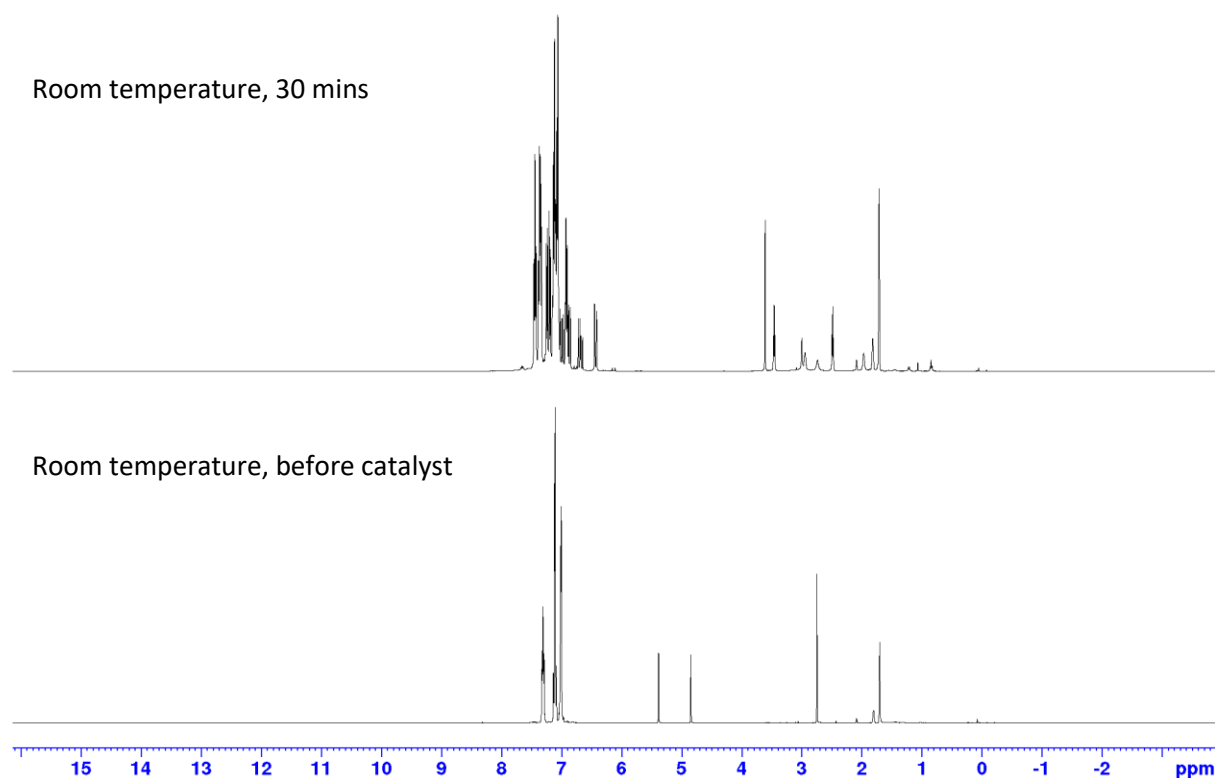


Figure S92: ¹H NMR spectrum for the hydrophosphination of 4'-trifluoromethylphenylacetylene catalysed by **4** (10 mol%) in d₈-toluene.

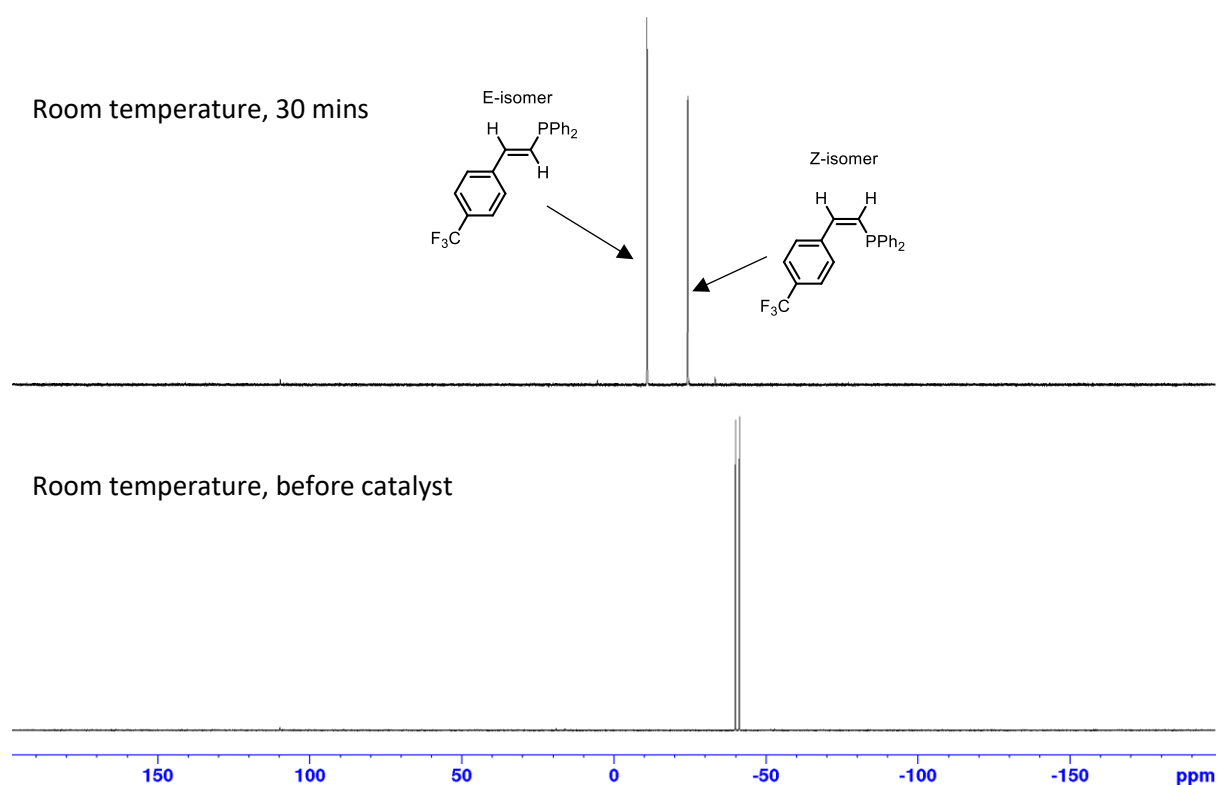


Figure S93: ³¹P NMR spectrum for the hydrophosphination of 4'-trifluoromethylphenylacetylene catalysed by **4** (10 mol%) in d₈-toluene.

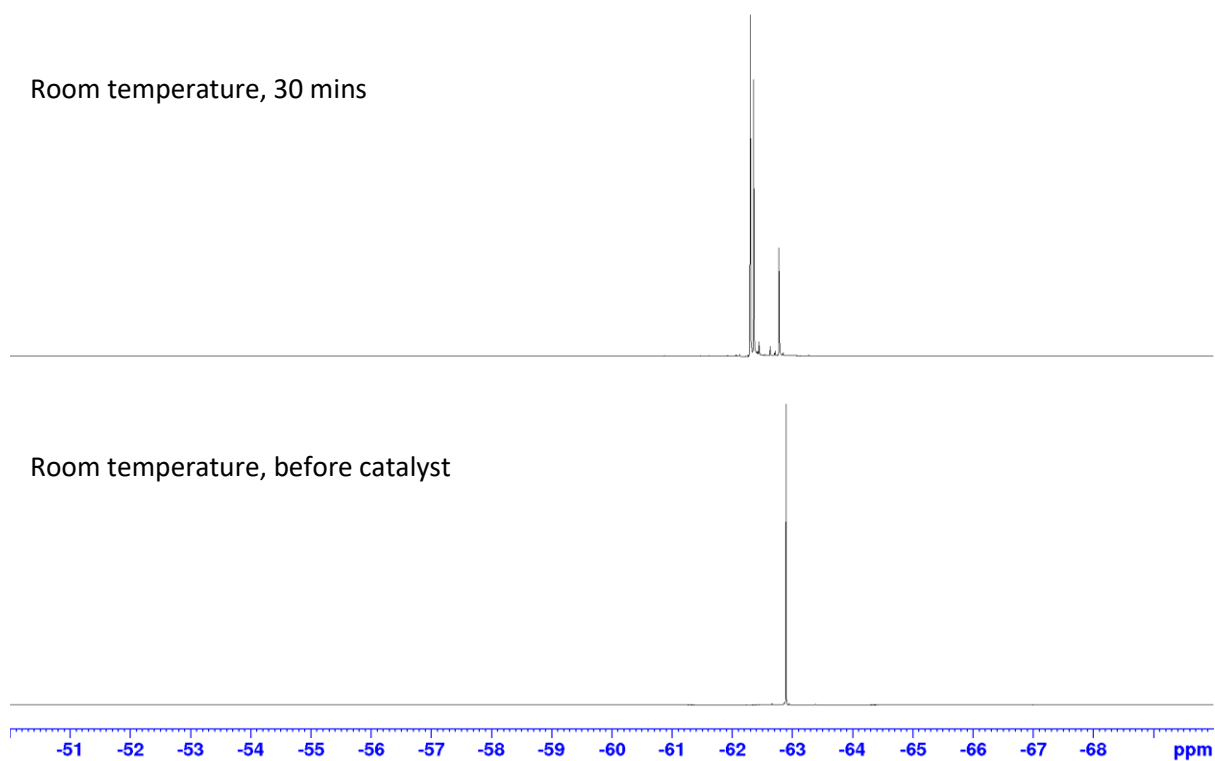


Figure S94: $^{19}\text{F}\{^1\text{H}\}$ NMR spectrum for the hydrophosphination of 4'-trifluoromethylphenylacetylene catalysed by **4** (10 mol%) in d_8 -toluene.

4-Cyanophenylacetylene catalysed by **4**

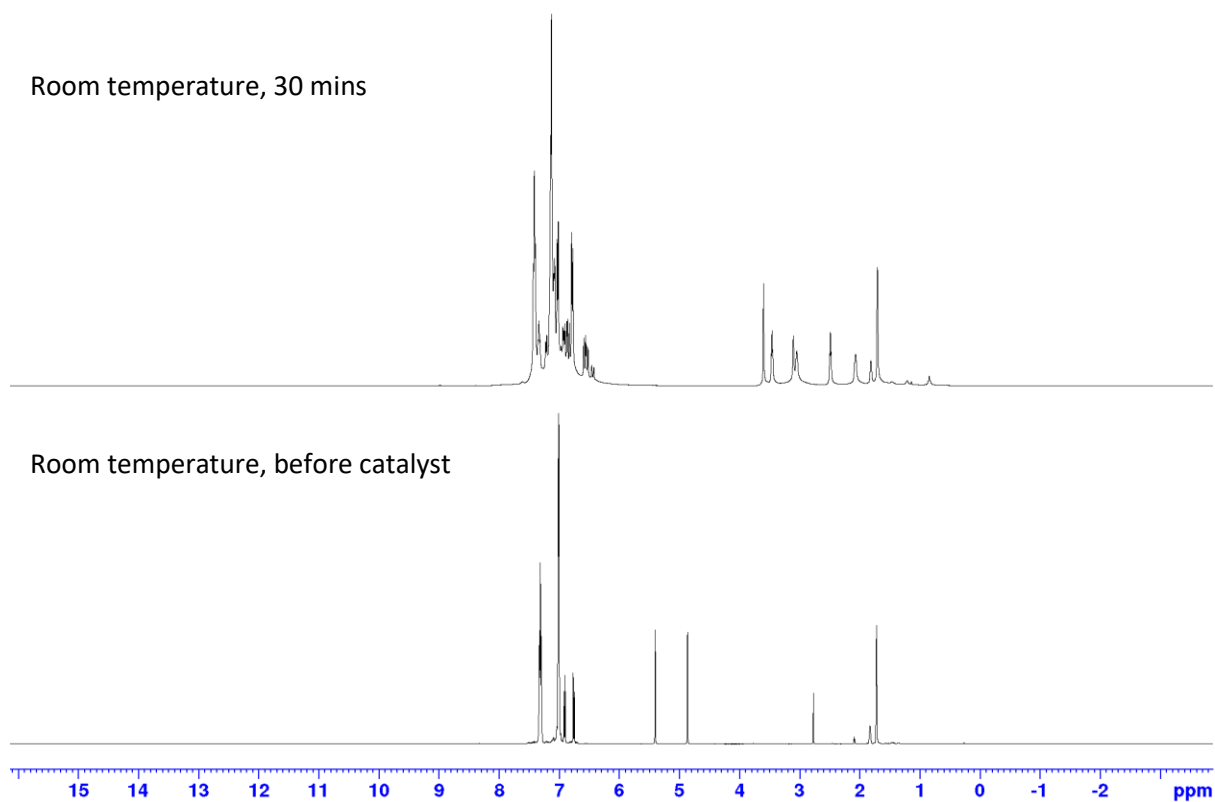


Figure S95: ^1H NMR spectrum for the hydrophosphination of 4-cyanophenylacetylene catalysed by **4** (10 mol%) in d_8 -toluene.

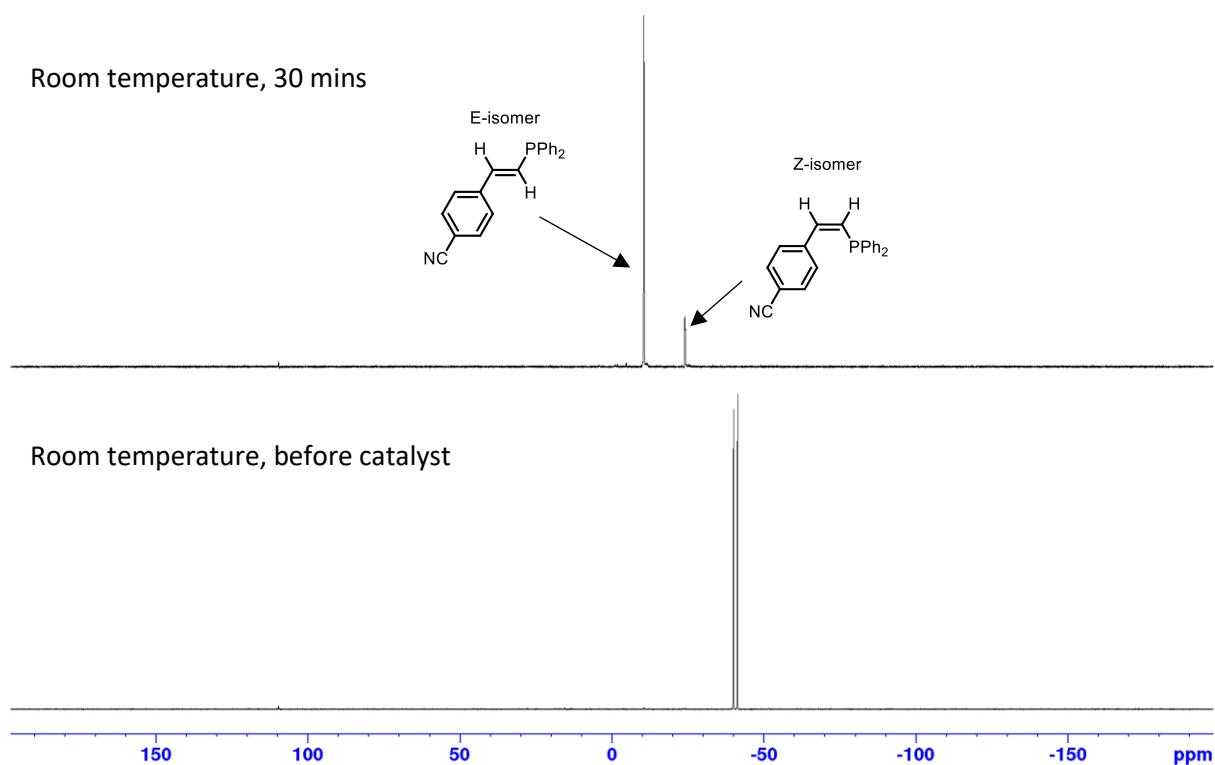


Figure S96: ^{31}P NMR spectrum for the hydrophosphination of 4-cyanophenylacetylene catalysed by **4** (10 mol%) in d_8 -toluene.

3-Phenyl-1-propyne catalysed by **4**

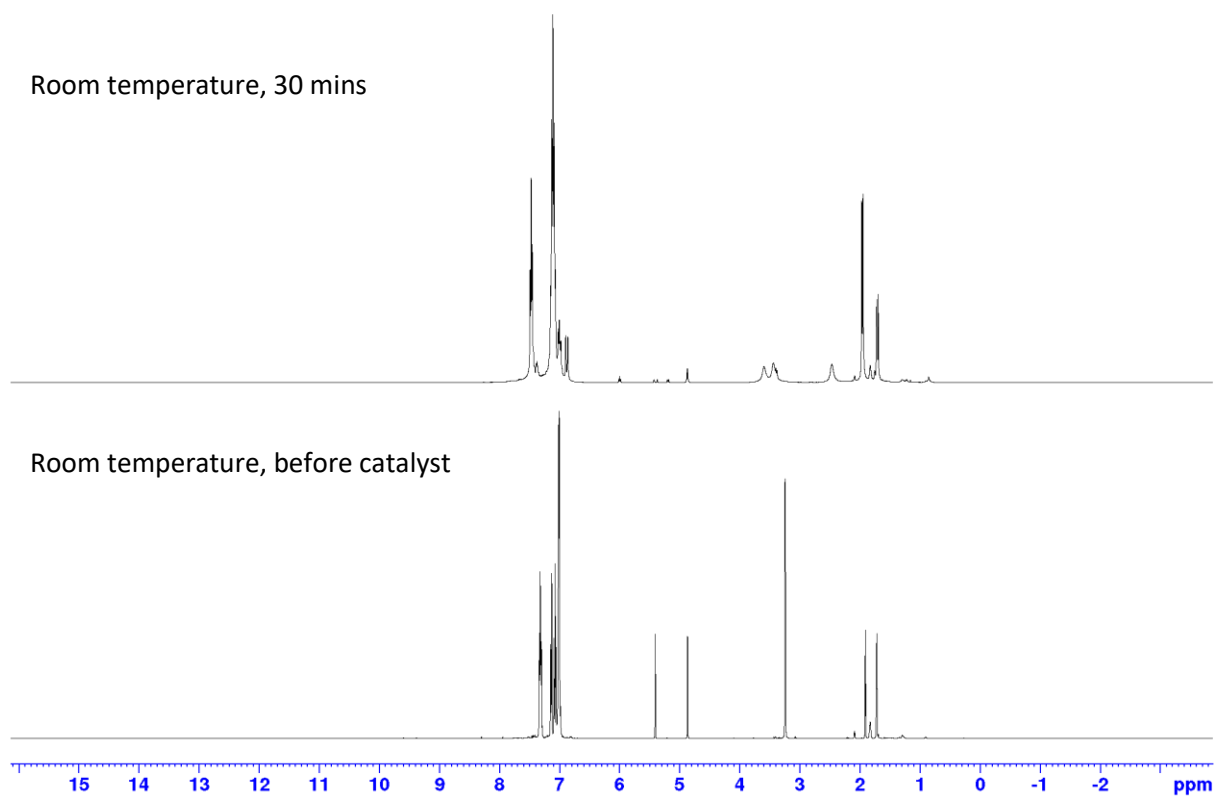


Figure S97: ^1H NMR spectrum for the hydrophosphination of 3-phenyl-1-propyne catalysed by **4** (10 mol%) in d_8 -toluene.

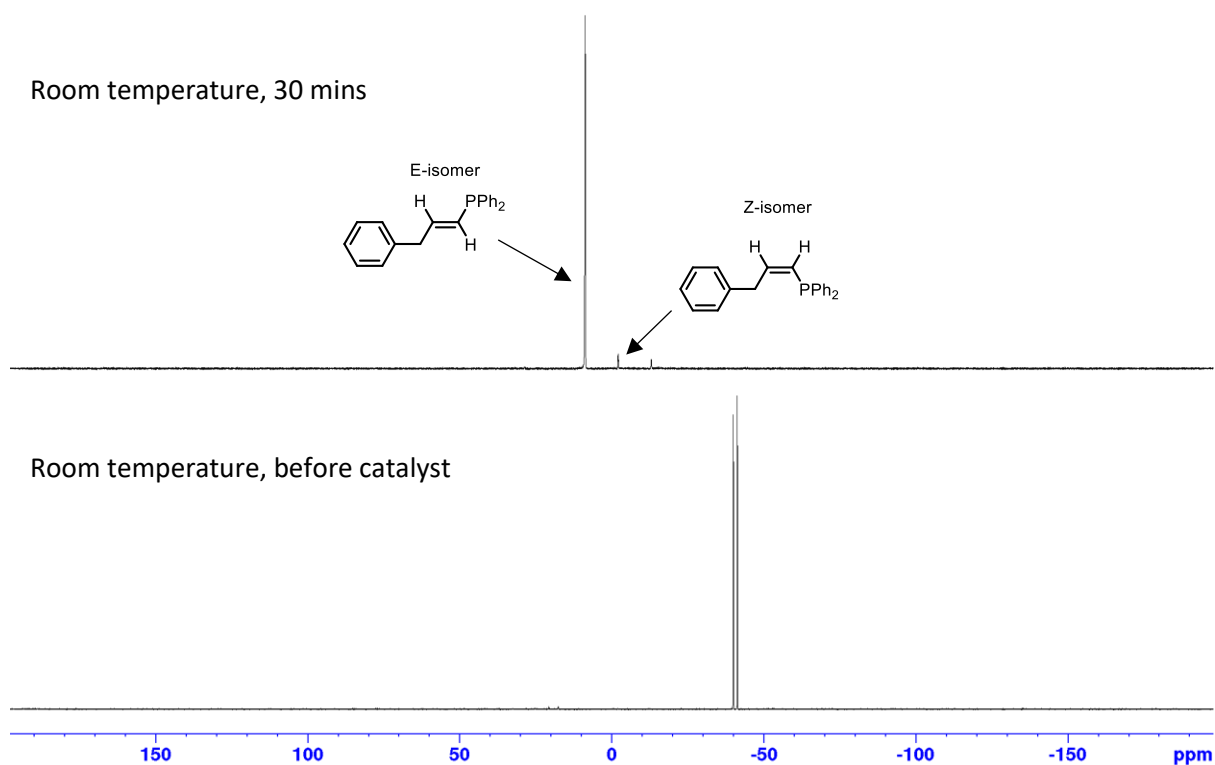


Figure S98: ^{31}P NMR spectrum for the hydrophosphination of 3-phenyl-1-propyne catalysed by **4** (10 mol%) in d_8 -toluene.

4-Phenyl-1-butyne catalysed by **4**

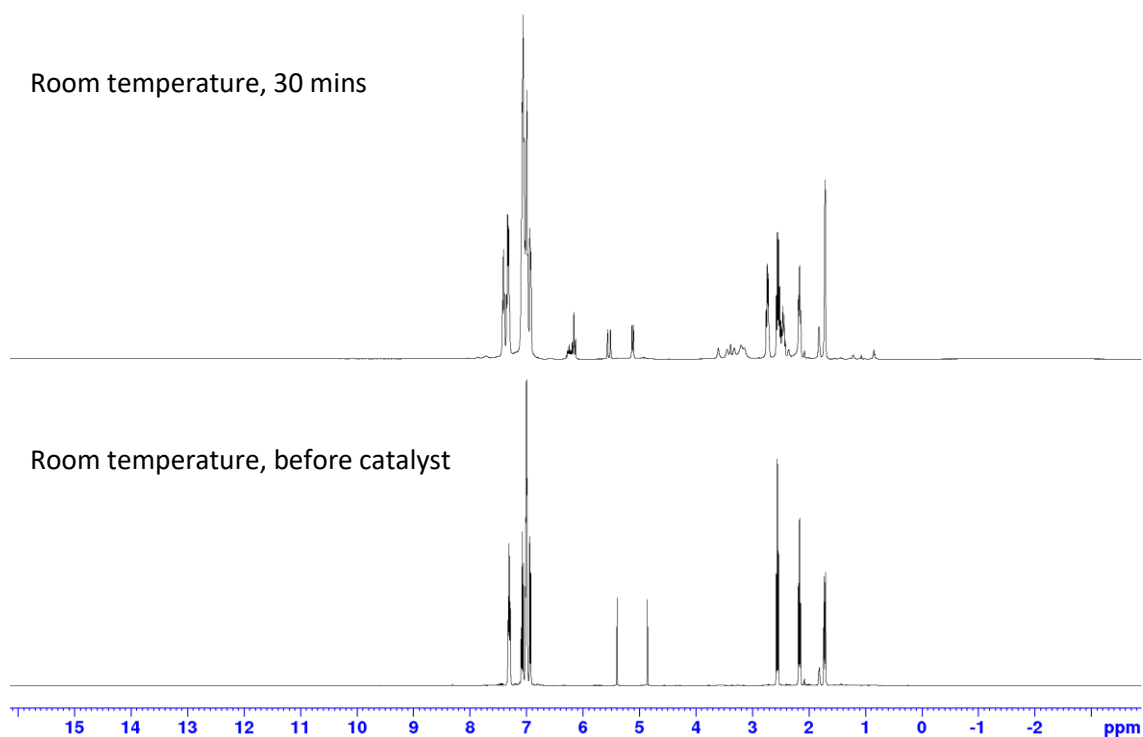


Figure S99: ^1H NMR spectrum for the hydrophosphination of 4-phenyl-1-butyne catalysed by **4** (10 mol%) in d_8 -toluene.

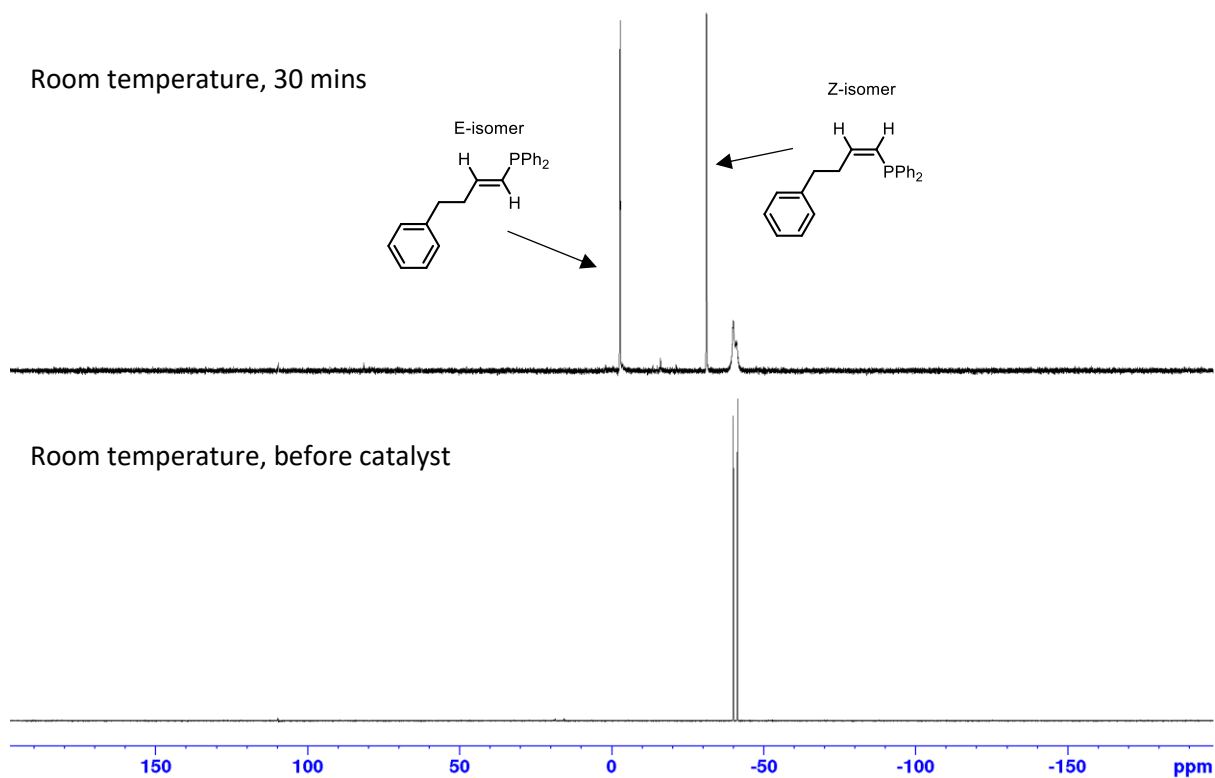


Figure S100: ^{31}P NMR spectrum for the hydrophosphination of 4-phenyl-1-butyne catalysed by **4** (10 mol%) in d_8 -toluene.

1-Octyne catalysed by **4**

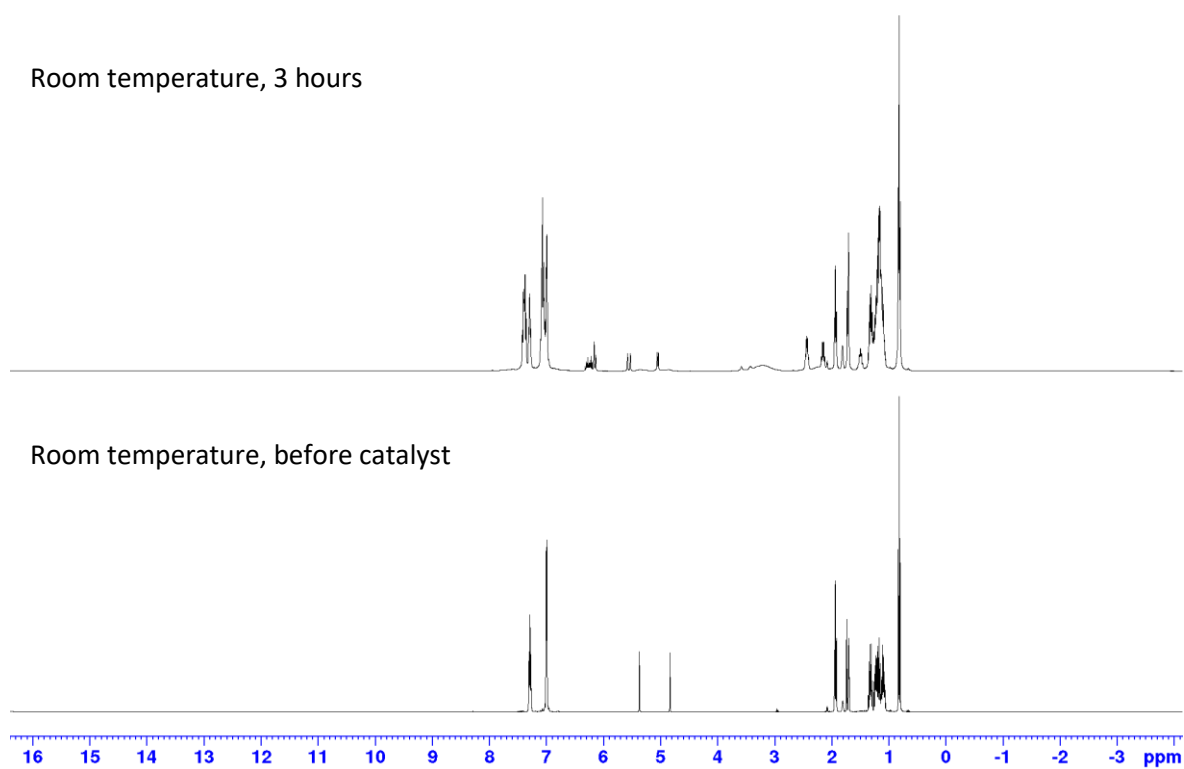


Figure S101: ^1H NMR spectrum for the hydrophosphination of 1-octyne catalysed by **4** (10 mol%) in d_8 -toluene.

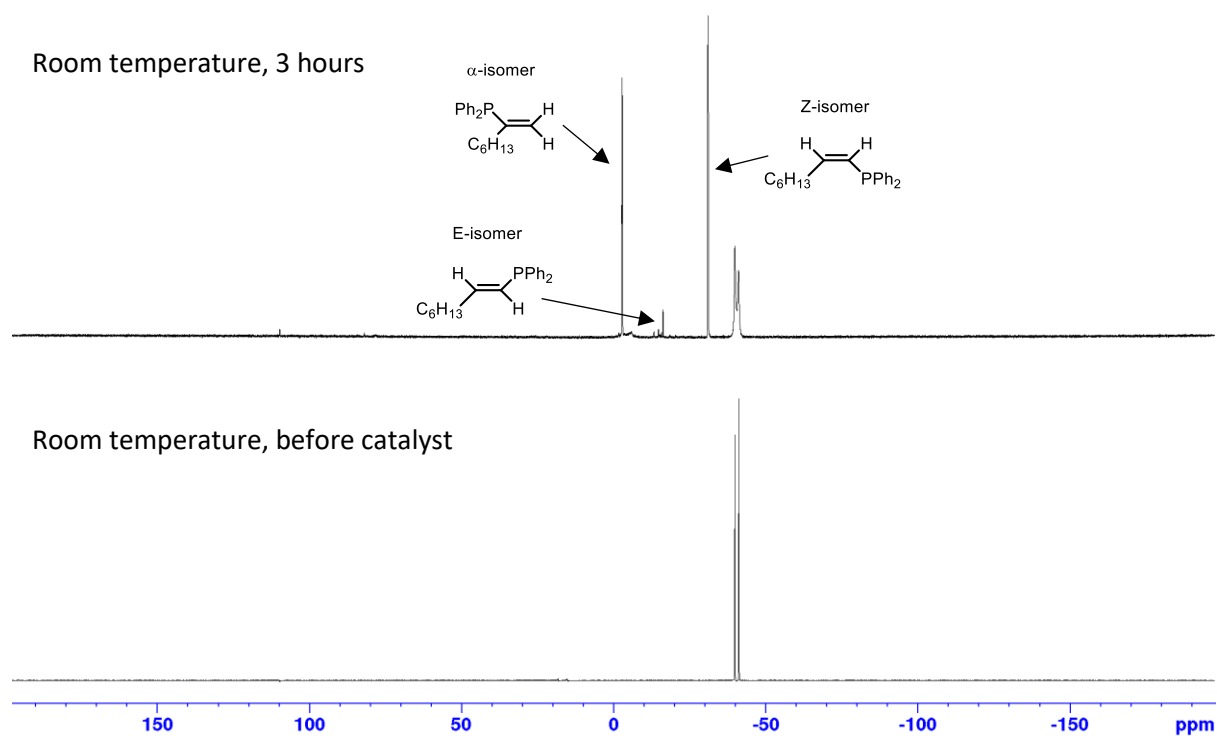


Figure S102: ^{31}P NMR spectrum for the hydrophosphination of 1-octyne catalysed by **4** (10 mol%) in d_8 -toluene.

3-Hexyne catalysed by **4**

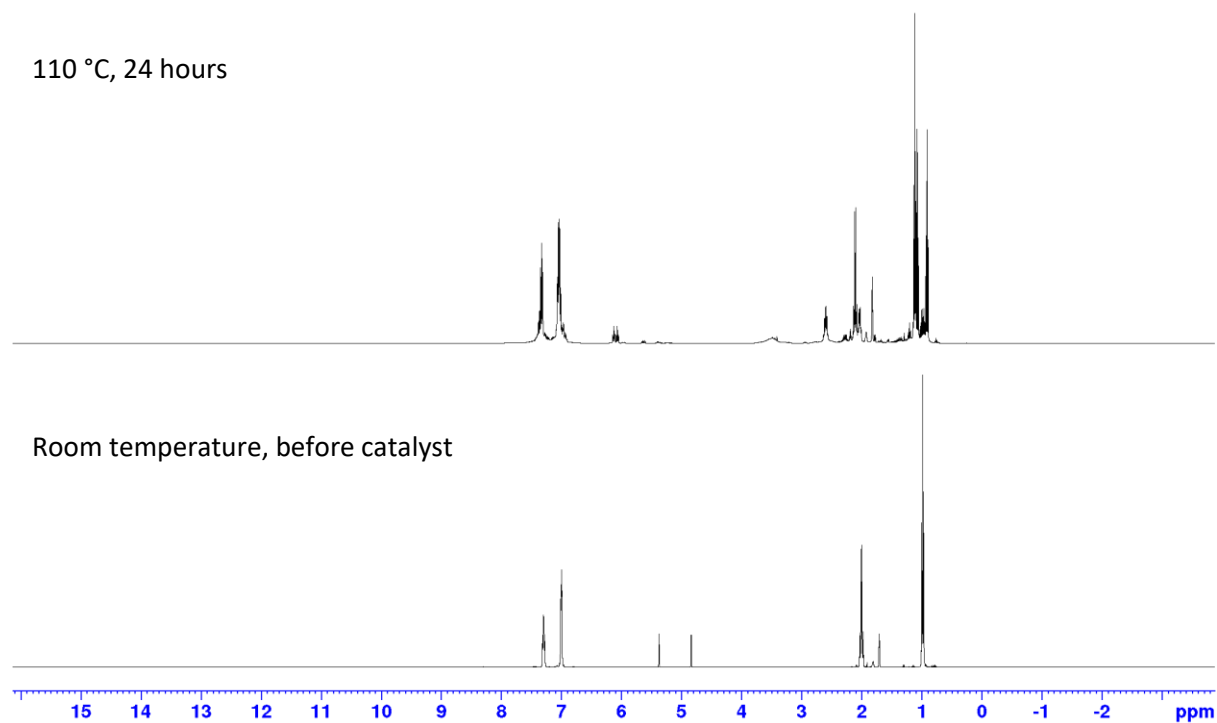


Figure S103: ^1H NMR spectrum for the hydrophosphination of 3-hexyne catalysed by **4** (10 mol%) in d_8 -toluene.

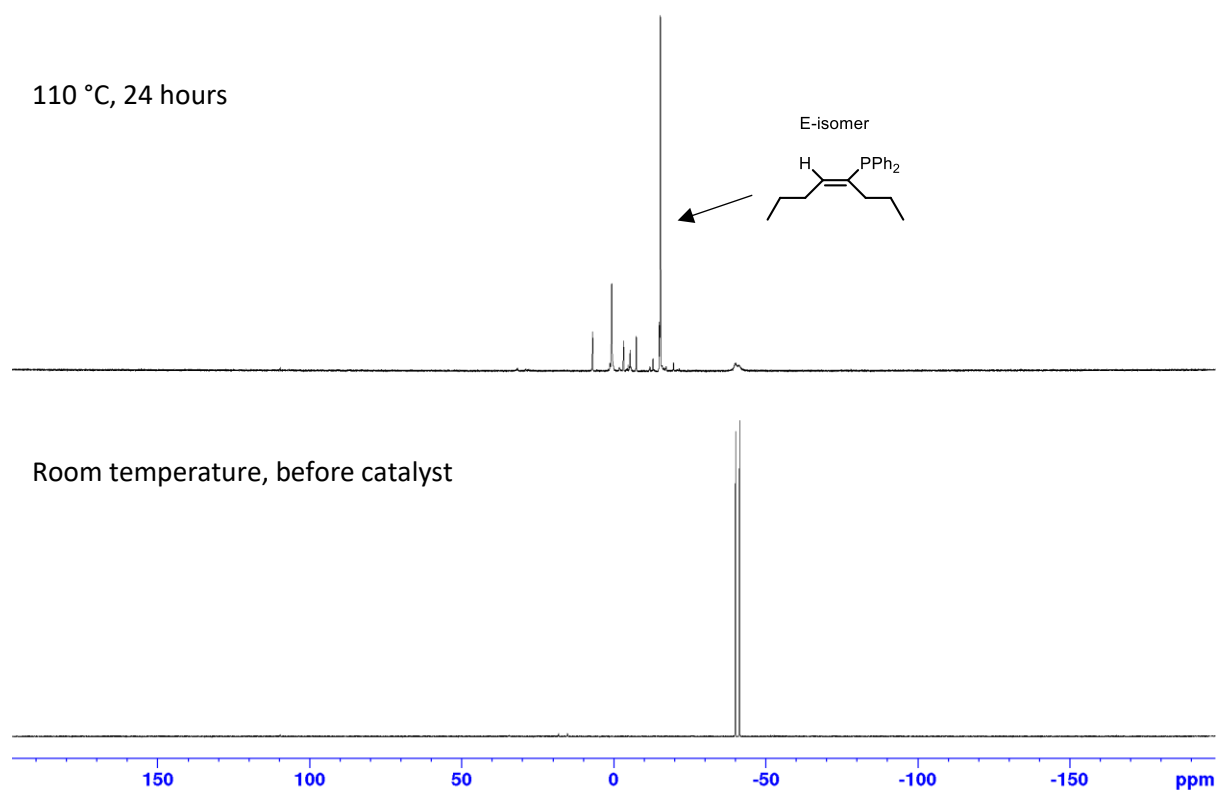


Figure S104: ^{31}P NMR spectrum for the hydrophosphination of 3-hexyne catalysed by **4** (10 mol%) in d_8 -toluene.

Styrene catalysed by **4**

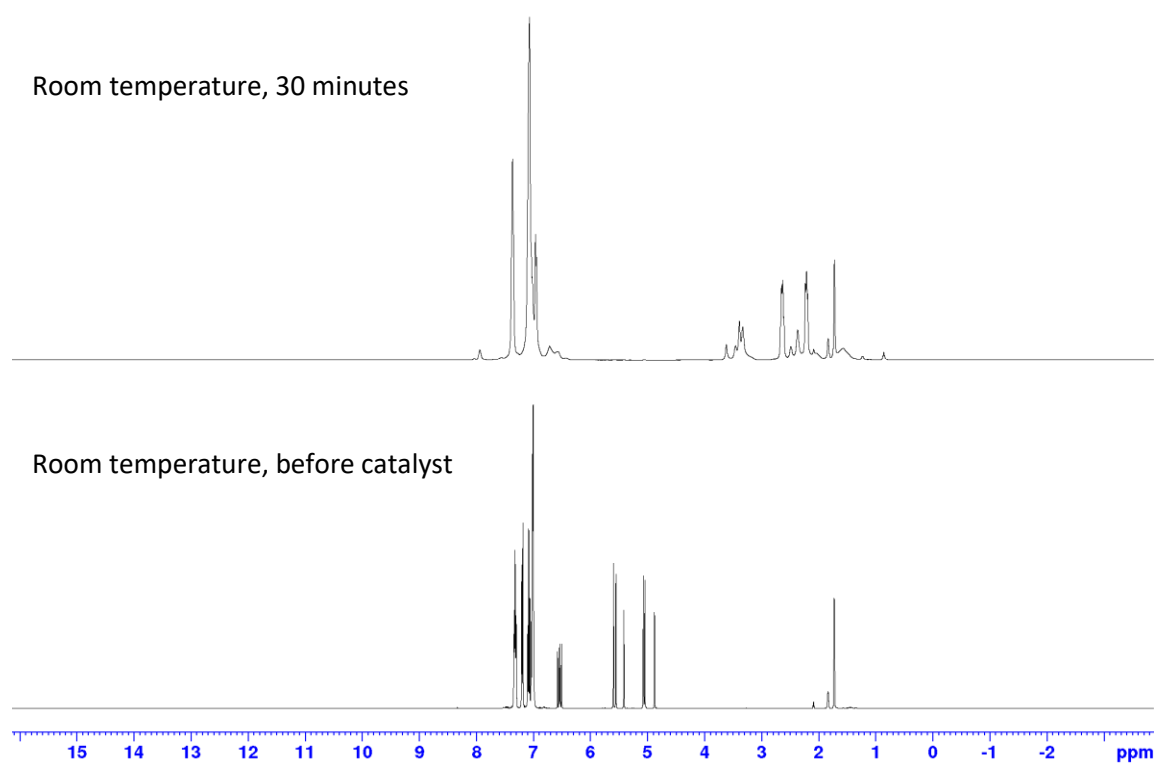


Figure S105: ^1H NMR spectrum for the hydrophosphination of styrene catalysed by **4** (10 mol%) in d_8 -toluene.

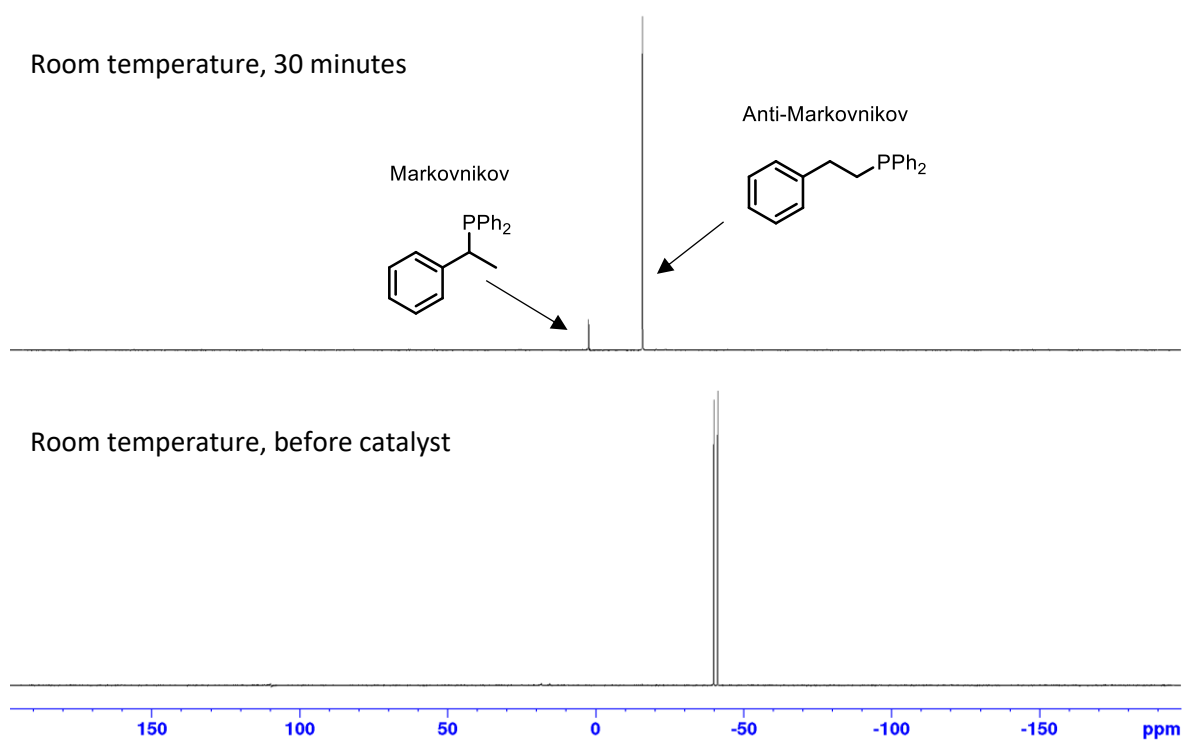


Figure S106: ^{31}P NMR spectrum for the hydrophosphination of styrene catalysed by **4** (10 mol%) in d_8 -toluene.

Methyl acrylate catalysed by **4**

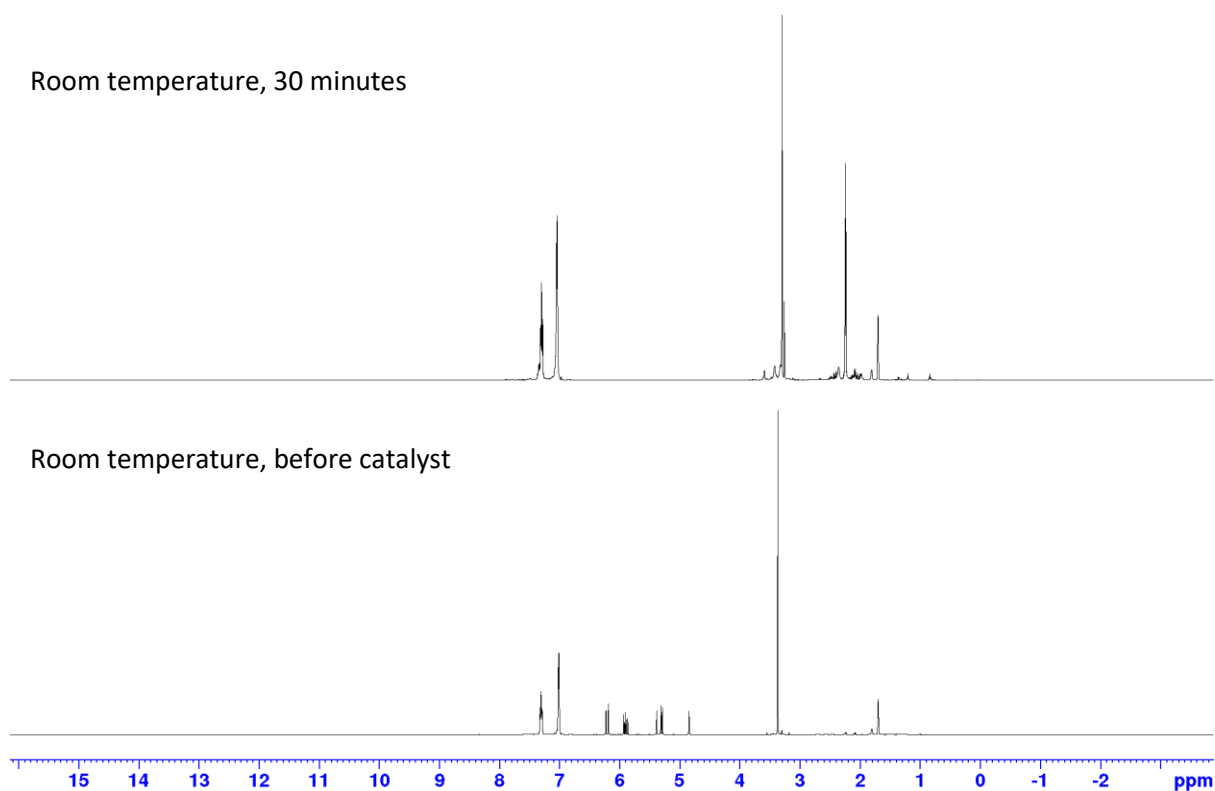


Figure S107: ^1H NMR spectrum for the hydrophosphination of methyl acrylate catalysed by **4** (10 mol%) in d_8 -toluene.

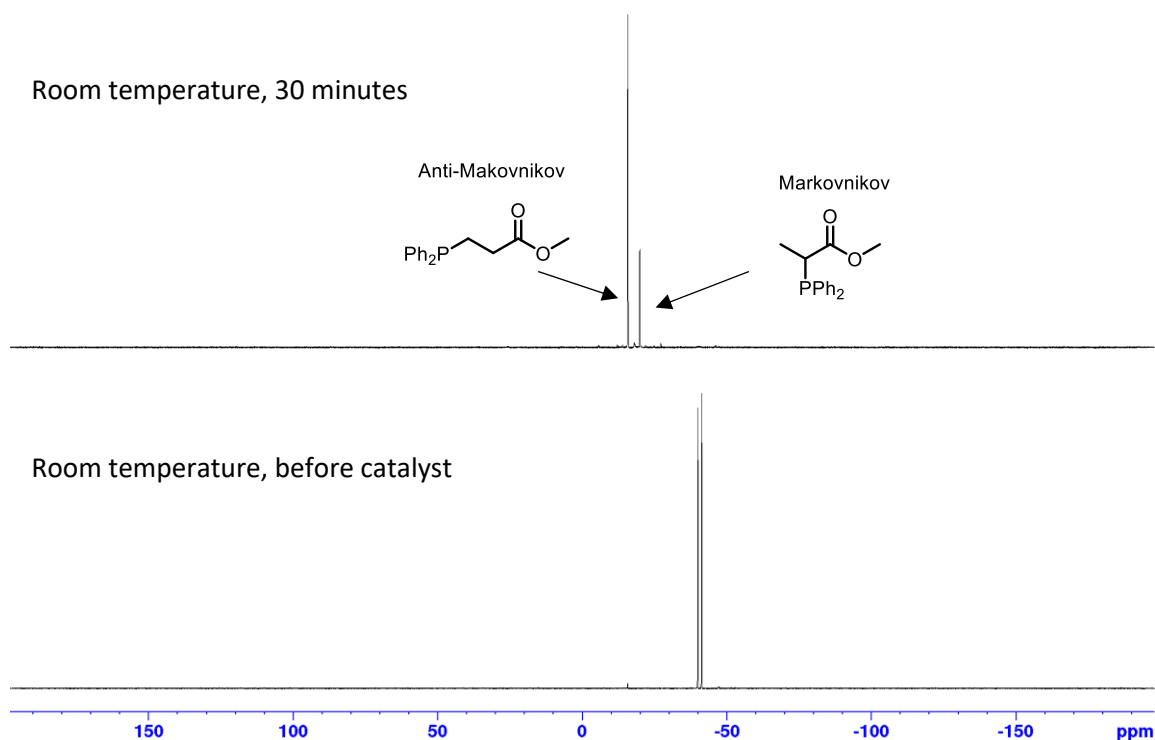


Figure S108: ^{31}P NMR spectrum for the hydrophosphination of methyl acrylate catalysed by **4** (10 mol%) in d_8 -toluene.

Stereoselectivity Study with Temperature

Heating with phenylacetylene

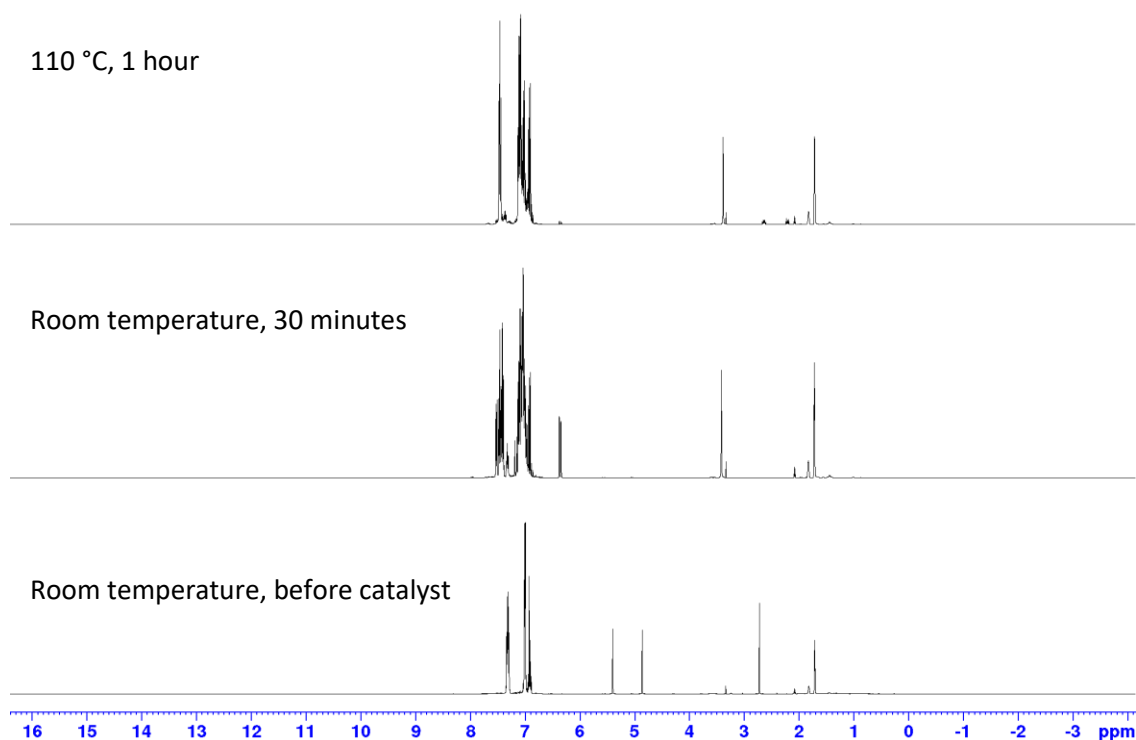


Figure S109: ^1H NMR spectrum for the hydrophosphination of phenylacetylene catalysed by **3** (10 mol%), followed by heating to demonstrate isomerisation, in d_8 -toluene.

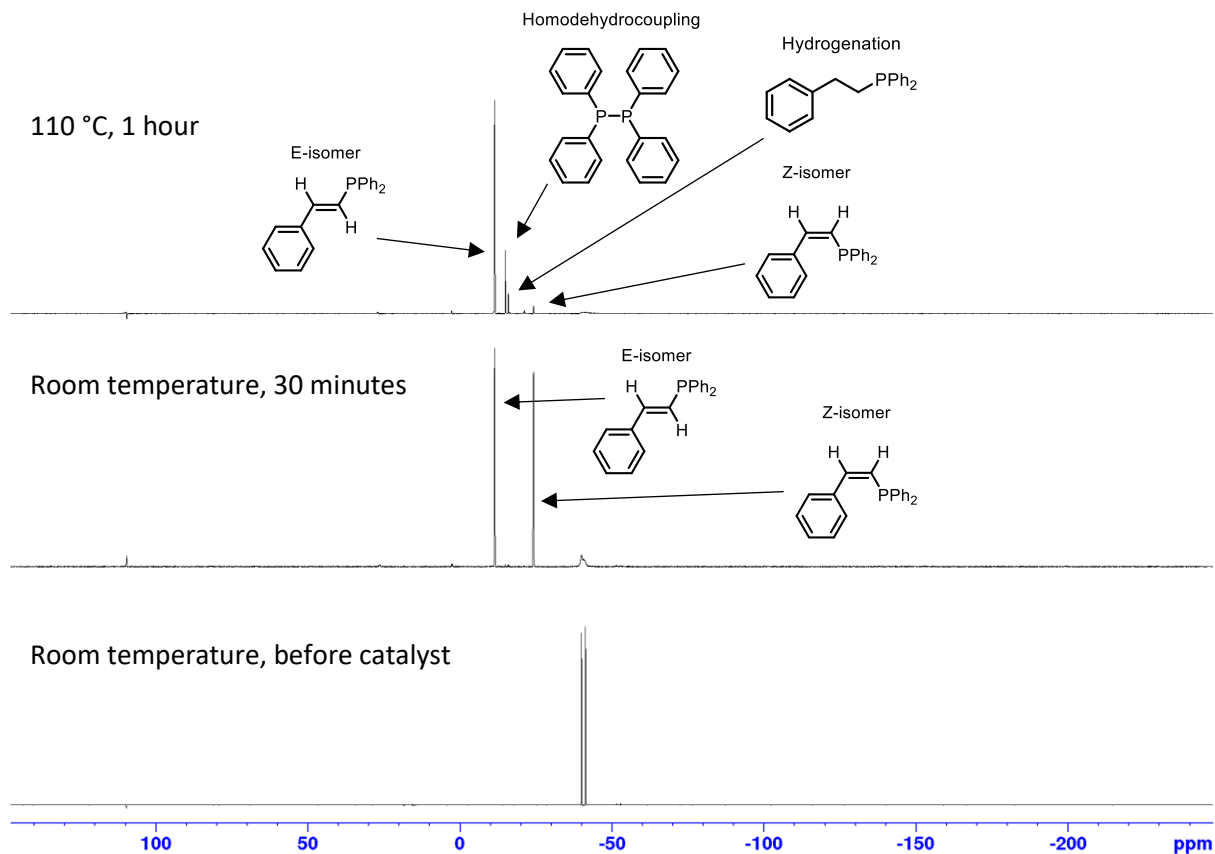


Figure S110: ^{31}P NMR spectrum for the hydrophosphination of phenylacetylene catalysed by **3** (10 mol%), followed by heating to demonstrate isomerisation, in d_8 -toluene.

Heating with diphenylacetylene

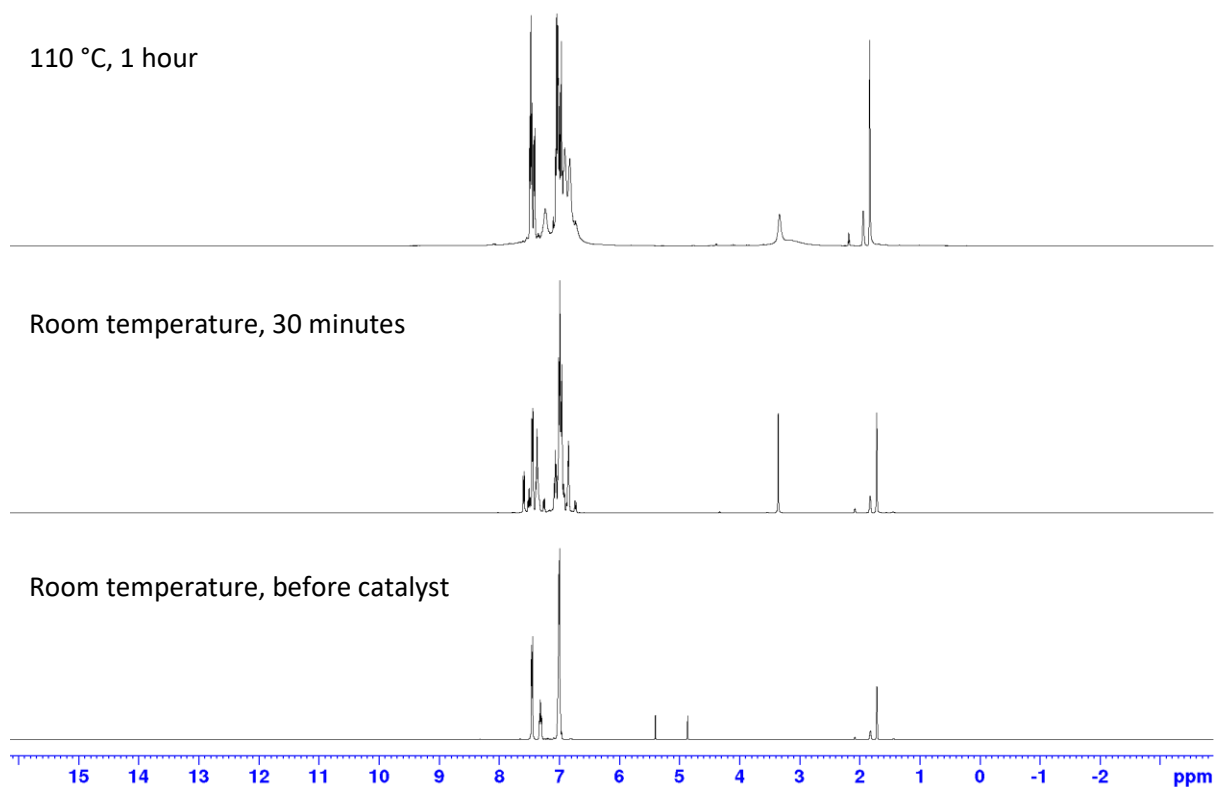


Figure S111: ^1H NMR spectrum for the hydrophosphination of diphenylacetylene catalysed by **3** (10 mol%), followed by heating to demonstrate isomerisation, in d_8 -toluene.

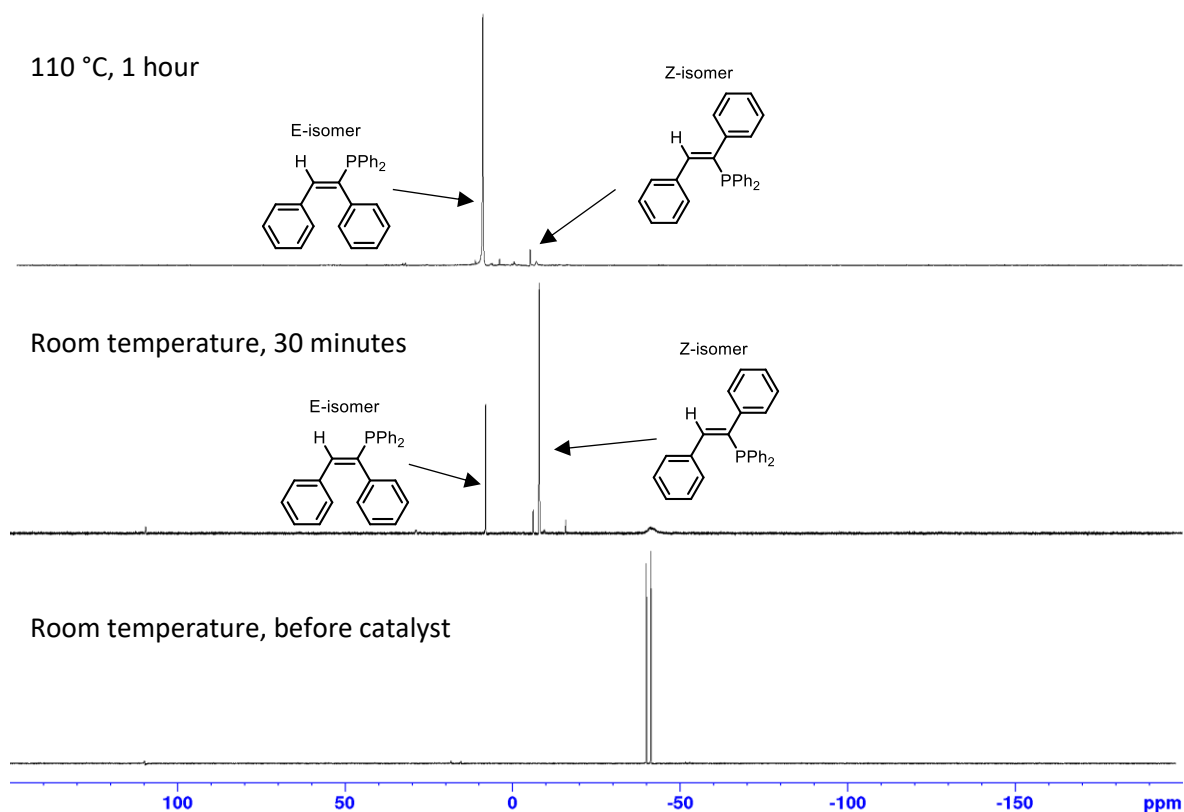


Figure S112: ^{31}P NMR spectrum for the hydrophosphination of diphenylacetylene catalysed by **3** (10 mol%), followed by heating to demonstrate isomerisation, in d_8 -toluene.

Heating with 4'-methylphenylacetylene

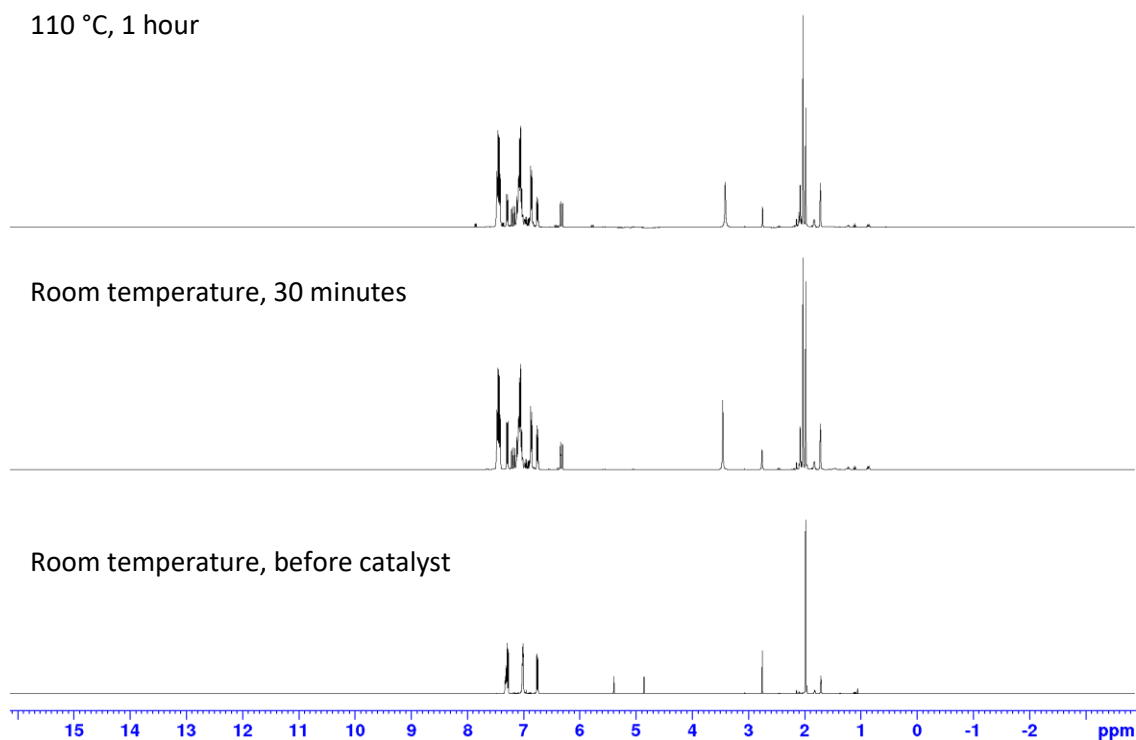


Figure S113: ^1H NMR spectrum for the hydrophosphination of 4'-methylphenylacetylene catalysed by **3** (10 mol%), followed by heating to demonstrate isomerisation, in d_8 -toluene.

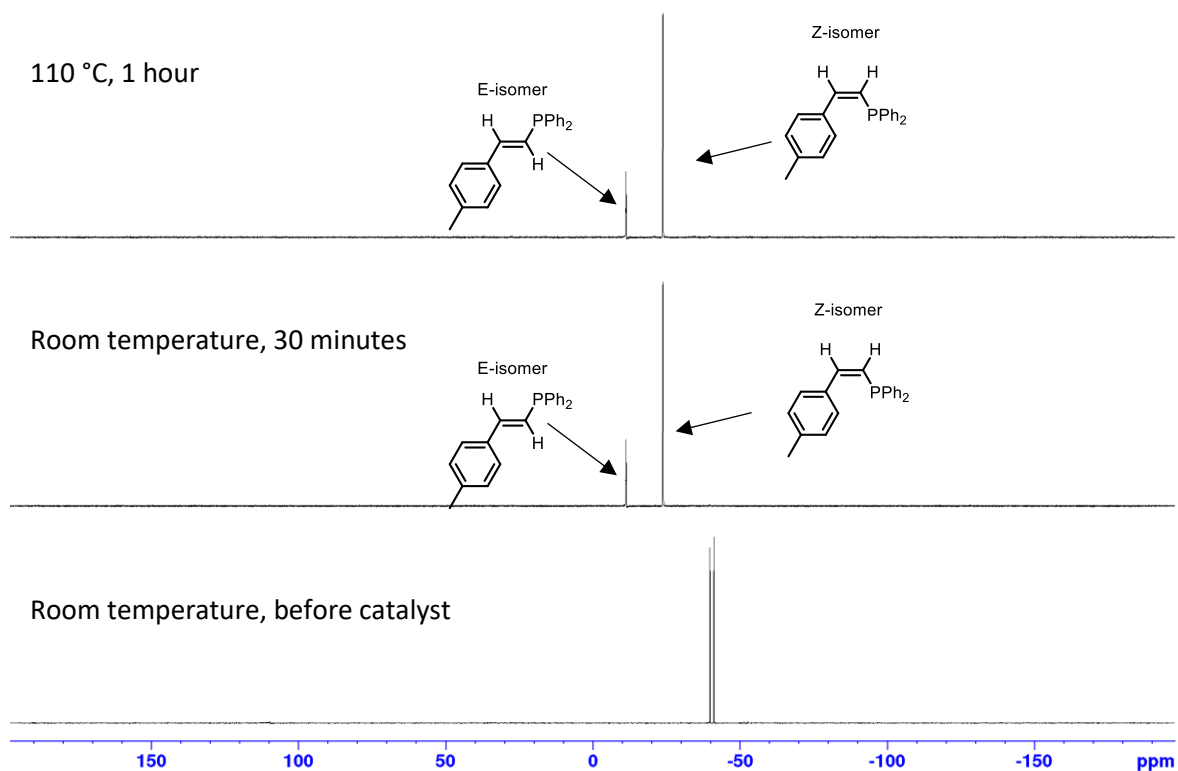


Figure S114: ^{31}P NMR spectrum for the hydrophosphination of 4'-methylphenylacetylene catalysed by **3** (10 mol%), followed by heating to demonstrate isomerisation, in d_8 -toluene.

Heating with 4'-trifluoromethylphenylacetylene

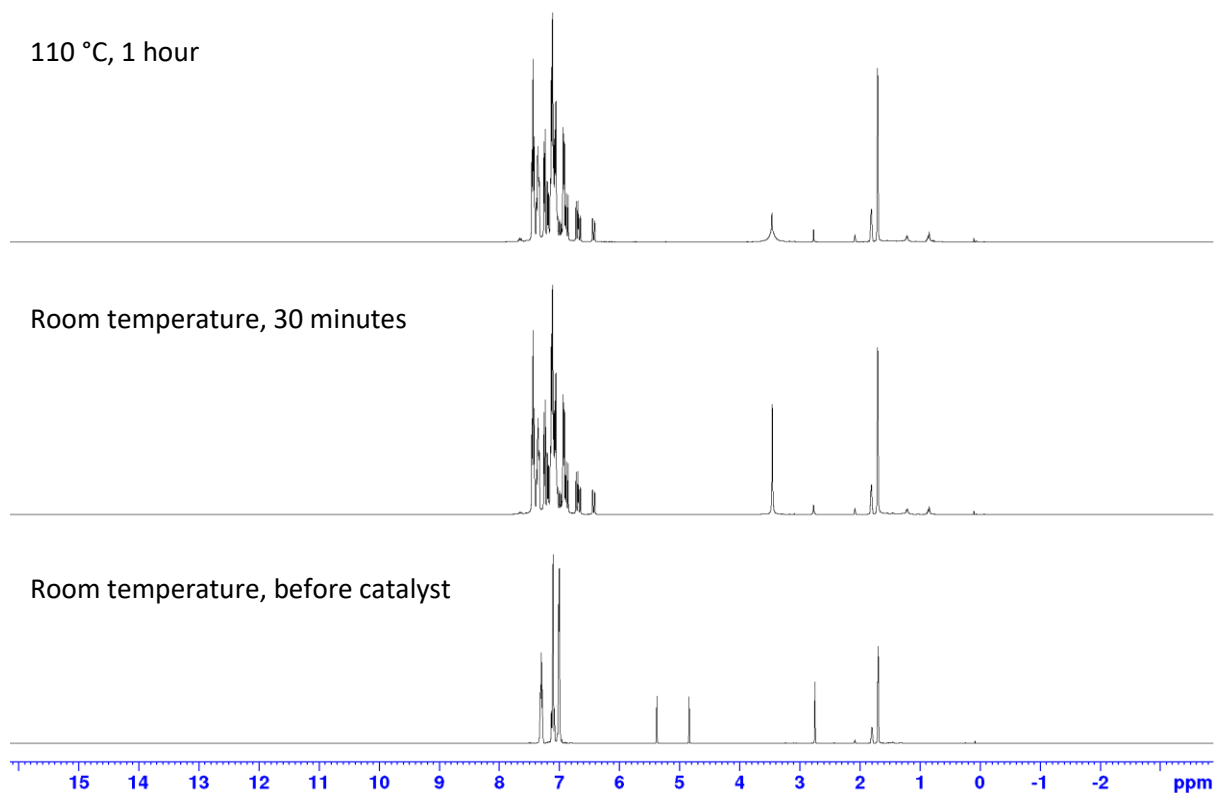


Figure S115: ^1H NMR spectrum for the hydrophosphination of 4'-trifluoromethylphenylacetylene catalysed by **3** (10 mol%), followed by heating to demonstrate isomerisation, in d_8 -toluene.

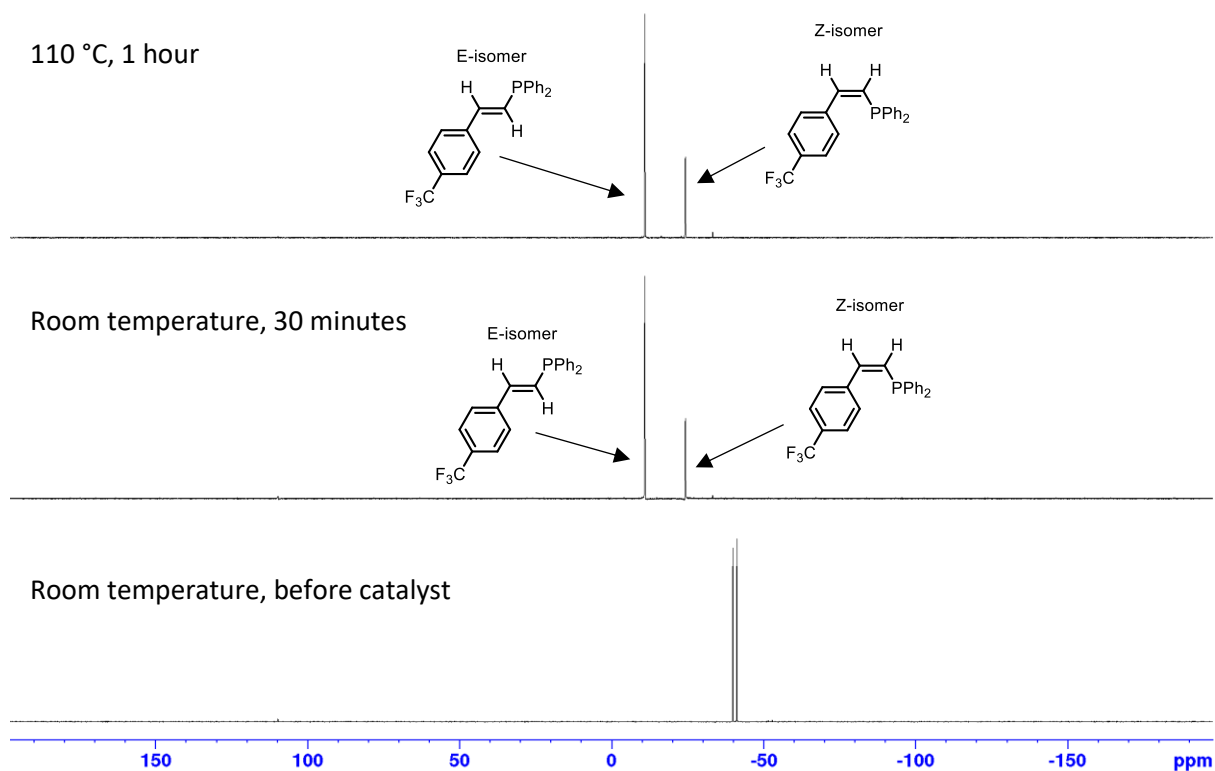


Figure S116: ^{31}P NMR spectrum for the hydrophosphination of 4'-trifluoromethylphenylacetylene catalysed by **3** (10 mol%), followed by heating to demonstrate isomerisation, in d_8 -toluene.

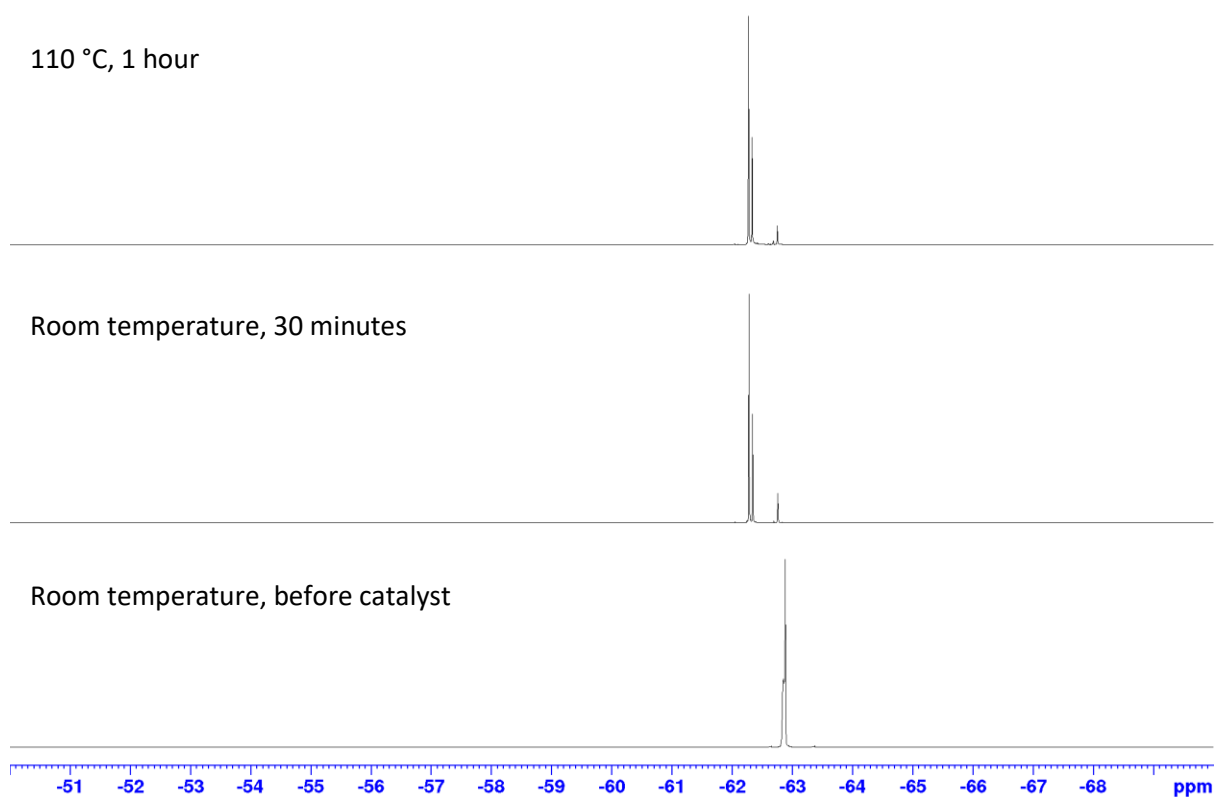
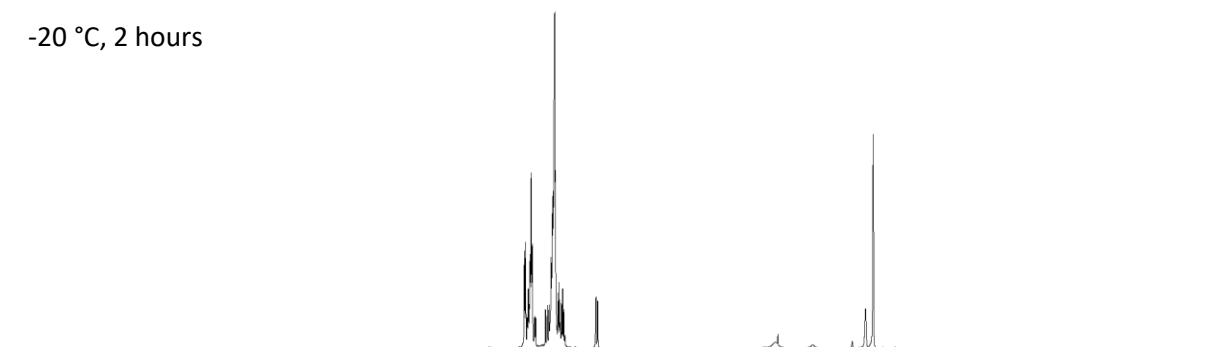


Figure S117: $^{19}\text{F}\{^1\text{H}\}$ NMR spectrum for the hydrophosphination of 4'-trifluoromethylphenylacetylene catalysed by **3** (10 mol%), followed by heating to demonstrate isomerisation, in d_8 -toluene.

Cooling with phenylacetylene

-20 °C, 2 hours



Room temperature, before catalyst

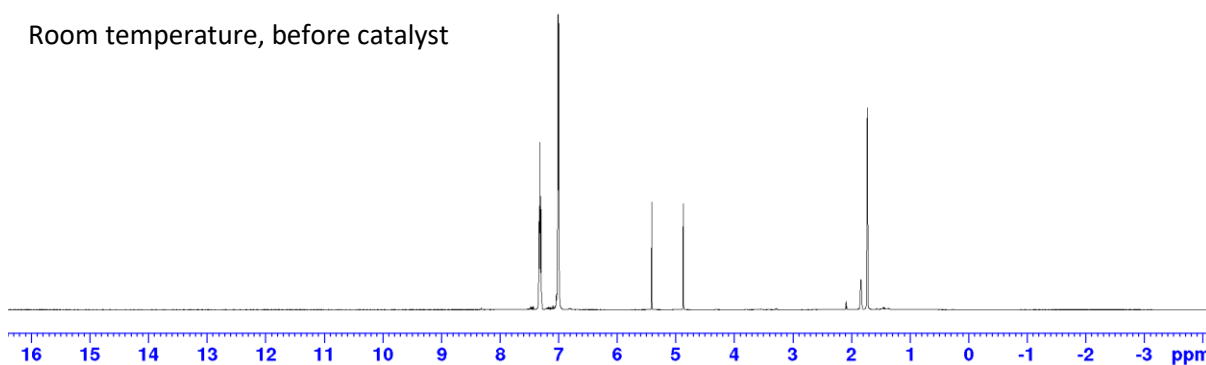
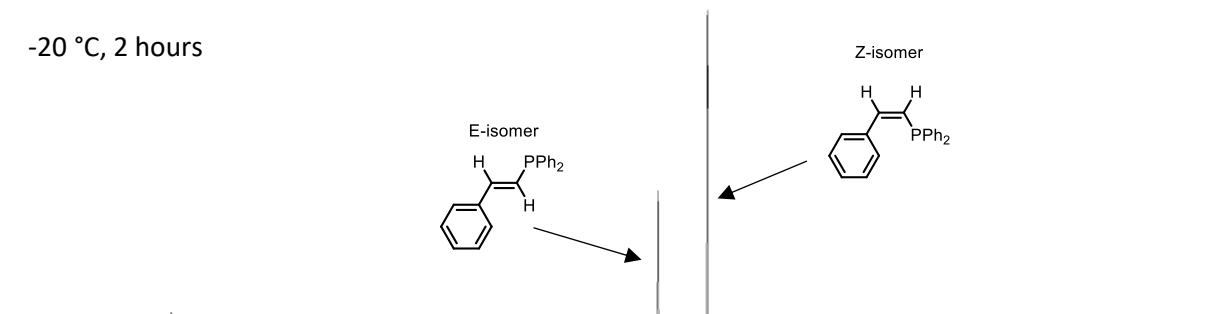


Figure S118: ¹H NMR spectrum for the hydrophosphination of phenylacetylene catalysed by **3** (10 mol%) at reduced temperature to demonstrate isomerisation, in d₈-toluene.

-20 °C, 2 hours



Room temperature, before catalyst

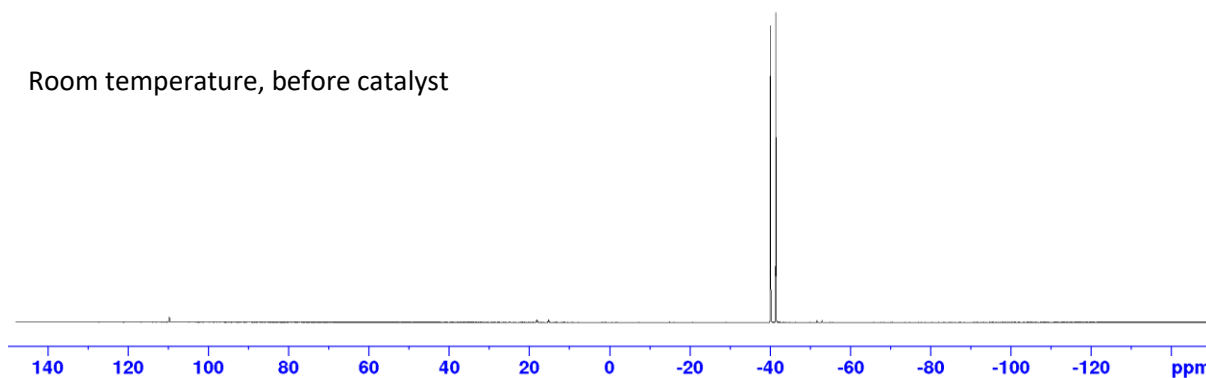
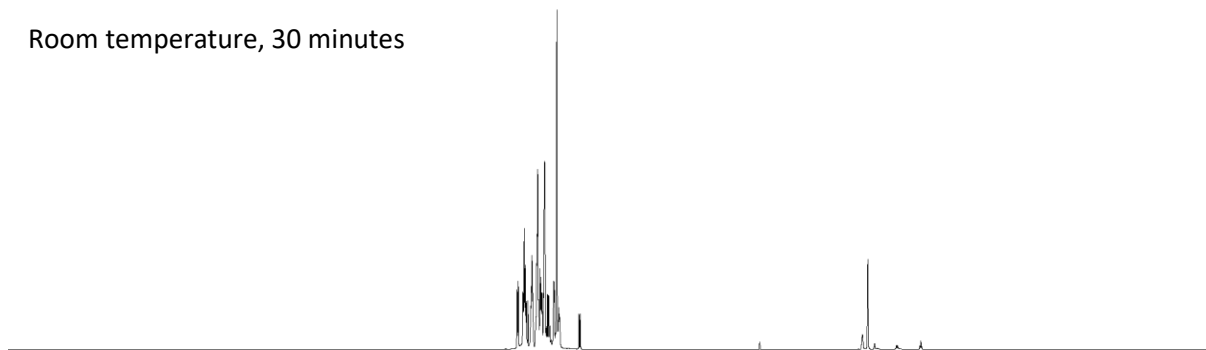


Figure S119: ³¹P NMR spectrum for the hydrophosphination of phenylacetylene catalysed by **3** (10 mol%) at reduced temperature to demonstrate isomerisation, in d₈-toluene.

Stereoselectivity Study with Amine Additives

Diphenylacetylene with $[\text{NaPPh}_2]_\infty$

Room temperature, 30 minutes



Room temperature, before catalyst

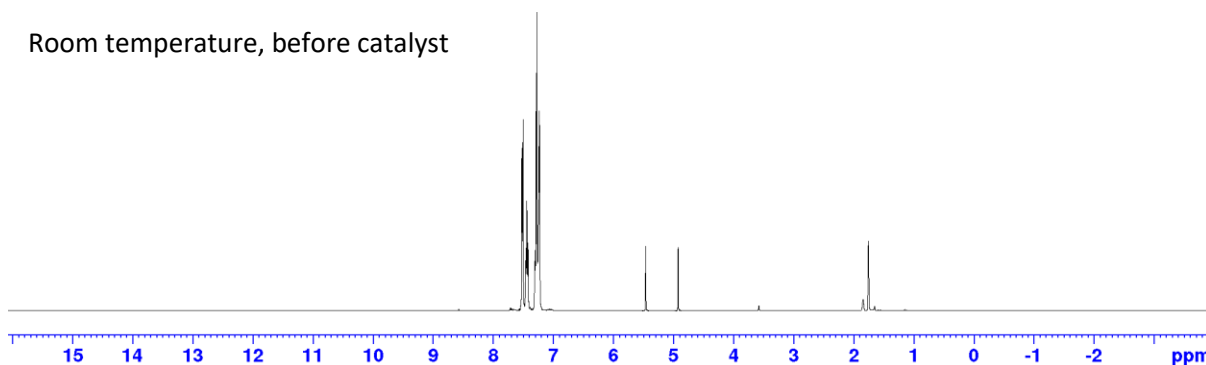
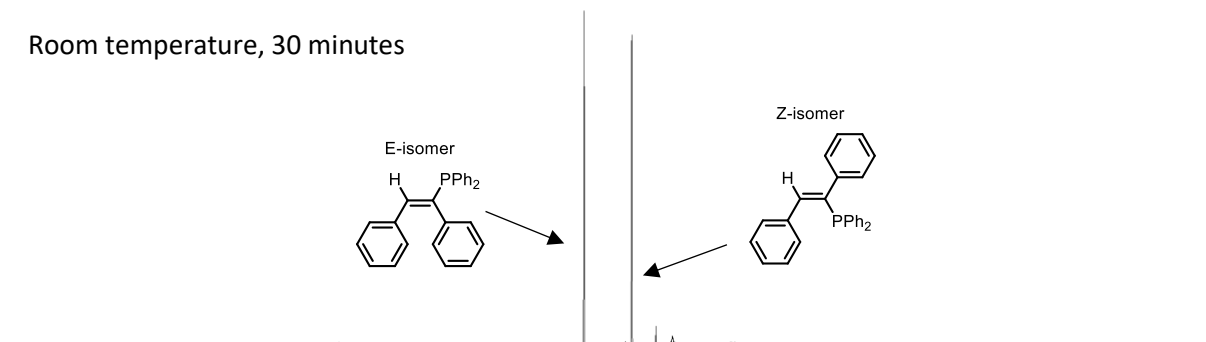


Figure S120: ^1H NMR spectrum for the hydrophosphination of diphenylacetylene catalysed by $[\text{NaPPh}_2]_\infty$ (10 mol%) in d_8 -THF.

Room temperature, 30 minutes



Room temperature, before catalyst

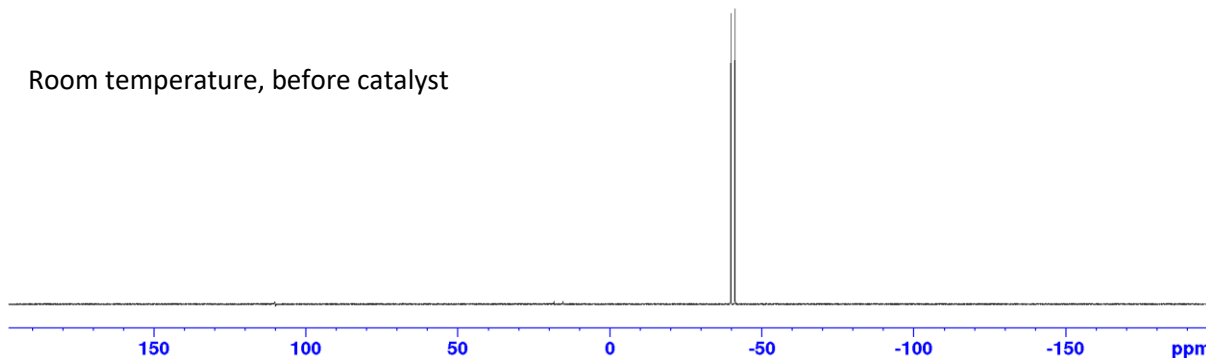


Figure S121: ^{31}P NMR spectrum for the hydrophosphination of diphenylacetylene catalysed by $[\text{NaPPh}_2]_\infty$ (10 mol%) in d_8 -THF.

Diphenylacetylene with $[\text{NaPPh}_2]_\infty$ and *n*-Butylamine

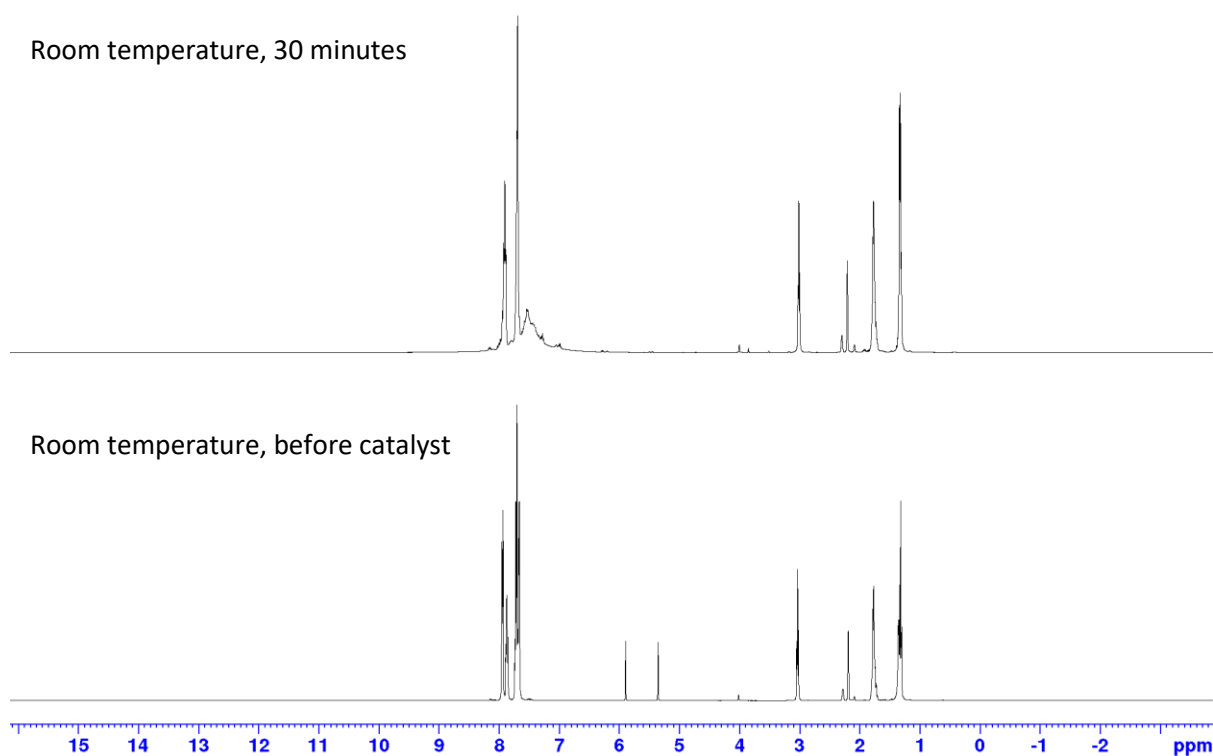


Figure S122: ^1H NMR spectrum for the hydrophosphination of diphenylacetylene catalysed by $[\text{NaPPh}_2]_\infty$ (10 mol%), with *n*-butylamine additive, in d_8 -THF.

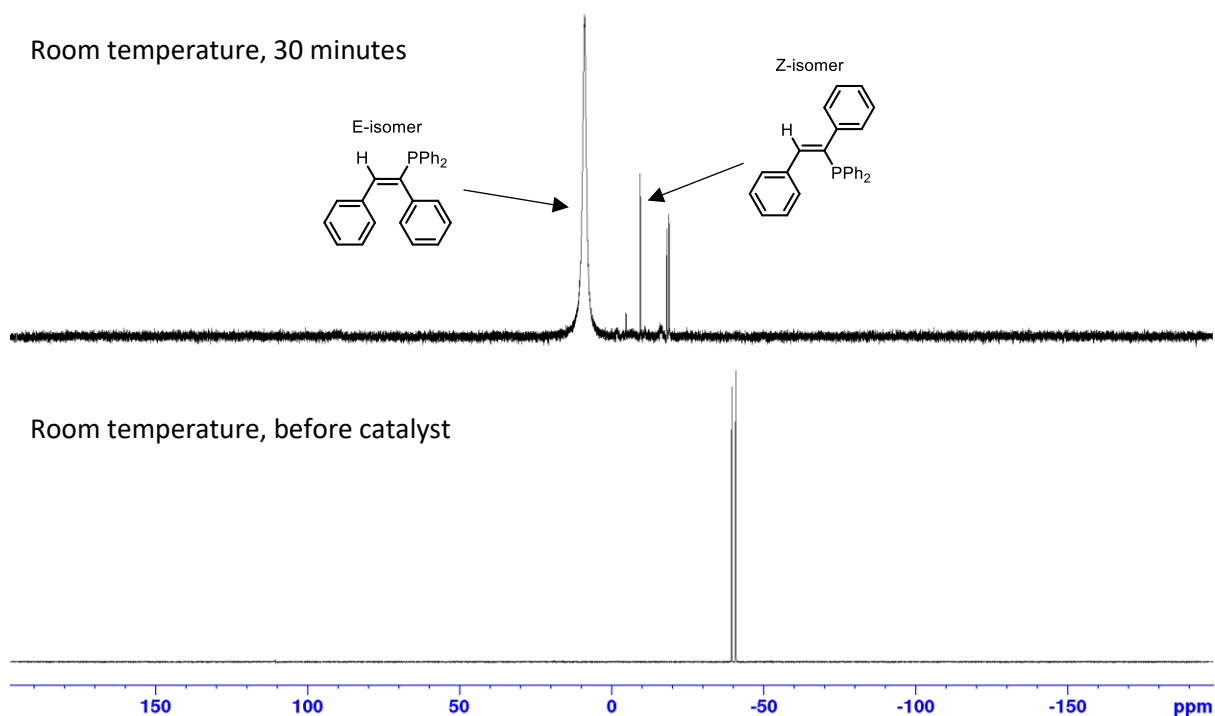


Figure S123: ^{31}P NMR spectrum for the hydrophosphination of diphenylacetylene catalysed by $[\text{NaPPh}_2]_\infty$ (10 mol%), with *n*-butylamine additive, in d_8 -THF.

Diphenylacetylene with $[\text{NaPPh}_2]_\infty$ and *N*-methylaniline

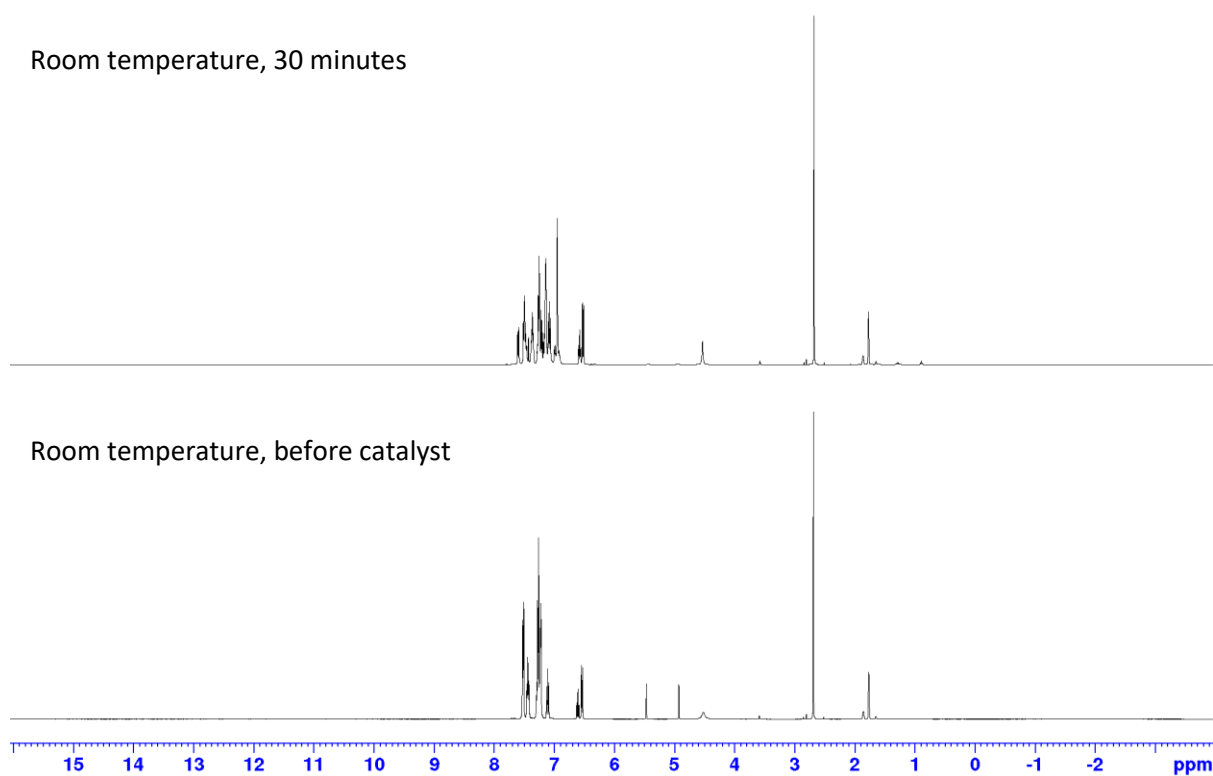


Figure S124: ^1H NMR spectrum for the hydrophosphination of diphenylacetylene catalysed by $[\text{NaPPh}_2]_\infty$ (10 mol%), with *N*-methylaniline additive, in d_8 -THF.

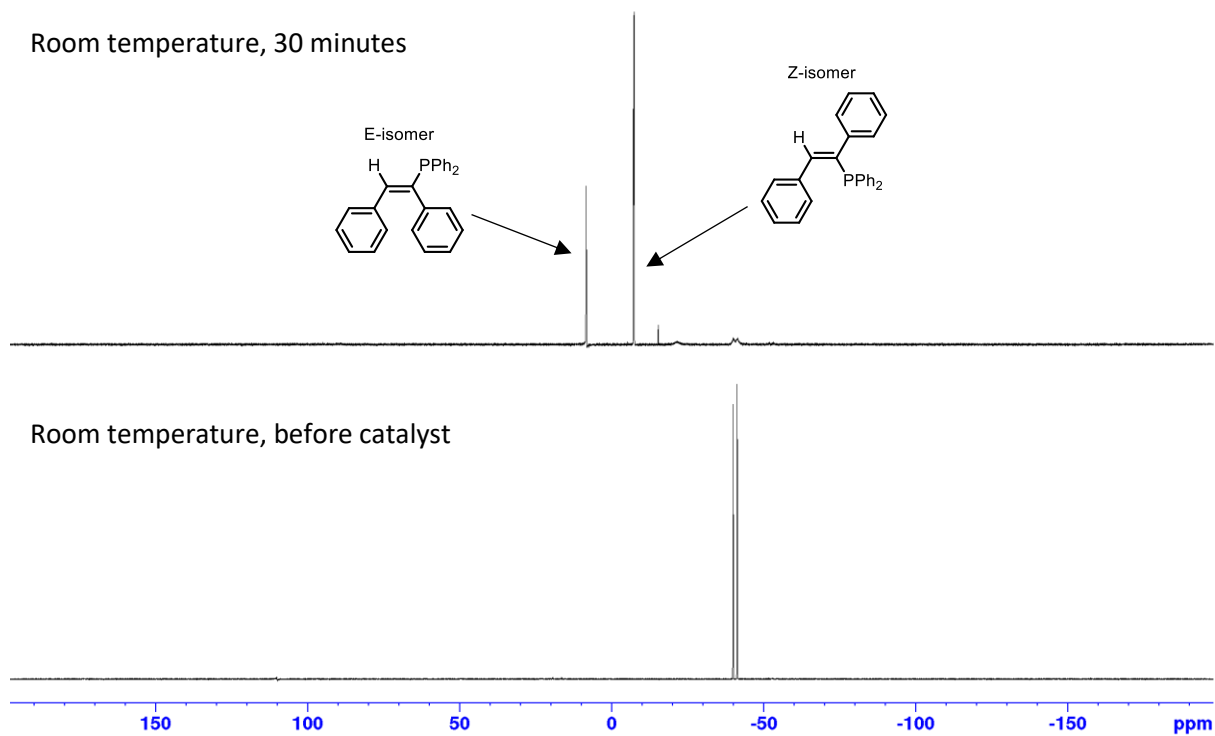


Figure S125: ^{31}P NMR spectrum for the hydrophosphination of diphenylacetylene catalysed by $[\text{NaPPh}_2]_\infty$ (10 mol%), with *N*-methylaniline additive, in d_8 -THF.

Diphenylacetylene with **3** and *n*-Butylamine (*d*₈-toluene)

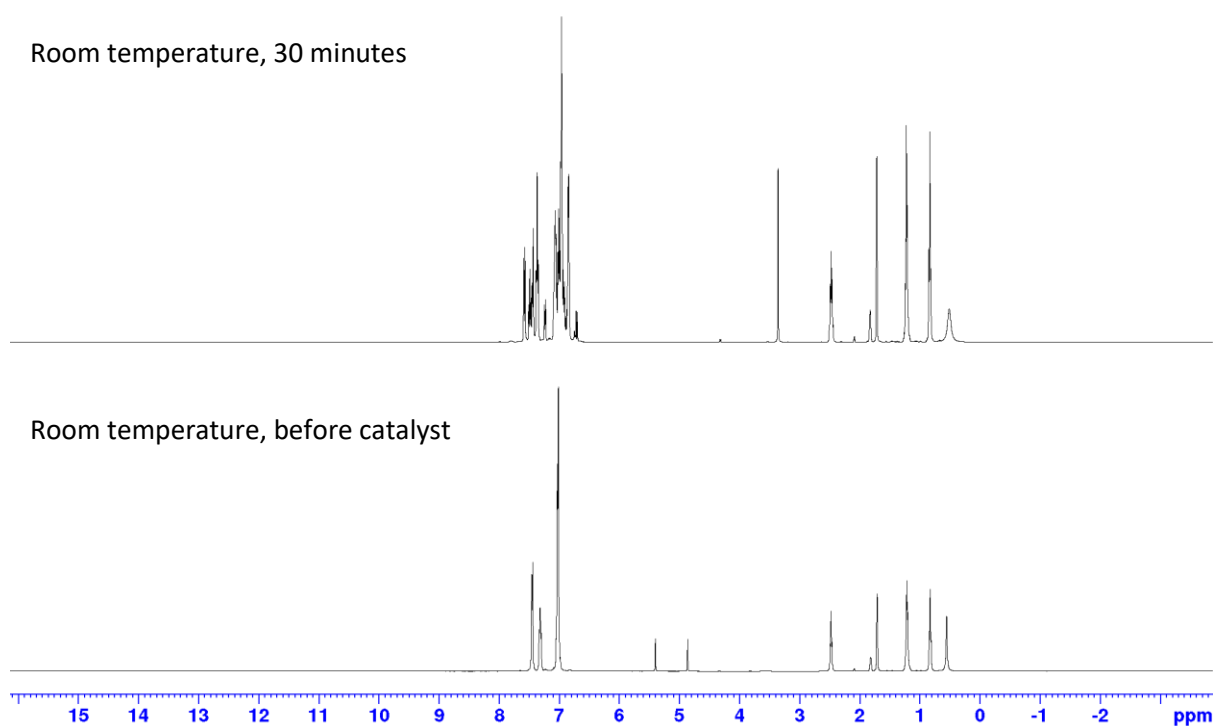


Figure S126: ¹H NMR spectrum for the hydrophosphination of diphenylacetylene catalysed by **3** (10 mol%), with *n*-butylamine additive, in *d*₈-toluene.

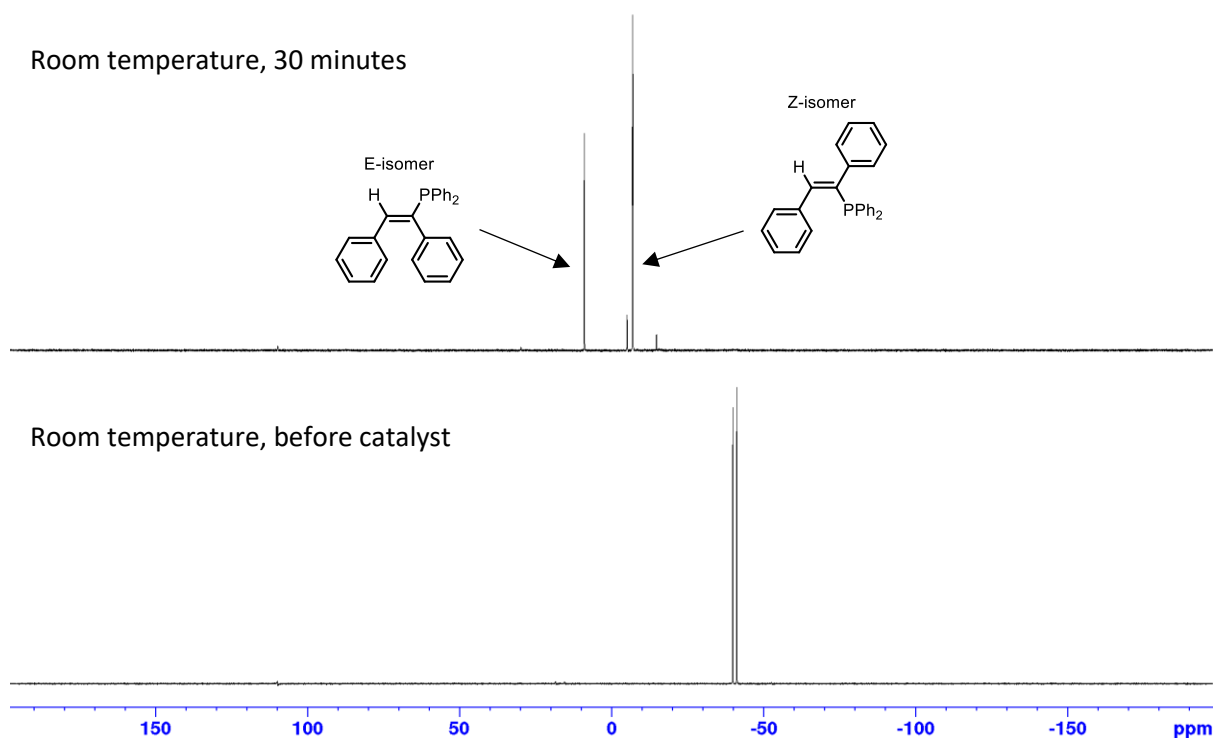


Figure S127: ³¹P NMR spectrum for the hydrophosphination of diphenylacetylene catalysed by **3** (10 mol%), with *n*-butylamine additive, in *d*₈-toluene.

Diphenylacetylene with **3** (d₈-THF)

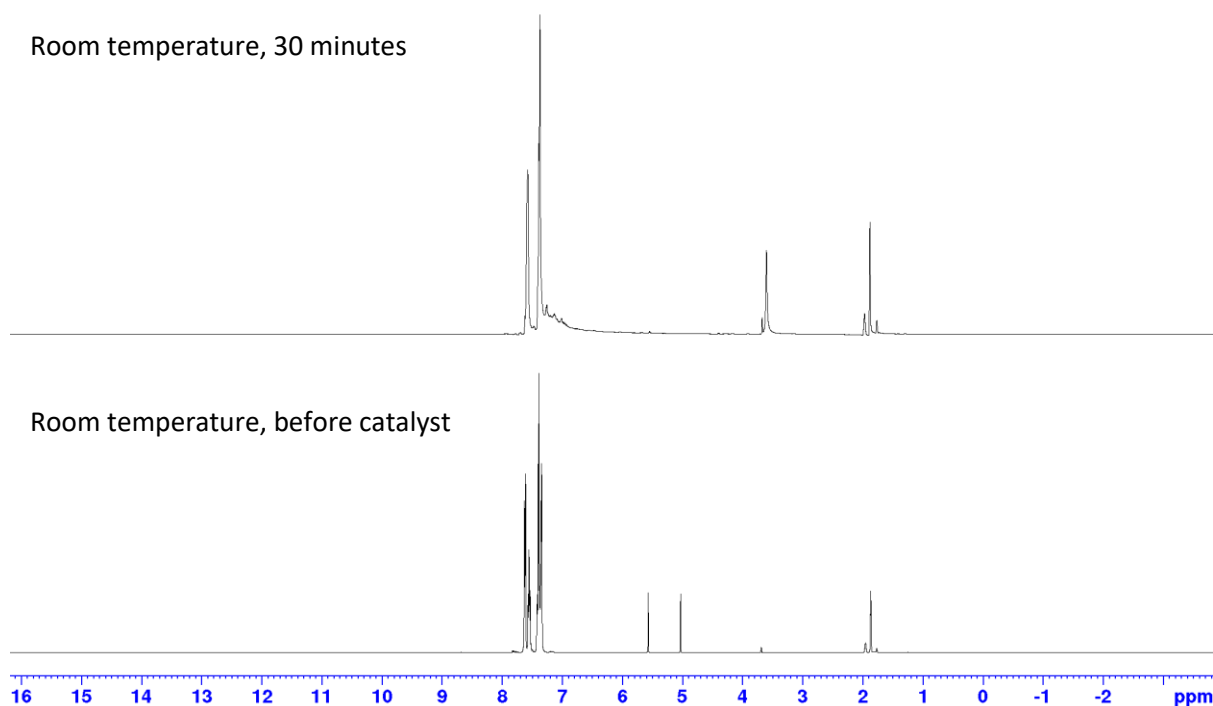


Figure S128: ¹H NMR spectrum for the hydrophosphination of diphenylacetylene catalysed by **3** (10 mol%) in d₈-THF.

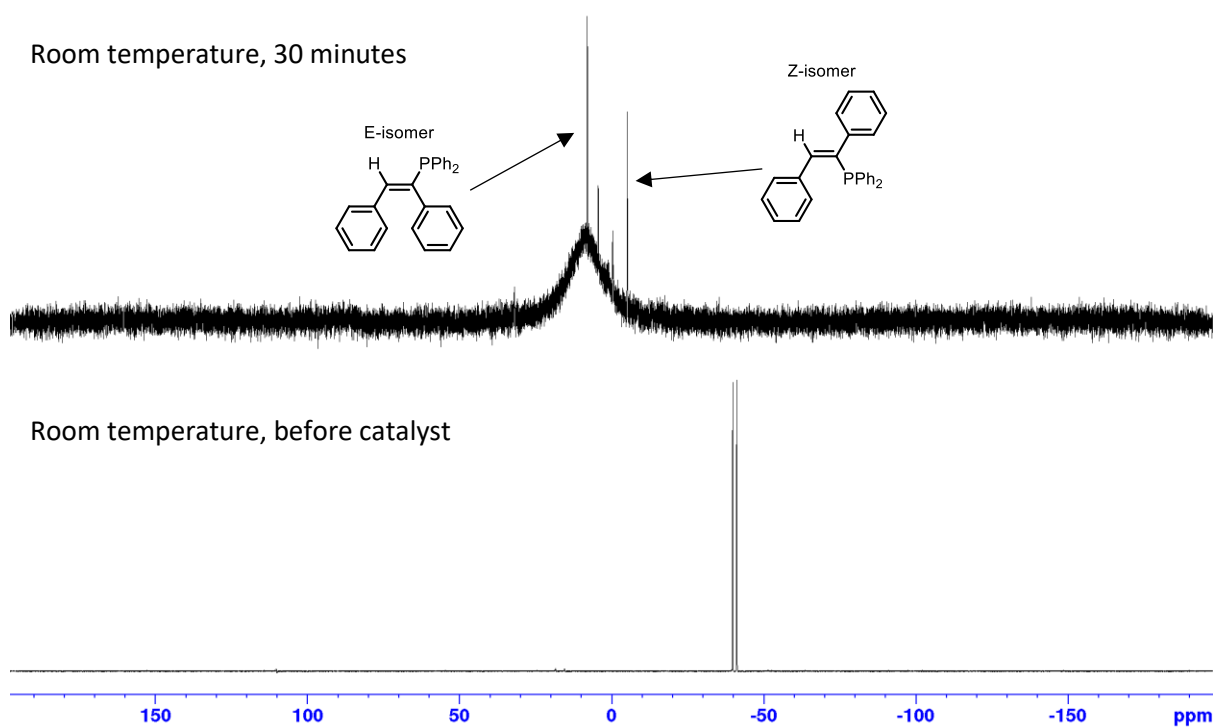


Figure S129: ³¹P NMR spectrum for the hydrophosphination of diphenylacetylene catalysed by **3** (10 mol%) in d₈-THF.

Diphenylacetylene with **3** and *n*-Butylamine (d₈-THF)

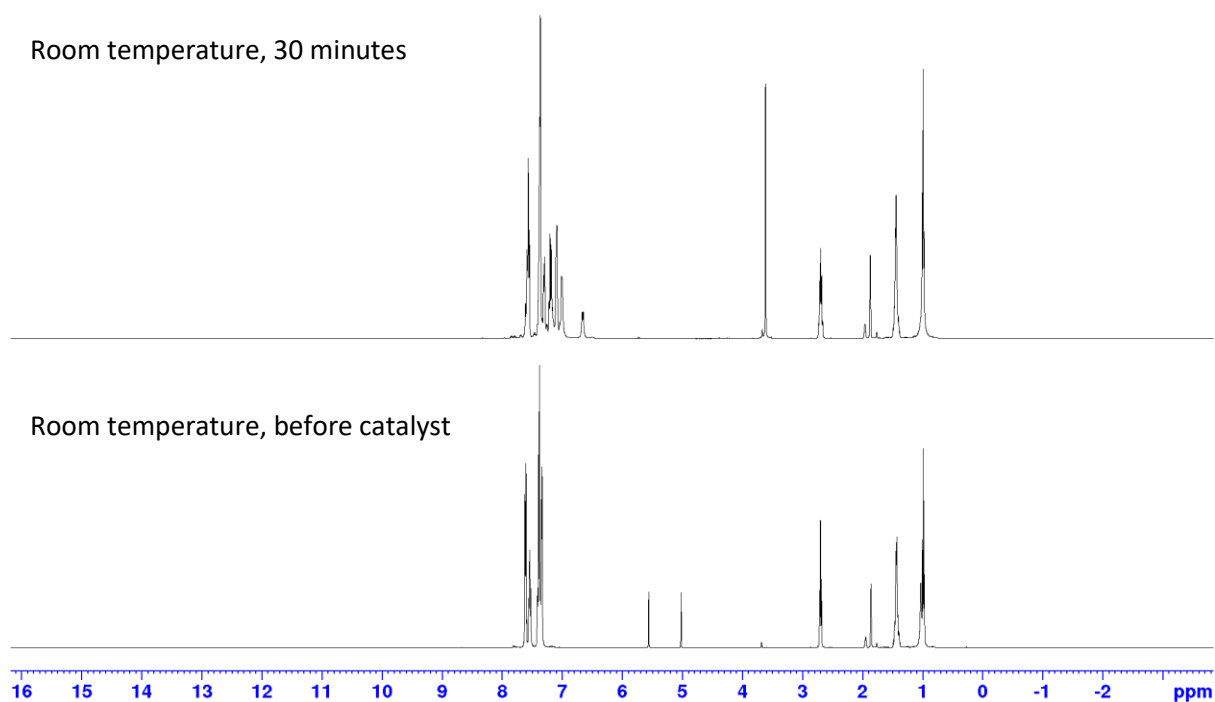


Figure S130: ¹H NMR spectrum for the hydrophosphination of diphenylacetylene catalysed by **3** (10 mol%), with *n*-butylamine additive, in d₈-THF.

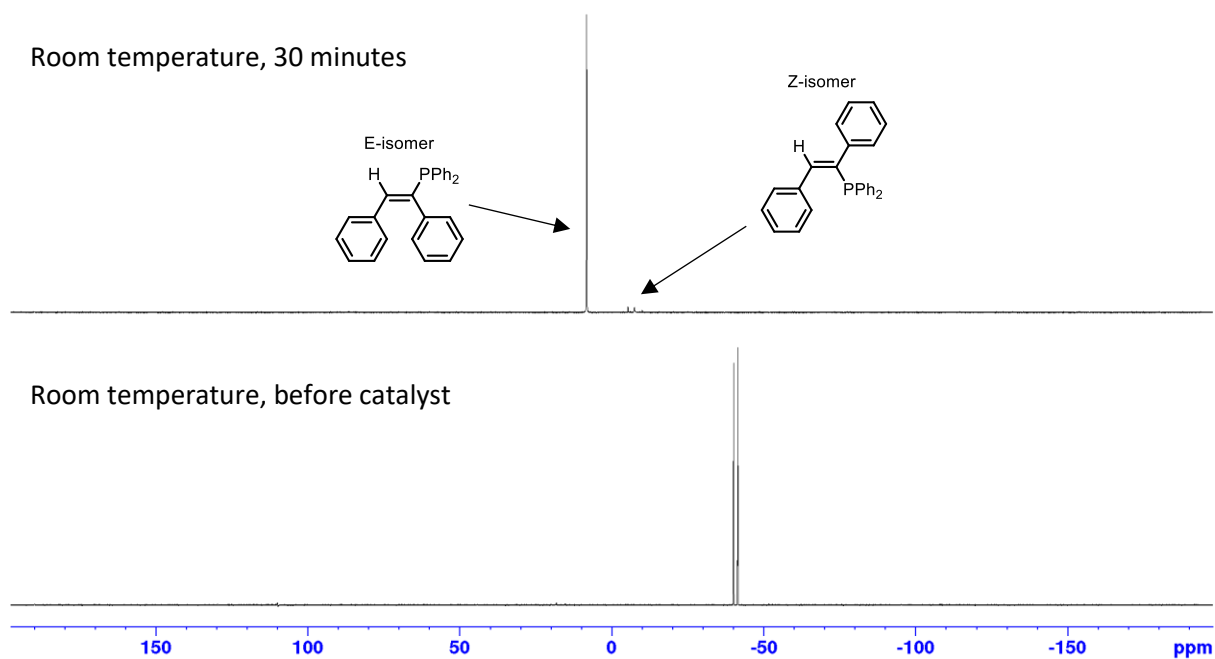


Figure S131: ³¹P NMR spectrum for the hydrophosphination of diphenylacetylene catalysed by **3** (10 mol%), with *n*-butylamine additive, in d₈-THF.

Diphenylacetylene with **3** and *N*-methylaniline

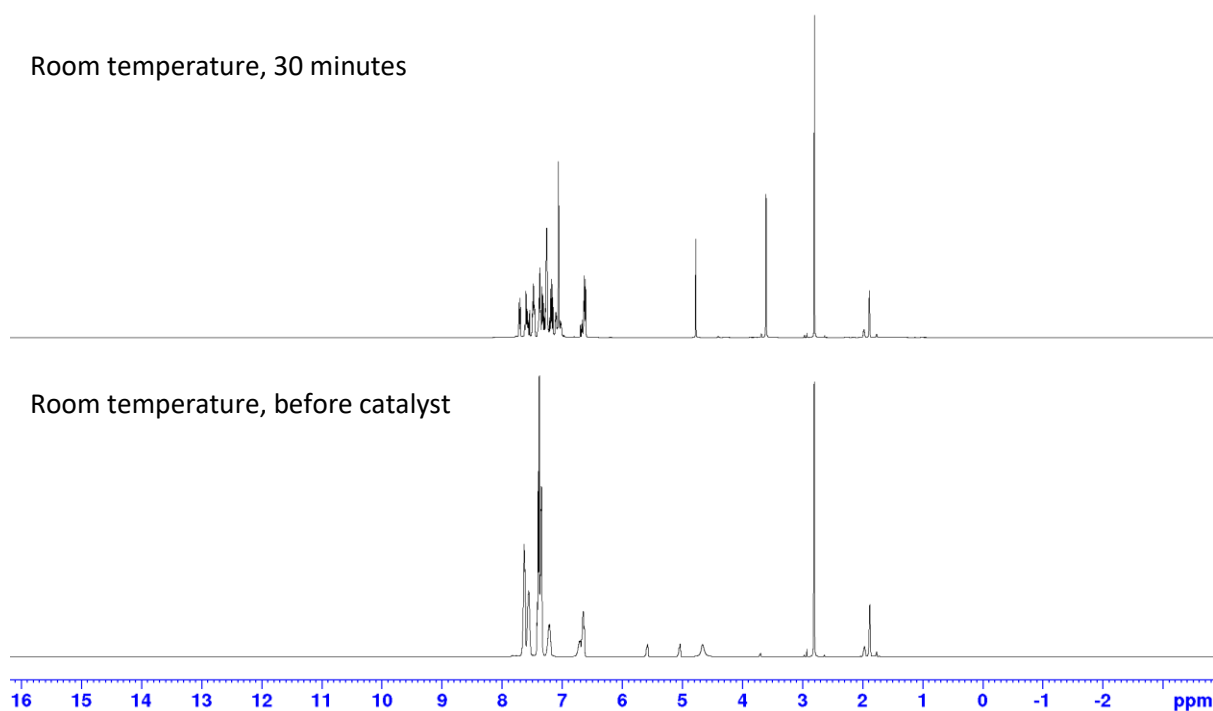


Figure S132: ¹H NMR spectrum for the hydrophosphination of diphenylacetylene catalysed by **3** (10 mol%), with *N*-methylaniline additive, in d₈-THF.

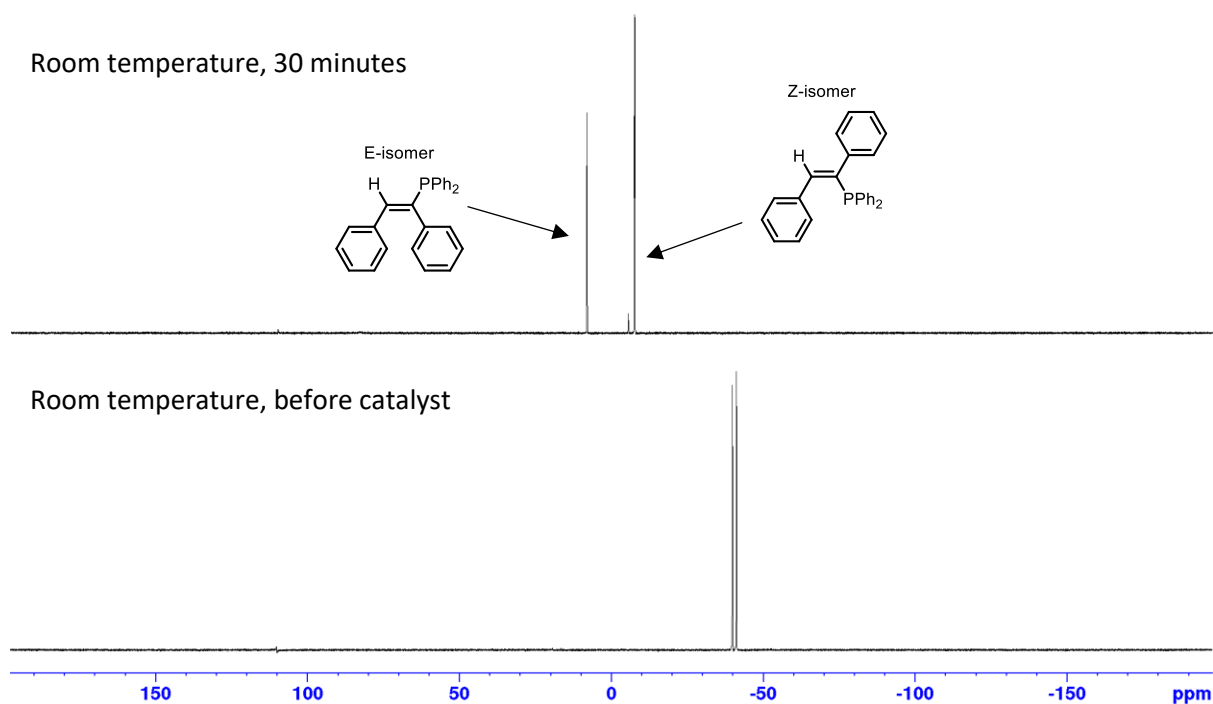


Figure S133: ³¹P NMR spectrum for the hydrophosphination of diphenylacetylene catalysed by **3** (10 mol%), with *N*-methylaniline additive, in d₈-THF.

4'-Methylphenylacetylene with **3** (d₈-THF)

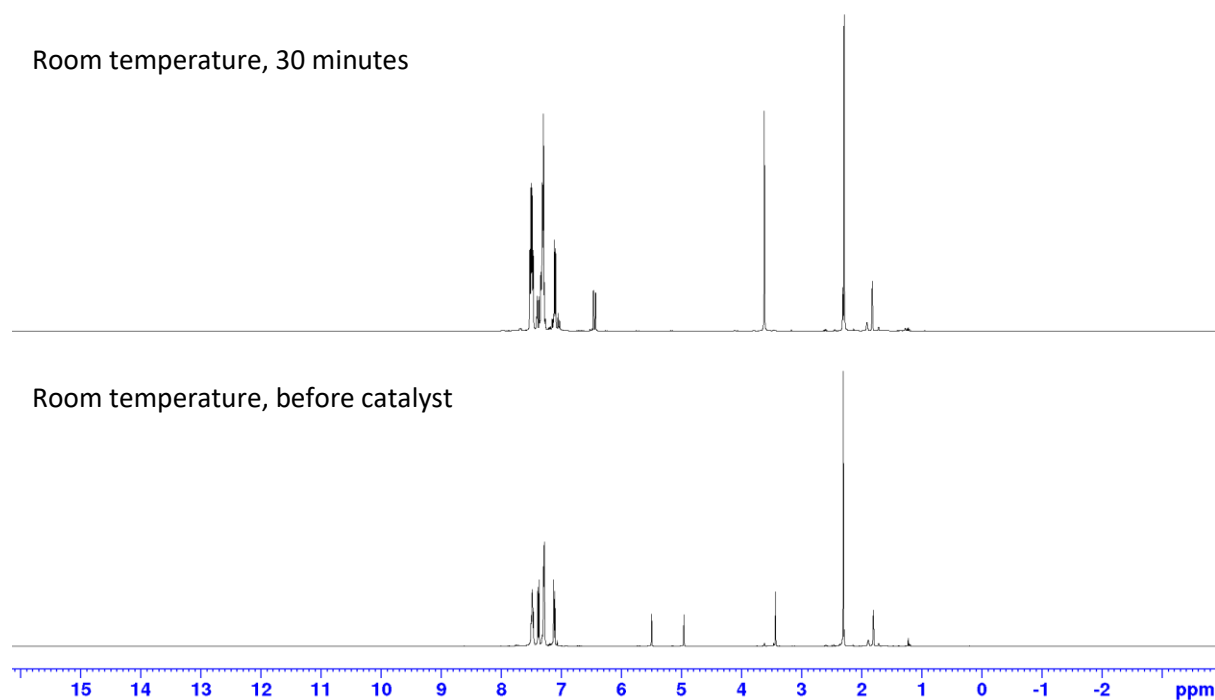


Figure S134: ¹H NMR spectrum for the hydrophosphination of 4'-methylphenylacetylene catalysed by **3** (10 mol%) in d₈-THF.

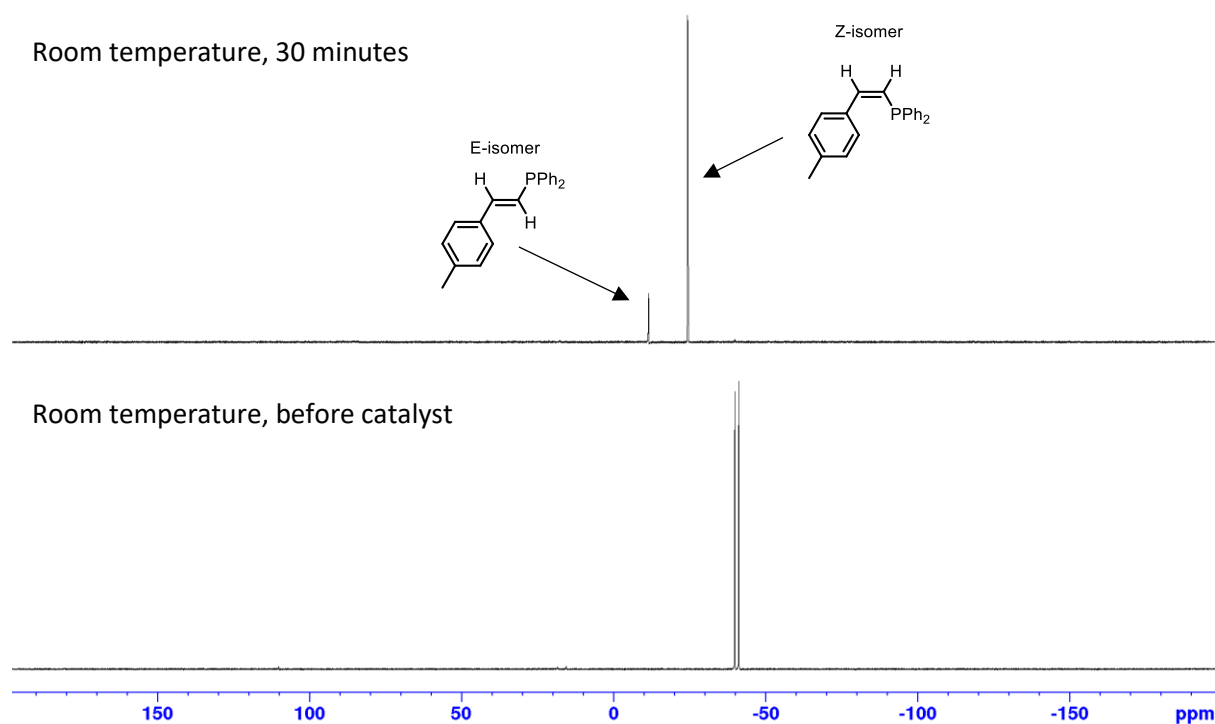
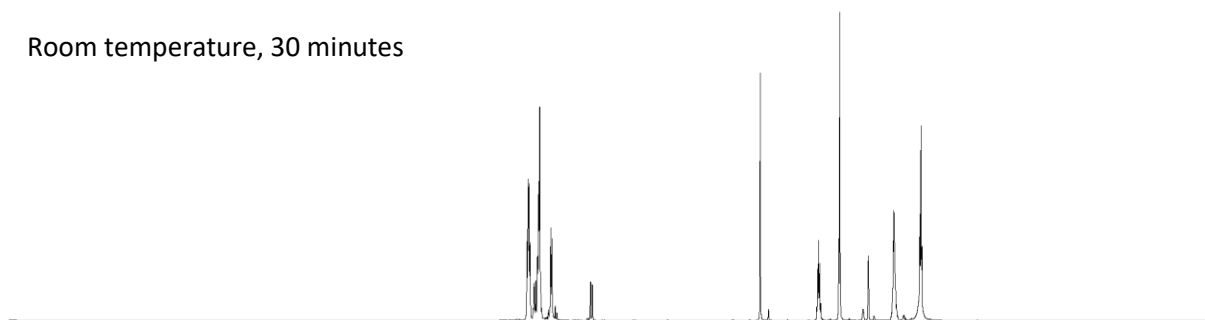


Figure S135: ³¹P NMR spectrum for the hydrophosphination of 4'-methylphenylacetylene catalysed by **3** (10 mol%) in d₈-THF.

4'-Methylphenylacetylene with **3** and *n*-Butylamine

Room temperature, 30 minutes



Room temperature, before catalyst

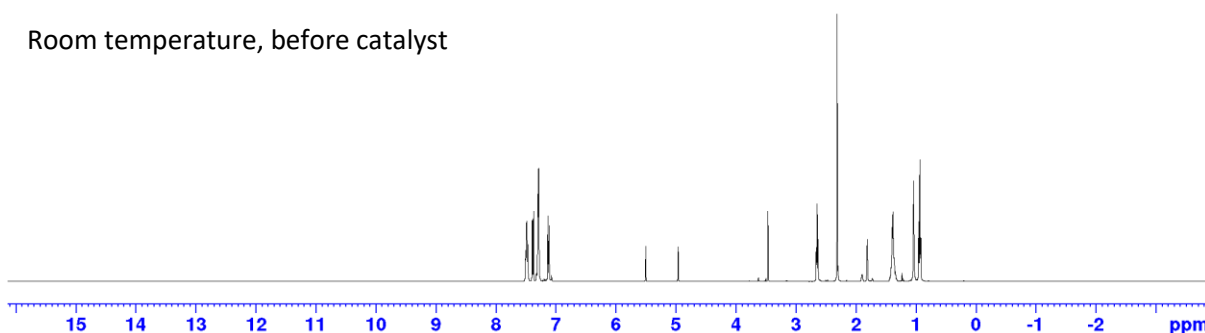
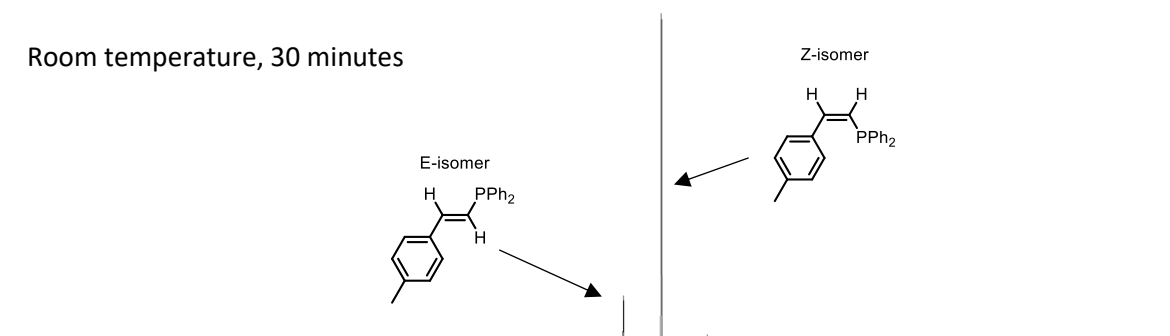


Figure S136: ¹H NMR spectrum for the hydrophosphination of 4'-methylphenylacetylene catalysed by **3** (10 mol%), with *n*-butylamine additive, in d₈-THF.

Room temperature, 30 minutes



Room temperature, before catalyst

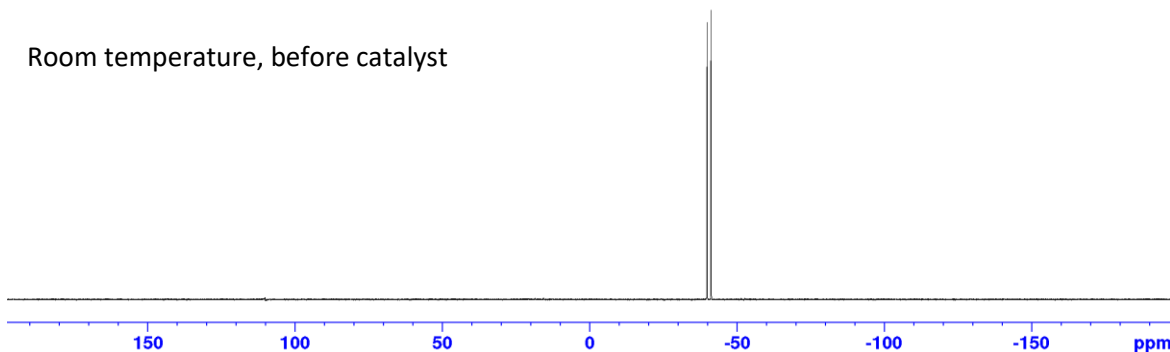


Figure S137: ³¹P NMR spectrum for the hydrophosphination of 4'-methylphenylacetylene catalysed by **3** (10 mol%), with *n*-butylamine additive, in d₈-THF.

4'-Methylphenylacetylene with **3** and *N*-methylaniline

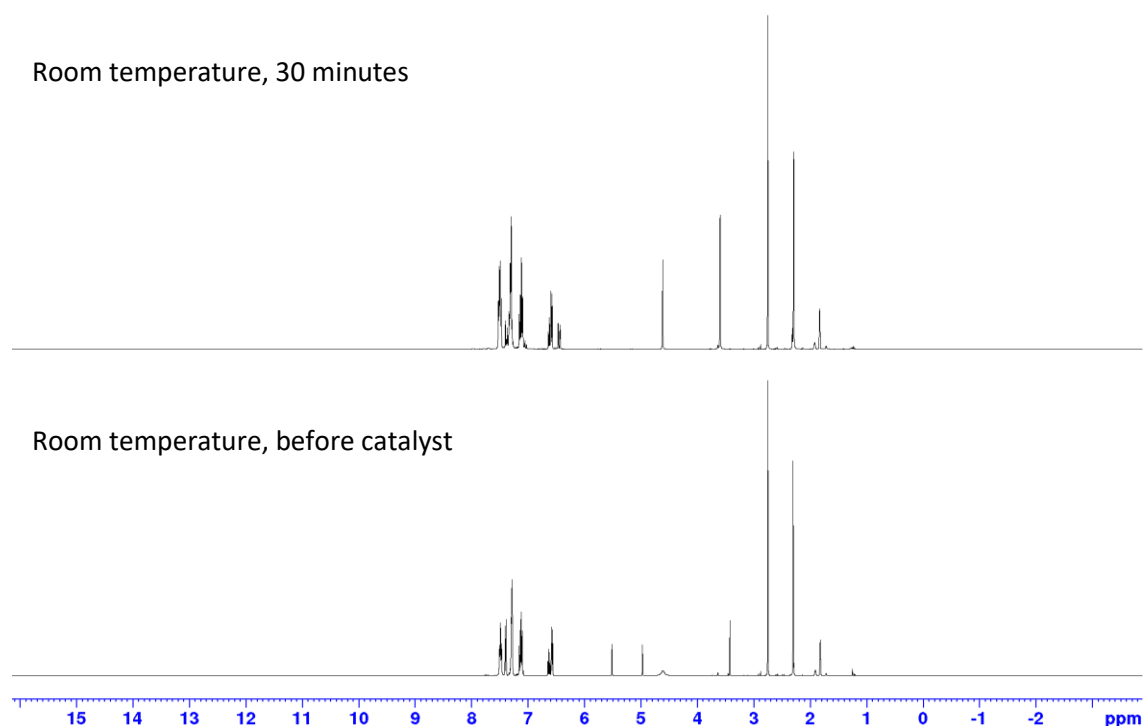


Figure S138: ^1H NMR spectrum for the hydrophosphination of 4'-methylphenylacetylene catalysed by **3** (10 mol%), with *N*-methylaniline additive, in d_8 -THF.

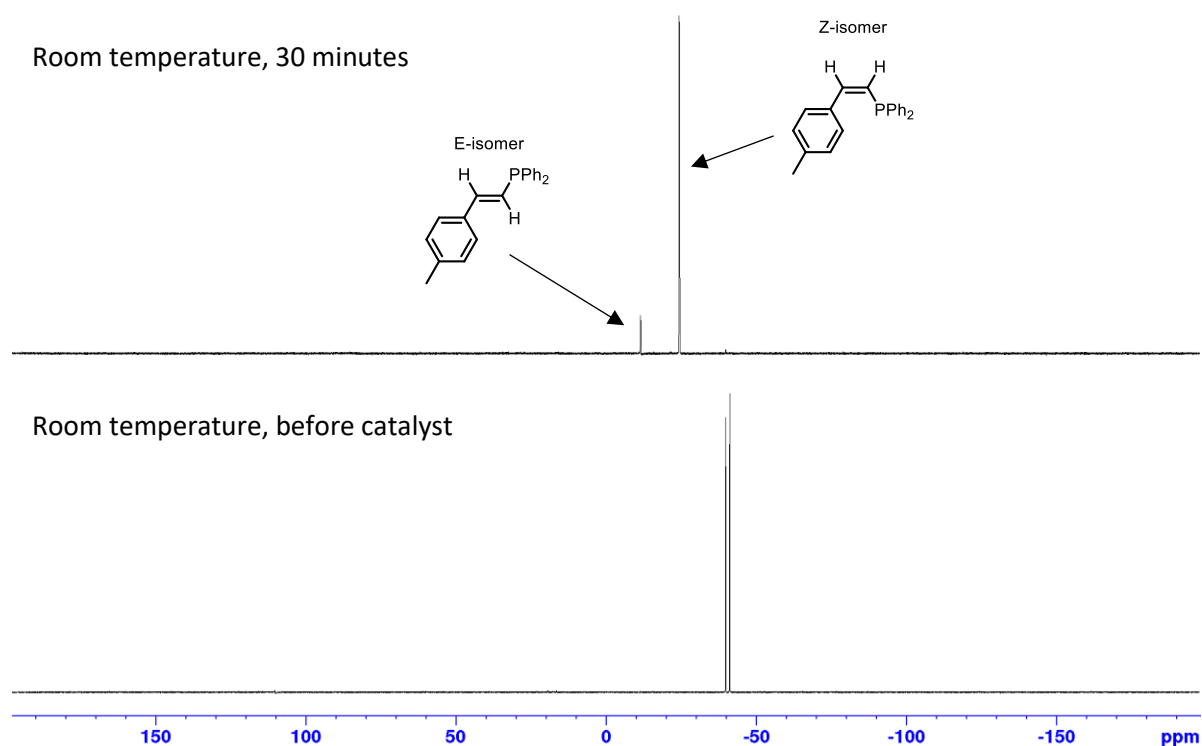


Figure S139: ^{31}P NMR spectrum for the hydrophosphination of 4'-methylphenylacetylene catalysed by **3** (10 mol%), with *N*-methylaniline additive, in d_8 -THF.

Isolation of Hydrophosphination Products

Phenylacetylene catalysed by **3**

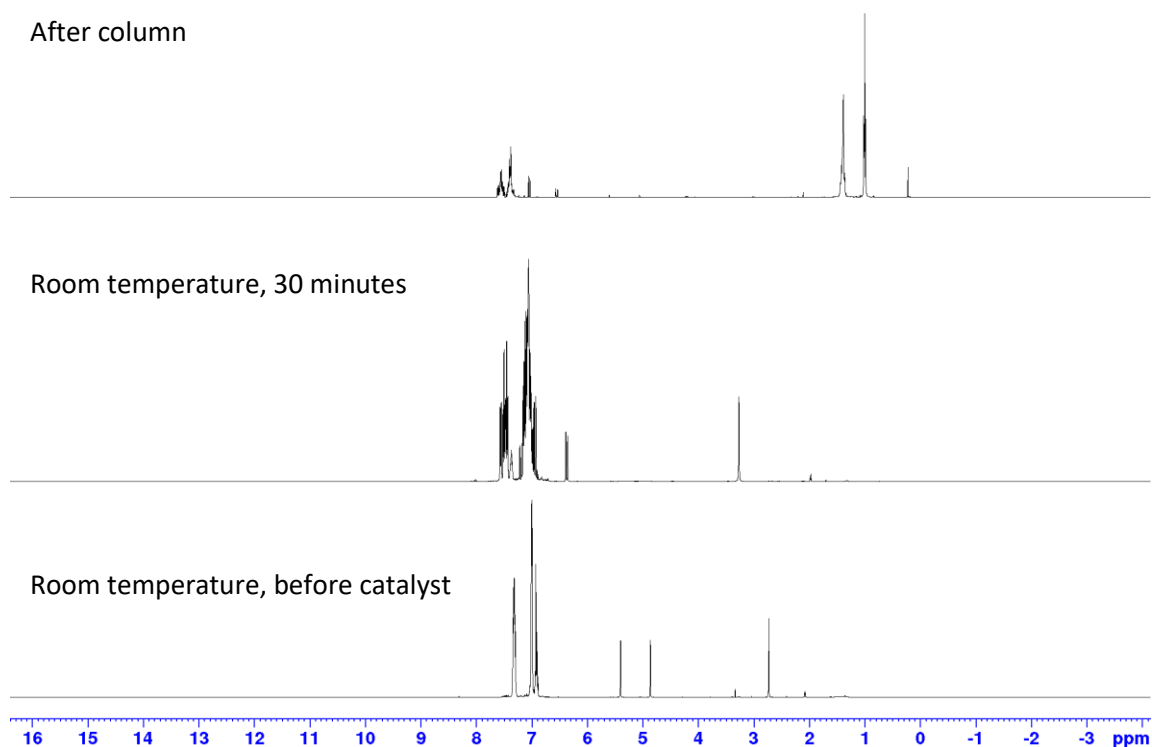


Figure S140: ^1H NMR spectrum for the hydrophosphination of phenylacetylene catalysed by **3** (10 mol%) in d_8 -toluene, followed by column chromatography and a final NMR carried out in CDCl_3 .

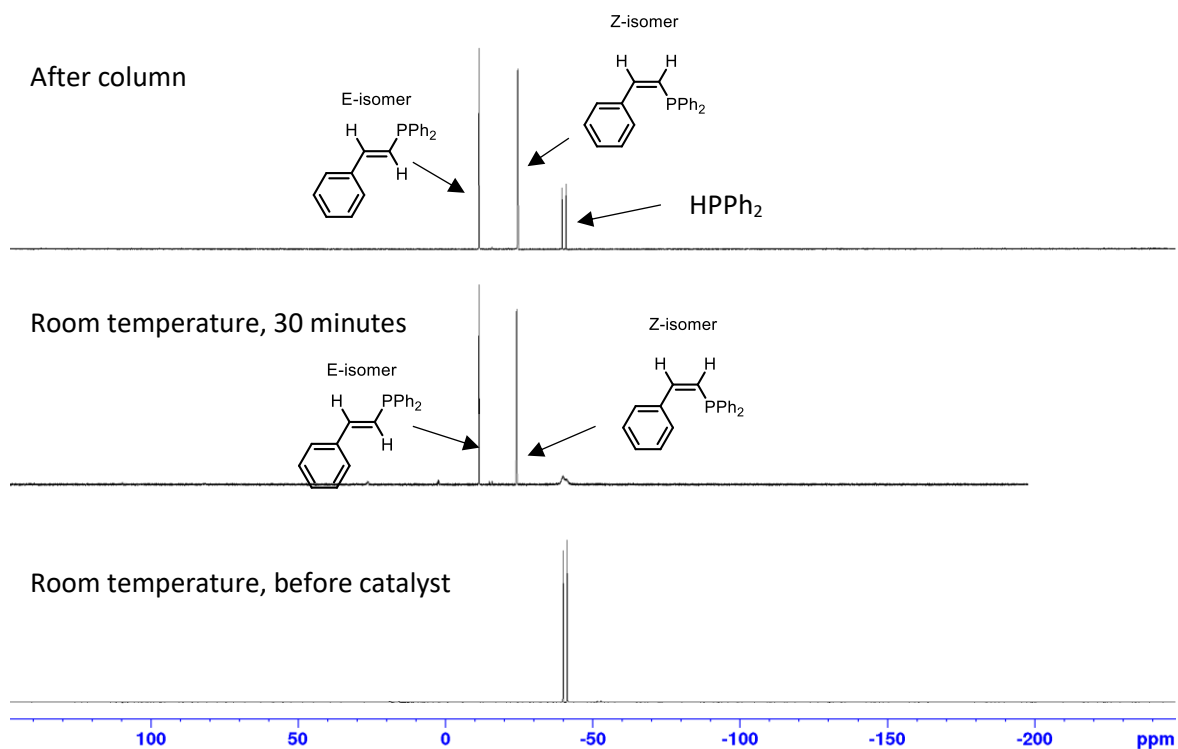


Figure S141: ^{31}P NMR spectrum for the hydrophosphination of phenylacetylene catalysed by **3** (10 mol%) in d_8 -toluene, followed by column chromatography and a final NMR carried out in CDCl_3 .

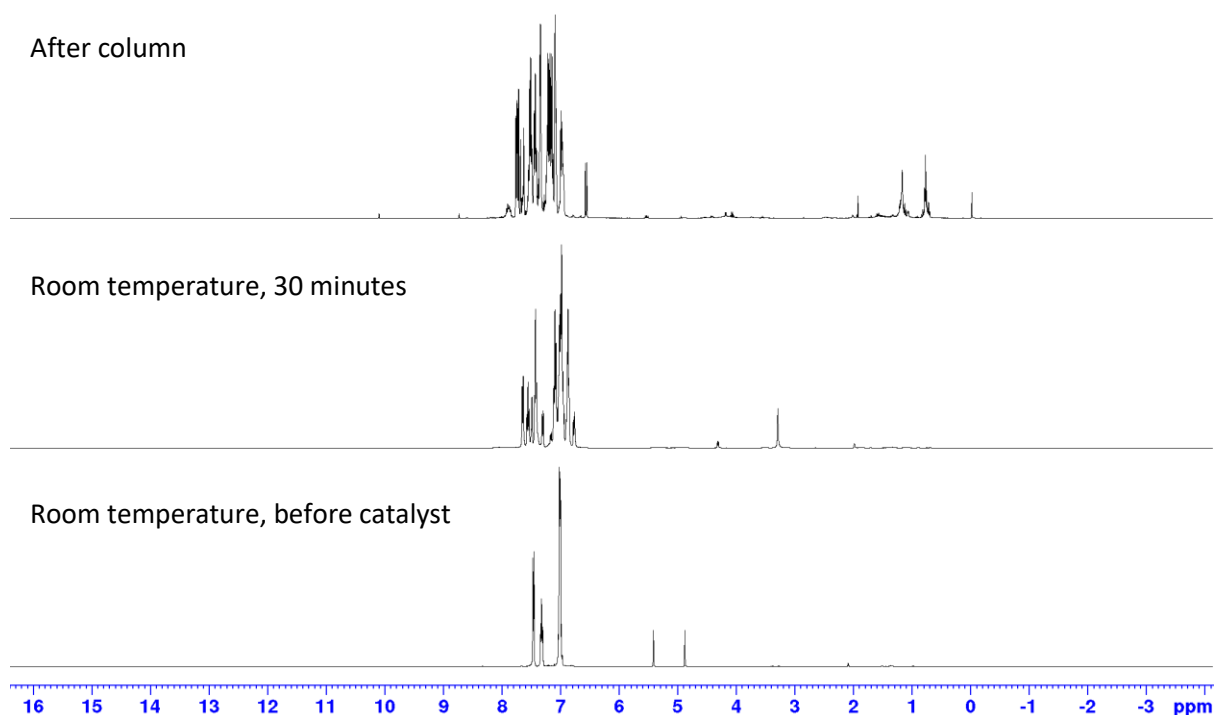


Figure S142: ^1H NMR spectrum for the hydrophosphination of diphenylacetylene catalysed by **3** (10 mol%) in d_8 -toluene, followed by column chromatography and a final NMR carried out in CDCl_3 .

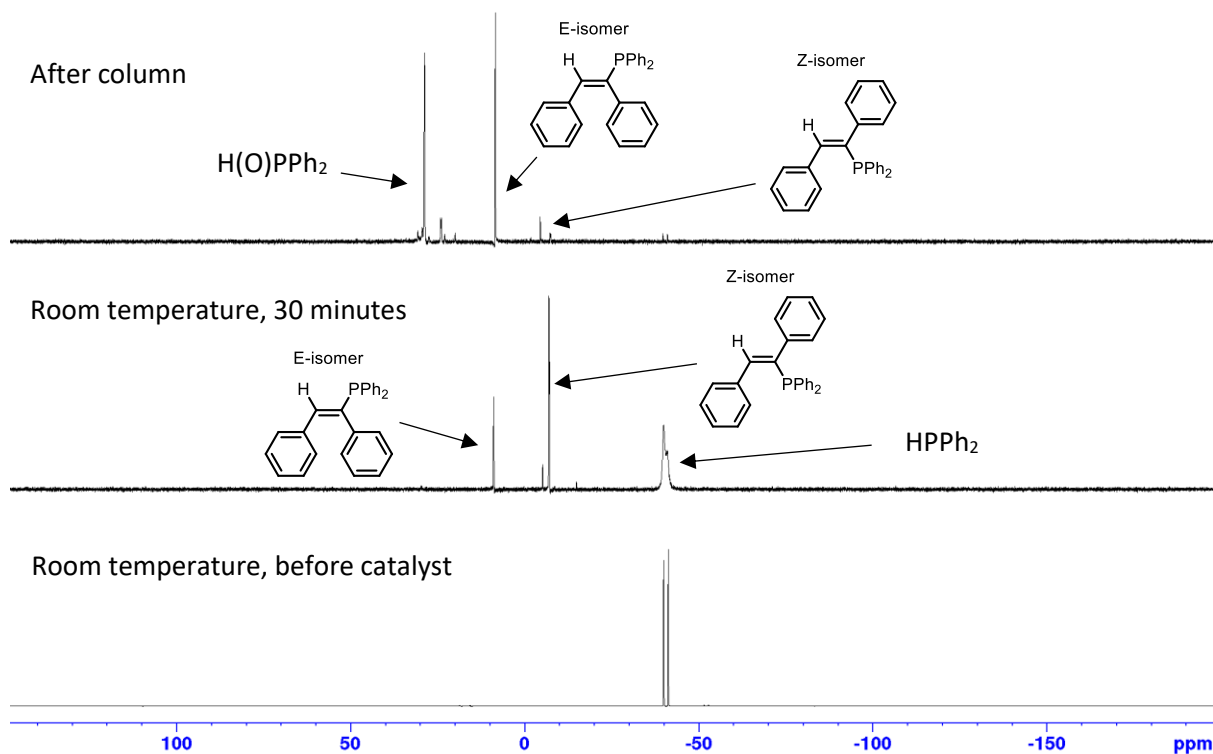


Figure S143: ^{31}P NMR spectrum for the hydrophosphination of diphenylacetylene catalysed by **3** (10 mol%) in d_8 -toluene, followed by column chromatography and a final NMR carried out in CDCl_3 .

4'-Methylphenylacetylene catalysed by **3**

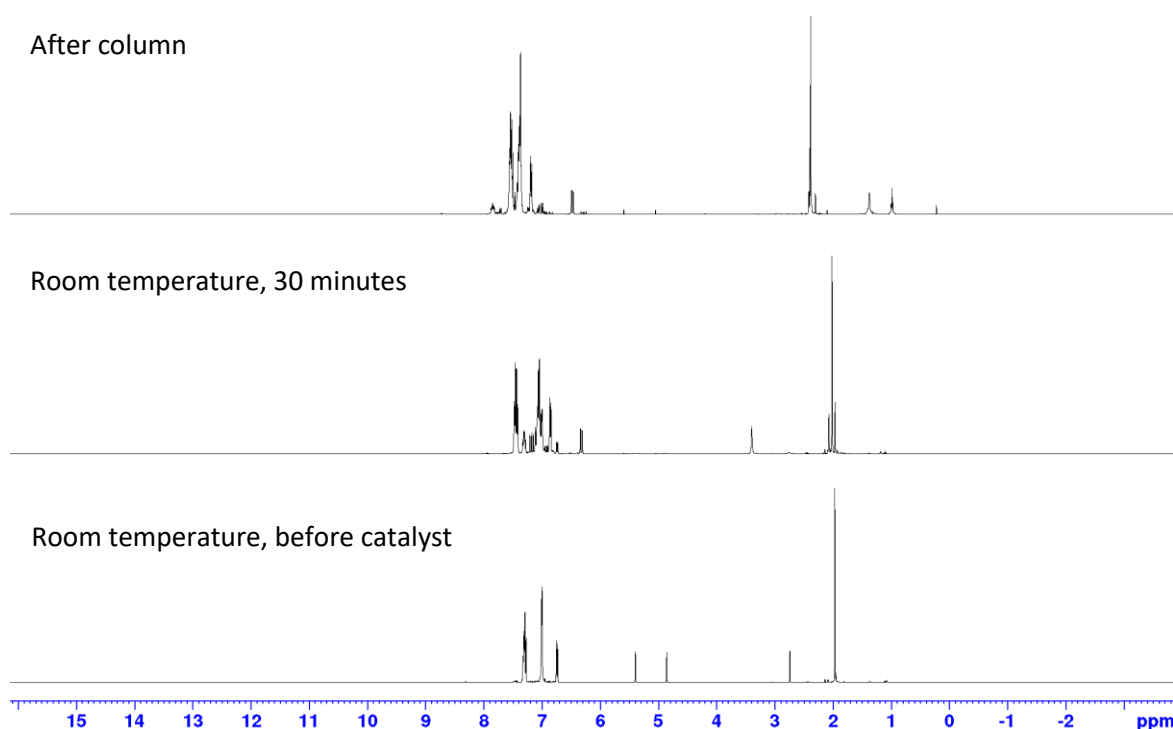


Figure S144: ^1H NMR spectrum for the hydrophosphination of 4'-methylphenylacetylene catalysed by **3** (10 mol%) in d_8 -toluene, followed by column chromatography and a final NMR carried out in CDCl_3 .

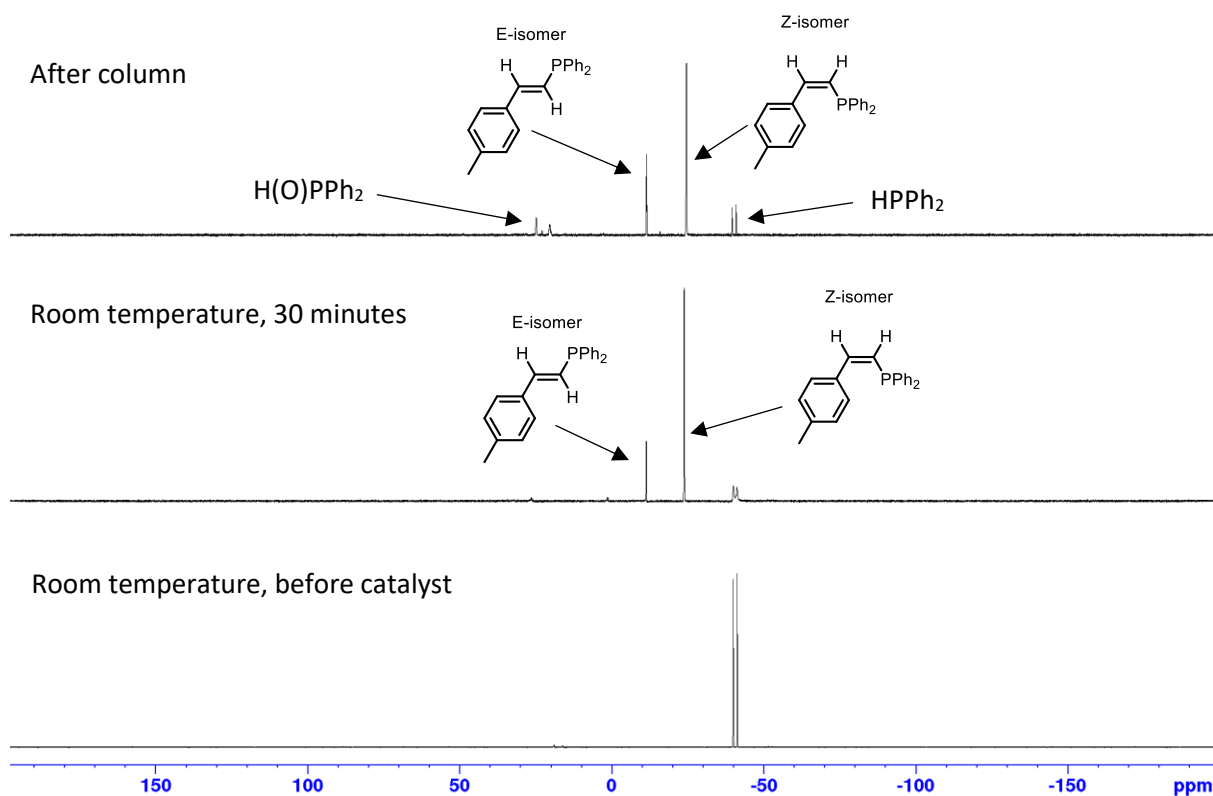


Figure S145: ^{31}P NMR spectrum for the hydrophosphination of 4'-methylphenylacetylene catalysed by **3** (10 mol%) in d_8 -toluene, followed by column chromatography and a final NMR carried out in CDCl_3 .

4'-Trifluoromethylphenylacetylene catalysed by **3**

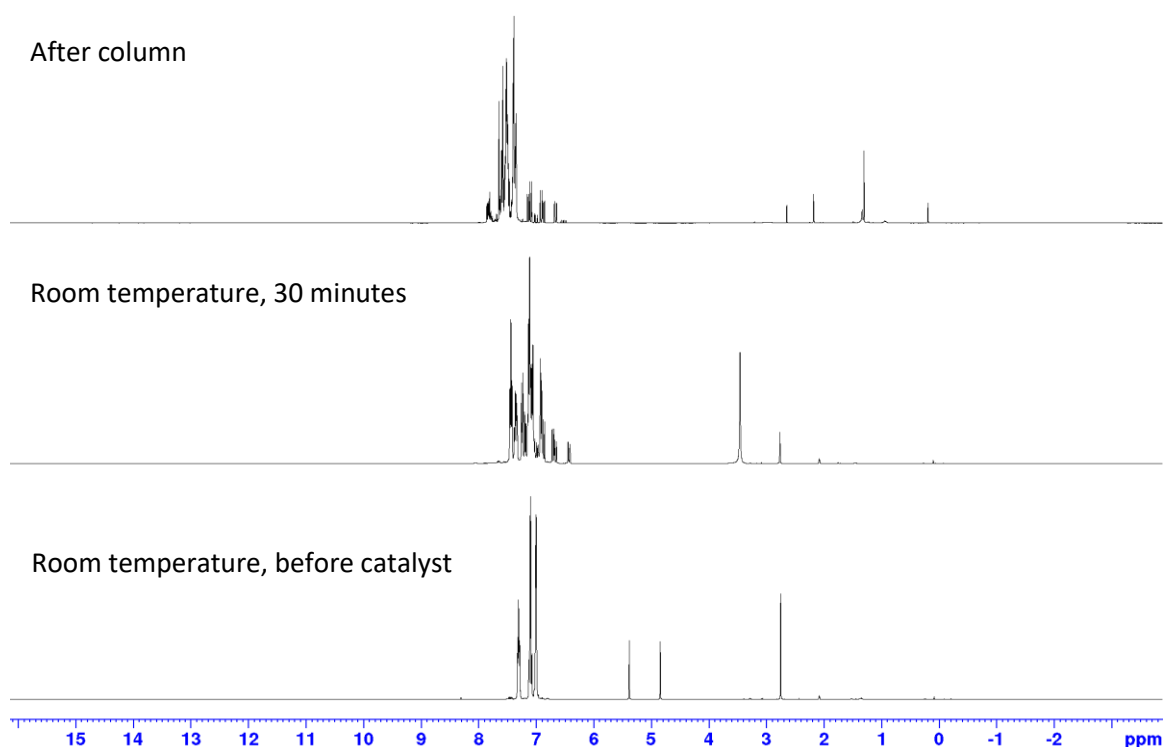


Figure S146: ^1H NMR spectrum for the hydrophosphination of 4'-trifluoromethylphenylacetylene catalysed by **3** (10 mol%) in d_8 -toluene, followed by column chromatography and a final NMR carried out in CDCl_3 .

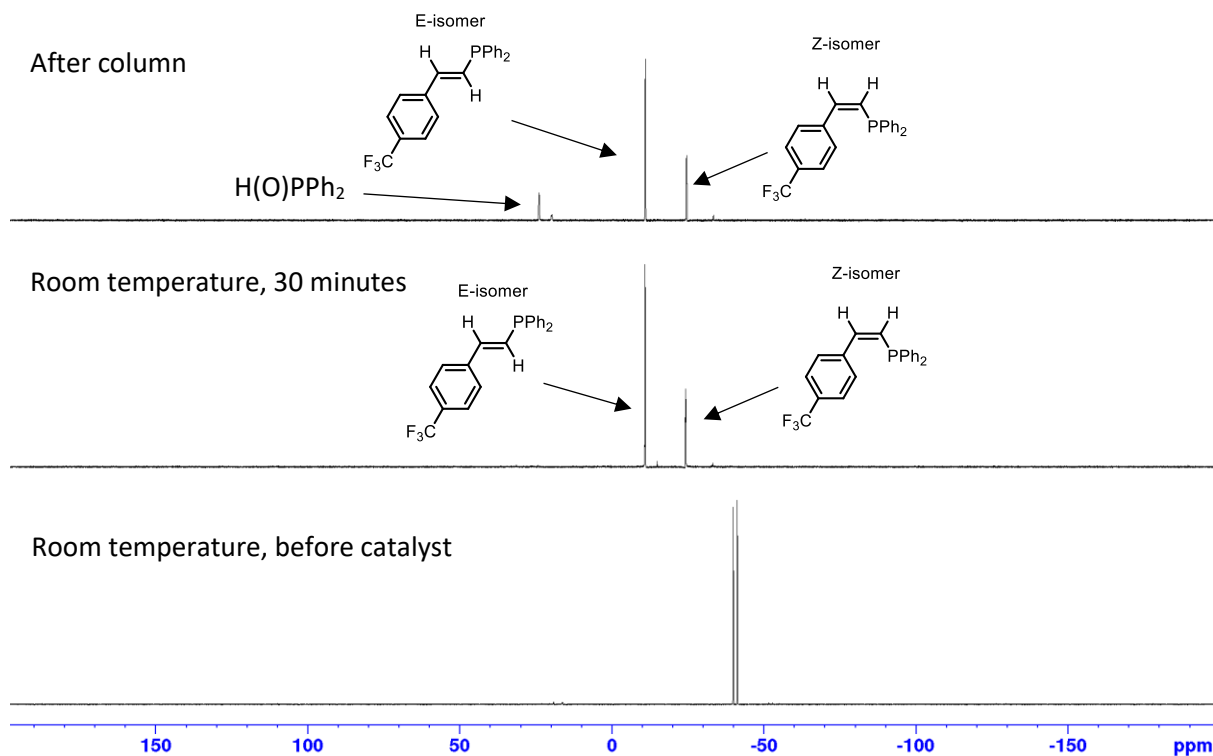


Figure S147: ^{31}P NMR spectrum for the hydrophosphination of 4'-trifluoromethylphenylacetylene catalysed by **3** (10 mol%) in d_8 -toluene, followed by column chromatography and a final NMR carried out in CDCl_3 .

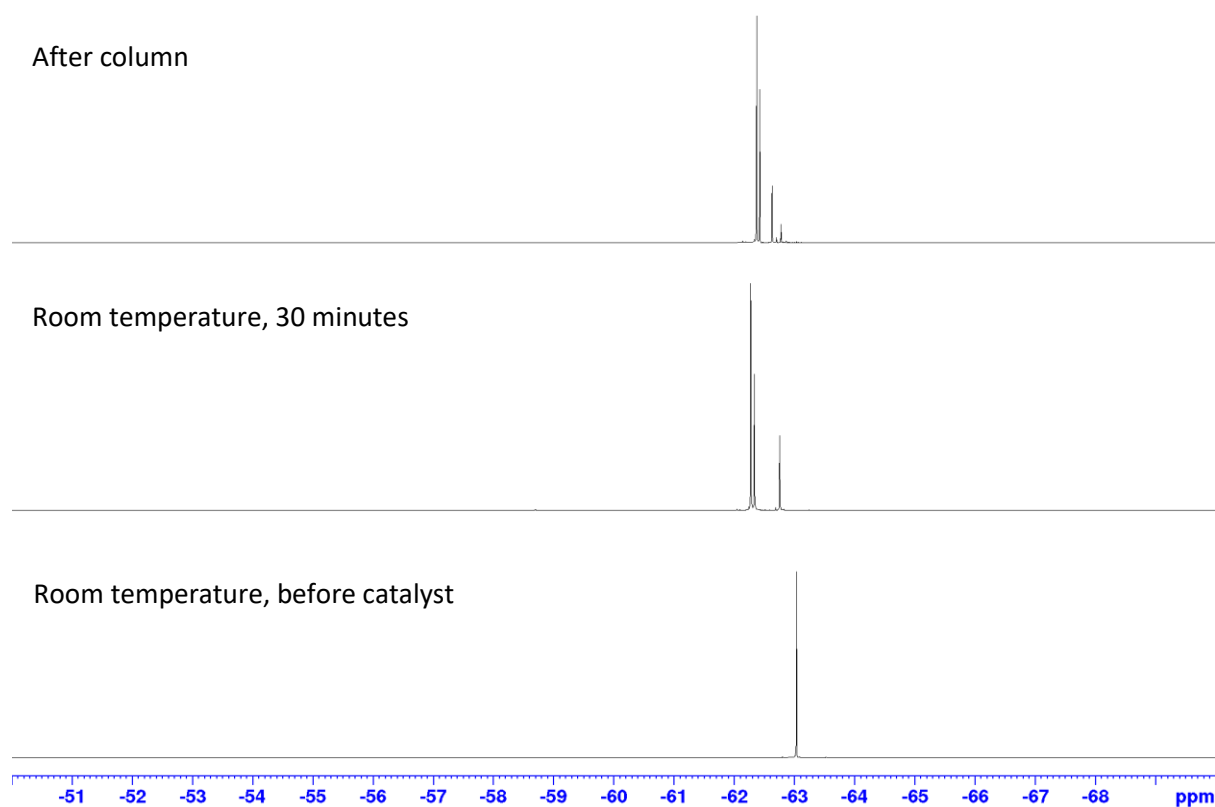


Figure S148: $^{19}\text{F}\{^1\text{H}\}$ NMR spectrum for the hydrophosphination of 4'-trifluoromethylphenylacetylene catalysed by **3** (10 mol%) in d_8 -toluene, followed by column chromatography and a final NMR carried out in CDCl_3 .

Computational Data

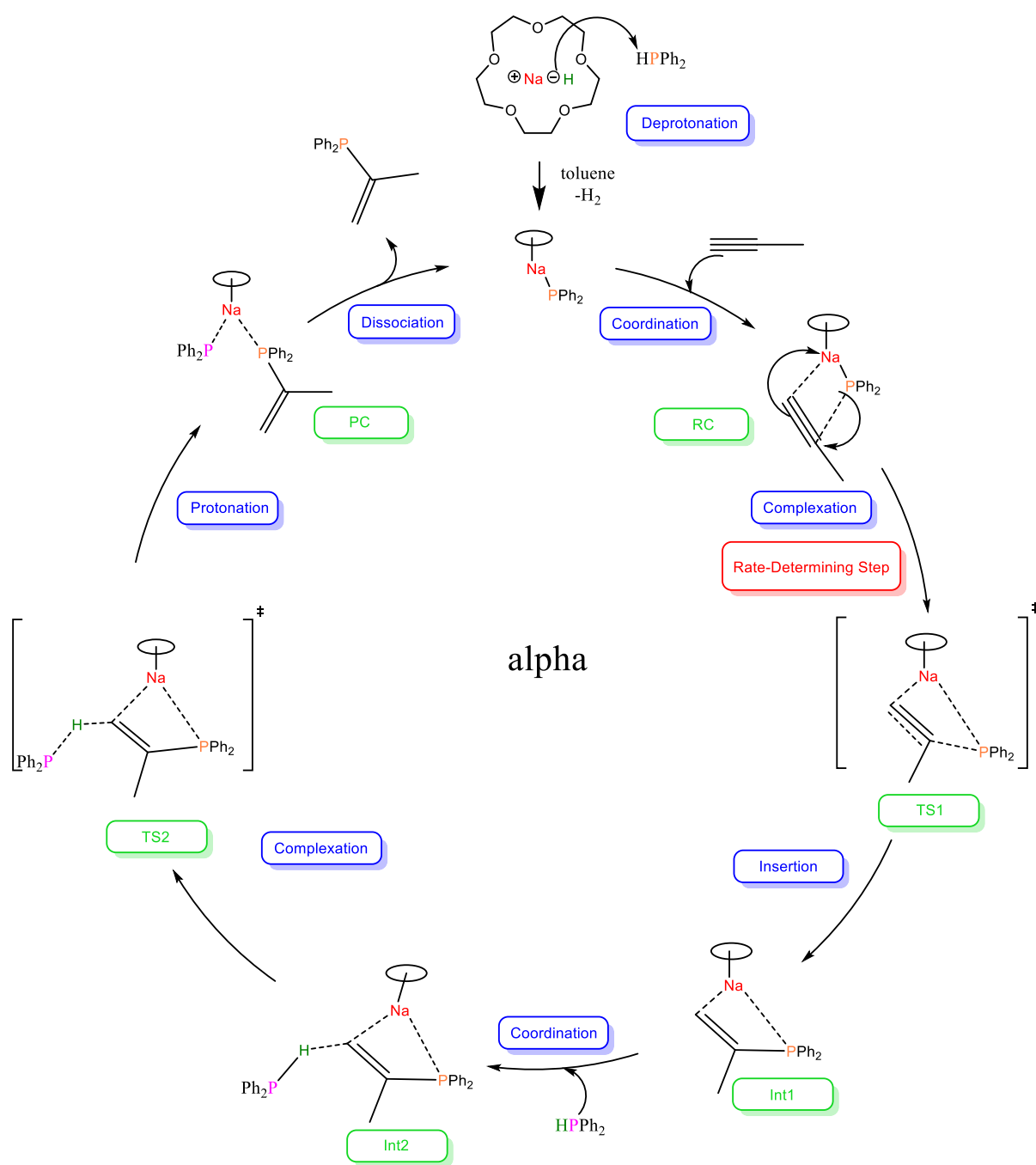


Figure S149: Proposed catalytic cycle for the formation of the α -isomer, following the hydrophosphination of 1-propyne with diphenylphosphine, catalysed by $\text{Ph}_2\text{PNa} \cdot 15\text{-crown-5}$, in toluene.

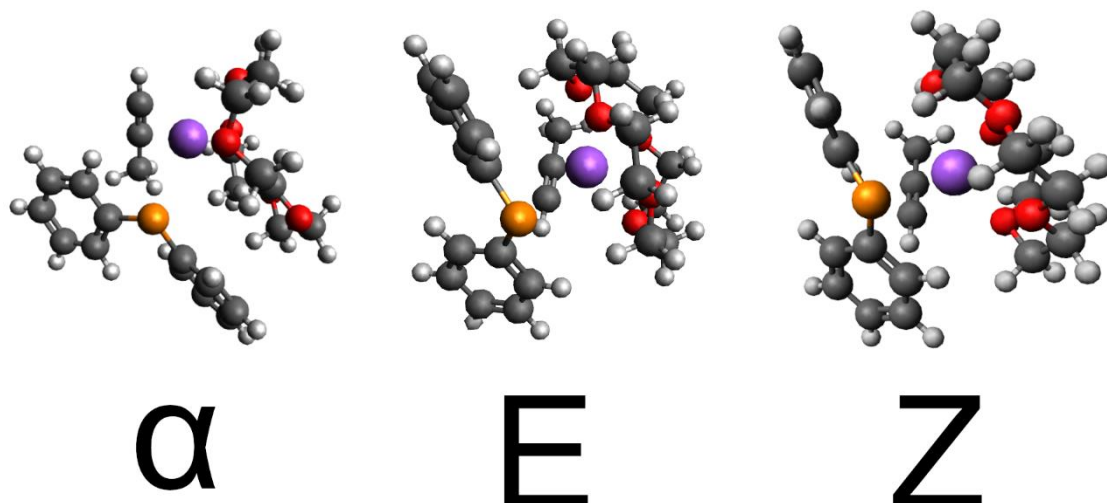


Figure S150: Reaction complex snapshots of each isomer, the reactant for the E and Z isomer are similar while the α isomer is oriented differently.

X-Ray Crystallographic Parameters for 1 – 4 Tables (S1-S4)

Table S1. Selected bond lengths (Å) of compounds 1 – 3. D = O (1), (3); N (2)

	1	2	3
<i>Na1–P1</i>	2.824(2)	2.9544(9)	2.8742(7)
<i>Na1–P1'</i>	2.824(2)	3.0326(11)	–
<i>Na1–D1</i>	2.280(17)	2.518(2)	2.428(3)
<i>Na1–D2</i>	2.317(6)	2.534(2)	2.3529(14)
<i>Na1–D3</i>	–	2.514(2)	2.4857(14)
<i>Na1–D4</i>	–	–	2.3781(12)
<i>Na1–D5</i>	–	–	2.430(5)
<i>P1–C1</i>	1.823(4)	1.8183(19)	1.8165(18)
<i>P1–C2</i>	1.826(4)	1.822(2)	1.8134(16)

Table S2. Selected bond angles (°) of compounds 1 – 3. D = O (1), (3); N (2)

	1	2	3
<i>Na1–P1–C1</i>	98.69(14)	116.17(6)	95.49(5)
<i>Na1–P1–C2</i>	87.44(13)	113.05(7)	105.78(5)
<i>C1–P1–C2</i>	105.01(18)	103.88(9)	105.67(7)
<i>P1–Na1–D1</i>	111.7(3)	119.25(6)	103.57(8)
<i>P1–Na1–D2</i>	102.37(16)	101.14(5)	122.64(4)
<i>P1–Na1–D3</i>	–	125.44(6)	93.33(3)
<i>P1'–Na1–D1</i>	106.7(4)	99.53(5)	–
<i>P1'–Na1–D2</i>	105.2(3)	170.12(6)	–
<i>P1'–Na1–D3</i>	–	106.84(5)	–
<i>P1–Na1–D4</i>	–	–	113.55(4)
<i>P1–Na1–D5</i>	–	–	110.98(8)
<i>D1–Na1–D2</i>	109.1(4)	71.82(7)	71.73(9)
<i>D1–Na1–D3</i>	–	110.12(7)	139.88(9)
<i>D1–Na1–D4</i>	–	–	132.15(8)
<i>D1–Na1–D5</i>	–	–	69.80(11)
<i>D2–Na1–D3</i>	–	72.77(7)	68.50(5)
<i>D2–Na1–D4</i>	–	–	108.75(5)
<i>D2–Na1–D5</i>	–	–	119.25(8)

<i>D3–Na1–D4</i>	–	–	68.14(4)
<i>D3–Na1–D5</i>	–	–	136.67(10)
<i>D4–Na1–D5</i>	–	–	69.35(10)

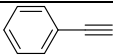
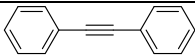

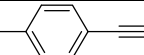
Table S3: Key bond lengths (Å) for compound **4**.

<i>P1–C1</i>	1.8151(15)
<i>P1–C2</i>	1.8259(14)
<i>Na1–N1</i>	2.7226(13)
<i>Na1–N2</i>	2.8056(14)
<i>Na1–O1</i>	2.5280(11)
<i>Na1–O2</i>	2.4193(11)
<i>Na1–O3</i>	2.4731(11)
<i>Na1–O4</i>	2.5111(11)
<i>Na1–O5</i>	2.5168(12)
<i>Na1–O6</i>	2.4728(11)

Table S4: Key bond angles (°) for compound **4**.

<i>C1–P1–C2</i>	101.50(6)
<i>N1–Na1–N2</i>	179.63(4)
<i>N1–Na1–O1</i>	67.63(4)
<i>N1–Na1–O2</i>	113.31(4)
<i>N1–Na1–O3</i>	112.16(4)
<i>N1–Na1–O4</i>	68.35(4)
<i>N1–Na1–O5</i>	68.13(4)
<i>N1–Na1–O6</i>	112.92(4)
<i>N2–Na1–O1</i>	112.48(4)
<i>N2–Na1–O2</i>	67.04(4)
<i>N2–Na1–O3</i>	67.77(4)
<i>N2–Na1–O4</i>	111.30(4)
<i>N2–Na1–O5</i>	112.11(4)
<i>N2–Na1–O6</i>	66.81(4)
<i>O1–Na1–O2</i>	68.99(4)
<i>O1–Na1–O3</i>	174.14(4)
<i>O1–Na1–O4</i>	106.53(4)
<i>O1–Na1–O5</i>	107.57(4)
<i>O1–Na1–O6</i>	79.04(4)
<i>O2–Na1–O3</i>	106.41(4)
<i>O2–Na1–O4</i>	173.14(4)
<i>O2–Na1–O5</i>	80.07(4)
<i>O2–Na1–O6</i>	105.42(4)
<i>O3–Na1–O4</i>	78.39(4)
<i>O3–Na1–O5</i>	67.54(4)
<i>O3–Na1–O6</i>	106.03(4)
<i>O4–Na1–O5</i>	106.49(4)
<i>O4–Na1–O6</i>	68.21(4)
<i>O5–Na1–O6</i>	172.78(4)

Table S5: Turnover numbers (TON) and turnover frequencies (TOF) of selected substrates in hydrophosphination catalysis by compound **3** [(15-Crown-5)NaPPh₂] in Toluene(D₈)

Entry	Substrate	Catalyst loading (mol%)	Time (h)	Conversion (%)	TON	TOF(h ⁻¹)
1		1	1	99	99	99
2		5	2.5	99	20	8
3		5	2	99	20	10
4		0.5	8	99	198	25

Reaction conditions: All reactions were performed under identical concentrations (0.5 mL by volume) and at room temperature. Conversion was determined by ¹H NMR spectroscopy.

Table S6: Selected Crystal Structure Data and Refinement Details for Compounds **1** and **2**

Compound	[(Ph ₂ PNa.(THF) ₂) ₂], 1	[(Ph ₂ PNa.PMDETA) ₂], 2
CCDC code		
Empirical formula	NaPO ₂ C ₂₀ H ₂₆	Na ₂ P ₂ N ₆ C ₄₂ H ₆₆
Formula weight	352.392	762.96
Temperature/K	230(2)	123(2)
Crystal system	monoclinic	Monoclinic
Space group	la	C2/c
a/Å	8.9988(3)	26.870(3)
b/Å	22.2544(6)	10.3785(6)
c/Å	10.5649(2)	20.9790(19)
α/°	90	90
β/°	101.590(2)	130.650(15)
γ/°	90	90
Volume/Å ³	2072.62(10)	4438.8(10)
Z	4	4
ρ _{calc} /g/cm ³	1.129	1.142
μ/mm ⁻¹	1.437	1.342
Radiation	Cu Kα (λ = 1.54184)	Cu Kα (λ = 1.54184)
2θ max/°	143.16	146.02
Reflections collected	10916	12532
Independent reflections	2969 [R _{int} = 0.0464, R _{sigma} = 0.0272]	4376 [R _{int} = 0.0597, R _{sigma} = 0.0450]
Data/restraints/parameters	2969/104/249	4376/0/241
Reflections obs [I>=2σ(I)]	2435	3753
Goodness-of-fit on F ²	1.0172	1.069
Final R indexes [I>=2σ(I)]	R ₁ = 0.0587, wR ₂ = 0.1801	R ₁ = 0.0580, wR ₂ = 0.1618
Final R indexes [all data]	R ₁ = 0.0652, wR ₂ = 0.1894	R ₁ = 0.0655, wR ₂ = 0.1701
Largest diff. peak/hole / e Å ⁻³	0.24/-0.14	0.56/-0.39

Table S7: Selected Crystal Structure Data and Refinement Details for Compounds **3** and **4**

Compound	[Ph ₂ PNa.15-crown-5], 3	[(Ph ₂ P) ⁻ (Na.2,2,2-cryptand) ⁺], 4
CCDC code		
Empirical formula	NaPO ₅ C ₂₂ H ₃₀	NaPO ₆ N ₂ C ₃₀ H ₄₆
Formula weight	424.41	584.67
Temperature/K	123(2)	123(2)
Crystal system	monoclinic	monoclinic

Space group	P2 ₁ /n	P2 ₁ /n
a/Å	9.27210(10)	12.7028(4)
b/Å	15.6269(3)	12.0142(3)
c/Å	15.4237(2)	19.7974(5)
α/°	90	90
β/°	91.5330(10)	91.118(3)
γ/°	90	90
Volume/Å³	2234.00(6)	3020.78(14)
Z	4	4
ρ_{calc}/g/cm³	1.2618	1.2855
μ/mm⁻¹	1.528	1.313
Radiation	Cu Kα (λ = 1.54184)	Cu Kα (λ = 1.54184)
2θ range for data collection/°	146.06	146.16
Reflections collected	14680	20410
Independent reflections	4426 [R _{int} = 0.0219, R _{sigma} = 0.0199]	5962 [R _{int} = 0.0289, R _{sigma} = 0.0228]
Data/restraints/parameters	4426/10/275	5962/0/361
Reflections obs [I ≥ 2σ (I)]	4096	5346
Goodness-of-fit on F²	1.337	1.050
Final R indexes [I ≥ 2σ (I)]	R ₁ = 0.0420, wR ₂ = 0.1190	R ₁ = 0.0398, wR ₂ = 0.1067
Final R indexes [all data]	R ₁ = 0.0447, wR ₂ = 0.1214	R ₁ = 0.0443, wR ₂ = 0.1105
Largest diff. peak/hole / e Å⁻³	0.71/-0.22	0.45/-0.23